nagra.

Arbeitsbericht NAB 08-15

Oftringen Borehole - Hydraulic Packer Testing

Text

October 2008

H.R. Fisch, U. Rösli, S. Reinhardt,
B. Yeatman (Solexperts AG)
R. Senger, T. Dale (Intera Inc.)

**Nationale Genossenschaft
für die Lagerung
radioaktiver Abfälle**

Hardstrasse 73
CH-5430 Wettingen
Telefon 056-437 11 11

www.nagra.ch

nagra.

Arbeitsbericht NAB 08-15

Oftringen Borehole - Hydraulic Packer Testing

Text

October 2008

H.R. Fisch, U. Rösli, S. Reinhardt,
B. Yeatman (Solexperts AG)
R. Senger, T. Dale (Intera Inc.)

KEYWORDS
EP-05, EWS, Oftringen, NOK, USM, Effingen-Member, Hydraulic Testing, Transmissivity, Conductivity, Head

**Nationale Genossenschaft
für die Lagerung
radioaktiver Abfälle**

Hardstrasse 73
CH-5430 Wettingen
Telefon 056-437 11 11

www.nagra.ch

This report was prepared on behalf of Nagra. The viewpoints presented and conclusions reached are those of the author(s) and do not necessarily represent those of Nagra.

Appendices

List of Tables

List of Figures

1. Introduction

1.1. Background and Project Summary

After drilling of the 719 m deep NOK-EWS Borehole at Oftringen, Switzerland, selected sections of the calcareous Malm and Dogger formations were hydraulically investigated using a double packer straddle system. The location of the NOK-EWS Borehole Oftringen is shown in Fig. 1.1. The investigation program was prepared and directed by Nagra. The main part of the in-situ experiments focused on eight hydraulic tests to the determination of the hydraulic properties of marls and interbedded limestones of the Effingen Member. A single hydraulic test was performed in limestone of the Geissberg layer above the Effingen strata. Additionally, a lower section of the NOK-EWS borehole that covers part of the Hauptrogenstein formation (Dogger) was investigated.

A project summary is presented in Tab. 1.1.

Tab. 1.1: Project summary

Project direction	Nagra
Project manager	Dr. Bernd Frieg
Drilling contractor	Daldrup & Söhne AG
Drilling period:	16 August – 17 October 2008
Geophysical logging + Fluid-Logging contractors	BLM, AF-Colenco, Albert Geo-Consult
Logging period:	17 – 19 October 2007
Hydraulic field testing campaign	
Duration:	19 October - 05 November 2007
Test engineers (Solexperts):	Hansruedi Fisch, Sacha Reinhardt Jörg Hayer, Dr. Andreas Kern
Technicians (Solexperts):	Fredi Portman, Peter Haller, Peter Stillhard, Stefan Caduff
Test analysis and reporting	
Solexperts:	Hansruedi Fisch, Dr. Ursula Rösli, Sacha Reinhardt, Bob Yeatman
Intera:	Dr. Rainer Senger, Tim Dale
Review	
Nagra:	Dr. B. Frieg
AF-Colenco:	Dr. Rainer Schwarz, Dr. Jean Croisé

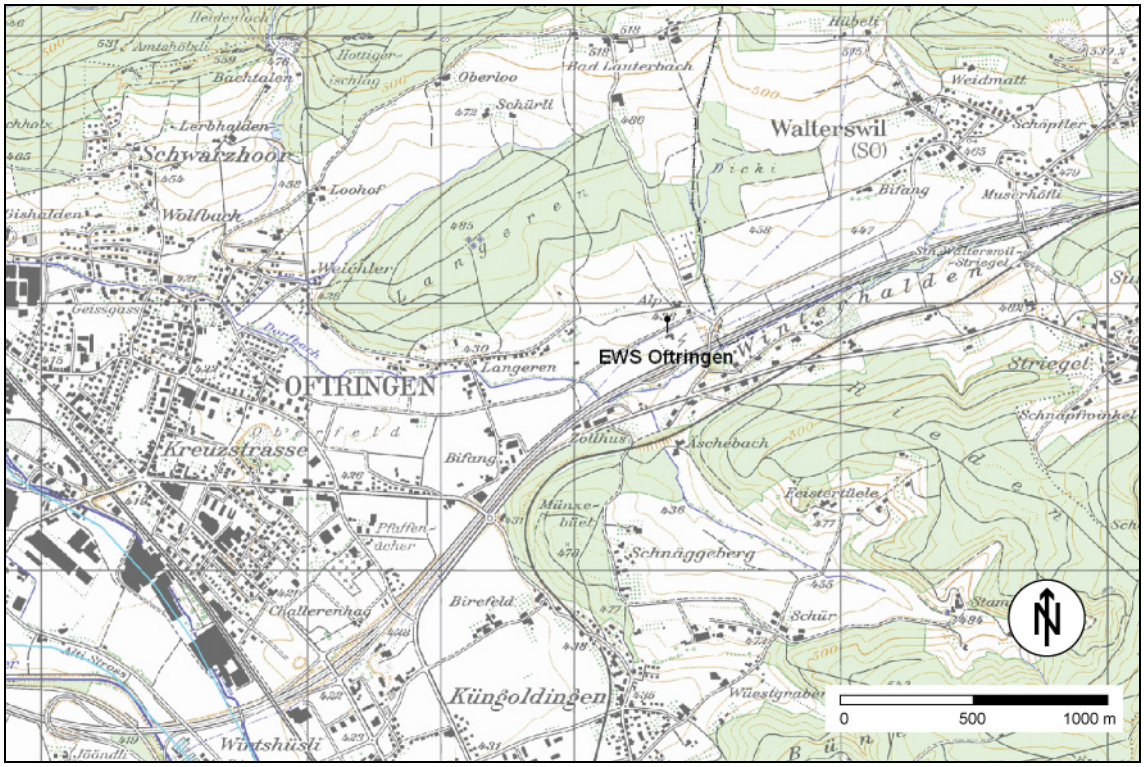

Fig. 1.1: Location of the NOK-EWS Borehole Oftringen (E 638'346 / N 240'887).

1.2. Scope of Report

This report summarizes field activities and results of hydrotesting in the NOK-EWS Borehole at Oftringen carried out between the 19 October 2007 and 05 November 2007. Transmissivity and hydraulic conductivity estimates of discrete borehole sections and corresponding measurements of hydraulic heads are provided.

1.3. Report Organization

Hydraulic testing of each test zone is presented in a separate chapter (Chapter 8 to Chapter 17). The Quick Look Reports (QLRs) are included in the Appendices A to J.

2. Overview of Hydraulic Testing

Hydraulic testing of the vertical borehole NOK-EWS 2007 was carried out between 19 October and 5 November 2007.

A total of 10 test sections were investigated using packer straddle lengths of 50.04 and 9.09 meters (Tab. 2.1). The test intervals are numbered in the order of testing. Coordinates and specifications of the NOK-EWS borehole are provided in Tab. 2.2. A geological profile is shown in Fig. 2.1.

The aim of hydraulic testing was to obtain reliable estimates on the transmissivity (T), hydraulic conductivity (K) and static hydraulic head (h_s) of the geologic units contained in the packer intervals. Intervals Oftr-i6 and Oftr-i10 have identical depth positions. During Test Oftr-i10, production of formation water was continued in order to obtain a representative formation water sample.

Equipment specifications are provided in Chapter 4.

Tab. 2.1: Investigated borehole sections of Borehole NOK-EWS 2007

Name	Depth	Length [m]	Geology	Main Goals [1)]
Oftr-i1	650.0 - 700.04 m bgl	50.04	limestone - marl interbedded strata and oolithic limestones	Flow model, T, K, h_s
Oftr-i2	590.0 - 640.04 m bgl	50.04	limestone - marl interbedded strata	Flow model, T, K, h_s
Oftr-i3	550.0 - 600.04 m bgl	50.04	mainly marl with interbedded limestone strata	Flow model, T, K, h_s
Oftr-i4	500.0 - 550.04 m bgl	50.04	marl - limestone interbedded strata	Flow model, T, K, h_s
Oftr-i5	449.85 - 499.89 m bgl	50.04	argillaceous limestone, marls and argillaceous marls	Flow model, T, K, h_s
Oftr-i6	408.5 - 417.59 m bgl	9.09	limestone (Geissberg Member)	Flow model, T, K, h_s , WS
Oftr-i7	632.5 - 641.59 m bgl	9.09	clay-marls and carbonate marls	Flow model, T, K, h_s
Oftr-i8	621.5 - 630.59 m bgl	9.09	limestone - marl interbedded strata	Flow model, T, K, h_s
Oftr-i9	583.0 - 592.09 m bgl	9.09	limestone - marl interbedded strata	Flow model, T, K, h_s
Oftr-i10	408.5 - 417.59 m bgl	9.09	limestone (Geissberg Member)	WS

[1)] Flow model, T= transmissivity, K = hydraulic conductivity, h_s = static formation head, WS = Water sample

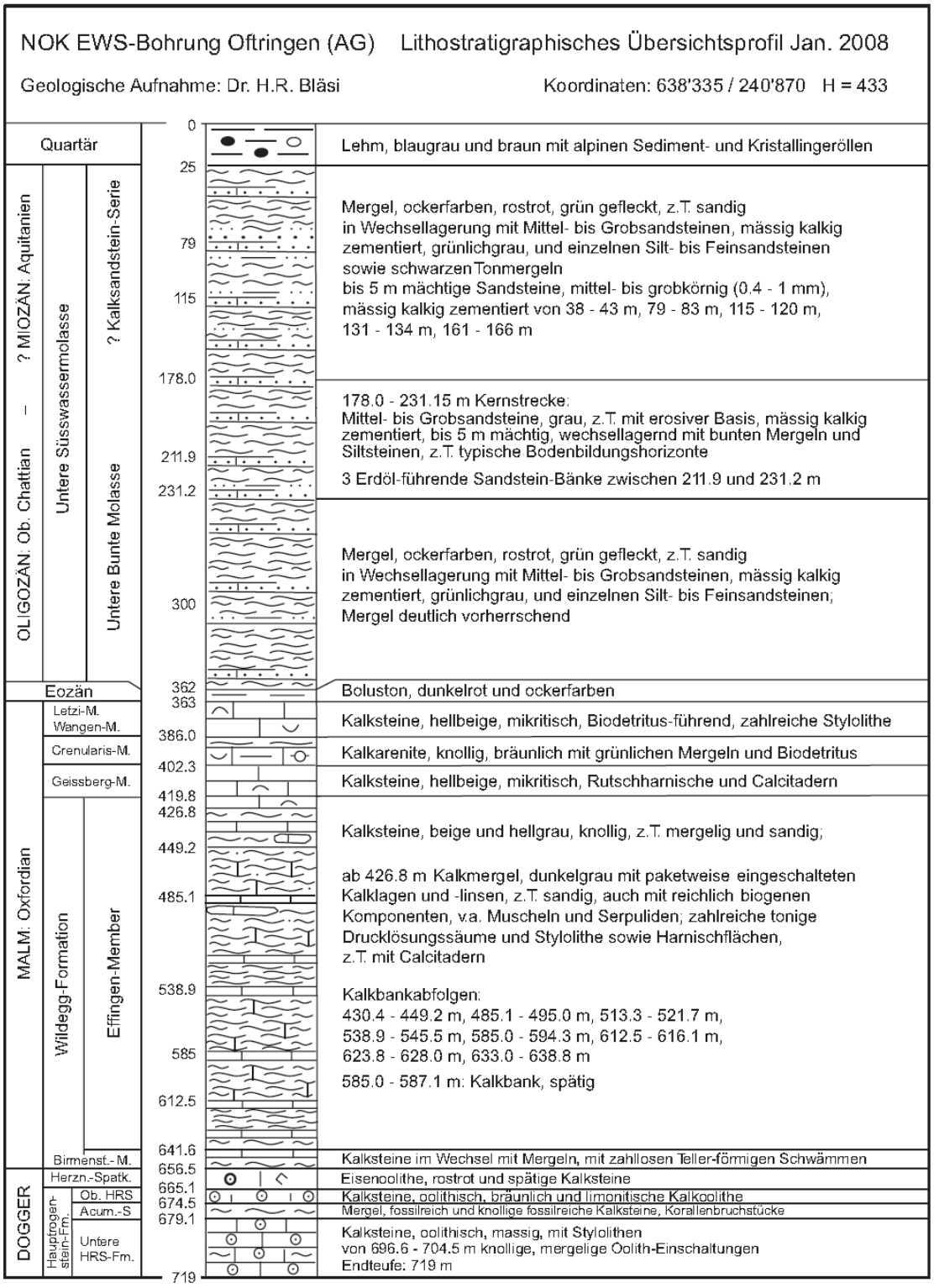

Fig. 2.1: Geological profile of the NOK-EWS borehole (Albert & Bläsi, 2008)

2.1. Depth reference

All depths provided refer, if not otherwise stated, to the drilling platform which was 1.42 m above ground level.

Tab. 2.2: Specifications of Borehole NOK-EWS 2007

Location:	Oftringen (AG), Switzerland	
Coordinates:	E 638'335 / N 240'870	
Elevation:	433	m asl
Drilling period:	16 August – 17 October 2007	
Drilling fluid:	Bentonite mud with polymer	
Geophysical logging:	- Caliper log (CAL) - Natural gamma (GR) - Temperature log (TEMP) - Salinity log (SAL) - Sonic log - Focused electric log (FEL)	
Borehole depth:	719.0 m bgl	
Borehole diameter:	216 mm 146 mm	(8 ½", 0 - 385 m bgl) (5 ¾", 385-719 m bgl)
7" Casing:		
- Casing inner diameter	163	mm
- Casing stick-up	1.42	m agl
- Casing shoe	382	m bgl

3. Borehole Pressure History

The borehole pressure history describes the chronology of the pressure disturbances for an individual test zone prior to start of hydrotesting. The natural static pressure of a specific test zone is perturbed by drilling. After drilling, the downhole pressure is controlled by the borehole water table and the fluid density. Flow to or from the specific test zone is controlled by the transmissivity of the test zone, potential borehole skin and the difference in hydraulic head between borehole and test zone. The flow process only stops when the test zone is hydraulically isolated, i.e. when the packers of the test tool are inflated or when the borehole pressure equals the formation pressure. The effects of the borehole pressure history are often only partly reversed during the initial pressure recovery phase of hydraulic testing (PSR phase). The borehole pressure history can be simulated using numerical analysis tools.

Pressure history records based on the specific borehole test zone drilling data were prepared prior to the interpretation of the hydraulic tests. The following information was used:

- Date and time of drilling through interval midpoint from drilling logs: SJ Geotec daily logbook
- Drilling fluid density: Nagra daily drilling reports (Tagesrapporte)
- Replacement of drilling fluid using fresh water: SJ Geotec logbook
- Open hole pumping during fluid logging and pressure recovery: SJ Geotec, AF-Colenco documentation
- Pressure records of antecedent hydrotesting: Solexperts

The density of the drilling fluid varied between 1.012 and 1.038 g/cm^3. The density of the clear borehole water is 0.997 g/cm^3 (measured by SJ Geotec). The duration of the borehole history is listed for each test interval in Tab. 3.1. An example for a pressure history record is shown in Tab. 3.2 and Fig. 3.1. The borehole history is shown for each test interval in the individual Quick Lock Reports (Appendices A to J). Where appropriate, consolidated test data from precedent tests (P1, P2 and P3) were used to prepare the borehole pressure history for an individual test. The procedure is demonstrated on example Oftr-i7 in Tab. 3.3.

The borehole pressure history data were incorporated into the numerical analyses using the software package nSights.

Tab. 3.1: Test specific duration of borehole pressure history

Interval name	Depth [m bgl]	Length [m]	Interval midpoint [m bgl]	Drilling through midpoint Date & time	Start hydraulic testing Data & time	Borehole history duration [hrs]
Oftr-i1	650.00 - 700.04	50.04	675.02	15.10.07 18:30	20.10.07 00:01	101.5
Oftr-i2	590.00 - 640.04	50.04	615.02	12.10.07 08:00	21.10.07 05:55	213.9
Oftr-i3	550.00 - 600.04	50.04	575.02	10.10.07 21:30	22.10.07 14:51	281.3
Oftr-i4	500.00 - 550.04	50.04	525.02	04.10.07 17:30	23.10.07 18:03	456.6
Oftr-i5	449.85 - 499.89	50.04	474.87	02.10.07 05:30	24.10.07 16:06	538.6
Oftr-i6	408.50 - 417.59	9.09	413.045	27.09.07 01:40	28.10.07 08:07	750.4
Oftr-i7	632.50 - 641.59	9.09	637.05	12.10.07 23:46	30.10.07 01:26	409.7
Oftr-i8	621.50 - 630.59	9.09	626.05	12.10.07 17:00	01.11.07 20:48	483.8
Oftr-i9	583.00 - 592.09	9.09	587.545	11.10.07 07:45	02.11.07 13:21	533.6
Oftr-i10	408.50 - 417.59	9.09	413.045	27.09.07 01:40	03.11.07 09:38	896.0

Tab. 3.2: Borehole pressure history for test Interval Oftr-i2.

Date and hour	Water table [m bgl]	Fluid density [g/cm^3]	Elapsed time [hrs]	Data source	Calc. P2 pressure [kPa]	Events
12.10.07 08:00	-1.42	1.028	-213.9	SJG	6030.7	Drilling through interval midpoint
15.10.07 18:30	-1.42	1.031	-131.4	Nagra	6048.0	Drilling
17.10.07 12:00	-1.42	0.997	-89.9	SJG	5851.8	Drilling fluid is replaced by fresh water
18.10.07 18:55	-1.40	0.997	-59.0	Col	5851.6	Start fluid logging
18.10.07 18:55 to 19.10.07 04:00	Series	0.997	Series	Col	Series	Drawdown & subsequent recovery (68 data points)
19.10.07 04:15	44.95	0.997	-49.7	Col	5398.3	End fluid logging
19.10.07 17:10	39.95	0.997	-36.9	SE	5447.2	WT measurement
20.10.07 00:01	20.30	0.997	-29.9	SE	5639.4	Start Test Oftr-i1
20.10.07 16:00	19.30	0.997	-13.9	SE	5649.2	Test Oftr-i1, P3 measure
21.10.07 04:10	18.42	0.997	-1.8	SE	5657.8	Test Oftr-i1, P3 measure
21.10.07 04:52	-1.42	0.997	-1.1	SE	5851.8	Fill up annulus
21.10.07 05:55	2.23	0.997	0.0	SE	5816.1	Start Test Oftr-i2

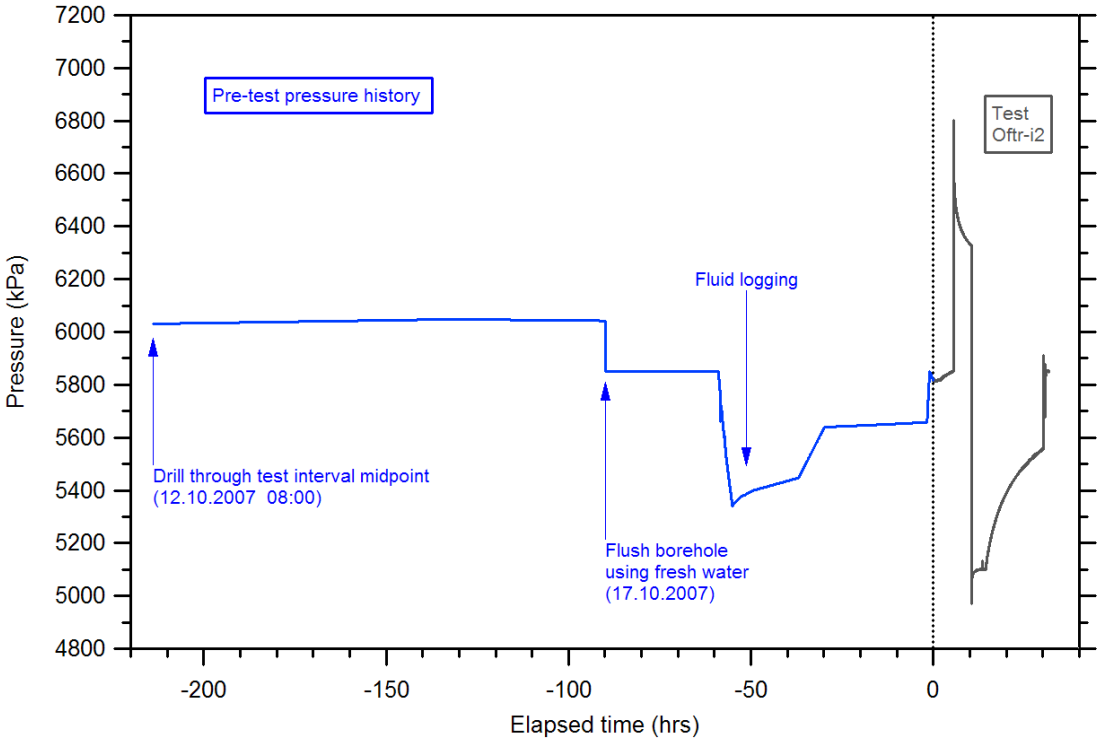

Fig. 3.1: Borehole pressure history for test Interval Oftr-i2.

The blue curve with negative elapsed time shows the pre-test borehole pressure data. Open-hole water table measurements were converted to pressures at the P2 sensor depth.

Tab. 3.3: Example procedure to establish a borehole pressure history data file.

The records listed below were used to build the borehole pressure history for test Interval Oftr-i7. Records 1 to 8 were processed in the indicated order and the resulting data set was reduced to 2000 data points by interpolation. The manually recorded data (record 9) were then added, completing the borehole history.

Sequence of data files or manually recorded data		**Comments**
1	Borehole history established for Oftr-i2	As shown in graph/table above
2	P2 pressure data from Oftr-i2	Oftr-i7 covers part of Oftr-i2
3	P1 (bottom hole) pressure data from Oftr-i3	Oftr-i7 has deeper position than Oftr-i3
4	P1 (bottom hole) pressure data from Oftr-i4	Oftr-i7 has deeper position than Oftr-i4
5	P1 (bottom hole) pressure data from Oftr-i5	Oftr-i7 has deeper position than Oftr-i5
6	P1 (bottom hole) pressure data from Oftr-i6	Oftr-i7 has deeper position than Oftr-i6
7	P1 (bottom hole) pressure data from Oftr-i6c	Oftr-i7 has deeper position than Oftr-i8c
8	P1 (bottom hole) pressure data from Oftr-i6d	Oftr-i7 has deeper position than Oftr-i6d
9	Manually recorded open hole WT data	From Oftr-i7 Daily Log Report (see QLR)

4. Testing Equipment

4.1. Downhole Equipment

The hydraulic tests were performed using a straddle-packer system referred to as the Heavy Duty Double Packer system (HDDP). This system consists of an upper and lower inflatable packer used to confine a test interval section of specified length. Inflow and out flow are through a perforated filter segment above the bottom packer. Pressure transducers, referred to as the Triple sub-surface probe (TSSP), measure the pressures below, within and above the test interval. Temperatures at the probes are also measured. A zero-displacement downhole shut-in tool (SIT) is used to isolate the test zone between the packers. A 3-inch downhole pump integrated in the test tubing was used for production pump tests. A generalized configuration of the test tool is presented in Fig. 4.1. Specific configurations of the downhole tools are provided in the Quick Look Reports in Appendices A to J.

4.1.1. Heavy Duty Double Packer System (HDDP)

The packers of the HDDP were inflated with an antifreeze-water mixture through separate hydraulic pressure lines connected to a surface pressure stabilization vessel. A third hydraulic line controls the downhole shut-in tool (SIT). The data from the TSSP are transmitted by an encapsulated single conductor cable. The technical data of the HDDP is provided in Tab. 4.1.

Tab. 4.1: Specifications of Heavy Duty Double Packer System (HDDP)

Tool Description	4 ¼” Heavy Duty double Packer System (HDDP)
Packer configuration	Double Packer
Packer type	IPI 4 ¼", natural rubber
Seal length	125 mm
Inflation Method	Surface controlled
Inflation Fluid	Antifreeze-water
Interval filter type	Johnson Filter Screen
Probe	Triple Sub Surface Probe (TSSP)
Shut-in tool (SIT)	2 ½" zero-displacement valve
Control Lines	4 Core Encapsulated Flatpack - Hydraulic line – Lower Packer (PA1) - Hydraulic line – Upper Packer (PA2) - Hydraulic Line – Shut-in tool (SIT) - 1/8” OD Tubing Encased Single Conductor Cable

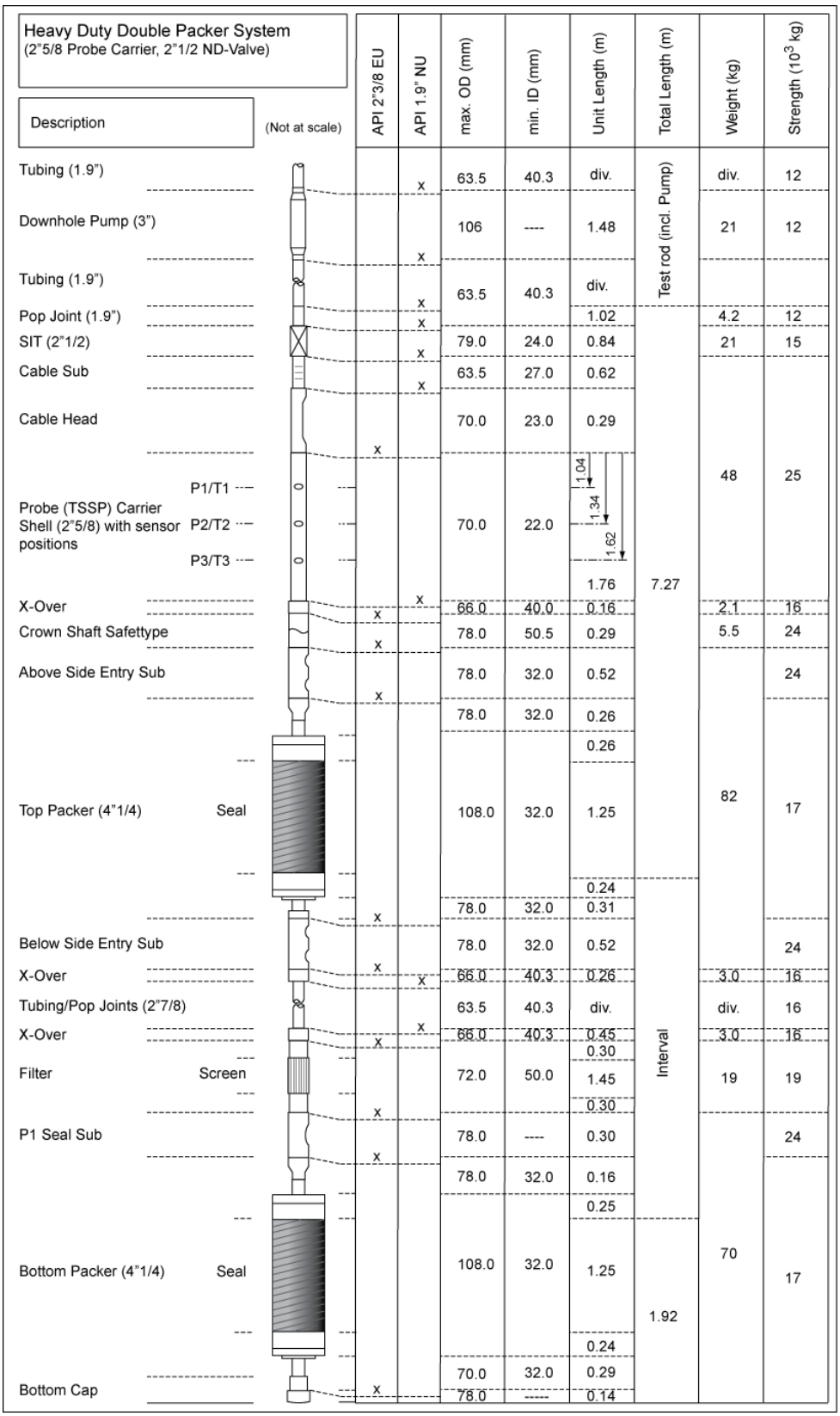

Fig. 4.1: General configuration and specifications of the Heavy Duty Double Packer System (HDDP)

4.1.2. Test Tubing

API Spec. 5 CT 1.9 - inch tubing was used as test rods. The detailed specifications of the test tubing are summarized in Tab. 4.2:

Tab. 4.2: Test tubing specifications

Size and type:	1.9” NU API, Grade N80
Inner diameter:	40.9 mm
Outer diameter:	48.3 mm
Coupling outer diameter:	56.1 mm
Thread:	API 1.9” NU
Weight per meter	4.1 kg
Volume per meter:	1.29 dm^3
Individual tubing length	6.5 m / 6.0 m
Lengths of pup joints	1.1 m, 1.9 m, 3.5 m

4.1.3. Slim Tubing

For slug or pulse tests in low permeable formations, a slim tubing was installed in the test tube. The slim tubing reduces the diameter of the test tube and therefore the wellbore storage is decreased. By reducing the wellbore storage the test data represent more quickly formation behaviour (out of wellbore storage period).

After lowering the water level in the test tube to the specified depth, the slim tubing was installed below the water level and the slim tubing packer pressurized. A 10 bar pressure sensor located above the packer measured the pressure of the water level in the slim tubing. The technical specifications of the slim tubing are summarized in Tab. 4.3.

4.1.4. Downhole Quadruple Flat-Cable

The downhole cable consists of three hydraulic steal pipes of ¼ inch and one electric conductor coated in a thermoplastic protective cover. The cable is also referred to as Quadruple Flat-Cable or Quadruple Flat-Pack.

Two steal pipes were used for packer inflation and one for the control of the shut-in valve (Tab. 4.1). The Quadruple Flat Cable was fixed at the test rods with cross coupling cable protectors for 1.9-inch non-upset tubing.

Tab. 4.3: Specifications of the slim tubing

High pressure tube type	Tecalto 520N-6 DN10, Aramid fiber reinforced Polyamide / Polyurethane tube
Inner diameter:	9.5 mm (3/8 inch)
Outer diameter:	16.5 mm
Length:	100 m
Packer type:	Petrometalic Bimbar 1, DN 30 mm
Packer pressure line:	Polyamide 6/3 mm
Pressure transducer type	Keller PA36XW/10 bar/80748.1
Linearity error:	± 0.005 %FS @ 25°C
Accuracy:	0.004 %FS @ 0… 50°C

4.1.5. Zero-displacement Shut-in Tool (SIT)

The downhole shut-in tool (SIT) was developed and manufactured by Solexperts. The SIT is a zero-displacement valve that is hydraulically operated using equipment located on the surface. The valve controls the fluid connection between the interior of the test rods and the test interval.

4.1.6. Triple Sub Surface Probe (TSSP)

Three Paroscientific Digiquartz 0-3000 psia transducers (see Tab. 4.4) were used to monitor fluid pressures in the interval below the bottom straddle packer (P1) within the testing interval (P2), and in the annulus between the tubing and borehole wall above the upper packer (P3).

These three transducers are mounted in the triple sub-surface probe (TSSP) carrier above the packers (Fig. 4.1). The depths to the transducer positions for P1, P2, and P3 for each test interval can be taken from the installation records in the QLRs (Appendices A to J).

Each quartz crystal pressure transducer has an associated temperature sensor for full thermal compensation of the pressure signal. The temperature sensor is mounted inside the pressure transducer housing. Because the temperature measurements are taken at the positions of the pressure transducers, they may not represent the actual/current temperature of the test interval fluid.

The calibrations for the pressure transducers in the TSSP, given in Tab. 4.4, are documented in Appendix K.

Tab. 4.4: Specifications of High Pressure Transducers mounted in Solexperts Triple Sub Surface Probe (TSSP)

Pressure Transducer Type:	Paroscientific Digiquartz Series 4000, Model 43K
Serial Numbers:	P1: 43224, P2: 50370, P3: 43231
Pressure Range (Full Scale):	0 - 3000 psia (0 - 207 bar)
Accuracy [1)]:	0.01 % (2.1 kPa)
Resolution:	0.01 ppm
Overpressure:	1.2 x Full Scale (FS)
Temperature Range (FS)[2)]:	0 – 125 °C
Accuracy (Temperature):	0.0008 % FS/ °C

[1)] Typical accuracy under difficult environmental conditions is according manufacturer 0.02%

[2)] Quartz Crystal Temperature Sensor integrated in transducer housing for full thermal compensation of pressure measurements

4.1.7. Additional pressure transducer in tubing string (P4)

A single transducer (P4), type Keller PAA26, 6 bar, was fixed at various depths to monitor the fluid level within the tubing string (Tab. 4.5).

Tab. 4.5: Specifications of the transducer mounted in the test rods (P4)

Pressure transducer:	Keller PA26 W/6 bar
Linearity error:	0.2 % FS
Cable length:	200 m (PVC cable)

It was mainly used during the initiation of the Pulse withdrawal (PW) tests to determine the volume change of the fluid in the test rods used in the calculation of the total compressibility of the system and the formation, respectively. During Pulse injection (PI) tests, the water level change in the 1.9" tubing (prior/after pulse) was measured without P4 sensor but using a dip meter.

4.1.8. Optional Pump Housing with 3-inch Pump

For constant rate or constant head withdrawal tests (pump tests) a submersible 3 inch pump of type SQE 1-110 from Grundfos was used. The pump was mounted in a tubing extension in the test rods at a depth of around 100 m (Fig. 4.1). A control unit allowed the infinite adjustment of the flow.

4.1.9. Downhole Sampler

Downhole sampling was conducted with an autonomous sampler which was attached to the wire rope of drilling machine and lowered in the 1.9" test tubing. Water samples could be taken directly above the shut-in tool using the adjustable non-return valve of the sampler. The volume of the sampler is about 1.3 litres.

4.1.10. Double Valve Pump

With help of the Double Valve Pump, water can be pumped out of the test tubing. It is often used to take water samples but also for water production for flow tests. The Double Valve Pump is installed into the 1.9” tubing. The provided Double Valve Pump has a maximum installation depth of 100 m.

A pump control unit controls the double valve mechanism over a pressure line and a production line. Two non-return valves prevent discharge from the pressure line to the interval during the pumping cycle and backflow from the production line to the interval and the pressure line during the production cycle.

During the pumping cycle, nitrogen is injected through the pressure line in order to move the water from the pressure line into the production line. In the following production cycle the nitrogen over-pressure is discharged before the water in the pressure line reaches the valve. Water from the test interval will flow into the pressure line.

4.2. Surface Equipment

The surface equipment consists of measuring instruments (flow, pressure, and chemistry), controlling instruments (e.g. SIT control, packers) and the data acquisition system. The instruments were installed in a mobile measuring container.

4.2.1. Flowboard

For the control and measuring of pump- and injection rates a flowboard with three flow meters of type Yokogawa AXF was available. The flow meters cover a flow range between 0.03 up to 1’178 litres per minute (Tab. 4.6). An additional mobile flowmeter was stored on site as a back-up.

Tab. 4.6: Specification of flow meters

Flow meters					
	Measuring range			Accuracy	
	Lower limit		Upper limit	3 - 100 % of FS	1 - 3 % of FS
	[l / min]	[% of FS]	[l / min]	[%]	[%]
AXF DN2	0.030	1	2.95	0.35	0.5
AXF DN5	0.118	1	11.80	0.35	0.5
AXF DN50	11.78	1	1'178.10	0.35	0.5
Additional mobile flow meter					
	[kg/h]		[kg/h]	[% of FS, effective range]	
Coriolis Mass Flow Controller	0.5		25	0.2	

4.2.2. Packer Pressure Control Unit

Two transducers, type Keller PA-23/25, 600 bar, mounted at the surface inflation control panel, were used to monitor the packer inflation pressures. To keep constant packer pressures, the packer were connected over the whole test time on a pressure vessel.

4.2.3. Additional recorded measurements at surface

A single pressure transducer, type Keller PAA-23, 0.85 – 1.15 bar absolute was mounted in the monitoring trailer and used to monitor barometric pressures.

Temperature sensors were located at ground surface to measure the surface temperature and temperature in the mobile monitoring container.

During pump tests, the physico-chemical parameters (e.g. pH, electrical conductivity, Eh and oxygen concentration) and the temperature of the extracted fluid were recorded.

4.3. Data Acquisition System (GeoMonitor II)

Data acquisition was performed through the SOLEXPERTS GeoMonitor II (GMII) software. The downhole pressure and temperature measurements were read in real time through the Quadruple Flatpack cable assembly and a frequency counter. The surface measurements were read with a Solexperts interface with the same scan rate.

The base scan rate for data collection was set at 5 seconds. At the initiation of pulse and slug sequences, the scan rate was increased to 1 second and then decreased to 2 second and then back to 5 seconds at times based on the rate of the observed pressure recovery.

The measurements were written to a data file on the PC hard drive in real-time. From the PC hard drive the data were transferred to another network PC every 10 seconds for “online” analysis and data back-up. An uninterruptible power supply was utilized to protect the system from short power interruptions.

5. General Testing Strategy and Testing Methods

5.1. General

Hydraulic tests conducted in low permeability formation can be affected by borehole pressure history, equipment compliance (i.e. normally mainly packer compliance), fluid temperature changes, presence of gas, or de-gassing effects. The hydraulic tests were conducted in a way to minimize any perturbing effects.

Testing goals and requirements were communicated by Nagra. The scheduled interval positions and packer seats were checked against the geophysical logs (BLM), in particular against the caliper log.

5.2. System Installation

Prior to installation of the double packer test tool, an installation plan was prepared specifying packer and tool positions, length of test tubing and tubing stick-up at surface. The installation rods were arranged on the stands (support frame), the length of each rod was measured and each rod was labelled using consecutive numbers. An installation record and a tally list (list of test rods used) are supplied for each test interval (see QLRs, Appendices A to J).

The pressure signals of the Triple Sub Surface Probe (TSSP) were checked at the surface (at atmospheric pressure) and during lowering of the system in the borehole at several depth and pressure conditions. The readings of the pressure probe were checked against manual measurements of the borehole water table. The shut-in tool was at open position during the entire system installation.

All threads of the testing tool and the test tubing were lubricated using the Nagra-approved grease "Bio-Schmierfett L2" (carbon free; provided by the drilling contractor) in order to limit the number of substances in the borehole that could compromise further production of undisturbed formation water samples for the analysis of isotopes in the groundwater, especially carbon 14.

Once the system reached the scheduled depth position, the two packers were inflated individually using water with 30 % of antifreeze of type “Panolin Propylene-Glycol Basic”. The packer pressures were controlled at surface using pressure vessel, pressure control (manometers mounted at vessel and cable winch) and two pressure transducers mounted on cable winch measuring the inflation pressure.

5.3. Open hole water table

Before start of first double-packer test in the Oftringen borehole, Oftr-i1, the open hole water table was at 20.3 m bgl because recovery from the preceding pump test (fluid-logging, see Section 3) was not complete. After test Oftr-i1, the open-hole water level was kept near surface. Decrease of water table due to volume displacement when moving the packer-straddle to a higher position was compensated by adding fresh water to the annulus. The purpose of this approach was twofold: (1) keep the borehole pressure history simple, and (2) anticipate that hydraulic formation heads would be close to surface level, the effect of borehole pressure history is minimized.

5.4. Typical Test Sequence

Several test methods can be combined in a test sequence. The reliability of estimated formation parameters is increased by carrying out several test procedures (methods) for the same test interval. A typical combined test in a low to medium permeable test section was conducted as follows:

1. Packer inflation (INF)
2. Compliance period (COM)
3. Pressure shut-in recovery (PSR) to allow the test zone pressure to recover toward the formation pressure
4. Pulse withdrawal test (PW) in order to obtain a rough transmissivity estimate.
5. Slug withdrawal test (SW), representing the main flowing phase
6. Shut-in phase (SWS)
7. Pulse injection test (PI)
8. Packer deflation (DEF)

All test sequences started with a packer inflation (INF) and compliance period (COM), followed by a pressure recovery phase (PSR). Then the principal tests were conducted such as a pulse injection (PI) or pulse withdrawal (PW) test, slug withdrawal test (SW) and a final short duration PI or PW test. The final PI/PW enables to check if the system compressibility parameter remained constant during the test sequence.

Pulse and slug tests with subsequent shut-in tests were the preferred test methods in the low permeable test intervals of the Oftringen borehole. Only one constant head injection test was carried out in the slightly more permeable test interval Oftr-i1.

5.5. Compliance Period (COM)

The shut-in tool is open. In case of tight formation, the water level in the test tubing is approximately equal to the borehole water level. Test interval volume changes caused by equipment compliance and temperature effects are compensated by water level change in the test tubing, and do not exert pressure pulses on the formation. Equipment compliance is mainly due to small shape changes of the packer sleeve which are likely to occur subsequent to packer inflation.

5.6. Initial Static Pressure Recovery (PSR)

The shut-in tool is closed and pressure is monitored to establish a pressure trend that can be extrapolated for the subsequent test period. Ideally, the pressure stabilizes at the end of the PSR phase, indicating that the effects of the borehole pressure history are dissipated.

5.7. Pulse Test (PI, PW)

At the beginning of a Pulse Test, the test section is exposed to an instantaneous overpressure (PI, Pulse Injection Test) or an instantaneous underpressure (PW, Pulse Withdrawal Test) with respect to the test interval pressure. The pressure difference is produced by filling the testing rods with water or by emptying the testing rods. When opening the shut-in valve, the pressure

difference is transmitted to the test zone instantaneously. The shut-in valve is closed immediately after imposing the pressure pulse to the test section. Ideally, there is no water flow between the test section and the formation. During pulse tests in low permeable formation, the propagation of the imposed pressure perturbation into the formation is small, often less than 1 m, depending on permeability.

In general, in comparison with slug, constant head and rate tests the pulse test yields less representative results for the formations parameters due to the normally short duration of the test. However, the pulse test is useful to obtain a rough conductivity estimate within a short time period and to assist in the planning of further tests at the beginning of a test sequence. Pulse tests are also used to determine the compressibility of the test zone (c_{tz}).

5.8. Slug Test (SI, SW)

At the beginning of a Slug Test, the test section is exposed to an instantaneous overpressure (SI, Slug Injection Test) or an instantaneous underpressure (SW, Slug Withdrawal Test). The pressure difference is produced by filling the testing rods with water or by emptying the testing rods. When opening the shut-in valve, the pressure difference is transmitted to the test zone instantaneously. During the test period, the shut-in valve remains open and the water level in the test tubing tends to recover to the static formation pressure corresponding to the fluid level in the tubing. The falling off or the rise of the water level in the tubing is recorded continuously. The duration of the pressure recovery during a slug test depends on the formation transmissivity and the diameter of the test tubing, which defines the storage of the test system during the slug. A slim tubing with reduced diameter compared to the test tubing can be installed to accelerate the slug test response.

5.9. Constant Head Test (HI, HW)

A constant head test can be performed either as an injection test (HI) or as a withdrawal test (HW), depending on the actual formation water pressure. In practice, maintaining a stable injection pressure is much easier to achieve than a stable drawdown. Therefore, constant head tests are mostly conducted as injection tests where water is injected into the formation under constant pressure. The change in the flow rate is recorded as a function of time for the analyzes of formation properties. During a constant head test, the wellbore storage effect is overcome immediately after the test begins (no head variation occurs afterwards), and analyzable test data is usually acquired a few minutes after the test starts. In the Oftringen Borehole, a single constant head injection test was carried out in test interval Oftr-i1 which has slightly higher permeability compared to most of the other test intervals.

5.10. Constant Rate Test (RI, RW)

During a constant rate test, the injection rate (**RI** test) or the pumping rate (**RW** test) is kept constant during the entire injection/pumping phase, while the pressure increase/decrease is recorded. In low permeable rock, constant rate tests are time consuming because the transient flow phase is delayed by wellbore storage effects. Constant rate withdrawal tests can be combined with formation water sampling (Test intervals Oftr-i6 and Oftr-i10). Constant rate injection test are rarely conducted in vertical boreholes using double-packer configuration. If the water table is below surface, the test tubing and injection lines require to be fully saturated prior to start of a RI test. As soon as the shut-in valve is opened to start RI, the water column in the test rod is accelerated by gravity and flow control is discontinued.

5.11. Injection vs. Withdrawal Tests

Extraction tests were generally preferred against injection tests. Theoretically, the analysis of hydraulic test should provide the same results, if it is conducted as an injection or withdrawal test provided that the borehole conditions and fluid properties are stable.

However, under certain circumstances, withdrawal and injection can produce different results. Decrease of fluid pressure during a withdrawal test can initiate degassing of dissolved gas, not only within the test interval between packers but also in the formation resulting in two-phase flow conditions.

Withdrawal tests help in removing, recognizing and determining potential borehole skin. In contrary, injection tests tend to increase skin effects in case of muddy borehole water.

5.12. Recovery Tests (RIS, RWS, SWS, SIS, HWS, HIS)

A recovery test period is initiated by closure of the shut-in tool, either after a flow test (e.g. constant head, HW) or a slug test (SW). After shut-in, the interval pressure recovers towards its static level if the test duration is long enough.

Similar to the above mentioned test methods, the recovery tests can be used to estimate the hydraulic formation properties, to evaluate the flow model and to provide information on the inner boundary parameters such as borehole skin and wellbore storage.

5.13. Groundwater Sampling

Groundwater sampling is ideally combined with a constant rate (pumping) test. In the Oftringen borehole, groundwater samples were taken from a relatively permeable, karstic limestone section of the Geissberg Member. Two attempts to take samples were undertaken, during tests Oftr-i6 and Oftr-i10 using identical interval positions, (408.0 - 417.59 m). Formation water was produced either by pumping (using a three-inch submersible pump installed in a pump housing roughly 100 m below surface), by air-lifting techniques or by series of consecutive slug withdrawal tests. In order to get the most representative formation water, the system and the test string were moved out with the Shut-in tool closed after completing water production. The water sample was finally pumped out from the tubing as soon as the Double Valve Pump could be installed above the Shut-in tool.

Ground water sampling in the Oftringen borehole was affected by degassing effects, which prevented to obtain representative water samples. The decrease in fluid-pressure during drawdown causes degassing of dissolved gas from the water in the test interval. Gas entering the pump housing causes the pump to stop. The accumulated gas trapped in the test zone was released by temporarily deflating the upper packer of the test tool (Oftr-i6). The constant rate drawdown tests were run at low production flow in order to limit drawdown and associated degassing effects.

6. Analysis Methods

6.1. Field test documentation and preliminary analysis

During the field analysis of the hydraulic tests the software Hugo TM (Solexperts) was used. Hugo is designed for online well test analysis, derivative analysis and test documentation. Hugo TM supports online analysis of hydraulic tests and interfaces directly with Solexperts data acquisition software GeoMonitor II. The test data can be automatically imported in the Hugo environment through the local network at short time intervals set by the user (e.g. every 5 seconds). Hugo TM supports type-curve-matching and straight-line analysis methods (see Chapter 6.3.1). Estimation of EPM (equivalent porous media) conductivity can be assessed by combining derivative diagnostics and straight-line analysis.

Field documents such as daily log report, equipment installation records and preliminary analyses (using Hugo) were prepared during field work. Numerical test interpretation was not included during field work.

6.2. General Interpretation Methodology

The interpretation levels were defined for each test interval by the Nagra project manager. Three levels of test interpretation are distinguished:

- Quick-look analysis (Quick-Look Report level)
- Standard analysis (Interval Report level)
- Detailed analysis (Interval Report level)

Test specific interpretation levels are shown in Tab. 6.1.

Tab. 6.1: Test interval specific interpretation levels

Interval	Depth [m bgl]	Analysis Level	Comments / Main goals
Oftr-i1	650.0 - 700.04	Standard	Limit uncertainty range of static head
Oftr-i2	590.0 - 640.04	Detailed	Limit uncertainty range of static head
Oftr-i3	550.0 - 600.04	Detailed	Compare with i9 (head)
Oftr-i4	500.0 - 550.04	Standard	Standard Plus
Oftr-i5	450.0 - 500.04	Standard	Standard Minus
Oftr-i6	408.5 - 417.59	QLR only	No additional analysis
Oftr-i7	632.5 - 641.59	Standard	Standard Minus / Focus on static head
Oftr-i8	621.5 - 630.59	Standard	Standard Minus / Focus on static head
Oftr-i9	583.0 - 592.09	Standard	Compare with i3 (head)
Oftr-i10	408.5 - 417.59	QLR only	No additional analysis

Detailed borehole history records (Section 3) were included already for the test numerical interpretation of the Quick Look reports. These analyses were refined for the standard and detailed interpretation.

The general interpretation methodology used is shown in the flowcharts of Fig. 6.1 and Fig. 6.2. Test interpretation begins with flow model identification for all interpretation levels.

QLR analysis

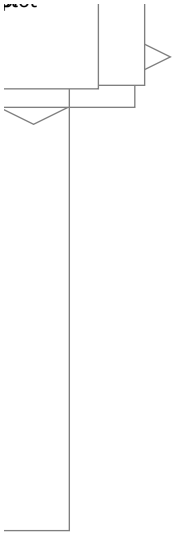

Standard analysis

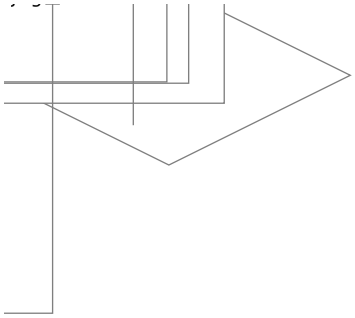

Fig. 6.1: General analysis strategies for QLR analysis (left) and standard analysis (right).

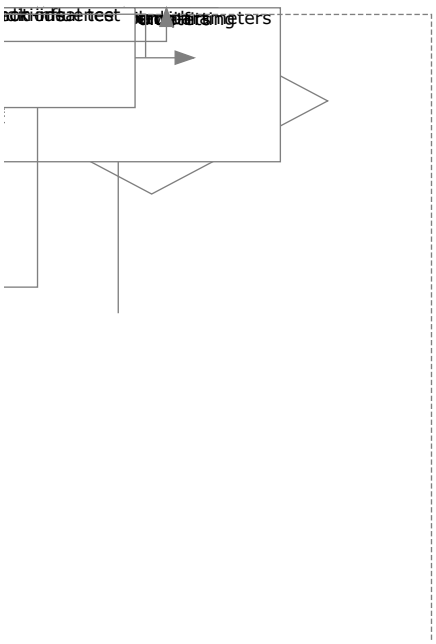

Fig. 6.2: General analysis strategy for detailed analysis.

6.3. Quick Look Report Analysis

6.3.1. Analytical analysis

A summary of the applied test analysis methods is presented in Tab. 6.2. References are given in Chapter 20. The Cooper-Bredehoeft-Papadopulos type-curves (abbreviated: CBP) are used to analyze both slug and pulse tests (Cooper et. al, 1967, Bredehoeft & Papadopulos, 1980). Constant head injection tests are analyzed according to Jacob & Lohman (1952) and Doe & Geier (1990), recovery tests after Agarwal (1980). An overview of analytical analysis methods is provided in Adams & Wyss (1994) and Nagra (2001).

Tab. 6.2: Summary of analytical analysis methods.

Test Type	**Analysis method**	**Abbreviation**	**Reference**
Pulse test	Type-curve matching	CBP	Bredehoeft & Papadopulos (1980)
Slug test	Type-curve matching	CBP	Cooper, Bredehoeft & Papadopulos (1967)
Constant head test	Straight-line analysis	SLA	Jacob & Lohman (1952)
	Spherical flow analysis	SLA-3D	Doe & Geier (1990)
Steady state conditions during constant head or constant flow test	Equation using steady-state ΔP, flow and R_i (estimated radius of investigation) as input parameters	SSA	Hvorslev (1951) Zeigler (1976)
Pressure recovery after constant head/rate tests	Diagnostics: log-log plot showing ΔP and derivative versus "equivalent time" (Agarwal) Straight-line analysis on transient pressure data	RSLA	Agarwal (1980) Bourdet et al. (1989) Agarwal (1980)

6.3.2. Numerical analysis

For the Quick Look Reports, numerical analyses were performed using the software nSights. The formation parameters were estimated by inverse parameter estimation to match the Cartesian pressure of the entire test sequence. The effect of borehole history pressure was included in the simulations. The parameters obtained from the Cartesian fit were used to produce fits to the individual test sequences (e.g. log-log diagnostic plot for SWS sequence) in order to verify the quality of the conceptional model used.

6.4. Standard Analysis

The standard analysis represents a complete reassessment of the results of the Quick-Look Report (QLR).

This includes the analysis of the flow geometry, the verification of consistency of test results, the formation parameters and confidence intervals, and additional simulations of the main test events if required.

6.4.1. Diagnostics (Flow Model Identification)

The diagnostic analysis follows the standard approaches in the literature (Bourdet, 1989; Horner, 1951; Horne, 1994; Ostrowski & Kloska, 1989; Peres et al., 1989; Ramey et al., 1975, Chakrabarty & Enachescu, 1997).

The flow model and parameter estimates from the diagnostic analysis are used as input in the forward simulation with nSights. The advantage of including nSights (see Section 6.6) forward simulations rather than just stopping with the diagnostic analysis of individual events is the simulation of multiple-consecutive test events and accounting for non-ideal conditions, such as pre-test borehole pressure transients, thermally-induced borehole pressure responses, time-varying pumping of flow rates, etc. For example, borehole pressure history effects are not accounted for when using simple straight-line methods or type-curve matching techniques.

The flow model and parameter estimates are also used as a starting point for inverse parameter estimation using non-linear regression techniques. The result of the inverse simulation gives best-fit parameters and statistical information; the latter will be used to check the validity of the flow model using model assumption diagnostics, i.e., residual analysis.

6.4.2. Inverse parameter estimation

The best-fit parameters for a particular flow model are obtained from the test data with inverse parameter estimation techniques. The inverse simulations involve fitting the measured data, primarily pressure data but can also include flow rate data depending on the type of test, and optimizing the hydraulic parameters that produce the best fit of the measured data. The conceptual flow model is regarded as adequate only when the objective function residuals are minimized and the residuals can be defined as normally distributed (Residual analysis).

6.4.3. Residual analysis

The model errors are compared to the normal curve to determine their distribution. If the errors are normally distributed, the inferred flow model is considered statistically verified. If the residual errors are not normally distributed, then the flow model has to be reevaluated in a second phase of analysis, which may require consideration of potential non-hydraulic phenomena that may be relevant for testing in argillites.

6.5. Detailed Analysis

The detailed analysis builds on the standard analysis and involves a detailed assessment of the test response in an attempt to identify possible non-hydraulic phenomena, particularly in argillites, which have to be considered in the analysis.

6.5.1. Multi-component objective function

The inverse simulation for the entire sequence is repeated. This time, the analyst can define a multi-component objective function. For example, the objective function may be comprised of several different data types (pressure, pressure derivatives, and flow rates, to list a few); that is, the inverse simulation can be fitted to either the Cartesian, log-log, derivative, or most any other diagnostic plot. This feature helps to constrain the inverse problem and increase the uniqueness of the solution.

The validity of the flow model is checked using the residual analysis. If the distribution of the errors is not normal, then the flow model is re-evaluated and another inverse procedure is executed. This step is repeated until an appropriate flow model can be obtained. Once the flow model is validated, the resulting parameter set is termed the "base case" set of parameters. In addition to the best-fit parameters, the inverse solution provides the joint confidence regions of the base case parameters to account for uncertainty arising from data noise, parameter sensitivity, and correlation among fitting parameters.

6.5.2. Perturbation analysis

The uniqueness of the base case parameters is evaluated by means of perturbation analysis. New starting values are assigned to each of the model parameters by random perturbations and an inverse procedure executed. This process is repeated a number of times to determine if the non-linear regression algorithm is converging to a unique global minimum or, if local minima are obscuring the results. The results from the global minima are then used for the analysis of the formation parameters.

6.5.3. Final step / Role of non-fitting parameters

In the final step, the potential uncertainties of the model parameters which are not-fitting parameters (i.e., fixed parameters such as borehole radius and test-zone length) are evaluated. Typically it is assumed that the values of the non-fitting parameters are known with 100% accuracy, however, this is not a conservative assumption. Pressure history, for example, is usually estimated based on driller's logs which can indicate significant uncertainty. The potential uncertainty of the parameter is represented by a statistical distribution which is sampled using either Monte Carlo or Latin Hypercube methods. For each sampled set of non-fitting parameters, an inverse procedure is executed. The optimization results provide information which can be used to quantify the uncertainty of the non-fitting parameters on the uncertainty of the fitting parameters.

6.5.4. Non-hydraulic effects

For the tests in the clayey rock sections, special attention is given to identifying non-hydraulic effects, which can be inferred from the test response or identified based on inconsistent results of the analysis. If non-hydraulic effects are indicated, the impact will be assessed and, if

possible, incorporated in the nSights simulation. For example, plastic behaviour of the clay due to swelling or geomechanical effects can be incorporated in nSights analysis through time-varying well-bore volume or test-zone compressibility.

6.6. Numerical Analysis using nSights

6.6.1. General description

The code used in the analytical and numerical analysis is nSights (n-dimensional Statistical Inverse Graphical Hydraulic Test Simulator). nSights is a numerical well-test analysis code developed by INTERA for Sandia National Laboratories (Intera Engineering Ltd., 2005) to analyze data from well tests that are performed in complex hydrogeologic systems under non-ideal conditions, i.e., data that are not amenable to analysis using conventional analytic methods. nSights is based on a statistical inverse graphical hydraulic analysis technique. The well-test analysis process allows estimating the hydraulic parameters of interest such as hydraulic conductivity (K) and specific storage (S_S) from measured pressure and flow-rate data. The code has a full suite of statistical routines that allow the analyst to quantify the uncertainty in the estimates of the fitting parameters of interest (K, S_S, n, etc.).

nSights has wellbore (inner) boundary conditions that can be used to simulate pulse-injection/withdrawal tests, specified borehole-pressure conditions, specified formation flow rates, and slug-injection/withdrawal tests. The cumulative effects of consecutive tests are incorporated in the simulations. A description of the nSights governing equations can be found in Pickens et al., (1987) which discusses the well-test analysis code GTFM (Graph Theoretic Field Model), the DOS-based precursor code to nSights. nSights has been fully verified following Sandia National Laboratories Nuclear Waste Management Program Procedure NP 19 1, “Software Requirements,” Rev. 4 to meet NQA 2 requirements (ASME, 1990).

Well-test interpretation is a process during which a mathematical model is matched to an observed formation response. Pressure-derivative analysis has been demonstrated as a powerful method for determining the appropriate conceptual (mathematical) flow model. nSights permits the analyst to calculate pressure derivatives not only for single-rate tests but also includes time-superposition functions to properly analyze multi-rate tests. Pressure-derivative analysis allows the analyst to provide the client with real-time information which can be used to optimize test duration and provide parameter estimations in the field or it can be used to provide analysis of the tests after they are completed.

The conceptual flow models available in nSights comprise the following:

1. Wellbore Responses: line source, open-hole and isolated wellbore storage, and well-bore skin.
2. System Responses: homogenous, unconfined, leakage, composite, dual porosity, fracture, fractional dimensions.
3. Outer Boundary conditions: infinite acting, circular, no-flow, and constant pressure boundaries, Carter – Tracey boundaries.
4. Fluid Phases: single-phase fluid, single-phase gas.

The available flow models enable simulations of a wide variety of geologic environments typically encountered during testing.

With head/pressure data, flow rate data, and knowledge of the testing geometry, the analyst can build a simulation which includes pump, recovery, slug, pulse, constant-head, and history events. nSights was designed to simulate test campaigns consisting of multiple consecutive test events. Simulating consecutive events is accomplished by using the pressure value at each model node at the end of a test event as the initial condition for the subsequent test event. This feature enables the analyst to incorporate in the simulation complex borehole pressure histories which existed in the borehole resulting in pressure transients in the formation prior to testing.

6.6.2. Diagnostic plots

nSights provides a broad capability for developing and displaying diagnostic plots to assist in interpretation of the testing sequence. The graphical interface in nSights allows the analyst to set up a simulation such that all of the events may be singled out, displayed and simulated together in Cartesian coordinates and separate events may be singled out, displayed, and simulated with their pressure derivative in log-log or semi-log space. Built-in data transformations to aid in the construction of log-log and semi-log plots include multiple-derivative algorithms and time superposition functions. The ability to sequentially simulate test events with different boundary conditions and to simultaneously view them on screen in Cartesian, semi-log, and log-log space is a feature unique to nSights.

- One of the main advantages of nSights over codes which employ analytical solutions is the ability to account for non-ideal test conditions including:
- Pre-existing borehole pressure transients
- Thermally induced borehole pressure responses
- Packer compliance and test-tool movement
- Borehole closure, i.e., non-constant test-zone volume
- Variable wellbore storage (test-zone compressibility as a function of time or pressure)
- Variable pumping rates
- Pressure dependent parameters (fluid density & viscosity, and test zone compressibility)

6.6.3. Non-ideal conditions

By accounting for non-ideal conditions, tests that otherwise would not be interpretable using conventional analytical techniques now can be analyzed. Interpretation of hydraulic tests where compliance effects are active requires that factors be quantified and accounted for in the analysis. nSights handles factors such as test-tool compliance, thermal effects, test-zone volume, and variable pumping rates by reading a file of compressibility, temperature, volume, or pump rate versus time or pressure and calculating the pressure response due to that factor. The combined net pressure response of the formation and non-ideal factors is then compared to the measured data. These features make it possible to estimate formation parameters for tests conducted under very complex and difficult conditions.

6.6.4. Inverse Parameter Estimation

nSights has fully inverse parameter estimation and error analysis capabilities. The solving routines include a choice of either Levenberg – Marquardt or the Simplex methods. Up to 20 parameters may be simultaneously optimized, although typically only three to four are optimized at a time. Parameters which can be optimized include:

- Formation and skin K & S_S
- Skin thickness
- Initial formation pressure
- Distance to boundary
- Fractional flow dimension
- Fractional flow dimension as a function of distance from the well
- K & S_S as a function of distance from the well, and multiple ring composite

One powerful feature of the optimization implementation in nSights is the ability to simultaneously optimize the calibration of data from several test types. For example, if a test sequence is composed of a slug test followed by a constant-head flow test and a final pressure recovery period, nSights can simultaneously optimize the pressure data from the slug and recovery tests and the flow rate data from the constant-head flow test. This powerful feature constrains the optimization process, providing a more unique and consistent parameter set for the full hydraulic test sequence.

6.6.5. Perturbation analysis

When the best-fit solution is found, a check for the global minimum is performed by randomly perturbing the fitting parameters and allowing the optimization to find a new solution. The potential variation of the best-fit parameters identifies possible local minima and the global minima as indicated by the smallest error.

6.6.6. Uncertainty of matched parameters

All parameters that are used in the analysis are identified and categorized as measured, calculated, assumed, or fitted. The fitted parameters (typically the hydraulic conductivity, specific storage and static formation pressure) are then subject of the subsequent test interpretation. In addition to the best-fit estimation of matched parameters, the statistical analyses associated with the inverse simulation provide important information on the uncertainty of the parameter estimates and degree of interdependence (covariance) with other fitted parameters.

In addition to the uncertainty of the fitted parameters, potential uncertainty of calculated or assumed parameters (i.e., non-fitting parameters) can be analyzed using the sampling analysis described above. It is also possible to define correlations between the sampled parameters. The results of the inverse simulations for the different sampled parameters will then provide fields of uncertainty ranges for the fitted parameters and typically increases the overall uncertainty range.

6.6.7. Superposition functions

nSights incorporates different superposition functions (Horner, Agarwal, Bourdet), which are particularly important for testing in low-permeability formation when the pressure recovery has not reached the static formation pressure. The Horner superposition allows the extrapolation of the pressure recovery to estimate the static formation pressures. The Agarwal and Bourdet superposition of a recovery sequence following variable-rate flow tests allows the identification of the stabilization of the derivative that corresponds to the infinite active radial flow (IARF) conditions. With the standard derivative analysis, this stabilization is not seen because of the transient pressure history prior to the recovery phase.

The main advantages of utilizing the superposition function are:

- Analysis of multi rate tests
- Early testing after drilling
- Early testing after previous test activities
- Simulation of entire test sequences
- Higher confidence level

6.6.8. Borehole history

In addition to superposition functions, borehole history effects associated drilling-related activities in the test interval before the test-tool installation will be incorporated in the analysis. For this, the information from the mud logger, the drillers logs, and other pretest observations will be incorporated as a pressure-history curve in the nSights analysis.

7. Hydraulic Parameters and Plausibility Ranges

7.1. Introduction

In this section the significance and the general use of the main hydraulic parameters are briefly discussed. During numerical test analyses, a hydraulic parameter can either be used as a fitting parameter or as a non-fitting parameter. A non-fitting parameter is an unvaried input parameter whose value is known with sufficient precision and which is supposed to stay constant during the entire test. The fitting parameter is varied during simulation within specified limits corresponding to the parameter-specific plausibility range. The plausibility range is estimated based experience from experiments in similar rock type or from other in-situ or rock laboratory measurements.

7.2. Parameters of Inner Boundary Conditions

7.2.1. Borehole Radius

The nominal boreholes radius is 0.073 m (expected radius based on size of used drill bit). Caliper logs were run before and after the hydrotesting campaign, on 18.10.07 and on 05.11.07, respectively. The 4-arm-caliper logs for the investigated borehole sections show a mostly smooth wellbore with a few peaks corresponding to radii up to 115 mm, indicating possible outbreaks, drilling irregularities or confined zones of weaker rock. Below 640 m, the caliper does not show any noticeable changes in borehole diameter. The second caliper log (of 05.11.08) shows more distinct deviations from the nominal borehole diameter, generally at locations where the first caliper log (of 18.10.07) indicated an irregular diameter.

The borehole radius (r_w) was used as a non-fitting parameter with a fixed value of 0.073 m in all presented test simulations. The effect of a potential deviation from the actual value was investigated during a sampling analysis for test interval Oftr-i4 (Section 11.6.2, Tab. 11.7). The exercise was based on a homogeneous flow model and showed that the r_w parameter did not correlate with the fitting parameters K, P_f and S_S.

The borehole radius parameter affects the calculation of the interval test zone volume (V_{tz}) which in turn is used to determine the test zone compressibility (Section 7.2.2). Despite the effect of the r_w parameter on the c_{tz} parameter, this relation is not relevant to the test simulation using nSights, as explained in Section 7.2.2.

7.2.2. Total Test Zone Compressibility

The total test zone compressibility (c_{tz} or c_{SC}) is defined as the wellbore storage at shut-in conditions (C_S) divided by the test zone volume ($V_{interval}$).

$$c_{tz} = C_S / V_{interval} \quad [Pa^{-1}]$$

where:

C_S = wellbore storage [m^3 / Pa^{-1}]

$V_{interval}$ = test zone volume [m^3]

As a simplification, the nominal interval volume was used. The nominal interval volume is the cylindrical volume of the hydraulically isolated borehole section without considering the volume of the test equipment in this zone. The test zone compressibility is also known as the so-called system compressibility.

For the test equipment used in the Oftringen borehole, and for interval lengths ranging from 5 to 50 meters the c_{tz} plausibility range can be indicated as 6E-10 Pa^{-1} to 3E-9 Pa^{-1} based on pulse test results of earlier similar projects using the same testing equipment. The c_{tz} parameter can be measured during a pulse injection (PI) or pulse withdrawal test (PW). If the measured c_{tz} is higher than expected, then the potential presence of a gas phase should be checked. An unexpected high c_{tz} value can also be due to a partially deflated packer.

A c_{tz}-value equal or smaller than the fluid compressibility at actual depth and temperature conditions should be considered as mismeasurement. Water compressibility values were calculated for each test zone using the PVT-tool of the software Saphir.

The c_{tz} -parameter was used as a fixed input (non-fitting) parameter for the majority of the cases where pulse tests provided reliable and consistent c_{tz}-estimates. If the c_{tz}-parameter was used as fitting parameter, the corresponding c_{tz}-parameter is shown in the result table.

If c_{tz} is estimated from a pulse test, $c_{tz} = C_{S\text{-}MEASURED} / (L * rw^2)$, the potential error due to an imprecise r_w value cancels out because the controlling parameter in nSights is $C_S = c_{tz}\ V_{interval} = c_{tz}\ L\ r_w^2$.

If c_{tz} is used as assumed parameter (c_{tz} is estimated based on comparable experiment cases), the effect on the calculated C_S is proportional to r_w^2. Given that C_S and c_{tz} are composite parameters and the r_w-dependent volume of compressible water between packers contributes only in part to the test zone compressibility (see above), the effect of an imprecise r_w parameter on a the actual deviation from true the C_S-value is less than expected. The role of c_{tz} as non-fitting parameter was investigated during a sampling analysis for the low-permeable test interval Oftr-i4. The exercise using a homogeneous flow model showed that the c_{tz} parameter did correlate significantly with the fitting parameters P_f , K and S_S (Section 11.6.2, Tab. 11.7).

As the C and c_{tz} are parameters describing the borehole or inner boundary conditions, their influence is decreasing with increasing elapse time during a test. The influence for the borehole parameters is smaller for more transmissive intervals because larger radii of investigation are reached within shorter test duration.

7.2.3. Wellbore Storage Coefficient

The wellbore storage coefficient C is one of the most sensitive parameters when testing in low transmissivity formations. It controls the duration of the wellbore storage dominated testing phases of constant rate and pressure recovery test events and, in the case of slug and pulse events, directly scales the derived transmissivity.

The wellbore storage coefficient is defined as the volume of fluid additionally stored or released by the interval while changing the pressure in the system by one unit (e.g. 1 Pa). The wellbore storage coefficient C can be expressed as:

$$C = \Delta V / \Delta P \qquad [m^3/Pa]$$

where:

ΔV = volume change $[m^3]$

ΔP = pressure change [Pa]

The above equation assumes no volume exchange with the formation and can be used for the calculation of the wellbore storage after applying a pressure pulse of known magnitude to the test interval. The wellbore storage coefficient C can also be expressed as the sum of a number of components:

$$C = C_1 + C_2 + C_3 + C_4 \qquad [m^3/Pa]$$

where:

C_1 = storage due to water level change in test tubing $[m^3/Pa]$
C_2 = storage due to fluid compressibility $[m^3/Pa]$
C_3 = storage due to elastic deformation of the borehole $[m^3/Pa]$
C_4 = storage due to elastic deformation of the test equipment $[m^3/Pa]$

At shut-in conditions (shut-in tool closed), C_1 equals to zero, C is denoted as C_S and depends mainly on the elastic behaviour of the packers and the compressibility of water. The wellbore storage parameter can be measured during pulse tests (see chapters 5.7 and 7.2.2).

In the petroleum industry, where C_3 and C_4 terms are commonly assumed to be insignificant, the simplest method of estimating the wellbore storage coefficient (at shut-in or artesian conditions) is to calculate it directly using the following equation:

$$C_S = V_i \, c_{fl} \quad [m^3/Pa]$$

where:

V_i = interval volume $[m^3]$

c_{fl} = fluid compressibility $[Pa^{-1}]$

There are various other methods of determining the wellbore storage e.g. by matching in the superposition analysis when using a wellbore storage and skin flow model (Enachescu et al., 1997). Depending on the method used, the calculated wellbore storage coefficients usually differ in a range of approximately one and a half orders of magnitude. Sources for this inconsistency could be inaccurate volume change measurements or limitations of the methods of calculation. It is also possible that the wellbore storage coefficient changes during a test. This phenomenon can often be observed and is probably caused by changing system behaviour at different pressure levels or by the presence of gas.

7.2.4. Borehole Skin

The skin effect describes the relation between formation permeability and the (altered) permeability near to the borehole wall (see Section 21.3). A positive skin can be caused by clogging of the rock pores with drill mud near the wellbore. In fractured medium, a decrease in fracture aperture towards the well results in a positive skin effect. A negative skin can be due to rock loosening and/or the appearance of fractures as a result of the rock stress redistribution around the borehole.

During drilling of the lower part of the Oftringen borehole (376 - 719 m), the drilling fluid contained relatively low quantities of additives. Nonetheless, it is likely that drilling through clayey limestone and marls added fine particles to the drilling fluid which could have resulted in clogging of rock pores. Skin effects could also have been (partly) removed during flushing of the borehole with fresh water or during the pumping for fluid-logging, prior to double-packer testing.

During test interpretation of single borehole tests, skin effect cannot be precisely quantified if the formation storage (S) is unknown. Conversely, the estimate of formation storage depends on the skin estimate. Some analysis methods such as Gringarten-Bourdet type-curve fitting (Gringarten et al., 1979) combine skin, formation storage and wellbore storage into a lump parameter ($C_D e^{2s}$) where storage S_S is included in the dimensionless storage parameter C_D (see Section 21.3) and the skin factor (s) appears in the exponent of e^{2s}.

For all Oftringen double-packer test analyses using nSights, the skin was simulated as a composite shell around the wellbore with specified hydraulic conductivity (K_S), specific storage (S_S) and radial thickness (t_s). The skin factor was calculated outside of nSights using the equation below (Earlougher, 1977; Horne, 1995):

$$s = \left(\frac{K_f}{K_s} - 1 \right) \ln \left(\frac{r_w + t_s}{r_w} \right)$$

where:

K_f = formation hydraulic conductivity [m/s]

K_s = specific hydraulic conductivity [m/s]

r_w = wellbore radius [m]

t_s = radial thickness of skin zone [m]

$r_w + t_s$ = altered zone radius r_s [m]

An estimate of the plausibility range for the skin parameter is difficult. As a conservative estimate, the potential variation of this parameter is assumed to be in the range of -4 to 50.

7.3. Formation Parameters

7.3.1. Transmissivity (T) and Hydraulic Conductivity (K)

The transmissivity describes the ability of an entire fluid conducting unit, such as an aquifer or aquitard, to transport water. It is a water based parameter. Hydraulic conductivity values K can be calculated from the derived transmissivity using the following relationship:

$$K = T / L \qquad [m/s]$$

where:

L = thickness of interval [m]

T = transmissivity [m^2/s]

For a packer test it is generally assumed that flow to the well is radial and L represents the distance between the packers. The estimated K-value corresponds to an average hydraulic conductivity. In heterogeneous medium the average K-value may be lower than the K-value of an individual higher transmissive feature (e.g. fracture) or higher than the actual K-value of the matrix or the undisturbed low porosity rock section. The estimated K-value depends on the physical properties of the fluid, given by

$$K = \frac{k \rho g}{\mu} \qquad [m/s]$$

where:

k = intrinsic permeability [m^2]

ρ = fluid density [kg/m^3]

μ = dynamic viscosity [Pa s]

g = acceleration of gravity [m/s^2]

The Saphir PVT correlation tool from Kappa Engineering was used to estimate water viscosity (μ_w) and water density (ρ_w) at interval depth conditions. Compressibility and density of the water at interval depth condition was calculated using the Dodson and Standing correlation. The water viscosity at interval depth conditions was calculated using the Van-Wingen & Frick correlation. A salinity of 10'000 ppm was assumed for all PVT calculations. Note that the water viscosity and water compressibility (Tab. 7.1) were not used as nSights input parameters but were estimated to provide intrinsic permeability values for K-values obtained using nSights.

The measured and estimated formation water properties for each test interval are summarised in the following Tab. 7.1. Note that these values are used during QLR analysis und subsequent analysis.

Tab. 7.1: Measured and estimated formation water properties of the test intervals

Test	Interval		P2 [1]	Pressure at interval midpoint [2]	Temperature T [3]	Density [4] ρ_w	Viscosity [4] μ_w
	Top [m bgl]	Bottom [m bgl]	[kPa]	[kPa]	[°C]	[kg/m^3]	[Pa s x 1E-4]
Oftr-i1	650.00	700.04	6426	6750	45.0	1001.2	6.739
Oftr-i2	590.00	640.04	5838	6150	42.0	1002.1	7.129
Oftr-i3	550.00	600.04	5447	5750	38.7	1003.3	7.594
Oftr-i4	500.00	550.05	4957	5250	35.7	1004.1	8.053
Oftr-i5	449.85	499.89	4466	4749	32.6	1005.0	8.567
Oftr-i6d	408.50	417.59	4059	4131	30.6	1005.4	8.922
Oftr-i7	632.50	641.59	6255	6371	45.0	1001.1	6.739
Oftr-i8c	621.50	630.59	6153	6261	44.1	1001.4	6.853
Oftr-i9	583.00	592.09	5774	5876	41.0	1002.4	7.266
Oftr-i10	408.50	417.59	4065	4131	30.9	1005.3	8.868

[1] P2 pressure prior to inflation of the packers (subartesian) plus theoretical pressure assuming a water table at surface level.

[2] The pressure at the interval midpoint was extrapolated based on the measured pressure P2 at the Triple Probe.

[3] Temperature (T) was measured at position of the triple probe.

[4] The ρ_w and μ_w parameters were calculated using the above mentioned PVT correlations.

7.3.2. Intrinsic Permeability (k)

The intrinsic permeability is a formation parameter which is independent from the physical fluid properties. The permeability is basically a function of size and shape of the openings through which the fluid moves (see e.g. Freeze & Cherry, 1979).

$$k = C_{sf}\ d^2 \quad [L^2],$$

where:

C_{sf} = dimensionless constant or shape factor [-]

d = mean pore diameter [L^2]

The larger the square of the mean pore diameter, the lower the flow resistance. The relationship between hydraulic conductivity and intrinsic permeability is given in Chapter 7.3.1.

7.3.3. Formation Storage

The storativity is the capacity of the formation to store a fluid while the storage coefficient is the capacity of a formation to store water. The term storativity is typically used in the petroleum literature, where different fluids have to be considered, while the storage coefficient is used in hydrogeology, where water is the only fluid of interest. The storage coefficient is a dimensionless coefficient defined as the volume of water that a formation unit will absorb or expel from storage per unit surface area per unit change in head. For a confined hydrogeologic unit, the formation storage coefficient is based on the elastic properties of the aquifer (or aquitard) and can be estimated using rock compressibility, formation porosity and water compressibility. The storage coefficient or storage (S) is expressed as:

$$S = \phi c_t L \rho_w g \qquad [-]$$

The storativity S' is expressed as:

$$S' = \phi c_t L \qquad [\text{m Pa}^{-1}]$$

where:
- S = storage coefficient [-]
- S' = storativity [m Pa^{-1}]
- $\rho_w g$ = specific weight of water [Pa m^{-1}]
- c_t = total compressibility [Pa^{-1}]
- ϕ = porosity [-]
- L = thickness of aquifer/aquitard or thickness of test interval [m]

The relation between S and S' is given by:

$$S = S' \rho_w g \qquad [-]$$

The total compressibility (c_t) is expressed as the sum of the compressibilities of the individual system components. For a two-phase system with gas and water, the total compressibility is given by:

$$c_t = c_f + S_w c_w + S_o c_o + S_g c_g \qquad [\text{Pa}^{-1}]$$

where the subscripts w and g refer to the water and gas phase, respectively, and the parameter S_x refers to the saturation of the individual phase. While the fluid compressibility can be derived from PVT correlation charts (as well as from laboratory measurements), the formation compressibility (c_f) is derived as rock compressibility (c_r) from geomechanical parameters (POISSON's ratio - ν - and YOUNG's Modulus – E), which are measured on core samples in the laboratory. The relation between rock compressibility and formation compressibility is:

$$c_r = c_f \phi \qquad [\text{Pa}^{-1}]$$

The rock compressibility is calculated as:

$$c_r = \frac{3(1-2\nu)}{E} \qquad [\mathrm{Pa^{-1}}]$$

To express the formation capacity to store fluid per unit of formation thickness, the parameters specific storativity ($S_s^{'}$) and specific storage (S_s) are used:

$$S_s^{'} = S'/L = \phi\, c_t \qquad [\mathrm{Pa^{-1}}]$$

$$S_s = S/L = \phi\, c_t\, \rho_w\, g \quad [\mathrm{m^{-1}}]$$

Based on the equations mentioned before the ratio between the storage coefficient (S) and storativity (S') for water is given by the fluid density ρ_w (1000 kg/m^3) times the gravitational acceleration g (9.81 m/s^2)

$$\frac{S}{S'} = \rho_w\, g \approx 10^4 \qquad [\mathrm{Pa\ m^{-1}}]$$

The storage parameter affects the transient response of a hydraulic test but does not interfere if a flow regime is at steady-state conditions. Storages values can theoretically be obtained from the analytical analysis of single-hole tests such as constant rate/head tests or slug/pulse tests. However, the storage results obtained from single-borehole tests are uncertain because of interference of borehole and skin effects. The storage parameter is constrained in the course of a numerical test interpretation but needs to be checked for plausibility. In case the plausibility criteria is not meet, test interpretation is continued using different assumptions, e.g. with respect to flow model.

The YOUNG's moduli can be converted into rock compressibility values using the above mentioned equation. The S_S values can be calculated based on rock compressibility data and the water compressibility using the following equation:

$$S_s = \phi\, \rho_w\, g\, c_t = \rho_w\, g\, (c_r + \phi\, c_w) \qquad [\mathrm{m^{-1}}]$$

Using a water compressibility of 4.4 E-10 Pa^{-1} (QLR Oftr-i5, Appendix E) and the below given ranges in rock porosity and rock compressibility (Tab. 7.2), gives specific storage values ranging from 6.2 E-7 m^{-1} to 1.2 E-6 m^{-1} for the marl (Tonmergel) and 6.4 E-7 m^{-1} to 6.9 E-7 m^{-1} for the argillaceous limestone.

A roughly estimated specific storage of S_s = 2.2 E-06 m^{-1} was used as preliminary information during preparation of the QLRs, Appendices A to J, based on assumed average formation compressibility of 7 E-09 Pa^{-1}, assumed rock porosity of 3 % and using the above mentioned relationship.

The preliminary estimate of S_s = 2.2 E-06 m^{-1} could represent an overestimation with regard to test intervals such as Oftr-i5 where the laboratory results suggest a factor 2 - 3 smaller S_s values (argillaceous marls ≈ two times smaller; argillaceous limestones ≈ three times smaller). Conversely, the rock samples cover only a relatively small volume of the formation, and the actual variation in rock properties could be significantly higher.

No rock samples with rock elasticity measurements are available for the hydrotest intervals Oftr-i1 to Oftr-i4 and Oftr-i6 to Oftr-i10. Therefore, a large plausibility range should be defined with respect to the values for the YOUNG's modulus.

In Nagra Technical Reports (2002a; 2002b), the estimated range of YOUNG's modulus is given as 0.1 to 40 GPa for the strata of the Lower Malm and as 2 - 30 GPa for Upper and Middle Dogger. These range estimated ranges were based on the results from the Benken borehole but were used to anticipate possible rock loosening effects with regard to potential underground construction works. Assuming similar rock properties for the same geologic units at Oftringen, and limiting the lower bound for plausible YOUNG's Modulus to 1 GPa (for relatively sound rock), the plausibility range of the specific storage is between 1.9 E-7 m^{-1} and 1.9 E-05 m^{-1} for the Lower Malm and between 2.4 E-7 m^{-1} and 1.0 E-05 m^{-1} for the Upper Dogger (Tab. 7.3.). These estimates are additionally based on POISSON's ratios between 0.18 and 0.4 and rock porosity values ranging from 1 to 15 volume percents.

Tab. 7.2: Results of laboratory rock tests (Albert & Bläsi, 2008) and calculated S_s values

Sample, Sample Name	Depth [m]	Confining Pressure [MPa]	Density [kg m^{-3}]	WC [vol%]	YOUNG Modulus [GPa]	POISSON Number [-]	c_r [Pa^{-1}]	S_s [m^{-1}]
Argillaceous Marls (Tonmergel)								
KM46-2_CP9_P	459.6	9	2610.4	5.7	20.25	0.37	3.9E-11	6.2E-07
KM46_2U-C2	459.39	0	2609.0	6.2	11.47	0.23	1.4E-10	1.7E-06
KM46-2_CP6	459.79	6	2600.0	6.1	11.72	0.32	9.2E-11	1.2E-06
Argillaceous Limestone (Kalkmergel)								
KM48-1_CP12	464.1	12	2671.3	4.1	29.53	0.24	5.3E-11	6.9E-07
KM48-1_CP9	464.1	9	2667.3	3.5	28.92	0.26	5.0E-11	6.4E-07
KM48-1_CP15	464.1	15	2666.8	4.6	25.75	0.3	4.7E-11	6.6E-07

Tab. 7.3: Plausibility ranges for the S_S parameter

Rock type		Depth range [m]	Intervals Oftr-xx	ϕ [-]	YOUNG Modulus [GPa]	POISSON Number [-]	c_r [Pa^{-1}]	S_s [m^{-1}]
Lower Malm: limestone - marl interbedded strata	min S_s	450	i2 to	1	40	0.4	1.5E-11	1.9E-07
	max S_s	to 650	i10	15	1	0.18	1.9E-08	1.9E-05
Upper Dogger limestone - marl interbedded strata, oolithic limestones	min S_s	650	i1	1	30	0.4	2.0E-11	2.4E-07
	max S_s	to 700		15	2	0.18	9.6E-10	1.0E-05

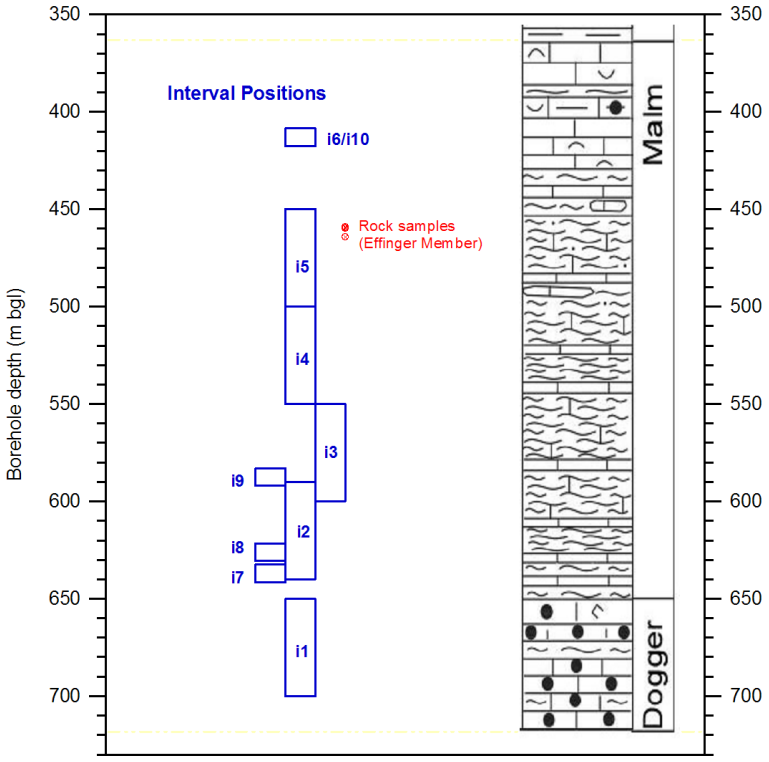

Fig. 7.1: Depth locations of rock samples for elasticity measurements shown with hydrotesting intervals and geologic units

7.3.4. Static Formation Pressure and Fresh-water Head

Characterizing the hydraulic head profile within the NOK-EWS borehole was one of the main objectives of the investigation. The static head estimate is based on the extrapolated or simulated static pressure and converted in fresh-water head assuming a vertical borehole.

The static hydraulic freshwater head is calculated using the following equation:

$$h_s = Z - z_2 + \left(\frac{P_S - P_{atm}}{(\rho_w \cdot g)} \right) \qquad \text{[m],}$$

where:
- hs = equivalent fresh water head [m asl]
- Z = reference point elevation [m asl]
- z2 = vertical distance between pressure transducer and reference level [m]
- Ps = static pressure at transducer depth [Pa]
- P_{atm} = atmospheric pressure [Pa]
- ρ_w = fresh-water density [1000 kg/m^3]
- g = acceleration of gravity [m/s^2]

The hydraulic heads in the Oftringen borehole were expected to be close to the land surface, i.e. slightly sub-artesian to slightly artesian. Although the location of the Oftringen NOK-EWS Borehole near to the southern foothills of the Jura would suggest the general possibility of distinct artesian heads, highly artesian conditions are unlikely in tight formations, as hydraulic potential is decreased when flow occurs through impermeable rock. As a working hypothesis, the static hydraulic heads are expected in a range from -50 to + 50 m below ground level (383 m asl to 483 m asl). Possible existence of fossil water pressures and coupled hydro-mechanical processes (pore pressure dependence on superimposed rock loads or regional stress fields) were not considered.

Tab. 7.4: Plausible static hydraulic heads and corresponding P2 pressures

Interval	**Depth**	**L**	**Sensor**	**Plausible range (h_s)**		**Plausible range (kPa)**	
Name	**from – to**		**depth [P2]**	**min.**	**max.**	**min.**	**max.**
	[m bgl]	**[m]**	**[m bgl]**	**[m asl]**	**[m asl]**	**[kPa]**	**[kPa]**
Oftr-i1	650.00 - 700.04	50.04	646.86	383	483	5955	6936
Oftr-i2	590.00 - 640.04	50.04	586.86	383	483	5367	6348
Oftr-i3	550.00 - 600.04	50.04	546.86	383	483	4974	5955
Oftr-i4	500.00 - 550.04	50.04	496.86	383	483	4484	5465
Oftr-i5	450.00 - 500.04	50.04	446.86	383	483	3993	4974
Oftr-i6	408.50 - 417.59	9.09	405.36	383	483	3586	4567
Oftr-i7	632.50 - 641.59	9.09	629.36	383	483	5784	6765
Oftr-i8	621.50 - 630.59	9.09	618.36	383	483	5676	6657
Oftr-i9	583.00 - 592.09	9.09	579.86	383	483	5298	6279
Oftr-i10	408.50 - 417.59	9.09	405.36	383	483	3586	4567

8. Test Interval Oftr-i1: 650 - 700 m

Interpretation Level: Standard analysis

8.1. Introduction

The initial analyses presented in the QLR (Appendix A) were expanded and additional numerical analyses were conducted to provide a greater level of confidence in the estimated formation properties. Borehole history effects were already included during the simulations for the QLR, as it was done for all intervals. The diagnostic plots presented in the QLR indicated that a homogeneous flow model is appropriate for this test interval, although the composite skin model produced a better overall fit in the Cartesian plot.

Downhole pressures and surface flow-rates of the entire test sequence of Test Oftr-i1 are shown in Fig. 8.1.

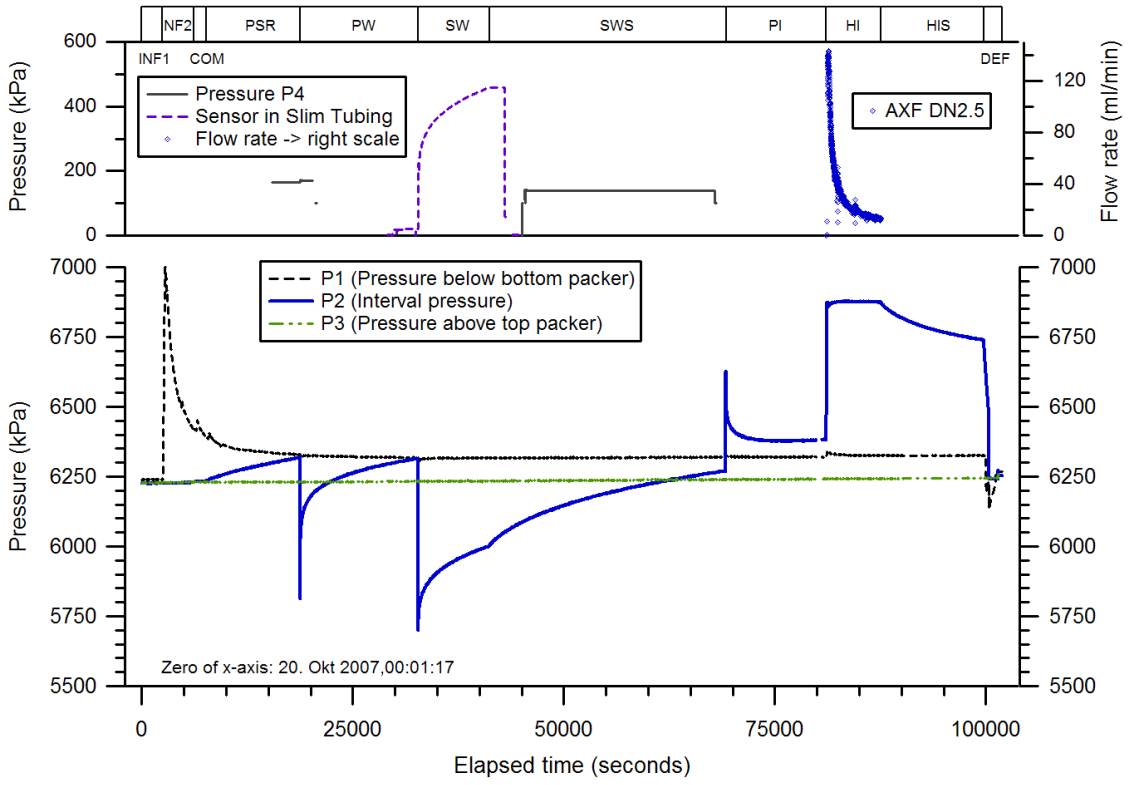

Fig. 8.1: Test Oftr-i1, 650.0 - 700.0 m: overview plot

8.2. Parameter Range from the QLR

For the QLR the analyses of individual test events resulted in wide range of estimated formation parameters. For the homogeneous model, the hydraulic conductivity estimates varied between 3.7E-12 m/s and 5.2E-11 m/s. The specific storage estimates ranged from 3.8E-06 m^{-1} to 1.0E-04 m^{-1} which was defined as upper bound of the plausibility range. Similarly, the matched static formation pressures ranged between 6676 and 7000 kPa, corresponding to hydraulic heads of 457 to 490 m asl, whereby the latter value corresponds to the upper limit of the plausibility range. A discrepancy in response character and associated parameters was indicated for the late sequences HI-HIS in comparison to the earlier test events SW-SWS. Generally better matches were obtained using a composite model (skin) but the fits for different test sequences produced considerably differing parameter estimates. The best estimates of the QLR are based on the Cartesian fit of the entire test sequence using a homogeneous flow model (Tab. 8.1; details in Appendix A).

Tab. 8.1: QLR result: Best-fit parameters estimates and 95% confidence intervals for homogeneous model.

Parameter	Units	Fit Value	95% Confidence Intervals	
		SSE = 1.01E+07	Lower Value	Upper Value
K_fm	[m/s]	5.53E-12	5.13E-12	5.97E-12
P_fm	[kPa]	6783	6762	6803
ss_fm	[1/m]	1.00E-04	8.75E-05	1.14E-04

The fit of the composite skin model resulted in a lower specific storage estimate but suggested a hydraulic head which was at the upper limit of the plausible range. The QLR parameter estimates for the composite skin model are shown in Tab. 8.2. Despite the significantly lower sum of square errors (SSE, Tab. 8.2), the composite model was discarded because the simulations produced distinct features in the diagnostic plots of PW and SW which were not seen in the test data.

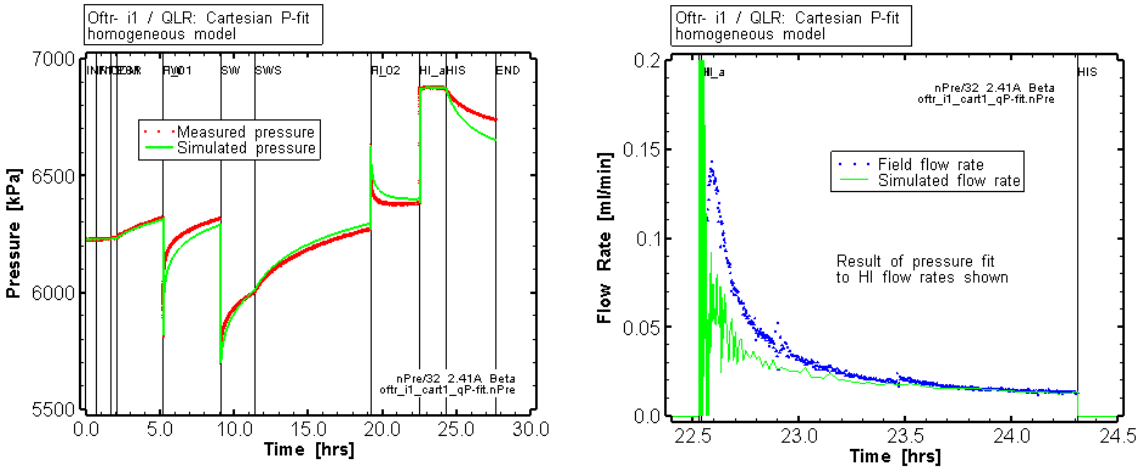

Fig. 8.2: Oftr-i1: Cartesian fit of the QLR best-estimate

Tab. 8.2: QLR composite model: Best-fit parameters estimates and 95% confidence intervals for composite model

Parameter	Units	Fit Value SSE=6.24E+06	95% Confidence Interval	
			Lower Value	Upper Value
K_fm	[m/sec]	3.95E-12	3.29E-12	4.75E-12
K_s	[m/sec]	2.46E-10	2.12E-10	2.86E-10
P_fm	[kPa]	7000	6945	7055
Ss_fm	[1/m]	3.37E-06	2.21E-06	5.13E-06
Ss_s	[1/m]	1.66E-06	1.15E-06	2.39E-06
t_s	[m]	2.56E-01	2.02E-01	3.11E-01

The residuals distributions for the homogenous and composite model (QLR analyses) are shown in Fig. 8.3. The range in the residuals is smaller for composite model. For both cases, considerable differences to the uniform distribution are recognizable.

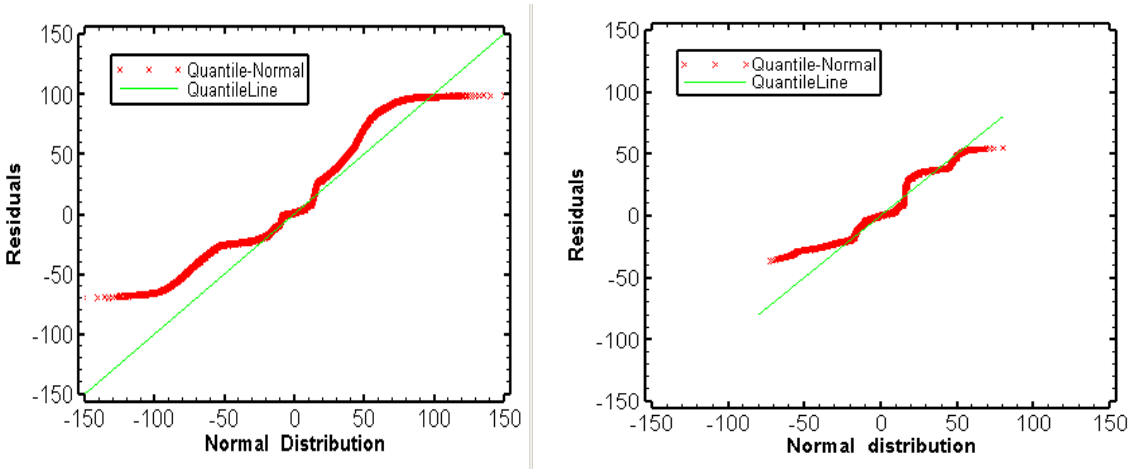

Fig. 8.3: Residual plots for the optimization of the all sequences fits to the Cartesian pressure response. Left: homogeneous model. Right: composite model (skin).

8.3. Cases for Standard Analysis

In view of recent rock elasticity measurements from core samples of the NOK-EWS Borehole the plausibility range for the Ss parameter was narrowed to 2.4E-7 m^{-1} - 1.0E-5 m^{-1} (see Section 7.3.3). The flow model identification was repeated based on the SWS sequence. Entire fits were performed by focusing on the SW-SWS-PI-HI period. As compliance effects may have affected the early test phase, the PSR-PW sequences are not fitted but incorporated as pressure history. The slow pressure recovery from the HI injection test is interpreted as an effect of changing borehole conditions (possible clogging during HI-injection) and is therefore not included in the simulation.

Check for possible test irregularities

Both pulse tests, PW and PI, showed consistent test zone compressibility values (PW: c_{tz} = 2.8E-9 Pa^{-1}, PI: c_{tz} = 3.3E-9 Pa^{-1}). This suggests that the fluid conditions remained constant during the entire test and no de-gassing occurred during the PW and SW-SWS drawdown sequences. A slim tubing was used during the slug withdrawal test. The P2 sensor of the Triple Probe and the P4 sensor in the slim tubing show identical differential pressures confirming the good quality of the measurements. The noise of the upper data in Fig. 8.4 is due to the influence of the high-voltage current transformer facility (NOK).

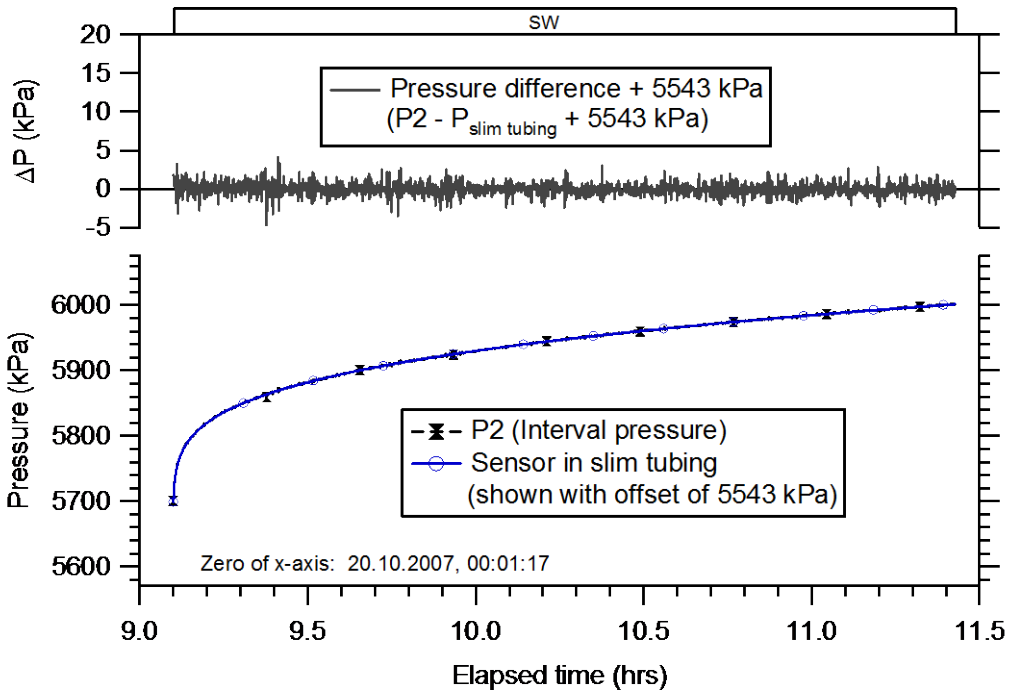

Fig. 8.4: Comparison of pressure signals of P2 and slim-tubing sensors during SW

8.4. Flow Model Identification

Log-log sequence fits were performed on the SWS sequence to test the homogeneous flow model identified during the QLR interpretation. It was assumed that the early test events (PSR, PW) were perturbed by equipment effects. For the investigation of the SWS phase, the period PSR-PW-SW was incorporated as pressure history, as well as the open-hole pressure history prior to testing (see Chapter 3). The optimization of the K, P_f and S_S parameters for the homogeneous model produced a good fit for the SWS log-log diagnostic plot, as shown in Tab. 8.3 and in the top left graph of Fig. 8.6. A composite fit with simultaneous matching of the pressure change (dP) and derivative (dP') curves was used. The estimated formation parameters were used to produce Cartesian pressures and flow rates (middle left and bottom left plots in Fig. 8.6). The discrepancies between measured and simulated pressure/flow in the Cartesian plots suggest that the homogenous model established based on the SWS sequence is not sufficient to adequately reproduce the measured pressure and flow responses.

The SWS sequence is re-evaluated using a composite model based on the combined log dP & dP' fit accounting for a skin zone of limited radial thickness (0.01 to 0.2 m). The results of the inverse parameter optimization are shown in Tab. 8.4 and in the plots on the right side of Fig. 8.6: The fit of the SWS log-log diagnostic plot (top right plot in Fig. 8.6) is slightly better compared to the fit of the homogeneous model (top left plot). The Cartesian plot (middle right plot) shows a significant better result for the non-fitted PI period. Note that the pre-SWS test data were incorporated as pressure history and were not fitted. The simulated HI flow rates (obtained by using the parameter estimates from the log-log diagnostic fit of the SWS sequence) match fairly well the measured flow, especially at middle/ late time of HI.

For both models, the calculated residuals (measured logP value minus simulated logP value) indicate significant discrepancies at the high and lower ranges and differ from a normal error distribution (Fig. 8.5).

Tab. 8.3: Sequence SWS optimization results fitted to dP & dP' of the log-log diagnostic plot: parameters estimates and 95% confidence intervals for homogeneous model.

Parameter	Units	Fit Value SSE = 13.45	95% Confidence Intervals	
			Lower Value	Upper Value
K_fm	[m/s]	7.02E-12	6.79E-12	7.26E-12
P_fm	[kPa]	6531	6524	6539
ss_fm	[1/m]	1.00E-05	8.98E-06	1.11E-05

Tab. 8.4: Sequence SWS optimization results fitted to dP & dP' of the log-log diagnostic plot: parameters estimates and 95% confidence intervals for composite model.

Parameter	Units	Fit Value SSE= 8.073	95% Confidence Interval	
			Lower Value	Upper Value
K_fm	[m/sec]	1.12E-11	8.92E-12	1.40E-11
K_s	[m/sec]	9.72E-11	3.28E-11	2.88E-10
P_fm	[kPa]	6562	6534	6590
Ss_fm	[1/m]	1.34E-06	1.66E-07	1.09E-05
Ss_s	[1/m]	2.42E-06	1.89E-07	3.08E-05
t_s	[m]	0.199	-0.093	0.491

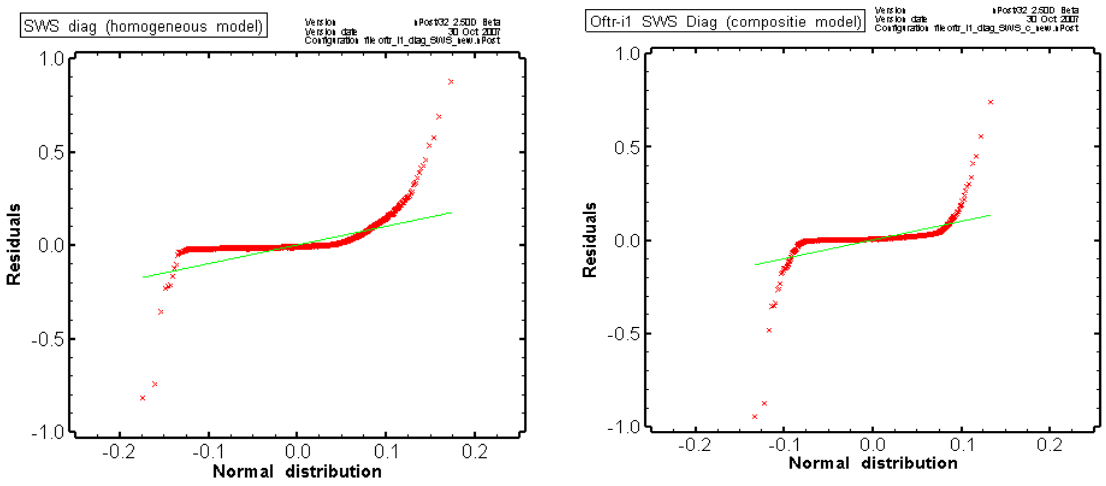

Fig. 8.5: Residual plot for log-log diagnostic composite fits of the SWS sequence. Left: homogeneous model. Right: composite skin model.

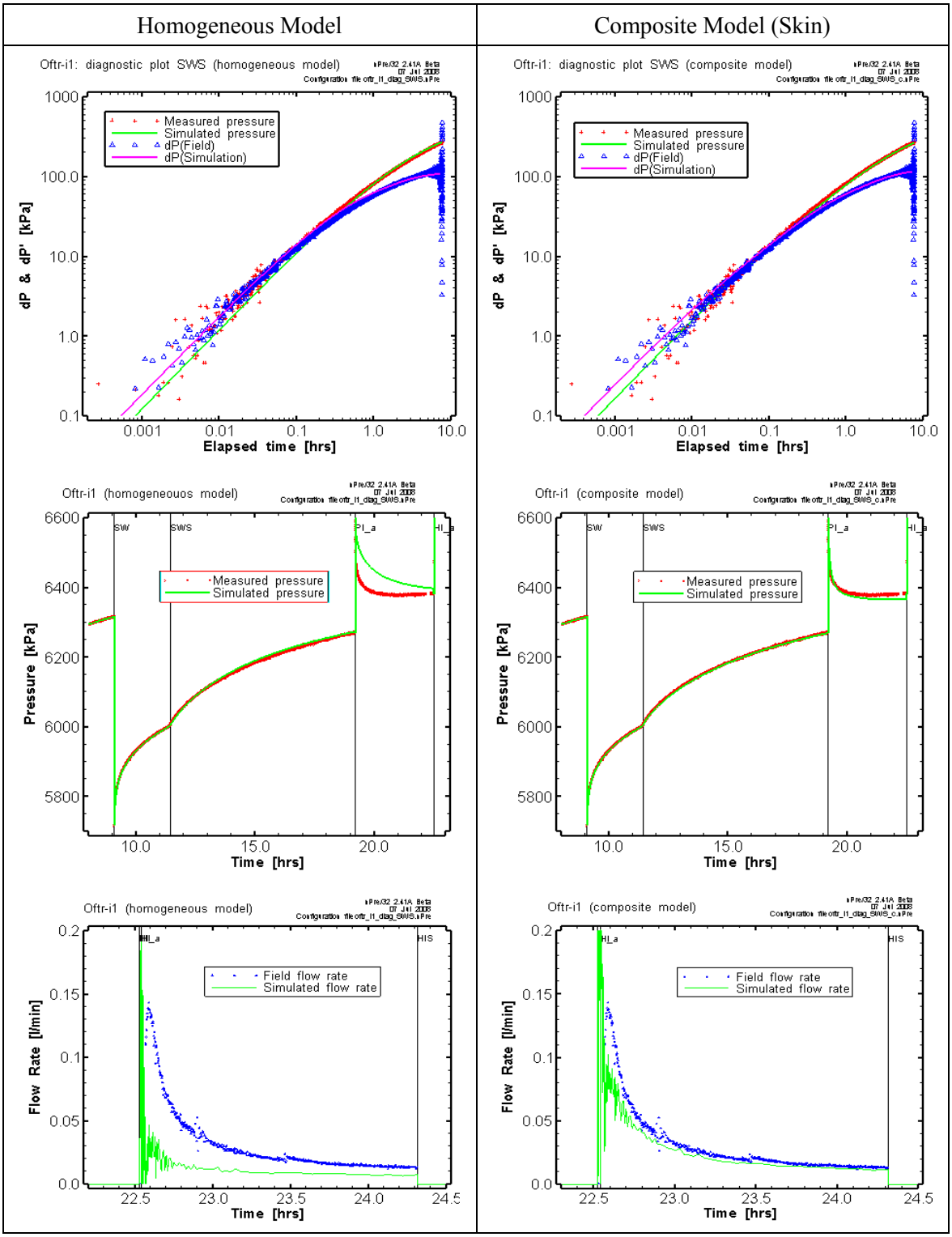

Fig. 8.6: Log-log fits for the SWS sequence for the homogenous (top left) and the composite model (top right). Simulated Cartesian pressure and flow are shown for both models using the formation parameter s obtained from the SWS fit.

8.5. Homogeneous Model -- Cartesian Fit SW-SWS-PI-HI

First simulations were carried out using the parameter ranges as defined in Section 7.3. However, the optimization of the Cartesian pressure response of the SW-SWS-PI-HI sequence showed a poor fit when the upper bound of the Ss parameter was limited to 1E-5 m^{-1} (according the defined plausibility range). Therefore, the upper limit of the Ss parameter was extended to 1E-4 m^{-1} which corresponds to upper bound S_S value of the QLR analysis. A composite fit was set-up to match both pressure (SW-SWS-PI) and flow (HI).

The simulation indicated a formation conductivity of 5.35E-12 m/s, a static formation pressure of 6657 and a specific storage estimate at the upper bound of range (1E-04 m^{-1}, Tab. 8.5). These results are very similar to the entire sequence fit (Tab. 8.1). The range between the upper and lower values for the 95th percentile confidence intervals are listed in Tab. 8.5 and shown in Fig. 8.7. The plot on the middle right side of Fig. 8.7 and the two plots on the bottom provide the 95th percentile confidence regions for the estimation of the S_s and K parameters (middle right), P_f and K parameters (bottom left) and P_f and S_s parameters (bottom right), with the shape of the ellipse indicating the degree of correlation between the parameters. Tab. 8.6 includes the covariance correlation matrix (shaded cells) which indicates that the three fitting parameters are well correlated. This correlation is also observed in the confidence intervals plots of Fig. 8.7 by small minor axis of the uncertainty ellipsoids.

The middle left plot in Fig. 8.7 shows a comparison of the residuals (measured value minus simulated value) to that of a normal distribution. The residuals are essentially normally distributed which indicates the absence of a systematic error and supports the conceptual model. The Cartesian fit to the measured flow rates and the corresponding residual distribution are shown in Fig. 8.8. The distribution of the flow rate residuals does not match the normal distribution. This may be due to the fact that the relatively low flow rates were measured at the surface. Due do the important length of the test tubing the storage of the injection hose, surface and downhole rates may differ significantly, especially at early time of HI.

Using the parameters estimates of the Cartesian fit (SW-SWS-PI-HI) for the diagnostic plots of the individual sequences resulted in good match of pressure and derivative for the SWS sequence but poor matches for the Ramey plots of the SW and PI sequences (not shown).

Overall, the homogeneous model is not satisfactory because the unrealistic high specific storage value and the poor fits of the individual sequence plots of SW and PI.

Tab. 8.5 Best-fit parameters estimates and 95% confidence intervals for homogeneous model.

Parameter	Units	Fit Value SSE=1.67E+06	95% Confidence Intervals		Initial Value
			Lower Value	Upper Value	
K_fm	[m/s]	5.35E-12	5.01E-12	5.71E-12	1.00E-11
P_fm	[kPa]	6656.66	6641.45	6671.88	6500
ss_fm	[1/m]	1.00E-04	9.13E-05	1.10E-04	1.00E-06

Tab. 8.6: Covariance-Correlation matrix for homogeneous model; SW-SWS-PI-HI Cart Fit (shaded cells denote correlation matrix elements).

Covariance/Correlation Matrix: Est. Cartesian Composite fit			
	K_fm	P_fm	ss_fm
K_fm	2.28E-05	-3.61E-05	-3.59E-05
P_fm	-9.95E-01	5.79E-05	5.67E-05
ss_fm	-9.96E-01	9.87E-01	5.70E-05

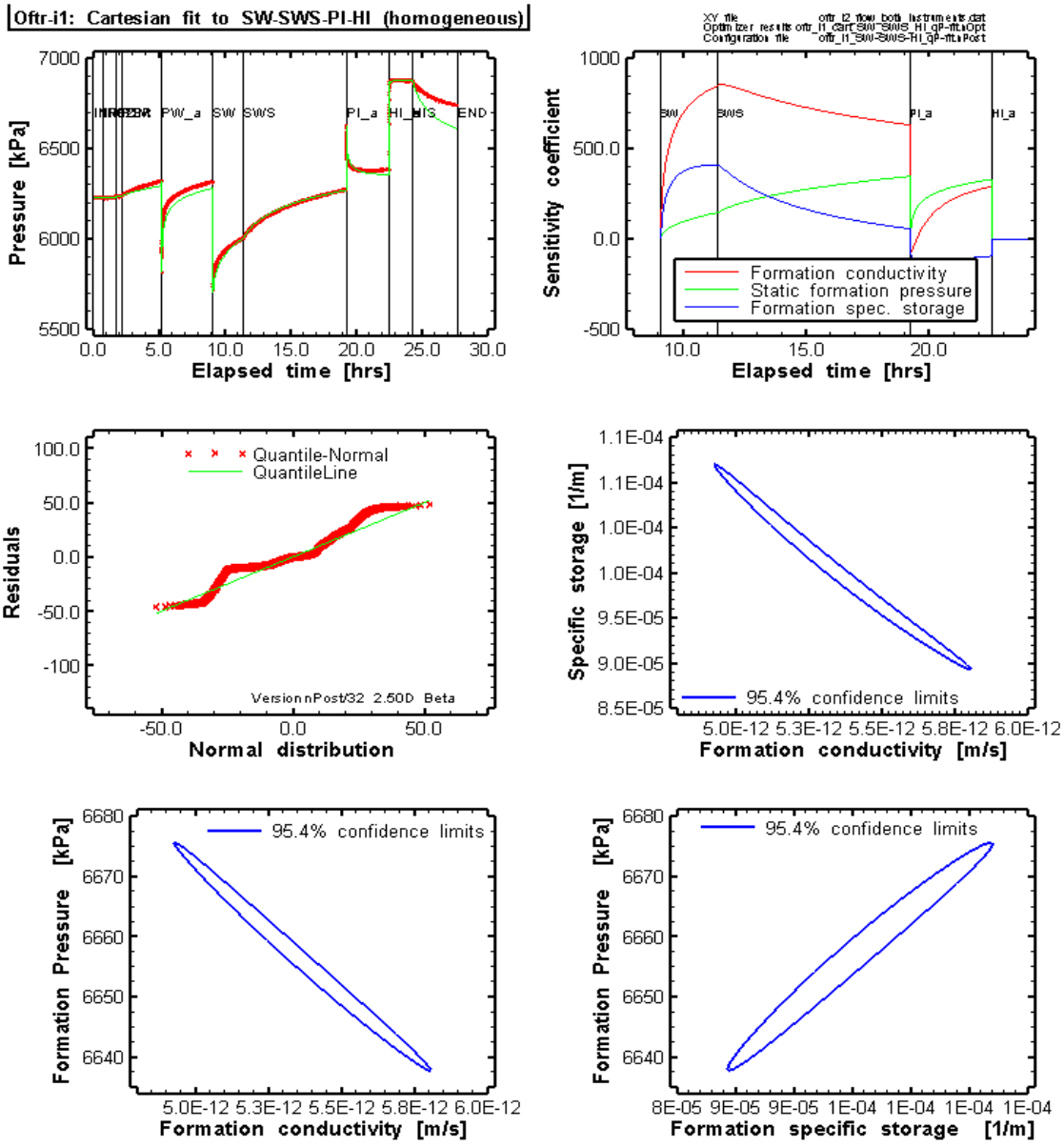

Fig. 8.7: Sequence SW-SWS-PI-HI optimization results fitted to the Cartesian pressure response (homogeneous model)

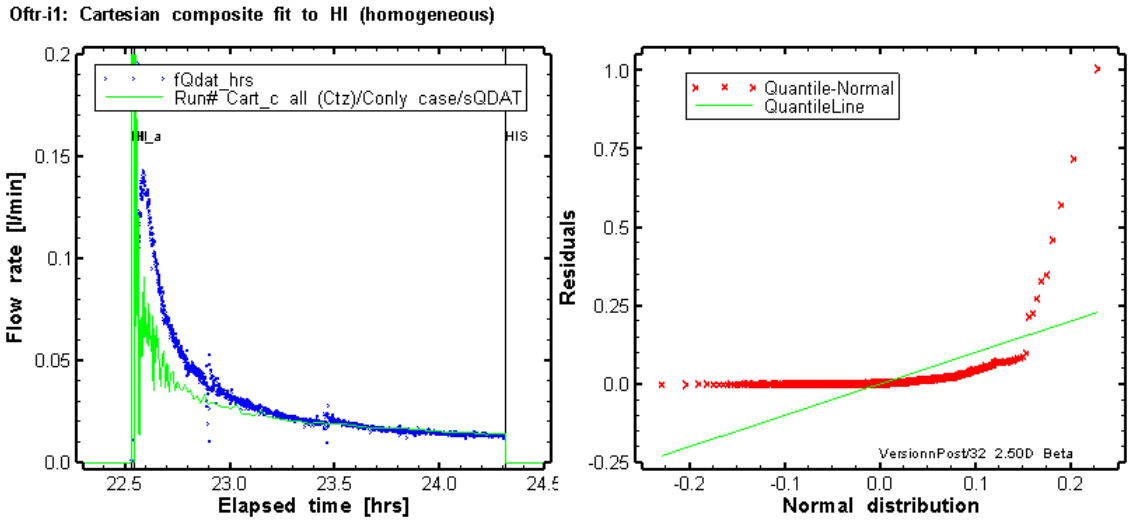

Fig. 8.8: Sequence SW-SWS-PI-HI optimization results fitted to the flow rate response (homogeneous model)

8.5.1. Composite Model -- Cartesian fit SW-SWS-PI-HI

The composite model is based on the homogeneous model but includes a skin zone of radial thickness t_s with skin-specific hydraulic conductivity and specific storage. During the simulations the Ss parameter for both skin zone and formation was allowed to vary between 2.4E-7 m^{-1} and 1.0E-5 m^{-1}. A composite fit was defined to match both pressure (SW-SWS-PI) and flow (HI).

The simulation indicated a formation conductivity of 6.96E-12 m/s, a static formation pressure of 6671 and a specific storage estimate at the upper bound of range (1E-05 m^{-1}, Tab. 8.7). The skin zone with a hydraulic conductivity of 1.55E-10 m/s and radial thickness of 0.08 m corresponds to skin factor of -0.69 (negative skin).

The sum of square errors for the composite model (SSE 6.0E+04; Tab. 8.7) is 1½ orders of magnitude lower compared to the homogeneous model (SSE=1.67E+06, Tab. 8.5)

The range between the upper and lower values for the 95th percentile confidence intervals are listed in Tab. 8.7 and shown in Fig. 8.9. The plot on the middle right side of Fig. 8.9 and the two plots on the bottom provide the 95th percentile confidence regions for the estimation of the S_s and K parameters (middle right), P_f and K parameters (bottom left) and skin parameters K_s and S_{SS} (bottom right), with the shape of the ellipse indicating the degree of correlation between the parameters. Tab. 8.8 includes the covariance correlation matrix (shaded cells) which indicates that the three skin fitting parameters are well correlated. The formation hydraulic conductivity is highly correlated with the static formation pressure but is fairly independent from the other fitting parameters. The correlations between the fitting parameters can also be observed in the confidence intervals plots of Fig. 8.9 by the elongation of the uncertainty ellipsoids. The skin parameters K_S, S_{SS} and t_s are highly correlated among each other (Tab. 8.8, bottom right plot in Fig. 8.9).

The middle left plot in Fig. 8.9 shows a comparison of the residuals (measured value minus simulated value) to that of a normal distribution. The residuals are significantly smaller compared to the residual of the fit for the homogeneous model (Fig. 8.7). The residuals are essentially normally distributed except for the negative residual values -10 to - 20 kPa which correspond to the early time data from the PI test. This indicates that test conditions were not ideal for the start of the pulse test (i.e. packer behaved not fully elastically). Apart from this, the residual plot suggests the absence of a systematic error and supports the composite model. The Cartesian fit to the measured flow rates and the corresponding residual distribution are shown in Fig. 8.10. Similar to the homogeneous case, the distribution of the flow rate residuals does not match the normal distribution. This may be due to the fact that the relatively low flow rates were measured at the surface. Due do the important length of the test tubing the storage of the injection hose, surface and downhole rates may differ significantly, especially at early time of HI. Overall, the flow rate match for the composite model is better for the composite model (negative skin) compared to the corresponding fit of the homogeneous model.

Tab. 8.7: Best-fit parameters estimates and 95% confidence intervals for composite model.

Parameter	Units	Fit Value SSE=5.98E+04	95% Confidence Interval		
			Lower Value	Upper Value	Initial Value
K_fm	[m/sec]	6.96E-12	6.75E-12	7.18E-12	1.00E-11
K_s	[m/sec]	1.55E-10	1.39E-10	1.72E-10	1.00E-11
P_fm	[kPa]	6671	6664	6678	6500
Ss_fm	[1/m]	1.00E-05	9.14E-06	1.09E-05	1.00E-06
Ss_s	[1/m]	6.08E-06	5.20E-06	7.10E-06	1.00E-06
t_s	[m]	0.078	0.070	0.086	0.100

Tab. 8.8: Covariance-Correlation matrix for composite model.

	K_fm	K_s	P_fm	ss_fm	Ss_s	t_s
K_fm	5.02E-06	-8.70E-06	-7.91E-06	7.83E-06	3.23E-05	-1.24E-05
K_s	-6.82E-01	3.24E-05	1.37E-05	-6.02E-05	-1.18E-04	4.77E-05
P_fm	-9.96E-01	6.81E-01	1.25E-05	-1.30E-05	-5.14E-05	1.99E-05
ss_fm	2.90E-01	-8.79E-01	-3.05E-01	1.45E-04	2.24E-04	-9.34E-05
ss_s	6.89E-01	-9.93E-01	-6.93E-01	8.91E-01	4.38E-04	-1.77E-04
t_s	-6.53E-01	9.87E-01	6.61E-01	-9.14E-01	-9.98E-01	7.21E-05

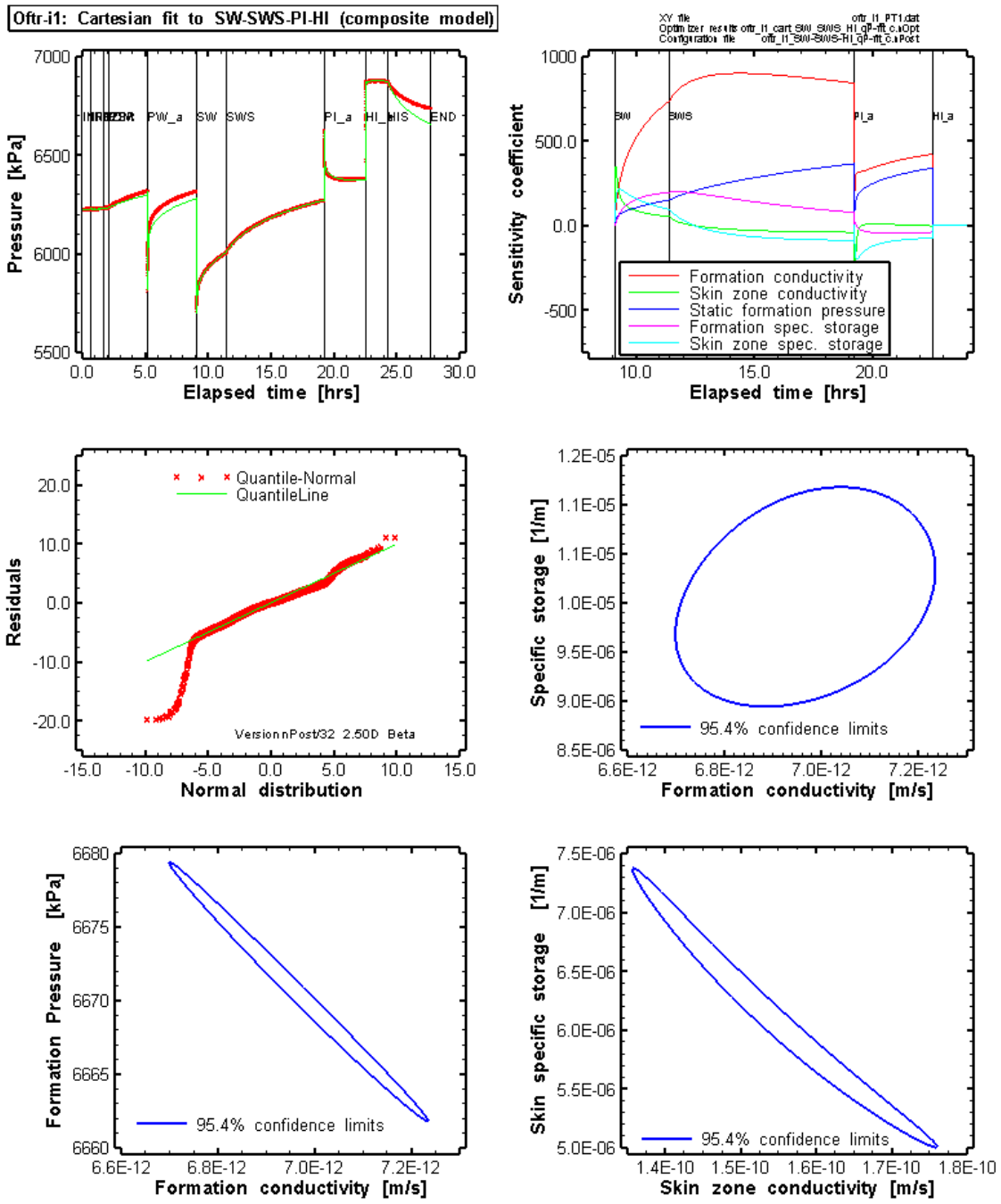

Fig. 8.9: Oftr-i1, Composite model: Sequence SW-SWS-PI-HI optimization results fitted to the Cartesian pressure response

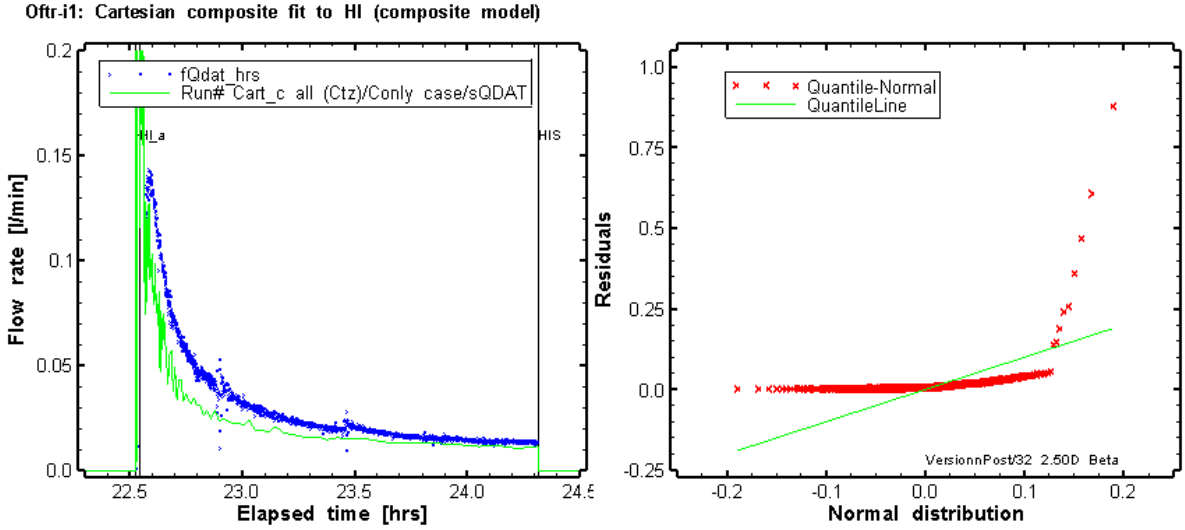

Fig. 8.10: Oftr-i1, Composite model: Sequence SW-SWS-PI-HI optimization results fitted to the flow rate response.

Fig. 8.12 shows the match for individual test sequences PW, SW, SWS, PI, and HI using the fit parameters from the Cartesian fit, composite model. The fits are of good quality for the SW-SWS sequence, medium quality for the PI sequence but rather poor for the PW and HIS test events. The bad matches for the PW and HIS sequences are not surprising as these test phases were not included in the Cartesian fit.

8.6. Analysis of Packer Squeeze in P1 Bottom Zone 701.3- 719 m

During packer inflation, a pulse like pressure response was recorded in the bottom borehole section (interval from base of lower packer to base of borehole) due to volume displacement. The pressure pulse is shown in the left graph of Fig. 8.11. The pressure pulse was analyzed as a pulse injection test assuming a test zone compressibility value (c_{tz}) of 2E-09 Pa^{-1}. Using the PI end pressure as initial (recovered) start pressure and assuming a radial flow model, the hydraulic conductivity becomes K =1.5E-10 m/s (T = 2.7E-09 m^2/s). By introducing a pressure trend to compensate for difference in start and end pressure, a K-value of 7.0E-11 m/s (T = 1.2E-09 m^2/s) is obtained. Note that the analysis of packer pressure squeezes provides very rough estimates only.

The P1 end pressure of 6326 kPa corresponds to a hydraulic fresh water head of 13.3 m bgl or 419.7 m asl.

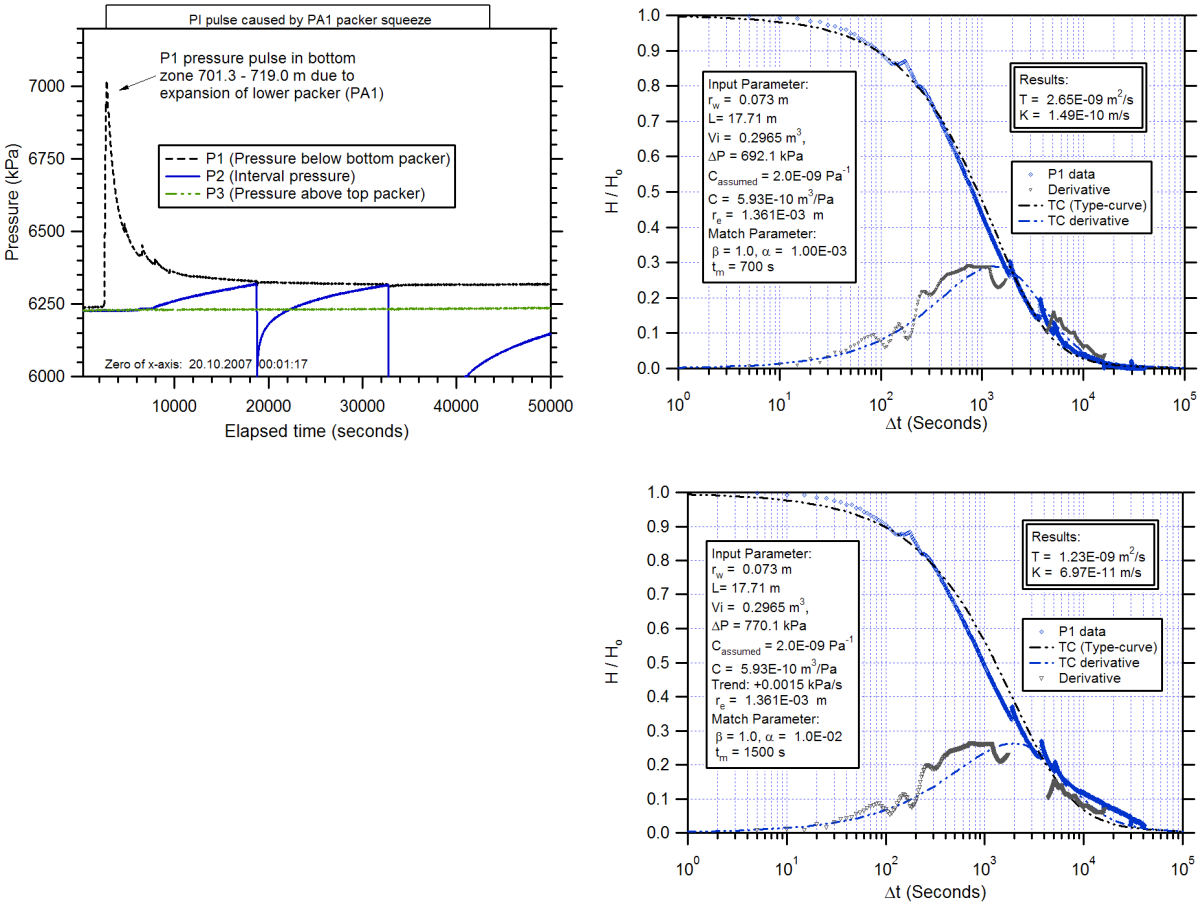

Fig. 8.11: Packer squeeze effect in P1 bottom zone analyzed as PI test.

Top left: Cartesian Plot. Top right: P1 pressure response analyzed as PI test assuming a c_{tz} value of 2E-09 Pa^{-1} (rough estimate). PI end pressure is used as PI initial pressure. Bottom right: P1 open-hole pressure used as PI initial pressure. P1 data are corrected using a trend of 0.0015 kPa/s. c_{tz} = 2E-09 Pa^{-1} (assumed). Analyses of packer squeeze pressure responses provide rough T, K-estimates only.

8.7. Summary

The homogenous flow model suggested during QLR interpretation was retested based on a narrowed plausibility range for the S_S parameter. Diagnostic analyses of the SWS sequence using both homogeneous and composite skin models produced acceptable fits but residuals distributions with considerable differences to a normal error distribution. The formation and skin parameter estimates obtained from the diagnostic analysis for the composite model produce good fits to the Cartesian pressure of the subsequent PI sequence and to the flow rate of the HI test, whereas the parameters from the homogenous model (SWS sequence) are not appropriate to reproduce the measured late test (PI-HI) pressure and flow responses. HIS matches were poor for both cases.

Additional simulations based on homogeneous and composite model, both with fits to the Cartesian pressure were run for the SW-SWS-PI-HI sequence. The early test sequences (PSR-PW) and the HIS phase were not considered during these simulations. The composite model produced significantly better matches to the Cartesian pressure and a lower sum of squared errors (SSE) compared to the homogeneous model. The homogeneous model suggested unrealistic high Ss values at the upper bound of the entered parameter range (1.0E-04 m^{-1}) and an order of magnitude higher than the upper limit of plausible values (1E-05 m^{-1}).

The formation and skin parameter estimates obtained from the Cartesian fit of the SW-SWS-PI-HI sequence, composite model, produced good fits to the sequence plots SW (Ramey A plot), SWS log-log diagnostic plot and PI Ramey A plot.

On the basis of the generally better fits and the revised S_S-plausibility range, the composite skin model is preferred over the homogeneous model. The best estimates for the hydraulic formation parameters are K = 7E-12 m/s (T = 3.4E-10 m^2/s), Ss = 1E-05 m/s and P_fm = 6671 kPa. The estimated static formation pressure corresponds to a hydraulic head of 456 m asl. This head is slightly artesian (+23 m above ground level). The head estimate is in general agreement with the P1 pressure measured at end of Test Oftr-i2 (443 m asl; rising trend with 0.16 m/hr), whose bottom interval (741.3 - 719.0 m) covers a similar borehole section as Test Oftr-i1 (750 - 700 m). The fairly well stabilized P1 pressure of Test Oftr-i1 suggests a head of 419.7 m (trend +0.37 m /hr) for the bottom borehole section 701.3 to 719 m.

The skin parameters K_S, S_{SS} and t_S should be considered with care as they are highly correlated among each other.

Based on the results of the good quality simulation cases (tagged with the √ symbol in Tab. 8.9), the following parameter ranges were assessed:

- formation conductivity: 3.3E-12 to 1.4E-11 m/s
- specific storage: 9E-07 to 1.1E-05 m^{-1}
- formation pressures: 6530 to 6678 kPa (with corresponding heads 442 to 457 m asl).

The above parameter ranges include the incertitude as indicated by the 95th percentile confidence intervals for the individual minimum and maximum values.

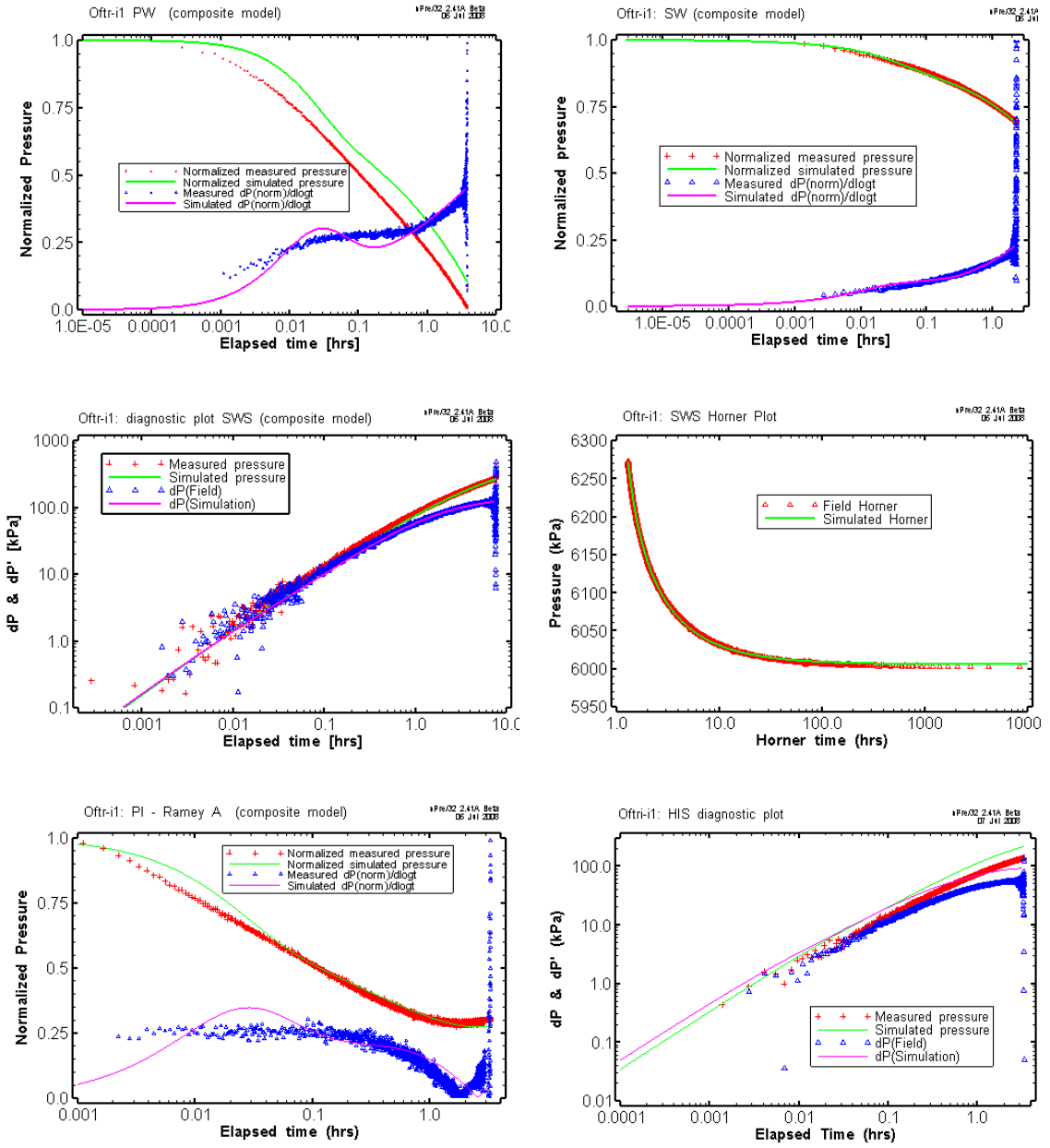

Fig. 8.12: Oftr-i1, Composite model: Individual sequence plots using the Cartesian fit parameters for the SW-SWS-PI-HI sequence.

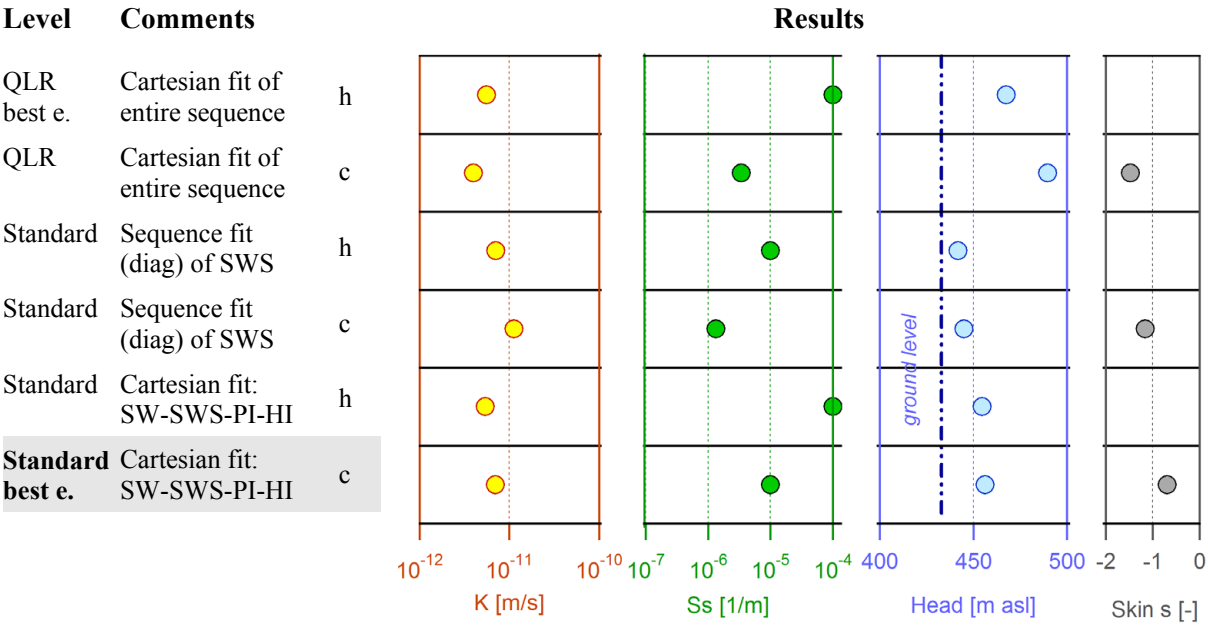

Fig. 8.13: Oftr-i1: Overview of results of inverse parameter estimations based on different models and fit configurations (abbreviations see Tab. 8.9).

Tab. 8.9: Oftr-i1: Overview of results of inverse parameter estimations

Case		K [m/s]	S_S [m^{-1}]	s [-]	h_s [m asl]	Fit quality	Remarks Plausibility	
QLR Cart ESF	h	5.53E-12	1.00E-04		467.5	-		
QLR Cart ESF, comp.P+q	c	3.95E-12	3.37E-06	-1.48	489.6	(+)		√
Standard analysis:								
Diag. sequence fit of SWS	h	7.02E-12	1.00E-05		441.8	(+)	Fit parameters disagree with meas. HI flow rates	
Diag. sequence fit (diag) of SWS	c	1.12E-11	1.34E-06	-1.16	445.0	+		√
Cart comp. P+q fit SW-SWS-PI-HI	h	5.35E-12	1.00E-04		454.7	-	Wide S_S range	
Cart comp. P+q fit SW-SWS-PI-HI	c	6.96E-12	1.00E-05	-0.69	456.1	(+)	**best estimate**	√

√ = good simulation results used to assess parameter ranges
QLR = Quick Look Report
c = composite skin model
Cart ESF = Cartesian entire sequence fit
Diag. Diagnostic plot, composite fit of dP and dP'
h = homogeneous model

9. Test Interval Oftr-i2: 590 - 640 m

Interpretation Level: Detailed analysis

9.1. Introduction

The initial analyses presented in the QLR (Appendix B) were expanded upon and additional numerical analyses were conducted on the hydraulic testing to provide a greater level of confidence in the estimated formation properties. The additional analyses focused on the PI and the SWS sequences, with a perturbation analysis conducted on the SWS sequence. The diagnostic plots presented in the QLR indicated that a homogeneous flow model is appropriate for this test interval. The majority of the analyses were conducted using the homogeneous flow model, however, due to overall poor fits to the PI_b sequence, the use of composite flow model was investigated.

Downhole pressures of the entire test sequence of Test Oftr-i2 are shown in shown in Fig. 9.1

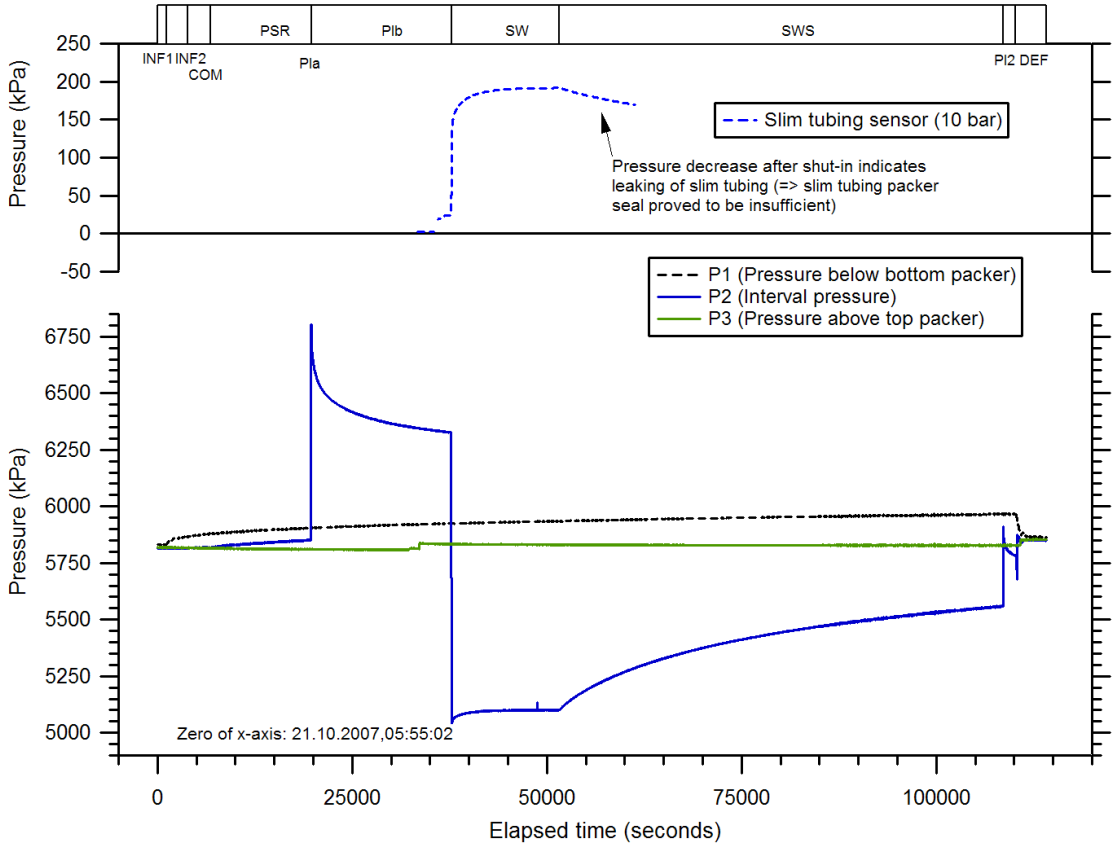

Fig. 9.1: Test Oftr-i1, 590.0 - 640.0 m: overview plot

9.2. Parameter Ranges and Best-estimate from QLR

The numerical analyses for the QLR provided the following parameter estimates:

$K = 3.6E\text{-}13$ m/s (2.4E-13 - 2.8E-11 m/s)
$S_S = 1.6E\text{-}05$ m^{-1} (9.7E-06 - 3.6E-05 m^{-1})
$P_f = 6066$ kPa (6045 - 6575 kPa)

The values in brackets indicate the lowest/highest estimates from several inverse parameter optimizations for different periods and fit constraints using nSights. The highest K-value of 2.8E-11 m/s was obtained from the single sequence fit of the PSR period using a homogeneous flow model. This value should be considered with care because the PSR pressure could be influenced by ongoing compliance effects. The QLR best-estimate fit was based on a Cartesian fit specification and a homogeneous flow model (no skin). The fitted formation specific storage (S_s) values from the QLR consistently indicated a relatively high range of 9.7E-6 to 3.6E-5 m^{-1}. Therefore, the bounding range in the S_s parameter for the detail analysis was specified from a low of 1.0E-7 to an upper value of 5.0E-5 m^{-1}. This wide range was kept for two simulation cases added (Sections 9.3 and 9.4) during revision of the Final Draft.

The best estimate of the formation fluid pressure (P_f) from the QLR was 6065.6 kPa which corresponds to an equivalent freshwater head of 454.5 m asl. This head is 23 m above the hydrostatic head of 433 m asl. For most of the detailed analyses, the bounding range for P_f was specified from a low of 5800 kPa to an upper value of 6300 kPa, which corresponds to an approximately equivalent freshwater head range of +/- 25 m about the QLR estimate of 456.2 m asl. Note that the detailed analysis for Oftr-i2 was completed before the plausibility ranges for the P_f and S_S parameters were reconsidered (Sections 7.3.3 and 7.3.4). Two simulation cases added during revision of the Final Draft (Sections 9.3 and 9.4) use the pressure range 5367 - 6348 kPa as indicated in Section 7.3.4, corresponding to hydraulic head +/- 50 m bgl.

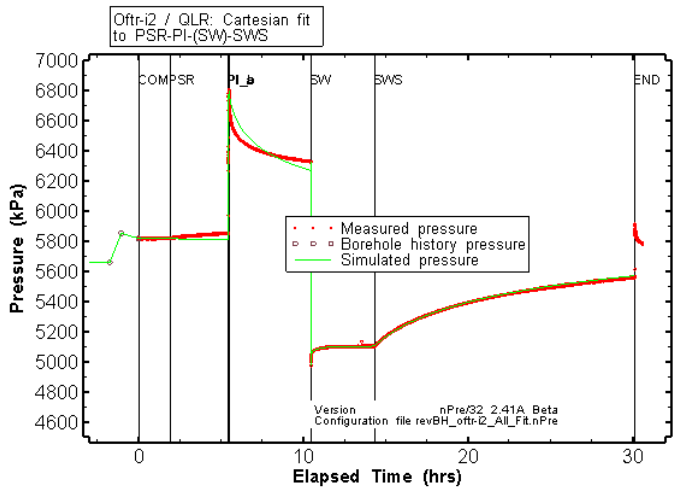

Fig. 9.2: Oftr-i2: Cartesian fit of the QLR best-estimate

9.3. Homogeneous Model: Cartesian PSR-PI-(SW)-SWS-PI2 Fit

(Section added during revision of Final Draft)

The Cartesian "entire sequence" fit presented in the QLR (Appendix B) does not include the PI2 period. Therefore, the inverse parameter optimization to fit the Cartesian pressure was repeated with inclusion of the PI2-period and with use of a slightly adapted P_f parameter range (Section 7.3.4). Due to by-passing of the slim tubing packer during the slug withdrawal test, the SW event was incorporated as pressure history period. The results of the parameter optimization are shown in Tab. 9.1, Tab. 9.2 and in Fig. 9.4. The inclusion of the PI2 period results in very similar parameter estimates and parameter confidence limits as presented in the QLR for the Cartesian fit to the PSR-PI-(SW)-SWS sequence (Appendix B). The fit is good for the SWS period but rather poor for the PSR, PI and PI2 sequences (Fig. 9.4). The result of the Cartesian fit to SWS log-log diagnostic plot is shown in Fig. 9.3. The simulated data are in almost perfect agreement with the measured pressure and the derivative. However, the SWS period is mainly dominated by wellbore storage and shows possible IARF conditions at late time only.

Tab. 9.1: Oftr-i2, homogeneous model, Cartesian Fit to PSR-PI-(SW)-SWS-PI2: Best-fit parameters estimates and 95% confidence intervals for homogeneous model.

Parameter	Units	Fit Value SSE=9.65E+06	95% Confidence Intervals	
			Lower Value	Upper Value
K_fm	[m/s]	3.61E-13	3.21E-13	4.06E-13
P_fm	[kPa]	6062	6036	6087
ss_fm	[1/m]	1.54E-05	1.28E-05	1.84E-05

Tab. 9.2: Covariance-Correlation matrix for homogeneous model; Cartesian Fit to PSR-PI-(SW)-SWS-PI2 (shaded cells denote correlation matrix elements).

Covariance/Correlation Matrix: Est. Cartesian Composite fit			
	K_fm	P_fm	ss_fm
K_fm	1.79E-05	-5.40E-05	-6.15E-05
P_fm	-9.86E-01	1.67E-04	1.85E-04
ss_fm	-9.99E-01	9.84E-01	2.12E-04

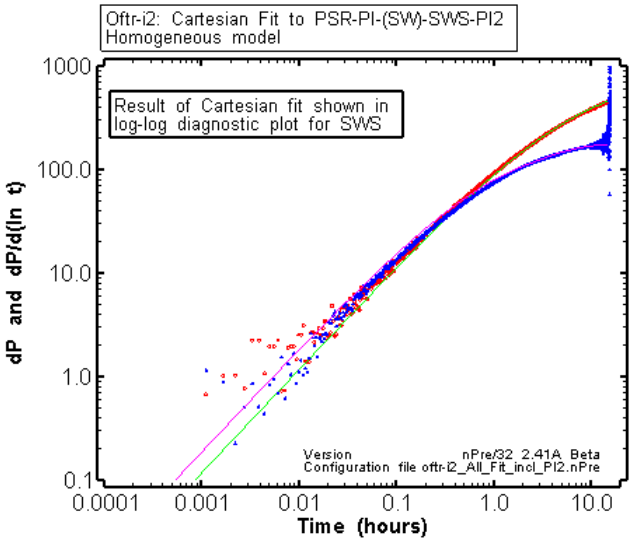

Fig. 9.3: Result of Cartesian fit shown for the SWS log-log diagnostic plot.

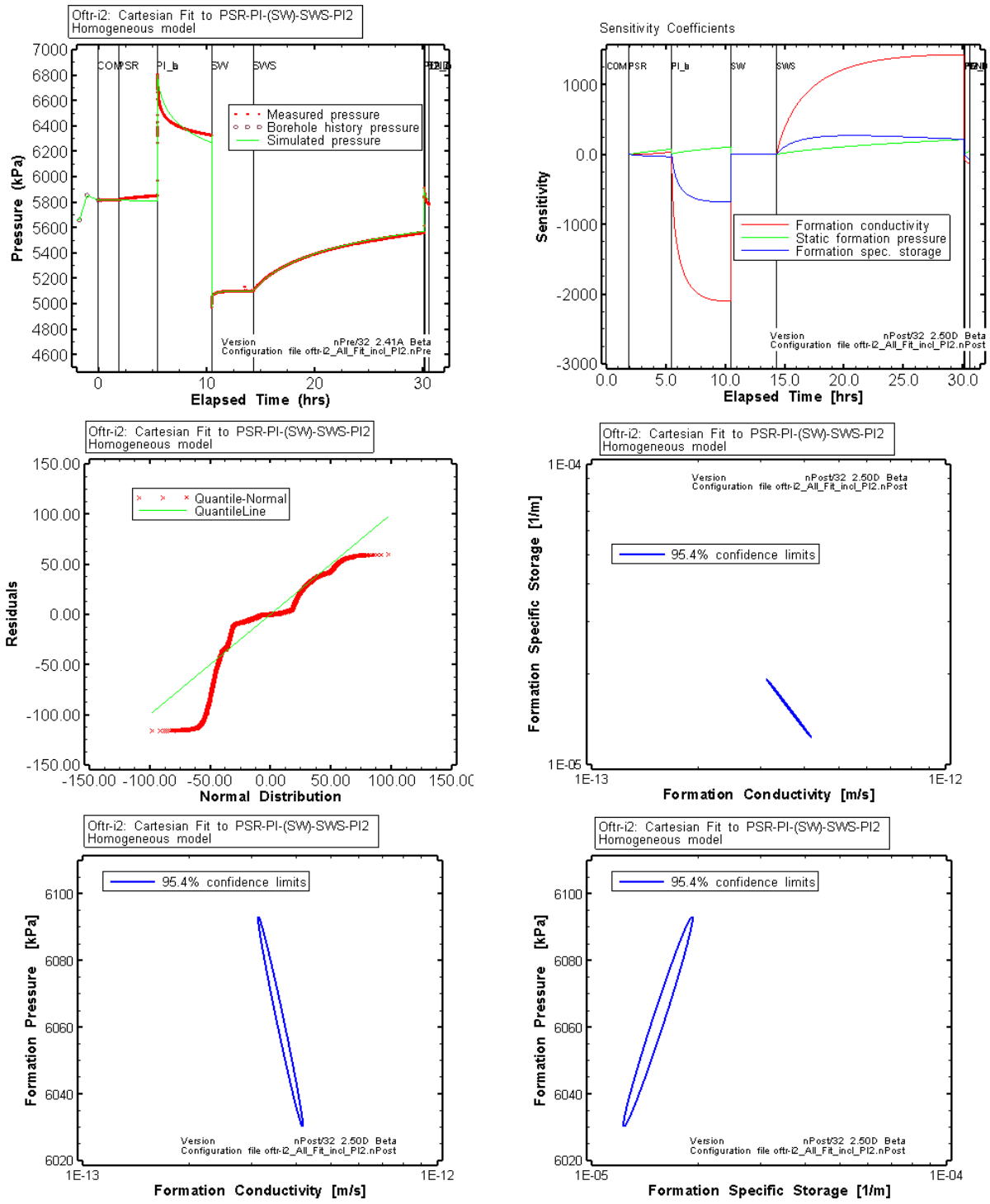

Fig. 9.4: Oftr-i2, homogeneous model, sequence fit PSR-PI-(SW)-SWS-PI2: Cartesian fit plot, sensitivity plot, residual plot and confidence regions.

Results from nSights inverse parameter estimation fitting the Cartesian pressures of the entire test (except SW which was incorporated as pressure history). Upper left: Cartesian plot of entire test. Upper right: sensitivity coefficients. Middle left: residual distribution. Confidence regions are shown for the joint parameters K-S_S (middle right), K-P_f (bottom left) and S_S-P_f (bottom right).

9.4. Homogeneous Model: Cartesian PI-(SW)-SWS-PI2 Fit

(Section added during revision of Final Draft)

This case is based on the simulation of the previous section but assumes that the interval pressure during the PSR period was affected by ongoing compliance effects. The PSR sequence is therefore not fitted but incorporated as pressure history. The results of the inverse parameter optimization (Tab. 9.3 and Tab. 9.6) are very similar to those of the Cartesian fits presented in the QLR (Appendix B) and Section 9.3. The fit is good for the SWS period but rather poor for the PSR, PI and PI2 sequences (not shown).

Tab. 9.3: Oftr-i2, homogeneous model, Cartesian Fit to PI-(SW)-SWS-PI2: Best-fit parameters estimates and 95% confidence intervals for homogeneous model.

Parameter	Units	Fit Value SSE= 7.66E+06	95% Confidence Intervals	
			Lower Value	Upper Value
K_fm	[m/s]	3.93E-13	3.45E-13	4.49E-13
P_fm	[kPa]	5995	5967	6022
ss_fm	[1/m]	1.46E-05	1.19E-05	1.78E-05

Tab. 9.4: Covariance-Correlation matrix for homogeneous model; Cartesian Fit to PI-(SW)-SWS-PI2 (shaded cells denote correlation matrix elements).

Covariance/Correlation Matrix: Est. Cartesian Composite fit			
	K_fm	P_fm	ss_fm
K_fm	2.28E-05	-6.62E-05	-7.81E-05
P_fm	-9.89E-01	1.96E-04	2.26E-04
ss_fm	-9.99E-01	9.86E-01	2.68E-04

9.5. Pulse Injection Analyses

As described in the QLR for the pulse-injection sequence (PI), the pressure increase at the start of the PI test was non-ideal as a result of equipment issues. As a result, the PI was divided into two portions for the analysis. The pressure increase portion of the test (PI_a) was not analyzed but included as a borehole history sequence. The recovery portion of the test (PI_b), following final pressure increase and shut-in, was used for the estimation of the formation parameters.

The fitted parameters for the PI_b analysis presented in the QLR included a P_f of 6300 kPa. However, the overall fit was poor (see Fig. 12 of QLR, Appendix B). The test analysis included the entire pre-sequence borehole pressure information as a borehole history curve. During the analysis conducted on the PI_b sequence for the QLR and this detailed analysis, the optimization routine consistently fitted a value for the P_f that was considered too large. This is

seen in the QLR analysis in which the reported P_f was actually the upper bound of the specified range. For the analysis in Section 9.5.1, the P_f was removed from the optimization process and was set at a constant value of 6000 kPa.

9.5.1. Homogeneous Model -- Ramey A Fit

The additional analysis utilized the normalized pressure (P_{norm}) of the PI_b diagnostic plot (Ramey A) as the optimization fitting criteria, assuming a homogeneous flow model. The left plot of Fig. 9.5 shows the measured data and simulation results for the optimization. The right plot of Fig. 9.5 shows the same simulation results but on a Cartesian plot scale. The optimized fit is poor with difficulty in simultaneously fitting both the early-time and late-time portions of the data curve. The best-fit parameters indicate a formation hydraulic conductivity (K) of 4.94E-13 m/sec and a specific storage (S_s) of 1.21E-05 m^{-1} (Tab. 9.5).

Tab. 9.5: Fitted parameter and 95% confidence interval values for sequence PI_b, assuming a homogeneous flow model.

95% Confidence Intervals				
Parameter	Units	Fitted Value	Lower Value	Upper Value
K	[m/sec]	4.94E-13	2.15E-13	1.13E-12
S_s	[1/m]	1.21E-05	3.80E-06	3.85E-05

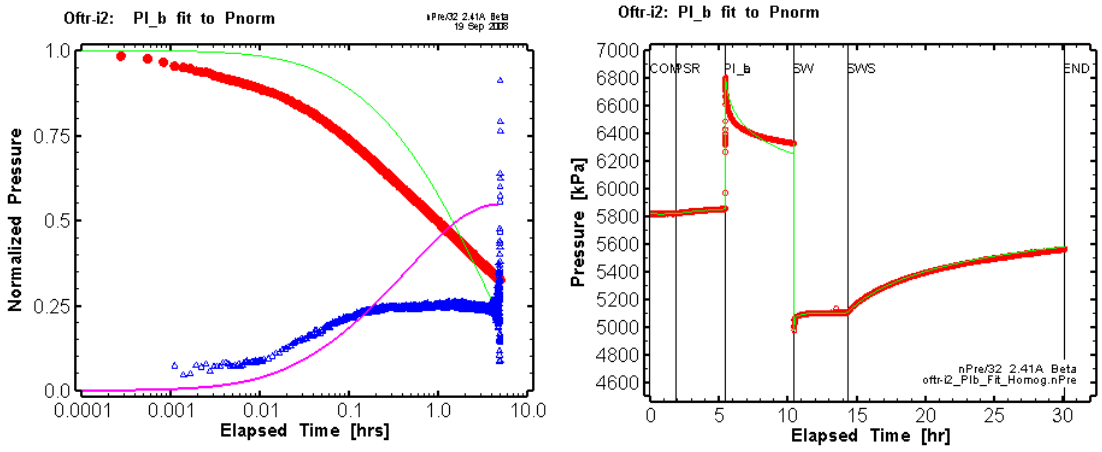

Fig. 9.5: Sequence PI_b optimization results fitted to P_{norm} showing the Ramey A diagnostic plot (left) and the Cartesian plot (right), assuming a homogeneous flow model.

9.5.2. Composite Skin Model -- Ramey A Fit

Given the difficulty in fitting the PI_b sequence assuming a homogeneous radial flow model, an analysis was conducted using a composite radial flow model to see if that conceptual model could better describe the observed pressure recovery. Fig. 9.6 shows the results of the optimization for the composite flow model. The simulated curve matches the P_{norm} data better after a time of 0.1 hours (Fig. 9.6 left; red data points and green simulated line) and looks better

on the Cartesian plot (Fig. 9.6 right). However, in Fig. 9.6, left plot, the pressure derivative of the diagnostic plot (blue data points) does not show the characteristic early time "hump" of a composite system as observed in the simulation (magenta curve). The best-fit formation parameters indicate a K of 1.99E-13 m/sec and an S_S of 3.73E-06 m^{-1}, and included an optimized P_f of 5949.3 kPa (Tab. 9.6).

Tab. 9.6: Fitted parameter and 95% confidence interval values for sequence PI_b, assuming a composite flow model.

95% Confidence Intervals				
Parameter	Units	Fitted Value	Lower Value	Upper Value
K	[m/sec]	1.99E-13	2.93E-15	1.36E-11
P_f	[kPa]	5949.3	5315.9	6582.6
S_s	[1/m]	3.73E-06	6.40E-07	2.17E-05
$K_{\_s}$	[m/sec]	6.40E-12	1.90E-13	2.15E-10
S_{s_s}	[1/m]	2.93E-06	1.81E-08	4.75E-04
$t_{\_s}$	[m]	0.049	-0.139	0.236

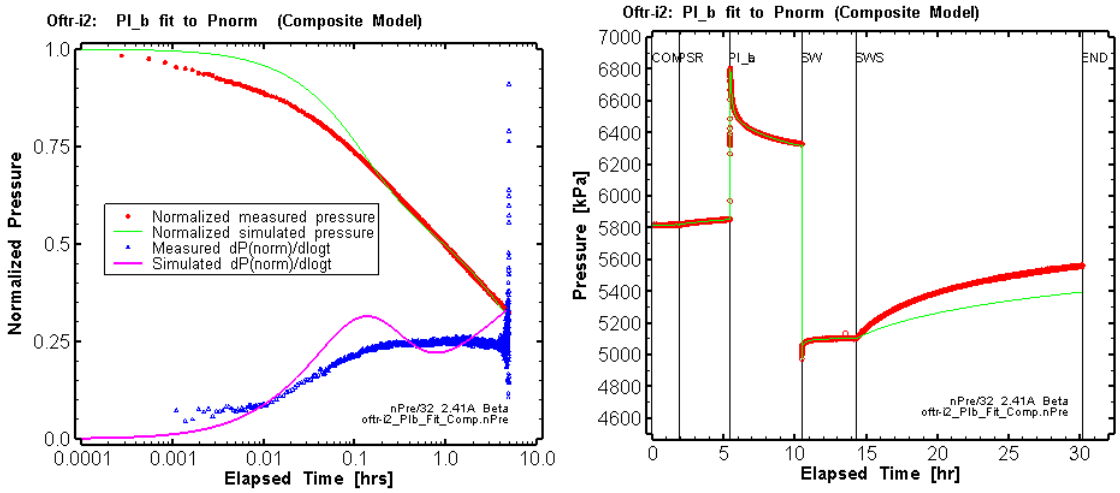

Fig. 9.6: Sequence PI_b optimization results fitted to P_{norm} showing the Ramey A diagnostic plot (left) and the Cartesian plot (right), assuming a composite skin model.

9.5.3. Homogenous Model / No Borehole History -- Ramey A Fit

The PI_b sequence was also analyzed as a stand-alone sequence assuming no prior borehole pressure history. The results of the analysis, which also assumed a homogenous flow model, are presented in Fig. 9.7. This optimized fit provides the best fit to both the diagnostic plot (Fig. 9.7, left) and the Cartesian plot (Fig. 9.7, right). The fitted formation parameters (Tab. 9.7)

indicate a K of 4.06E-12 m/sec, an S_S of 1.59E-05 m^{-1}, and a P_f of 6275.6 kPa. Compared to the analysis including borehole history (Fig. 9.5 and Tab. 9.5), the analysis without borehole history resulted in an increase in K by approximately one order of magnitude and an increase in P_f by 275 kPa. The 95% upper and lower confidence intervals presented in Tab. 9.7 show a relatively small range in each of the fitted parameters. However, the fitted P_f of 6275.6 kPa corresponds to an equivalent freshwater head of 478 m asl, which is approximately 45 m above ground surface (433 m asl).

Tab. 9.7: Fitted parameter and 95% confidence interval values for sequence PI_b, assuming a homogeneous flow model and no borehole pressure history.

95% Confidence Intervals				
Parameter	Units	Fitted Value	Lower Value	Upper Value
K	[m/sec]	4.06E-12	2.92E-12	5.64E-12
P_f	[kPa]	6275.6	6266.7	6284.5
S_s	[1/m]	1.59E-05	1.02E-05	2.49E-05

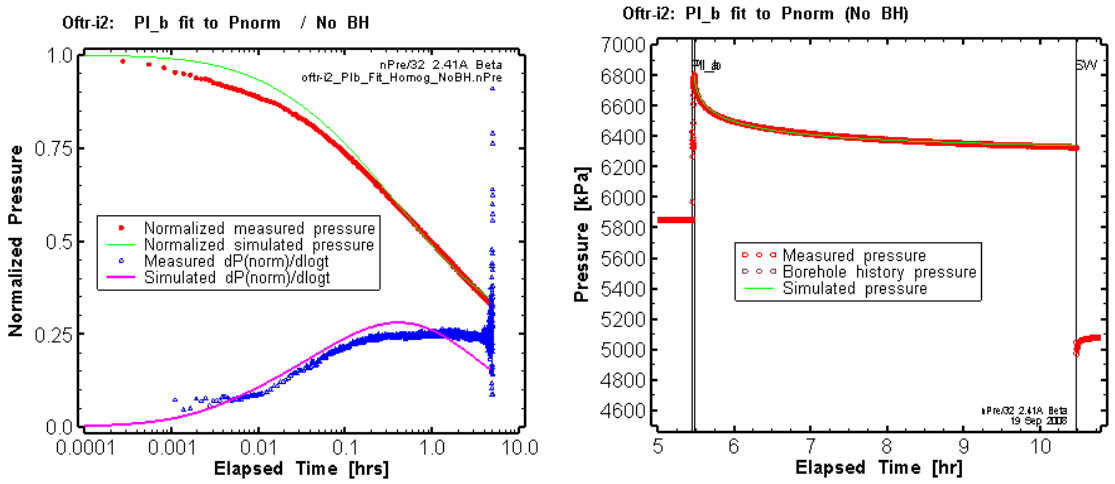

Fig. 9.7: Sequence PI_b optimization results fitted to P_{norm} showing the Ramey A diagnostic plot (left) and the Cartesian plot (right), assuming a homogeneous flow model and no borehole pressure history.

9.5.4. Summary of Pulse Test Analyses

Based on the three additional analyses conducted for the PI_b sequence, it appears that there are non-ideal conditions, such as tool compliance or borehole effects that are not accounted for. Each of the analyses with the homogeneous model yielded P_f estimates that are considered to be too high. The analysis with the composite model provided a more reasonable estimate of formation pressure, however, the observed data do not suggest the presence of a composite

system based on the diagnostic data plots. Therefore, emphasis has been placed on the analysis of the SWS for determination of the hydraulic flow parameters for this interval.

9.6. Slug-Withdrawal Recovery Analyses

As described in the QLR, a slug-withdrawal test (SW) was conducted following the PI test. During the SW, a leak was encountered whereby fluid was bypassing the slim-line packer (see QLR). Once this leak was discovered, the test interval was isolated, ending the SW and initiating the shut-in recovery phase (SWS). Analyses of the SWS sequence presented in the QLR were based on a homogenous flow model and included the PI sequence as a pulse sequence to be simulated. Additional analyses were conducted to where the PI sequence was included as part of the borehole pressure history from the drilling of the test-interval midpoint until the start of the SW sequence. In addition, the SW sequence was also included as a history file given the leakage of the slim tubing packer.

9.6.1. Homogeneous Model: Cartesian Fit SWS

Fig. 9.8 shows the results of the Cartesian fit to the SWS sequence. The upper left plot shows a good visual match to the SWS. The fitted formation parameters (Tab. 9.8) indicate a K of 2.42E-13 m/sec, a S_s of 2.94E-05 m^{-1}, and a P_f of 6072.9 kPa. The lower left plot in Fig. 9.8 shows the change in sensitivity coefficients of the three fitted parameters during the SWS sequence. This indicates that the K is the most sensitive parameter and P_f is the least sensitive parameter and is still increasing at the end of the SWS sequence. The range between the upper and lower values for the 95th percentile confidence intervals are listed in Tab. 9.8 and shown in Fig. 9.8. The two plots on the right side of Fig. 9.8 provide the 95th percentile confidence regions for the estimation of the P_f and K parameters (upper) and S_s and K parameters (lower), with the shape of the ellipse indicating the degree of correlation between the parameters. The confidence interval information indicates that the range in the fitted parameter values is relatively small for all three parameters. Fig. 9.9 presents a comparison of the residuals (measured value minus simulated value) to that of a normal distribution. The residuals are essentially normally distributed which indicates that the residuals can be attributed to measurement error and not a systematic error indicating an erroneous conceptual model. Tab. 9.8 also includes the covariance correlation matrix which indicates that the three fitting parameters are highly correlated. This correlation is also observed in Fig. 9.8 by the almost linear nature (small minor axis) of the uncertainty ellipsoids.

Tab. 9.8: Fitted parameter values, 95% confidence interval values, and covariance correlation matrices for the Cartesian fit to the SWS sequence

95% Confidence Intervals				
Parameter	Units	Fitted Value	Lower Value	Upper Value
K	[m/sec]	2.42E-13	2.18E-13	2.68E-13
P_f	[kPa]	6072.9	6053.0	6092.8
S_s	[1/m]	2.94E-05	2.58E-05	3.36E-05

Covariance/Correlation Matrix			
	K	P_f	S_s
K	1.37E-05	-7.36E-05	-3.97E-05
P_f	-0.9994	3.94E-04	2.13E-04
S_s	-0.9999	0.9989	1.15E-04

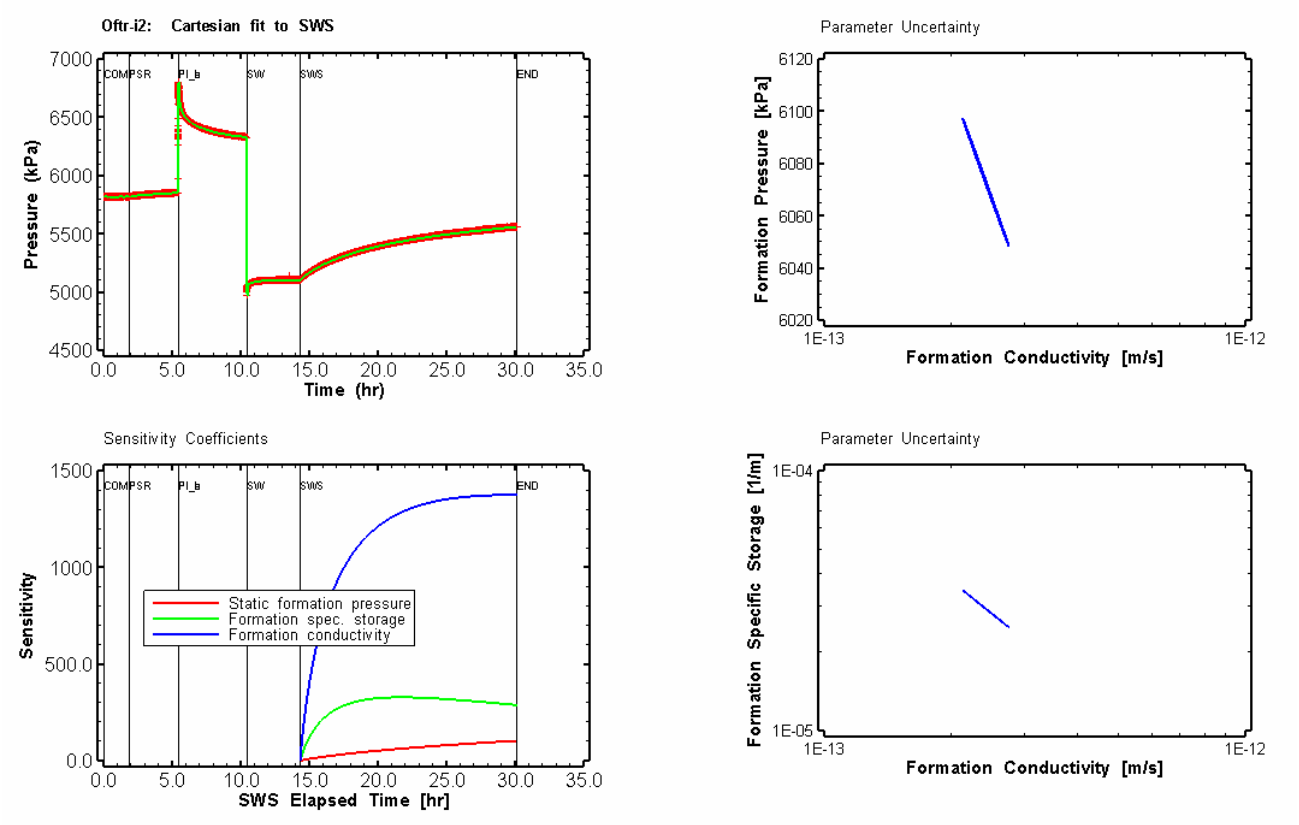

Fig. 9.8: Sequence SWS optimization results fitted to the Cartesian pressure response.

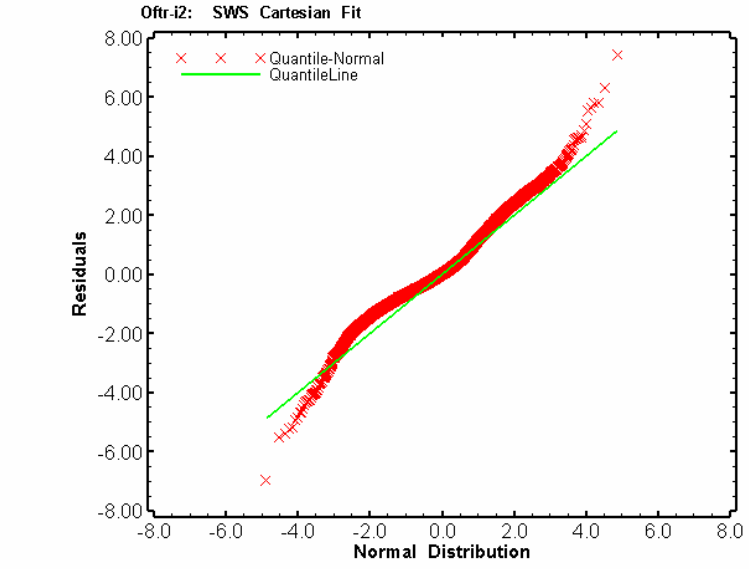

Fig. 9.9: Residual plot for the optimization of sequence SWS fitted to the Cartesian pressure response.

9.6.2. Homogeneous Model: SWS log-log diagnostic plot

Another optimized fit to the SWS was conducted on the change in pressure (dP) curve of the SWS log-log diagnostic plot. The results of this optimization are presented in Fig. 9.10, which shows the log-log plot. The optimized parameter values (Tab. 9.9) indicate a K of 4.73E-13 m/sec, a S_s of 1.53E-05 m^{-1}, and a P_f of 5862.8 kPa. Fig. 9.11 presents a comparison of the residuals (measured value minus simulated value) to that of a normal distribution, indicating that the residuals are essentially normally distributed with the residuals beyond a value of approximately 0.10 indicating a poor match to the scatter of data at early time (see log-log plot on Fig. 9.10). The range between the upper and lower values for the 95% confidence intervals on the optimized parameters are listed in Tab. 9.9 and shown in Fig. 9.12. The plots in Fig. 9.12 provide the confidence regions for the estimation of the P_f and K parameters (left) and S_s and K parameters (right), with the shape of the ellipse indicating the degree of correlation between the parameters. The confidence interval information indicates that the range in the fitted parameter values is relatively small for all three parameters. Tab. 9.9 also includes the covariance correlation matrix which indicates that the three fitting parameters are well correlated. This correlation is also observed in Fig. 9.12 by the small minor axis of the uncertainty ellipsoids.

Tab. 9.9: Fitted parameter values, 95% confidence interval values, and covariance correlation matrices for the SWS sequence fit to the dP portion of the log-log diagnostic plot.

95% Confidence Intervals				
Parameter	Units	Fitted Value	Lower Value	Upper Value
K	[m/sec]	4.73E-13	3.59E-13	6.24E-13
P_f	[kPa]	5862.8	5808.6	5917.0
S_s	[1/m]	1.53E-05	1.05E-05	2.23E-05

Covariance/Correlation Matrix			
	K	P_f	S_s
K	1.00E-04	-5.40E-04	-3.02E-04
P_f	-0.9949	2.94E-03	1.62E-03
S_s	-0.9993	0.9911	9.15E-04

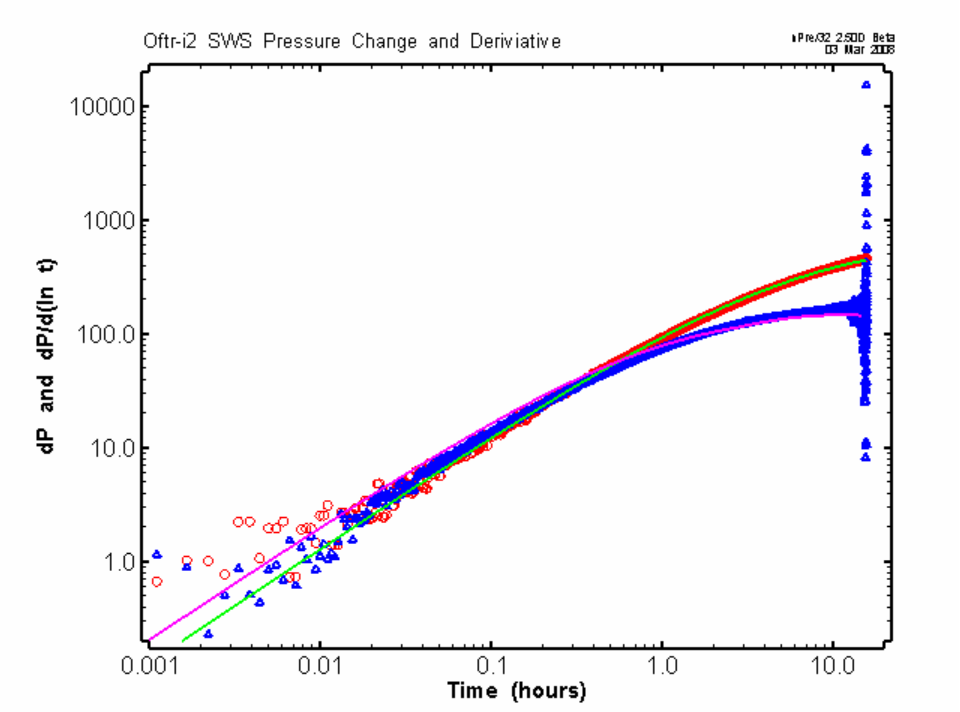

Fig. 9.10: Sequence SWS optimization results fitted to dP portion (red data circles) of the log-log diagnostic plot.

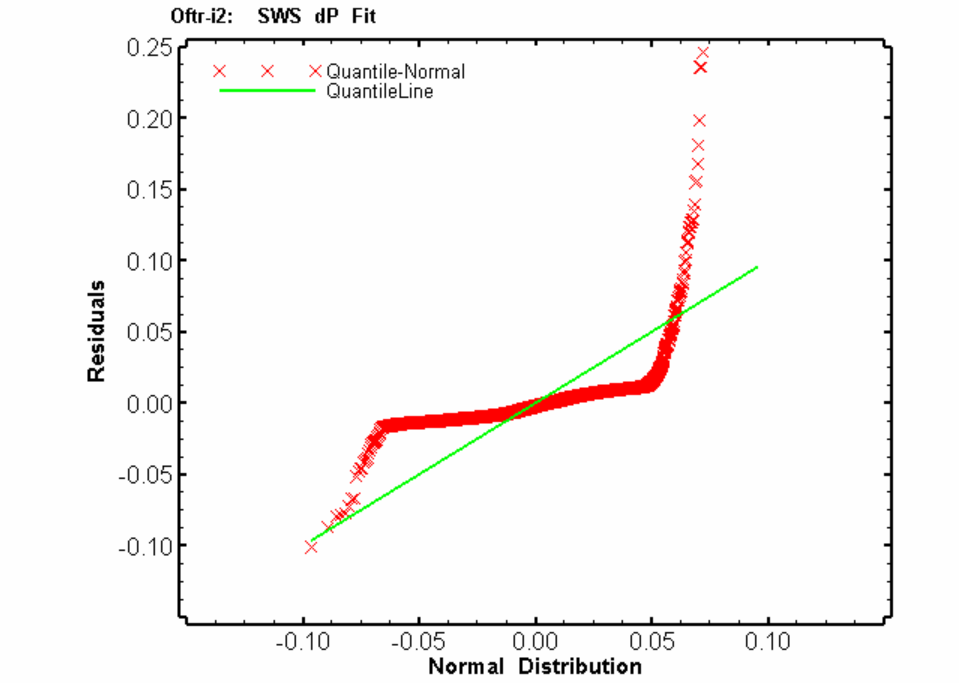

Fig. 9.11: Residual plot for the optimization of sequence SWS fitted to the dP portion of the log-log diagnostic plot.

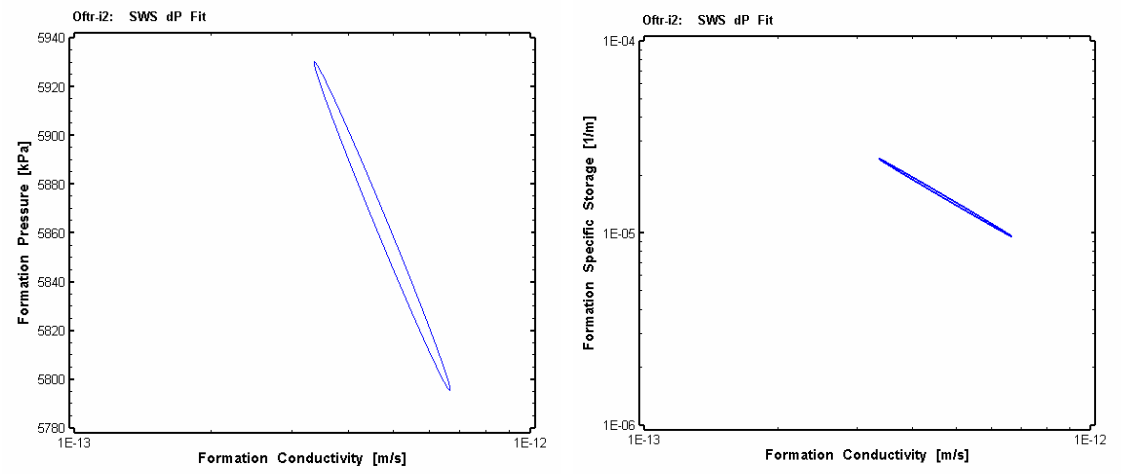

Fig. 9.12: Parameter uncertainty plots for the SWS optimization results fitted to dP portion of the log-log diagnostic plot.

9.6.3. Homogeneous Model: Perturbation Analysis for the SWS log(dP)-Fit

Following the determination of the best-fit solution to the SWS dP curve using the optimization process, a check was performed to determine if this best-fit solution was located at the global minimum of the parameter space. The uniqueness of the best-fit parameters is evaluated by means of a perturbation analysis. New starting values are assigned to each of the optimized parameters by random perturbations and the optimization analysis repeated. This process is conducted a number of times to determine if the non-linear regression algorithm continues to converge to a unique global minimum or if local minima are obscuring the results. If local minima are found, the objective function may need to be re-evaluated and re-defined such that a global minimum is found.

A set of 50 perturbation simulations were conducted using the same parameter ranges as for the previously presented single optimization. The 95% confidence intervals on the optimized parameters from the perturbation analysis are listed in Tab. 9.10 and shown in Fig. 9.13. The plots in Fig. 9.13 provide the confidence regions and the 50 values of the optimized parameters (red symbols), for the estimation of the P_f and K parameters (left) and S_s and K parameters (right). The results indicate that there is a cluster of 48 perturbations with two perturbations which lie outside of this cluster. Fig. 9.14 presents the sum of squared errors (SSE), which is a goodness-of-fit measurement, for each perturbation for the same parameter combinations as in Fig. 9.13. These plots indicate that the two outlier perturbation results have an SSE higher than those of the clustered results. The blue dot in the centre of the cluster of red symbols indicates the perturbation with the lowest SSE. A comparison of the 95% confidence interval information presented in Tables Tab. 9.9 and Tab. 9.10 and Fig. 9.12 and Fig. 9.13 indicate an agreement between the single best-fit optimized parameter set and the perturbation analysis. Thus the best-fit optimized parameter set can be considered located at the global minimum of the parameter space.

Tab. 9.10: Perturbation analysis fitted parameter values and 95% confidence interval values for the SWS sequence fit to the dP portion of the log-log diagnostic plot.

95% Confidence Intervals				
Parameter	Units	Fitted Value	Lower Value	Upper Value
K	[m/sec]	4.73E-13	3.59E-13	6.24E-13
P_f	[kPa]	5862.7	5808.5	5916.9
S_s	[1/m]	1.53E-05	1.05E-05	2.22E-05

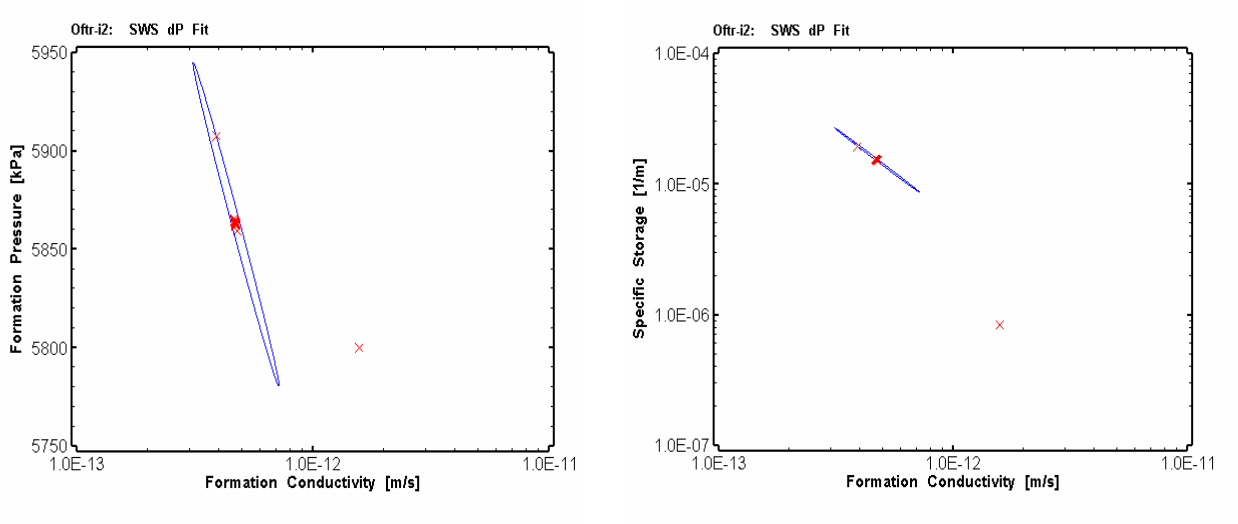

Fig. 9.13: Perturbation analysis parameter uncertainty plots for the SWS optimization results fitted to dP portion of the log-log diagnostic plot.

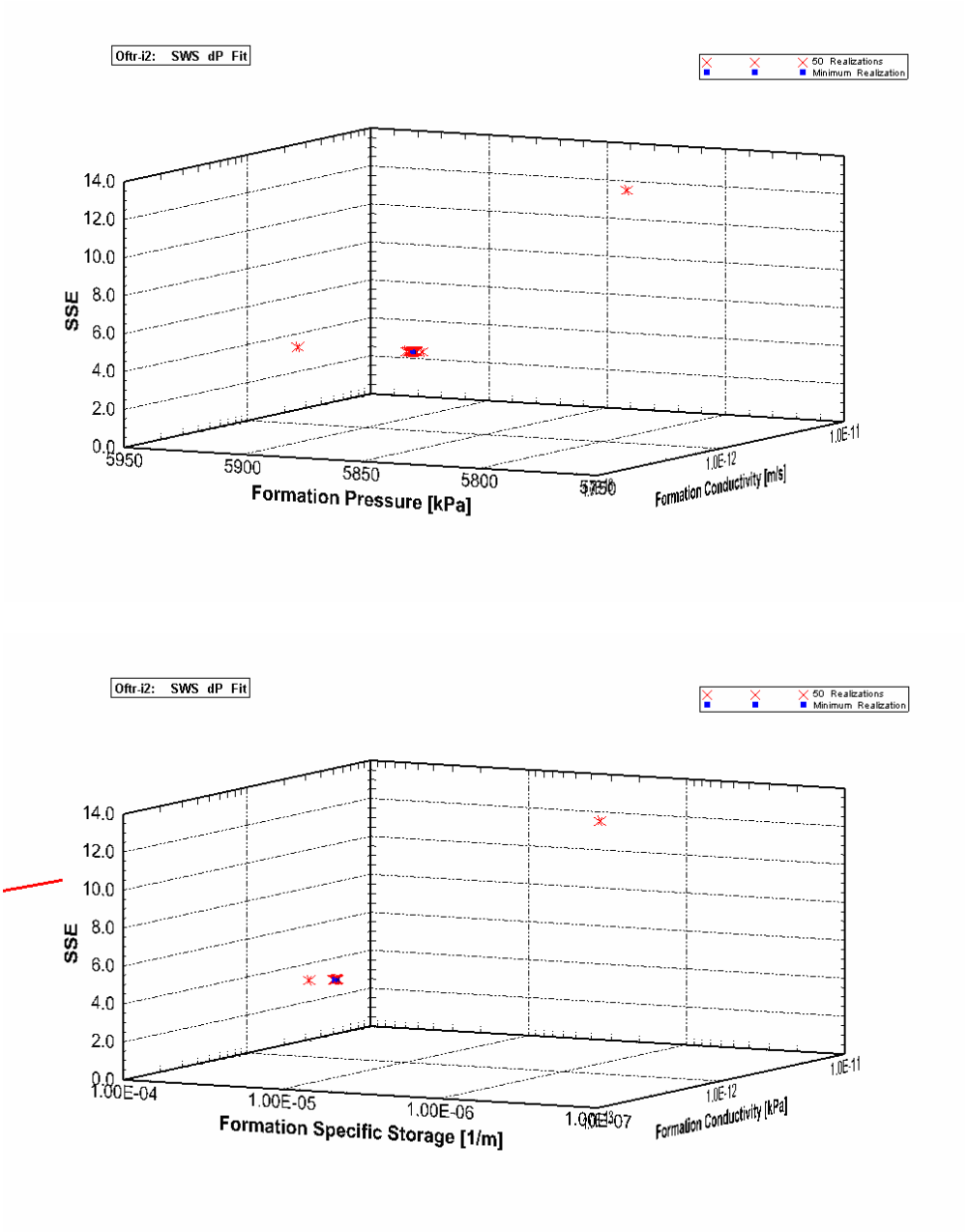

Fig. 9.14: Perturbation analysis sum of squared error (SSE) plots for the SWS optimization results fitted to dP portion (red data circles) of the log-log diagnostic plot.

9.6.4. Homogeneous Model: SWS without pre-test Pressure History

To look at the impact of the borehole pressure history on the SWS analysis, only the SW sequence was included as borehole pressure history. The SWS dP curve was used for fitting during the optimization process. Fig. 9.15 and Tab. 9.11 present the results from the optimization. The optimized parameter values were a K of 6.43E-13 m/sec, a S_s of 1.46E-05 m^{-1}, and a P_f of 5828.6 kPa, which are very similar to those presented for the analysis with the full borehole history included (Fig. 9.10 and Tab. 9.9). The range between the upper and lower values for the 95% confidence intervals on the optimized parameters is presented in Tab. 9.11 and Fig. 9.16. These results are similar to those presented in Tab. 9.9 and Fig. 9.12 and indicate that the effects of the pre-test pressure history are essentially dissipated within the formation prior to the conductance of the SW/SWS sequences.

Tab. 9.11: Fitted parameter values and 95% confidence interval values for the SWS sequence fit to the dP portion of the log-log diagnostic plot assuming no borehole pressure history.

95% Confidence Intervals				
Parameter	Units	Fitted Value	Lower Value	Upper Value
K	[m/sec]	6.43E-13	3.95E-13	1.05E-12
P_f	[kPa]	5828.6	5780.5	5876.8
S_s	[1/m]	1.46E-05	7.82E-06	2.74E-05

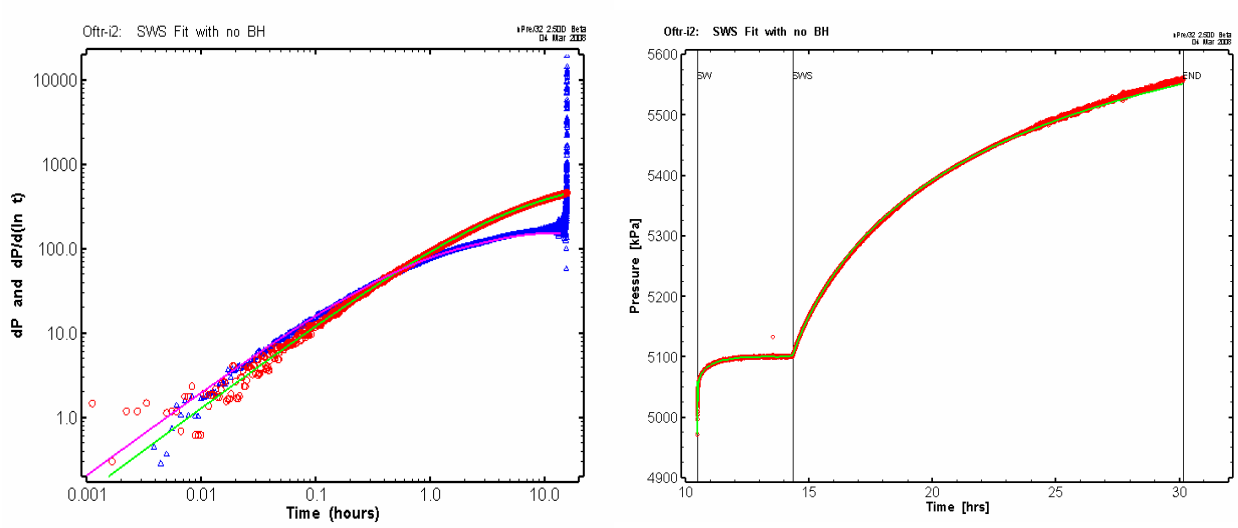

Fig. 9.15: Sequence SWS optimization results for the log-log diagnostic plot (left) and the Cartesian plot (right), based on the fit to the dP portion (red data circles) of the log-log diagnostic plot and assuming no borehole pressure history.

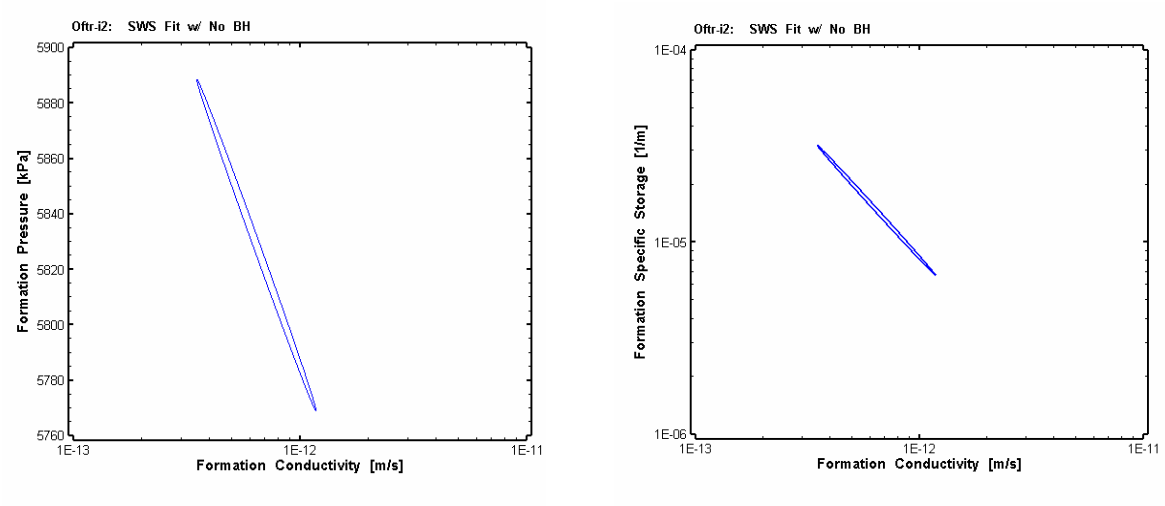

Fig. 9.16: Parameter uncertainty plots for the SWS optimization results fitted to dP portion of the log-log diagnostic plot assuming no borehole pressure history.

9.7. Summary

In addition to the simulation of the entire sequence for interval Oftr-i2, detailed analysis of the PI_b and SWS sequences were conducted. An overview of the simulation results is given in Tab. 9.13 and Fig. 9.17. Results of the analysis for PI_b indicated that non-ideal conditions had a significant impact on the observed pressure response and an estimate of the hydraulic parameters could not be made with confidence. The analysis of the SWS sequence provided a good fit to the pressure response with consistency in parameter estimates between the single optimization and the perturbation analysis. Based on the results of the perturbation analysis, the best-fit estimates were a hydraulic conductivity of 4.73E-13 m/sec (transmissivity of 2.37E-11 m^2/sec), a specific storage of 1.53E-05 1/m (storativity of 7.66E-04) and a formation pressure of 5862.7 kPa (equivalent freshwater head of 433.8 m asl) and listed in Tab. 9.12.

The detailed analysis confirmed that the homogeneous flow model fits best to the field data. Based on the results of the good quality simulation cases (tagged with the √ symbol in Tab. 9.13), the following parameter ranges were assessed:

- formation conductivity: 3.6E-13 to 5.6E-12 m/s
- specific storage: 1.0E-05 to 3.4E-05 m^{-1}
- formation pressures: 5810 to 6090 kPa, corresponding to heads from 428 to 457 m asl.

The above parameter ranges include the incertitude as indicated by the 95th percentile confidence intervals for the individual minimum and maximum values. The upper range limit for the S_S parameter listed above is higher than the plausibility range for this parameter, 1.9E-07 - 1.9E-05 m^{-1}, as defined in Section 7.3.3.

Tab. 9.12: Summary of parameter best estimates for the test interval Oftr-i2.

Parameter	Units	Best Estimated Value
K	[m/sec]	4.73E-13
T	[m^2/sec]	2.37E-11
S_s	[1/m]	1.53E-05
S	[-]	7.66E-04
P_f	[kPa]	5862.7
H	[m asl]	433.8

Level	Comments		Results
QLR best e.	Cart ESF except PI	h	
QLR	Cart ESF except PI	c	
Detailed	Cart ESF	h	
Detailed	Cart ESF, PSR as history	h	
Detailed	P(norm)-fit of PI, Ramey A Plot	h	
Detailed	P(norm)-fit of PI, Ramey A Plot	c	
Detailed	P(norm)-fit of PI, Ramey A Plot, no BH	h	
Detailed	P-fit of SWS, diag	h	
Detailed best. e.	log(dP)-fit of SWS, diag, Perturbation analysis [1)]	h	
Detailed	log(dP)-fit of SWS, diag, no BH	h	

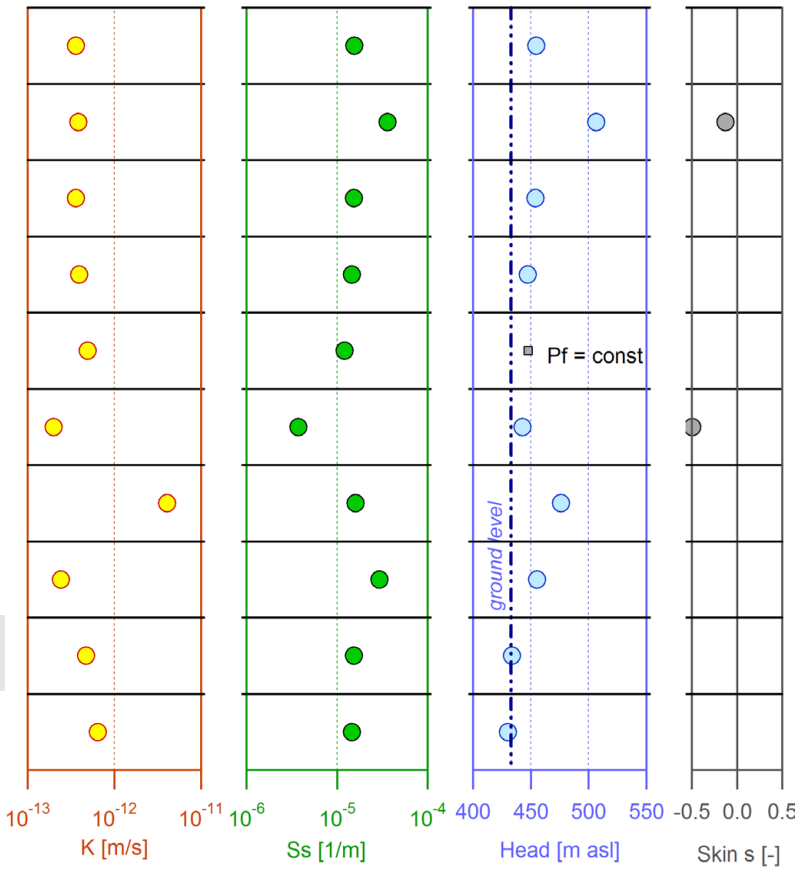

Fig. 9.17: Oftr-i2: Overview of results of inverse parameter estimations based on different models and fit configurations.

QLR = Quick Look Report
best e. = best estimate
c = composite skin model
Cart ESF = Cartesian entire sequence fit
diag = log-log diagnostic plot
h = homogeneous model
no BH the pre-test borehole pressure history is not considered
[1)] = global minimum of SSE confirmed during perturbation analysis

Tab. 9.13: Oftr-i2: Overview of results of inverse parameter estimations

Case		**K [m/s]**	**S_S [m^{-1}]**	**s [-]**	**h_s [m asl]**	**Fit quality**	**Remarks Plausibility**	
QLR Cart ESF except PI	h	3.58E-13	1.55E-05		454.5	+/-	PI not included	√
QLR Cart ESF except PI	c	3.84E-13	3.62E-05	-0.13	506.4	+	P_f above range, S_S above range, PI not included	
Detailed analysis:								
Cart ESF	h	3.61E-13	1.54E-05		454.1	+/-		√
Cart ESF, PSR as history	h	3.93E-13	1.46E-05		447.3	+/-		√
P_{norm} fit of PI	h	4.94E-13	1.21E-05		(447.8)	--	P_f assumed	
P_{norm} fit of PI	c	1.99E-13	3.73E-06	-0.50	442.6	-		
P_{norm} fit of PI, no BH	h	4.06E-12	1.59E-05		475.9	(+)		
P fit of SWS	h	2.42E-13	2.94E-05		455.2	+	S_S above range	√
log(dP) fit of SWS **best estimate**	h	4.73E-13	1.53E-05		433.8	+	Perturbation analysis [1)]	√
log(dP) fit of SWS, no BH	h	6.43E-13	1.46E-05		430.3	+		

√ = good simulation results used to assess parameter ranges
QLR = Quick Look Report
c = composite skin model
Cart ESF = Cartesian entire sequence fit
h = homogeneous model
no BH the pre-test borehole pressure history is not considered
[1)] = global minimum of SSE confirmed during perturbation analysis

10. Test Interval Oftr-i3: 550 - 600 m

Interpretation Level: Detailed analysis

10.1. Introduction

For the detailed analyses of the test interval 3, the earlier analyses presented in the QLR (Appendix C) were refined to better constrain the estimated formation properties with focus on the formation transmissivity and the static formation pressure. In the preliminary analyses presented in the QLR the estimates of specific storage were mostly at the upper limit of the expected values (S_s = 1.E-5 m^{-1}). Rock mechanic laboratory tests on core samples from the Oftringen borehole yielded values of specific storage ranging between 5.E-7 and 8.E-7 m^{-1}, which is significantly less than the lower range assumed in the optimizations. Estimates of storativity and transmissivity typically show a high degree of interdependence, rendering the optimization of formation properties, including the static formation pressure uncertain, particularly when only a single test sequence is available for inverse modelling.

.

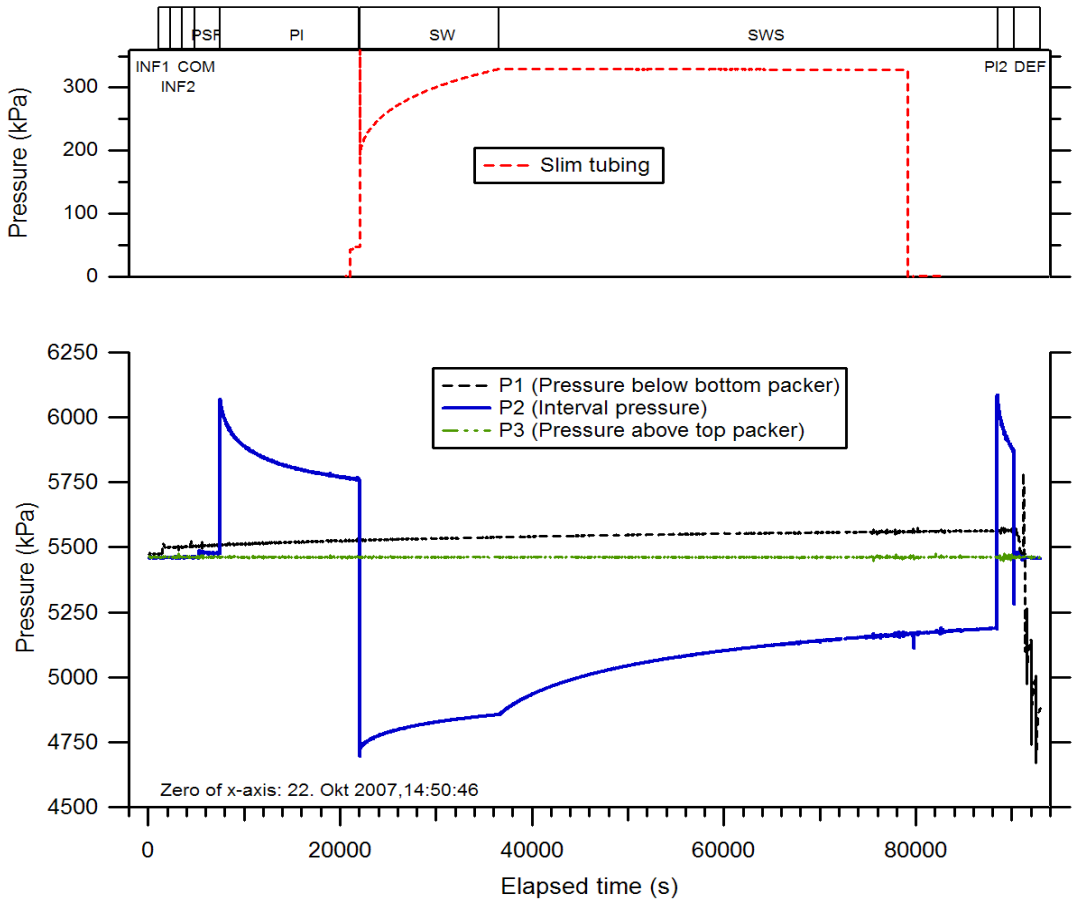

Fig. 10.1: Test Oftr-i3, 550.0 - 600.0 m: overview plot

For the detailed analysis, the validity of the underlying flow model is tested using residual analysis and the optimization for achieving the global minimum is tested using a perturbation analysis. The constraint of specific storage is tested by varying the upper range of the storativity value. Furthermore, the detailed analysis is aimed at better constraining the range in formation pressures.

Downhole pressures of the entire test sequence of Test Oftr-i3 are shown in Fig. 10.1.

10.2. Parameter Range from the QLR

The range in fitted parameters of formation conductivities (K) was from 1.4E-12 to 5.8E-12 m/s and the estimates for specific storage (S_s) ranged from 2.6E-6 to the assumed upper bound of 1.0E-5 1/m, indicating that higher values would have been possible. The estimated formation pressures indicated a relatively large range between 4600 and 6500 kPa, indicating hydraulic heads between about 345 m to 548 m asl which are significantly above and below, respectively, of the hydrostatic head of 426 m asl. The relatively high head values were based on the diagnostic fits of the PI sequences, which indicated relatively low sensitivity coefficients for the formation pressure.

The results of the QLR best estimate fit are shown in Fig. 10.2 and Tab. 10.2.

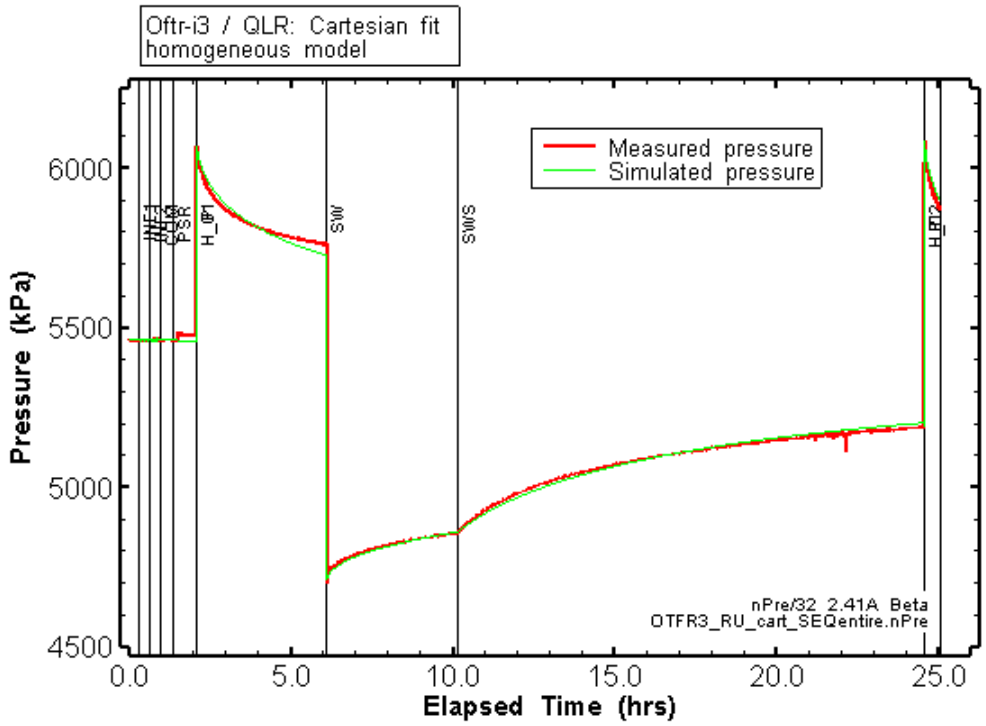

Fig. 10.2: Oftr-i3: Cartesian fit of the QLR best-estimate

Tab. 10.1: Oftr-i3: QLR best-fit parameters estimates and 95% confidence intervals for homogeneous model.

Parameter	Units	Fit Value SSE=6.04E+06	95% Confidence Intervals	
			Lower Value	Upper Value
K_fm	[m/s]	1.38E-12	1.33E-12	1.43E-12
P_fm	[kPa]	5389.7	5384.0	5395.4
Ss_fm	[1/m]	1.00E-05	9.43E-06	1.06E-05

10.3. Cases for Detailed Analyses

10.3.1. Case 1: Entire Test / Cartesian Pressure Optimization

This case corresponds to the optimization of the Cartesian pressure response of the entire test in the QLR (Fig. 12), assuming a homogeneous flow model and defining the upper bound of S_s at 1.E-5 1/m. The best fit parameters indicated relatively narrow confidence intervals (Tab. 10.2) but relatively large correlation coefficients between K and S_s (Tab. 10.3). The results in Fig. 10.3 show a good fit of the SW and SWS sequence, but indicates some deviations of the late-time PI response. The sensitivity coefficients during PI and SW-SWS are opposite indicating that they complement each other to better constrain the parameter estimate. The residual analysis indicates an overall uniform distribution which does support the underlying conceptual model.

The parameter variances (diagonal elements) are quite small (Tab. 10.3). Given that the parameters are estimated by nSights using a normalized scale of 0 to 1, the maximum theoretical variance would correspond to the case where all values in this range are equally likely represented by a uniform distribution with a theoretical variance of 1/12 or 8.33E-2. This theoretical value is much greater than the parameter variance (diagonal elements in Tab. 10.3), which indicates that the estimated parameter distributions are tightly clustered around the mean value. Moreover, the smaller the variance of the parameter, the larger is its sensitivity and the greater the likelihood that it can be properly identified from the available test response. Even though the correlation coefficients between two parameters (Tab. 10.3) are relatively high, indicating elongated confidence regions, the overall range of the confidence regions are relatively narrow (Fig. 10.3).

The diagnostic plots of the individual sequences, based on the Cartesian fit of the entire test, are shown in Fig. 10.4. The results indicate a good comparison of the measured and simulated responses for SW, SWS, and PI2, but some discrepancy for PI at late time. However, the diagnostic plots of the PI sequences do indicate a homogeneous characteristic, supporting the underlying conceptual flow model.

Tab. 10.2: Best-fit parameters estimates and 95% confidence intervals for homogeneous model.

Parameter	Units	Fit Value SSE=2.28E+06	95% Confidence Intervals		Initial Value
			Lower Value	Upper Value	
K_fm	[m/s]	1.38E-12	1.35E-12	1.41E-12	1.00E-12
P_fm	[kPa]	5389.4	5386.0	5392.9	5500.0
Ss_fm	[1/m]	1.00E-05	9.65E-06	1.04E-05	1.00E-06

Tab. 10.3: Covariance-Correlation matrix for homogeneous model (shaded cells denote correlation matrix elements).

Covariance/Correlation Matrix: Est. CART DAT_P			
	K_fm	P_fm	ss_fm
K_fm	1.423E-06	-1.782E-06	-4.565E-06
P_fm	-0.855	3.050E-06	6.41E-06
Ss_fm	-0.991	-0.814	1.491E-05

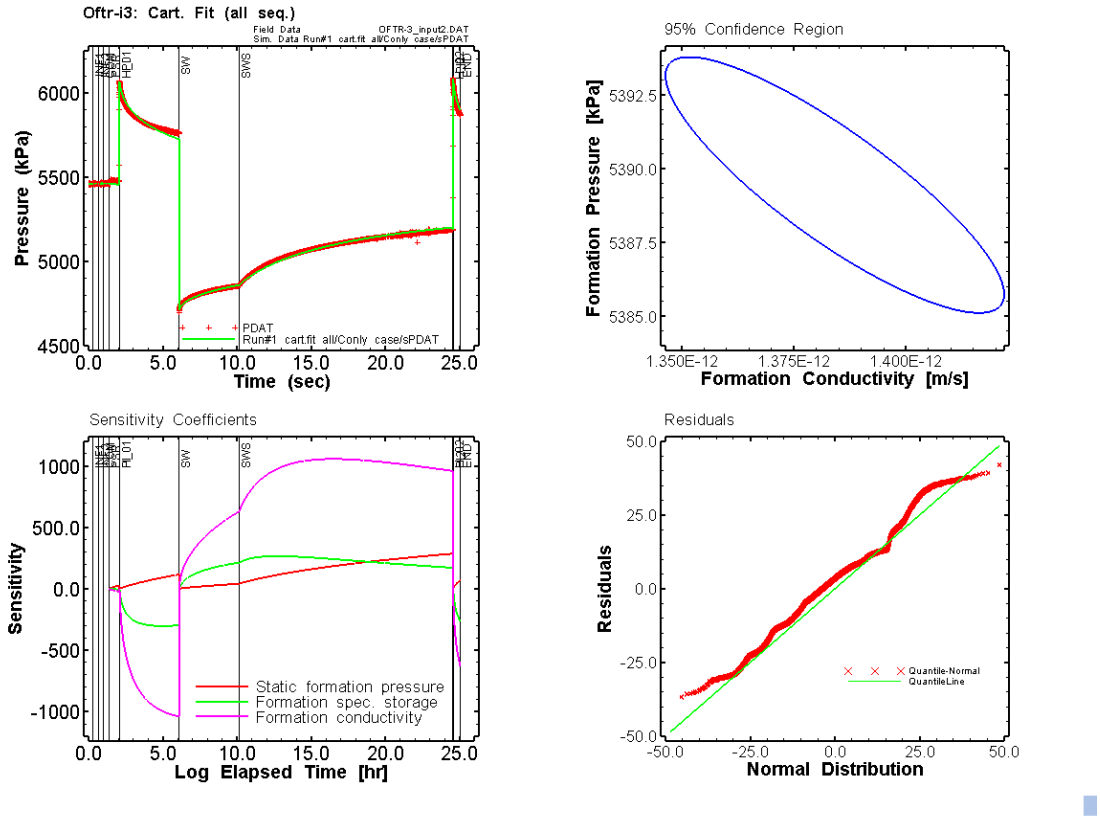

Fig. 10.3: Oftr-i3: Results from nSights inverse simulation of the Cartesian pressures of the entire test (upper left), the 95% confidence region for P_f and K (upper right), the Sensitivity (lower left), and the computed residual compared to a normal distribution (lower right).

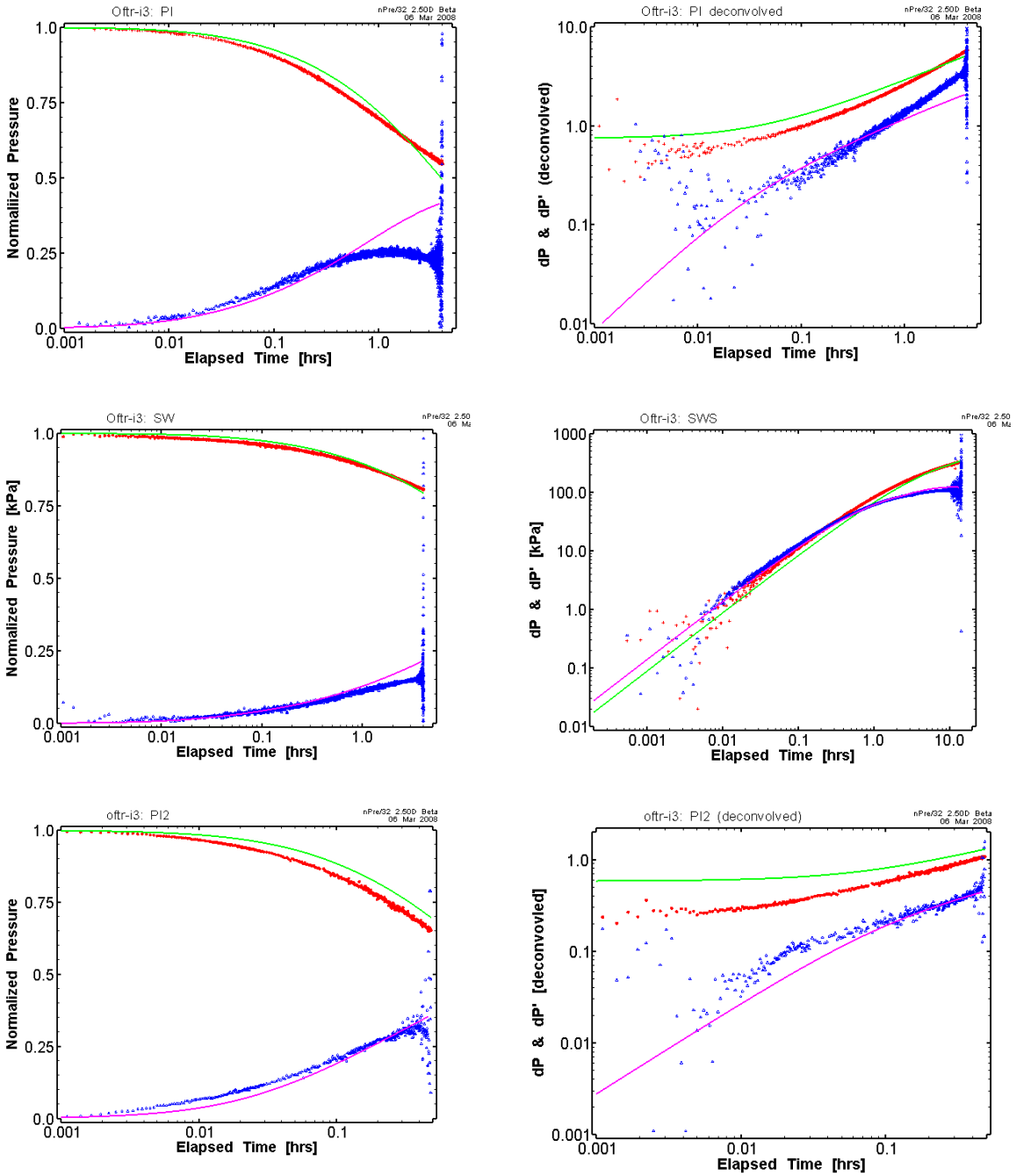

Fig. 10.4: Oftr-i3: diagnostic plots of the different sequences for the Cartesian fit of the entire test.

10.3.2. Case 2: Entire Test / Cartesian Pressure Optimization / Extended S_S Range

This case repeats the optimization of the Cartesian pressure response of the entire test but setting the upper bound for S_s to 5.E-5 1/m, in order to see if the parameter estimate converges to the value within the extended range and how the other parameter would change. The best-fit parameters and confidence intervals are summarized in Tab. 10.4 with the covariance/correlation matrix given in Tab. 10.5. Overall the fit slightly improved based on the computed Sum of Squared Errors (SSE) of 1.71E+6 (Tab. 10.4) compared to the value of SSE = 2.28E+6 for Case 1 (Tab. 10.2). The estimate of the formation conductivity noticeably decreased from a value of 1.38E-12 to 8.32E-13 m/s and the formation pressure slightly increased from 5389 kPa to 5455 kPa. The estimate of specific storage converged to a value of 2.2E-5 1/m within the given range. More importantly, the 95% confidence intervals for each parameter (Tab. 10.4) are above (Ss_fm, P_fm) or below (K_fm) the confidence intervals for Case 1 (Tab. 10.2). The statistical analysis indicate similar correlations as shown in the shape of the confidence regions (Fig. 10.5), whereby the residuals show a slight improvement compared to that in Case 1 (Fig. 10.3).

Tab. 10.4: Best-fit parameters estimates and 95% confidence intervals for homogeneous model.

Parameter	Units	FitValue	95% Confidence Intervals		Initial Value
		SSE=1.71E+06	Lower Value	Upper Value	
K_fm	[m/s]	8.32E-13	8.12E-13	8.53E-13	1.00E-12
P_fm	[kPa]	5455.2	5451.9	5458.50	5500.0
Ss_fm	[1/m]	2.20E-05	2.12E-05	2.29E-05	1.00E-06

Tab. 10.5: Covariance-Correlation matrix for homogeneous model (shaded cells denote correlation matrix elements).

Covariance/Correlation Matrix: Est. CART DAT_P			
	K_fm	P_fm	ss_fm
K_fm	1.768E-06	-1.690E-06	-4.058E-06
P_fm	-0.774	2.699E-06	3.690E-06
Ss_fm	-0.994	0.732	9.424E-06

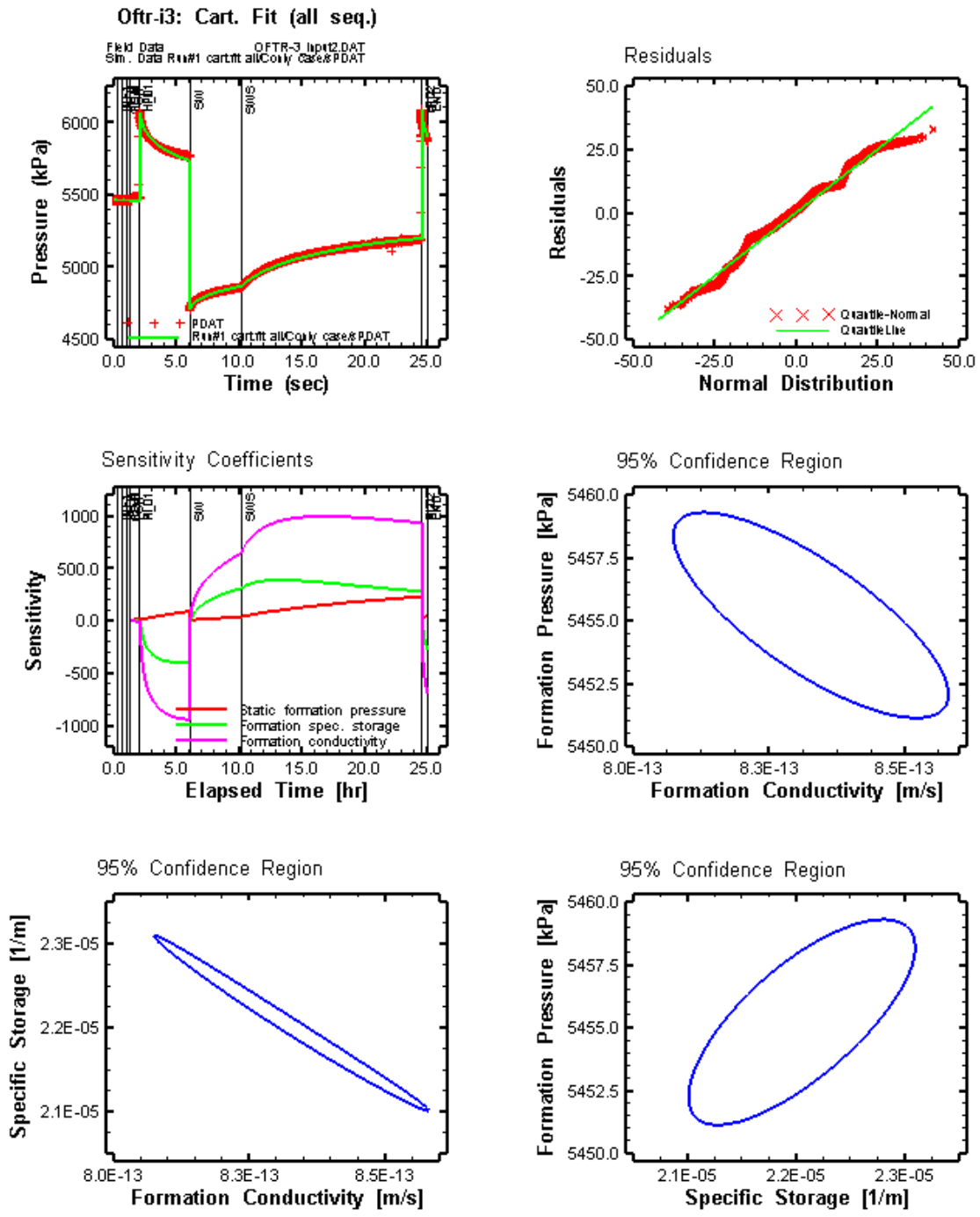

Fig. 10.5: Oftr-i3: homogeneous model: fit plots, residual and sensitivity plots and confidence regions of joint parameters.

Results from nSights inverse simulation of the Cartesian pressures of the entire test (upper left), the computed residual compared to a normal distribution (lower right), the Sensitivity (middle left), the 95% confidence region for P_f and K (middle right), the 95% confidence region for S_s and K (lower left), and the 95% confidence region for P_f and S_s (lower right).

A perturbation analysis was performed to test if the estimated parameters and differences were associated with a local minimum or represent a global minimum of the optimization. This was done by repeating the optimization with different starting values for the different parameters. For this case 100 optimization runs were performed for which individual fits were computed. Two different optimization algorithms were used: (a) Levenberg-Marquardt, and (b) Simplex method. The results are plotted as three dimensional plot of the SSE as a function of the best-fit values of formation conductivity and formation pressure (Fig. 10.6). In addition, the best-fit results from Case 2 are indicated as red squares for comparison with the distribution from the perturbation runs. Also indicated are the 95% confidence regions for Case 2 (Fig. 10.5) showing that all the best-fit values from the perturbation fall well within the 95% confidence region from the single optimization (Fig. 10.6).

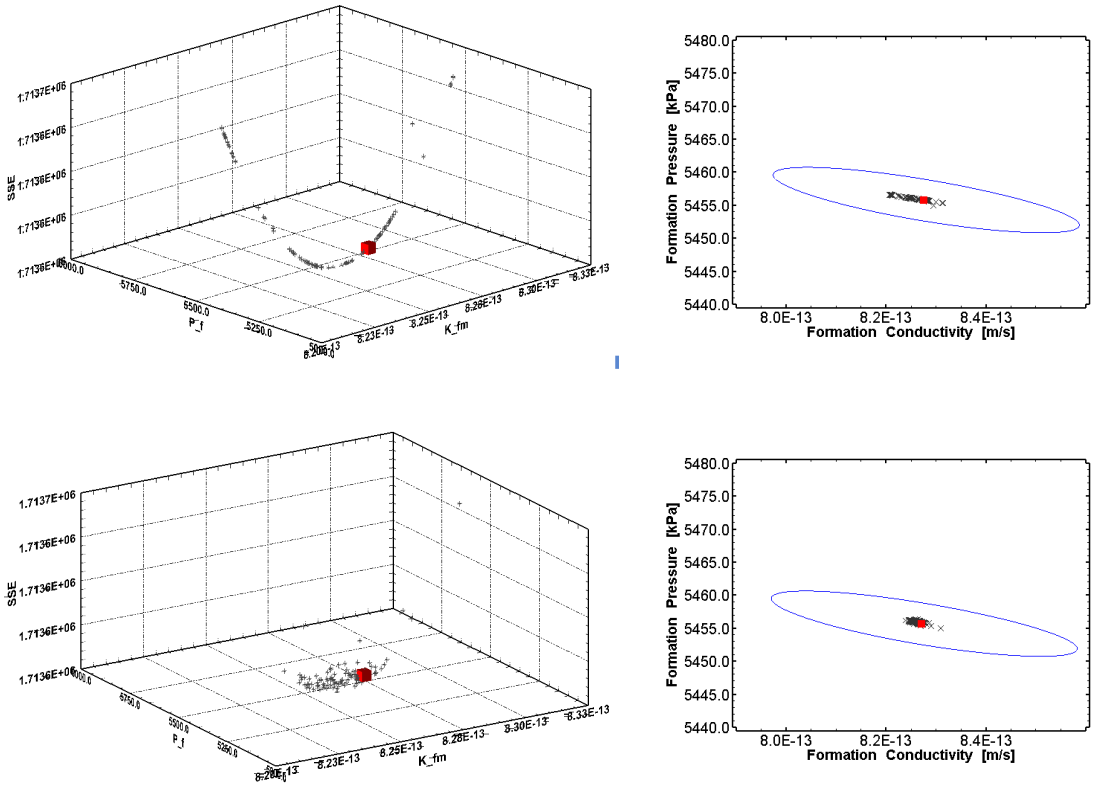

Fig. 10.6: Oftr-i3: Results from perturbation analysis of the nSights inverse simulation of the Cartesian pressures of the entire test.

Left: multiple realizations with computed SSE (sum of squared errors) versus P_f and K_fm estimates. Right: estimates of P_f and K_fm and associated confidence region for best-fit realization. The red symbol indicates the best-fit realization (lowest SSE). Top uses Levenberg-Marquardt optimization, Bottom uses Simplex optimization.

10.3.3. Case 3: SW-SWS-PI2 / Cartesian Pressure Optimization

The third case evaluated the impact of the PI sequence on the overall parameter estimates. As indicated above, the Cartesian fit of the entire test resulted in fits for PI that differed from the measured data, suggesting some phenomena that were not accounted for the conceptual model. By defining the PI response as a history curve, the measured response was explicitly incorporated in the transient response and in the fit of the SW-SWS-PI2 sequence. The results of the optimization are summarized in Tab. 10.6 and Tab. 10.7 and shown in Fig. 10.7. The overall fit improved from a value SSE = 1.71E+6 to a value of SSE = 3.68E+5. The formation parameters indicated slightly higher values for formation conductivity of 2.0E-12 m/s and lower formation pressure of 5242 kPa. The estimate for specific storage decreased from 2.0E-5 to 9.0E-6 1/m. All the parameter correlations increased to above 0.9, but the parameter variance (diagonal elements) are still relatively low resulting in a narrow range of the confidence intervals. Furthermore, the range in the residuals narrowed and followed the uniform distribution (Fig. 10.7). The corresponding diagnostic plots are shown in Fig. 10.8, indicating good fits for SWS and PI2 but some discrepancies for SW.

Tab. 10.6: Best-fit parameters estimates and 95% confidence intervals for homogeneous model.

Parameter	Units	Fit Value	95% Confidence Intervals		Initial Value
		SSE=3.68E+05	Lower Value	Upper Value	
K_fm	[m/s]	2.04E-12	1.99E-12	2.09E-12	1.00E-12
P_fm	[kPa]	5242.7	5239.1	5246.3	5500.0
Ss_fm	[1/m]	9.02E-06	8.71E-06	9.34E-06	1.00E-06

Tab. 10.7: Covariance-Correlation matrix for homogeneous model (shaded cells denote correlation matrix elements).

Covariance/Correlation Matrix: Est. CART DAT_P			
	K_fm	P_fm	ss_fm
K_fm	1.71E-06	-2.26E-06	-4.96E-06
P_fm	0.962	3.22E-06	6.41E-06
Ss_fm	-0.996	-0.940	1.45E-05

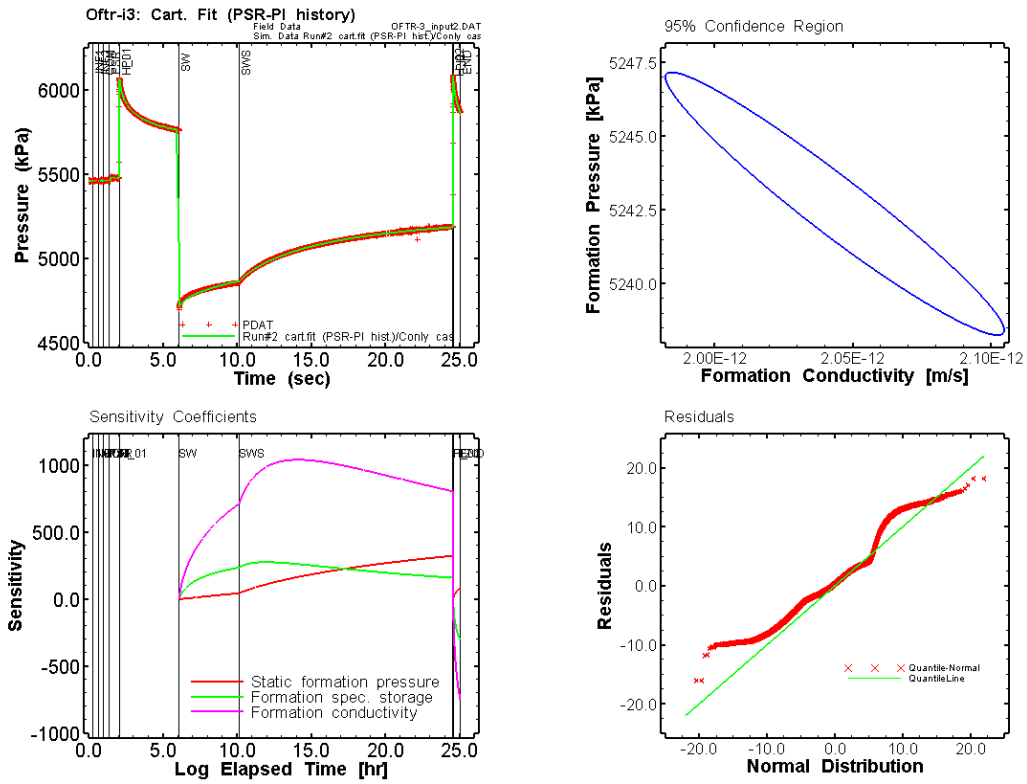

Fig. 10.7: Oftr-i3: Results from nSights inverse simulation of the Cartesian pressures of the entire test (upper left), the 95% confidence region for P_f and K (upper right), the sensitivity (lower left), and the computed residual compared to a normal distribution (lower right).

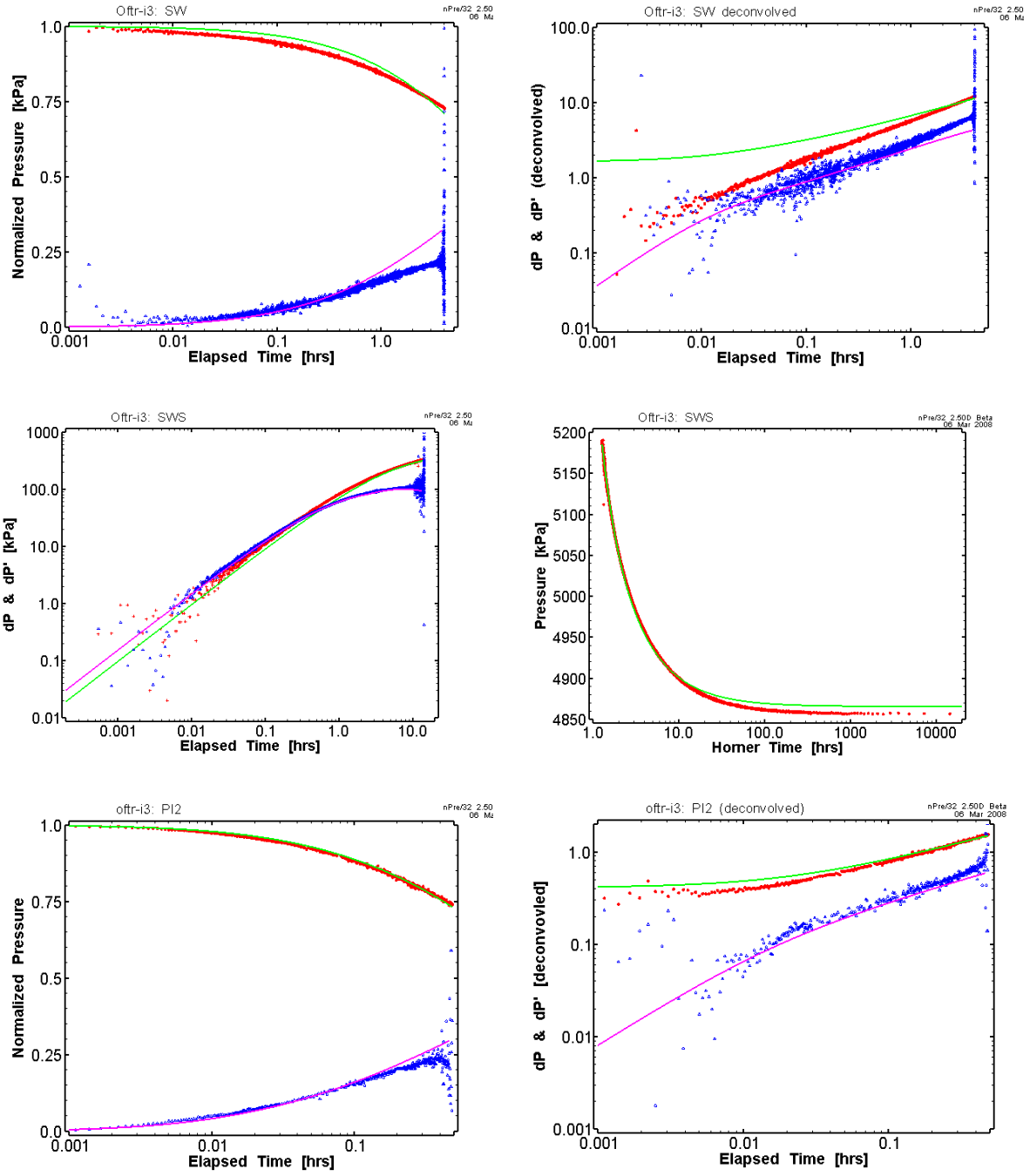

Fig. 10.8: Oftr-i3: diagnostic plots of the different sequences for the Cartesian fit of the SW – PI2 sequence.

10.3.4. Case 4: Entire Test / Cartesian Pressure Optimization / Low Ss

The fourth case attempted to force the optimization to a specific storage value of less than 1.E-6, based on the range of the laboratory data from Oftringen cores. The results of the best fit parameters are summarized in Tab. 10.8. The optimization yielded a significantly higher value of SSE = 1.0E+7 and the residuals showed a wider range and more deviation from a uniform distribution (Fig. 10.9). More importantly, a covariance analysis could not be performed because the estimate for S_s was consistently at the upper boundary. Overall, the parameter estimates yielded somewhat higher conductivities of 4.0E-12 m/s and slightly higher formation pressures of 5296 kPa compared to those for Case 2 (Tab. 10.4).

Tab. 10.8: Best-fit parameters estimates and 95% confidence intervals for homogeneous model.

Parameter	Units	Fit Value SSE=1.01E+07	95% Confidence Intervals		Initial Value
			Lower Value	Upper Value	
K_fm	[m/s]	3.98E-12	NA	NA	1.00E-12
P_fm	[kPa]	5296.3	NA	NA	5500.0
Ss_fm	[1/m]	1.00E-6	NA	NA	1.00E-06

Covariance-Correlation matrix could not be computed

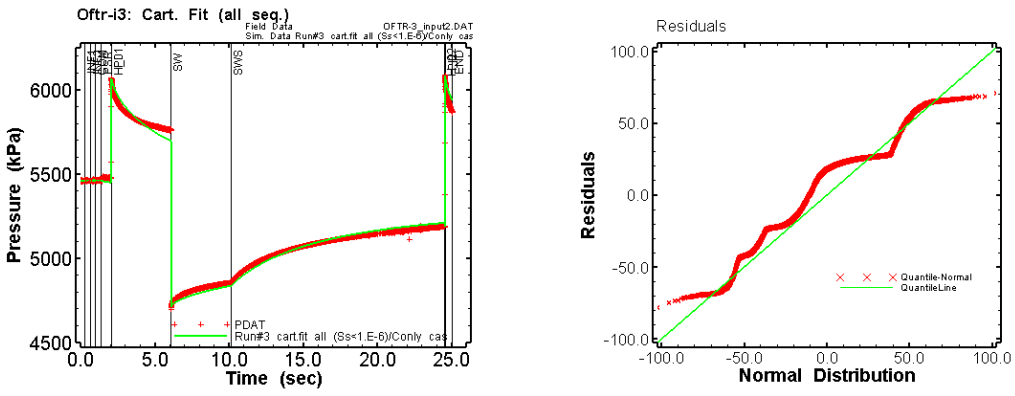

Fig. 10.9: Oftr-i3: Results from nSights inverse simulation of the Cartesian pressures of the entire test (left), and the computed residual compared to a normal distribution (right).

10.3.5. Case 5: Composite Flow Model (Skin)

The final case assumed a composite flow model. For the optimization, the starting values for K and S_s were the same from the inner and outer zone (i.e., homogeneous). The results of the optimization are summarized in Tab. 10.9 and Tab. 10.10. The estimated conductivity values for the inner skin zone (K_s) and for the outer undisturbed formation (K_fm) show only a relatively small difference, whereas the specific storage of the skin zone (Ss_s) and of the outer zone (Ss_fm) indicate more than two orders of magnitude difference. The value for the outer zone was at the lower bound of realistic values (Ss_fm = 1.E-7 1/m) and Ss_s of 2.2E-5 1/m corresponded to the specific storage value for the homogeneous model for Case 2 (Tab. 10.4). For several of the fitted parameters (K_fm, P_fm, Ss_s) no confidence intervals could be computed, because they showed correlation coefficients of 1, indicating complete interdependence. For these parameters, the computed variances were also significantly greater than the theoretical value (Tab. 10.10) indicating that these estimates were not be properly identified because of the negligible sensitivity coefficients in Fig. 10.10.

The overall fit (Fig. 10.10) was comparable to that for the homogeneous model (Fig. 10.5) and indicated approximately a uniform residuals distribution. However, the statistical analysis of the optimization showed negligibly low sensitivity coefficients which indicated that the test could not significantly perturb the outer zone to enable reasonably constrained estimates of undisturbed formation parameters. The diagnostic plots of the individual sequences did not indicate distinct characteristics of a composite model, due to the fact that there was only a relatively small permeability contrast between the inner and outer zone combined with the limited sensitivity of the outer zone parameters.

Tab. 10.9: Best-fit parameters estimates and 95% confidence intervals for composite model.

Parameter	Units	Fit Value SSE=1.45E+06	95% Confidence Interval		
			Lower Value	Upper Value	Initial Value
K_fm	[m/sec]	5.66E-13	NA	NA	1.00E-12
K_s	[m/sec]	8.19E-13	7.58E-13	8.86E-13	1.00E-12
P_fm	[kPa]	5450.2	NA	NA	5500.0
Ss_fm	[1/m]	1.00E-07	NA	NA	1.00E-06
Ss_s	[1/m]	2.20E-05	1.99E-05	2.43E-05	1.00E-06
t_s	[m]	1.73E-01	1.47E-01	1.99E-01	1.00E-01

Tab. 10.10: Covariance-Correlation matrix for composite model.

	K_fm	K_s	P_fm	ss_fm	Ss_s	t_s
K_fm	1.80E+02	5.86E-02	1.96E+01	-8.50E+02	-7.68E-02	1.51E-01
K_s	7.69E-01	3.21E-05	6.36E-03	-2.79E-01	-4.50E-05	2.75E-05
P_fm	1.00E+00	7.71E-01	2.12E+00	-9.21E+01	-8.36E-03	1.58E-02
ss_fm	-1.00E+00	-7.78E-01	-1.00E+00	4.01E+03	3.67E-01	-7.14E-01
ss_s	-7.16E-01	-9.94E-01	-7.18E-01	7.26E-01	6.39E-05	-2.00E-05
t_s	4.37E-01	1.88E-01	4.22E-01	-4.37E-01	-9.71E-02	6.65E-04

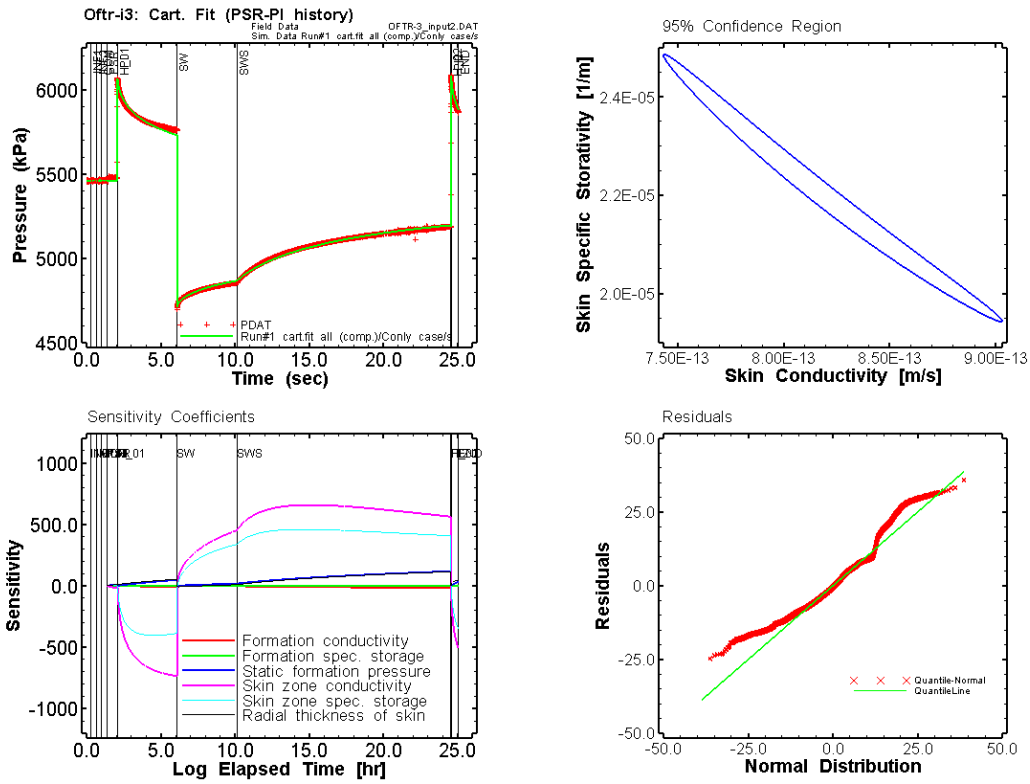

Fig. 10.10: Oftr-i3: Results from nSights inverse simulation of the Cartesian pressures of the entire test assuming a composite model.

Upper left: Cartesian plot. Upper right: 95% confidence region for K_s and Ss_s. Lower left: sensitivity plot. Lower right: computed residual compared to a normal distribution. Confidence regions for K_fm and Ss_fm could not be computed due to high correlation.

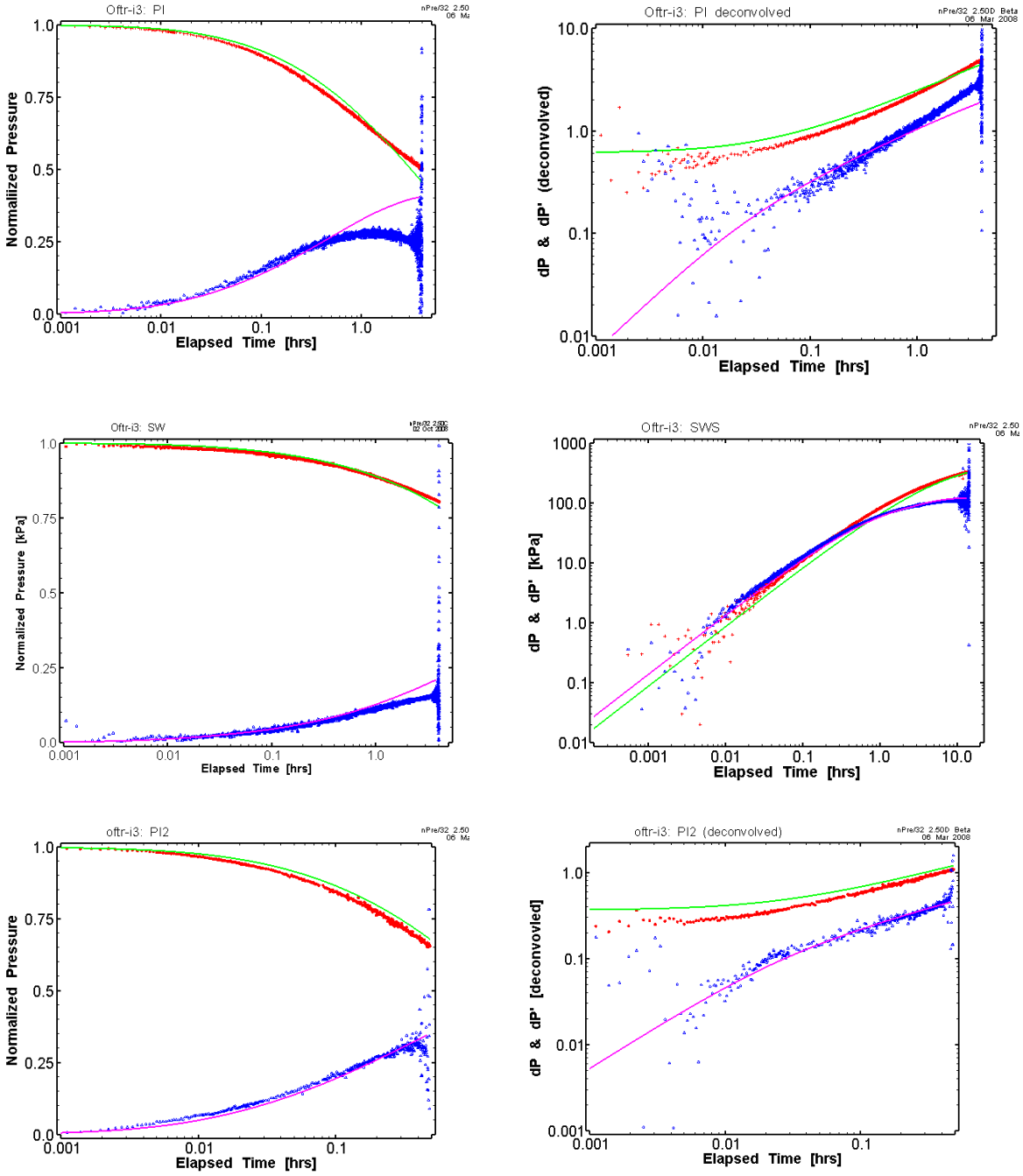

Fig. 10.11: Oftr-i3: diagnostic plots of the different sequences for the Cartesian fit of the entire test, assuming a composite model.

10.3.6. Summary of the Detailed Analyses

The results of the detailed analyses confirmed the homogeneous flow model. Based on the results of the good quality simulation cases (tagged with the √ symbol in Tab. 11.10), the following parameter ranges were assessed:

- formation conductivity: 8E-13 to 4E-12 m/s
- specific storage: 8.0E-6 to 2.3E-5 m^{-1}
- formation pressure: 5230 to 5460 kPa (with corresponding heads 409 - 433 m asl).

The above parameter ranges include (where applicable) the incertitude as indicated by the 95th percentile confidence intervals for the individual minimum and maximum values.

The statistical analyses of the different optimization cases indicated a relatively narrow range in formation properties which, for the homogeneous model, were characterized by low variance and relatively high sensitivity coefficients. Even though formation conductivity and specific storage were highly correlated (R>0.9), the uncertainty with the mutual variation of conductivity and specific storage is relatively small. However, the optimization of all the cases examined yielded significantly higher values of specific storage compared to those derived from geomechanical tests on cores from the Oftringen borehole. Even the composite model yielded high values for specific storage of the inner zone. The low value estimated for the outer zone (Ss_fm = 1.E-7 1/m) was not considered realistic, because of the lack of sensitivity and high variance of the outer zone parameters indicating that they could not be properly identified.

The above indicated formation pressure range seems too small given the known incertitude inherent in test performance. Therefore, the above given uncertainty range for the formation pressure parameter (derived from P_f values of good quality simulation cases) is discarded. Based on expert judgement, also taking into account the results from the QLR, the following range is given:

- formation pressure: 5100 to 5600 kPa (with corresponding heads 396 - 447 m asl).

Level	Comments	
QLR best e.	Cart ESF	h
Detailed *case 1*	Cart ESF, limited S_S range	h
Detailed *case 2*	Cart ESF, extended S_S range, perturbation a.	h
Detailed best estimate	Cart SW-SWS-PI fit *case 3*	h
Detailed *case 4*	Cart ESF - low S_S	h
Detailed *case 5*	Cart ESF	c

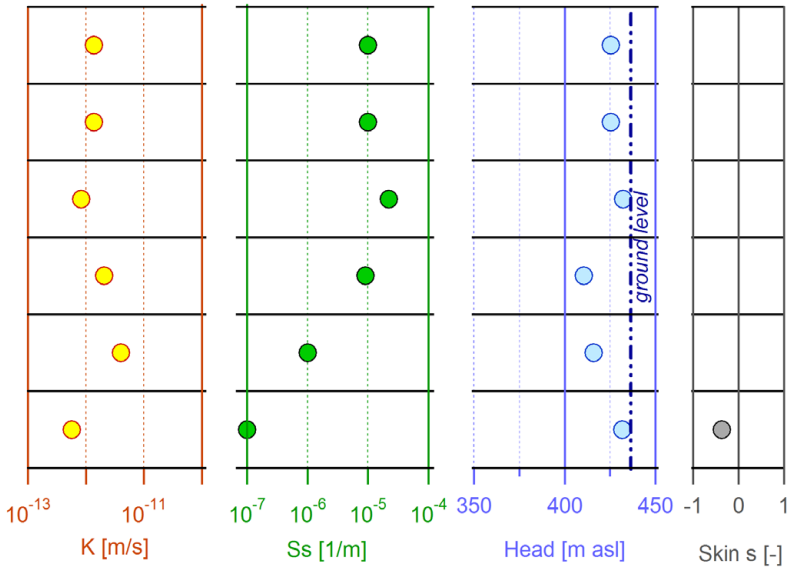

Fig. 10.12: Oftr-i3: Overview of results of inverse parameter estimations based on different models and fit configurations (abbreviations see Tab. 10.11).

Tab. 10.11: Oftr-i3: Overview of results of inverse parameter estimations

Case		K [m/s]	S_S [m^{-1}]	s [-]	h_s [m asl]	Fit quality	Remarks Plausibility	
QLR Cart ESF	h	1.38E-12	1.00E-05		425.5	+		
Detailed analysis:								
Cart ESF, limited S_S range	h	1.38E-12	1.00E-05		425.5	(+)	Poor match of PI2	
Cart ESF, extended S_S range, perturbation a.	h	8.32E-13	2.20E-05		432.2	+		√
Cart SW-SWS-PI fit	h	2.04E-12	9.02E-06		410.6	++	**best estimate**	√
Cart ESF - low S_S	h	3.98E-12	1.0E-06		416.0	(+)		√
Cart ESF	c	5.66E-13	1.0E-07	-0.37	431.7	++	Unrealistic low S_S; skin not confirmed in diag. plots	

√ = good simulation results used to assess parameter ranges
QLR = Quick Look Report
c = composite skin model
Cart ESF = Cartesian entire sequence fit
Diag. Diagnostic plot, composite fit of dP and dP'
h = homogeneous model

11. Test Interval Oftr-i4: 500 - 550 m

Interpretation Level: Standard "plus" analysis

11.1. Introduction

For the Standard Interpretation of the test interval Oftr-i4, the earlier analyses presented in the QLR were refined to better constrain the estimated formation properties with focus on the formation hydraulic conductivity and transmissivity. The preliminary analyses presented in the QLR suggested a very low hydraulic conductivity. The estimates of specific storage were mostly within the expected range. However, the best fits of the longer test periods (SWS sequence and entire test sequence) suggested very low static formation heads: 290.7 m asl for the SWS sequence fit and 349 m asl for the entire sequence fit, respectively. These heads are significantly lower than the estimated heads of the more transmissive intervals Oftr-i1 and Oftr-i6 which are situated below and above Oftr-i4. The hydraulic head of interval Oftr-i4 is expected within the range defined by the higher transmissive zones of the NOK-EWS borehole, above and below of Oftr-i4.

Estimates of formation storage and hydraulic conductivity typically show a high degree of interdependence, rendering the optimization of formation properties, including the static formation pressure uncertain, particularly when only a single test sequence is used for inverse modelling.

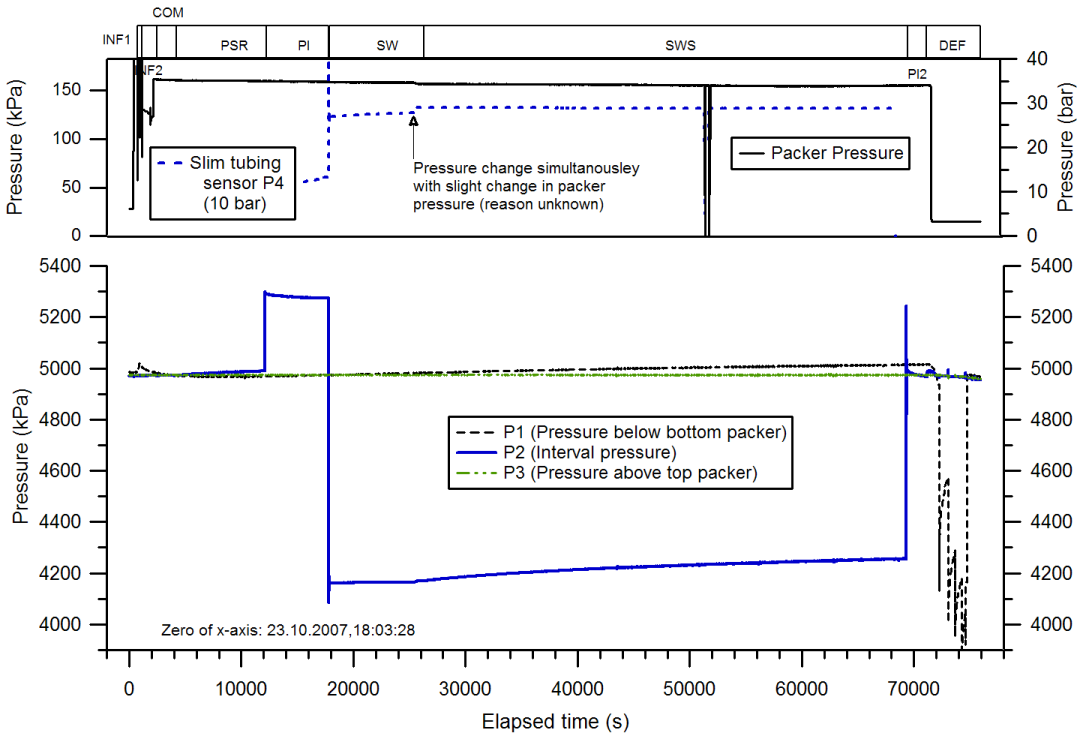

Fig. 11.1: Test Oftr-i4, 500.0 - 550.0 m: overview plot

11.2. Parameter Range and Best Estimates from QLR

At QLR stage, the individual test events resulted in significant range of estimated formation parameters based on a homogeneous flow model. The hydraulic conductivity estimates from inverse parameter optimizations varied between 1.3E-14 m/s and 1.8E-13 m/s. The specific storage estimates ranged from 2.1E-7 m^{-1} to 3.2E-6 m^{-1}. The matched static formation pressures ranged between 3576 to 5933 kPa, corresponding to hydraulic heads 291 - 531 m asl. This range is significantly larger than the plausibility range (4484 - 5465 kPa corresponding to 383 - 483 m asl.

The best estimates of the QLR are based on the Cartesian fit of the entire test sequence using a homogeneous flow model (Tab. 11.1; details in Appendix D). The measured and simulated Cartesian pressure and the residual distributions for the homogenous model (QLR) are shown in Fig. 11.2. The residual plot (right graph in Fig. 11.2) suggests that the residuals are essentially normally distributed which indicates the absence of a systematic error and supports the conceptual model.

Incertitude with regard to the P_f parameter

Considering the very low hydraulic conductivity of test interval Oftr-i4 with a hydraulic conductivity smaller than 1E-12 m/s, the duration of the individual test sequences are too short to obtain a reliable estimate of static formation pressure. The sensitivity plot at bottom right in Fig. 11.2 shows a very low sensitivity to the formation pressure parameter. Additional analyses focus on testing more models using a plausible range for the P_f parameter.

Tab. 11.1: QLR Oftr-i4: Best-fit parameters estimates and 95% confidence intervals for homogeneous model.

Parameter	Units	Fit Value SSE=2.72E+05	95% Confidence Intervals	
			Lower Value	Upper Value
K_fm	[m/s]	1.92E-14	1.81E-14	2.04E-14
P_fm	[kPa]	4384	4357	4411
ss_fm	[1/m]	1.79E-06	1.64E-06	1.95E-06

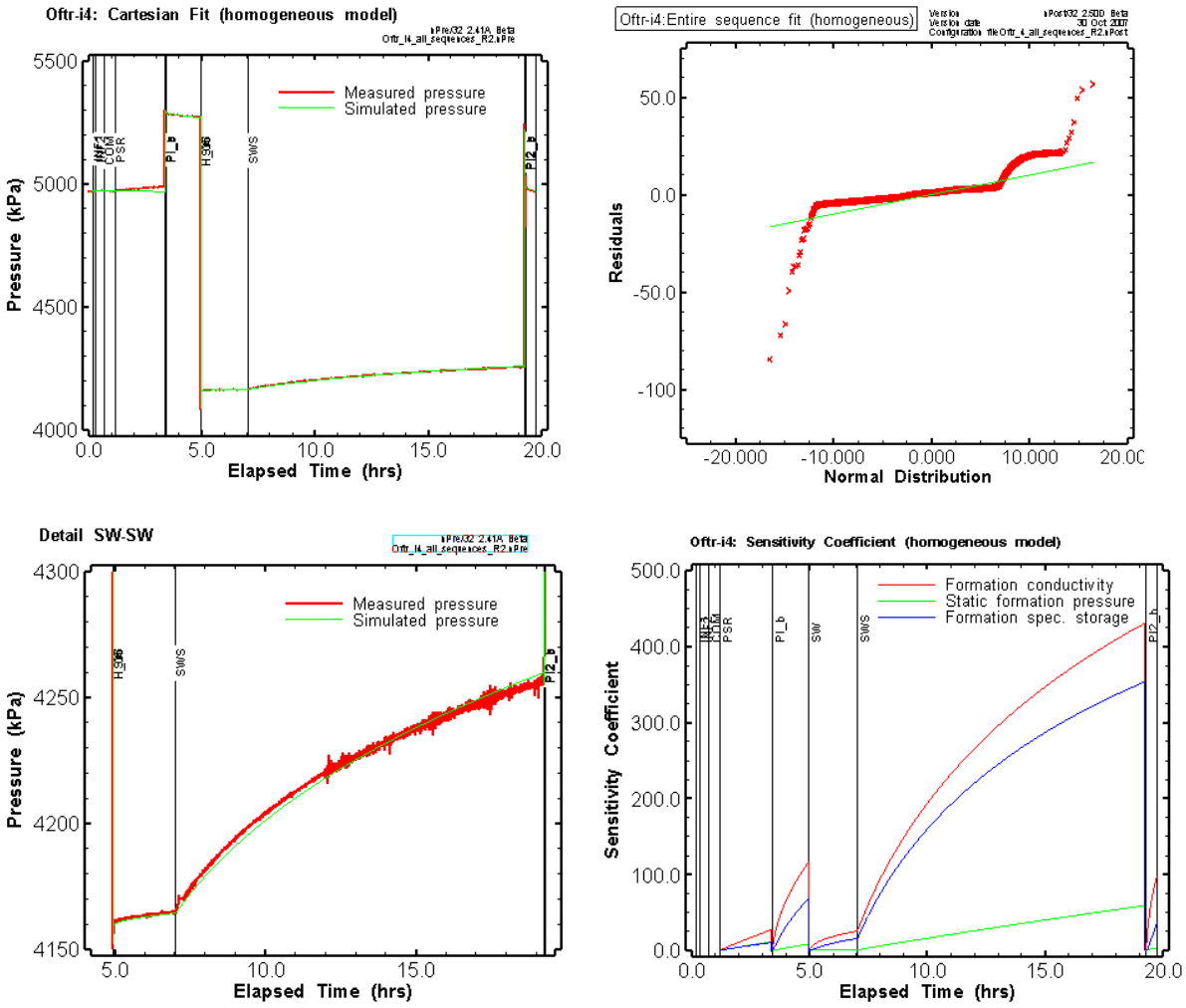

Fig. 11.2: Oftr-i4: QLR results from nSights inverse simulation of the Cartesian pressures of the entire test (top left and detail SW-SWS bottom left), the computed residual compared to a normal distribution (top right) and the sensitivity coefficients (bottom right)

11.3. SWS Fit in Log-log Diagnostic Plot Using Confined P_f-Range

The flow model is retested using a constrained parameter range for the static hydraulic pressure (P_fm ranging from 4500 to 5500 kPa). The pre-SWS test sequences INF-COM-PSR-PI-SW are incorporated as pressure history, as well as the pre-test borehole history. The c_{tz} was set to 8.0E-10 Pa^{-1} which is deemed more realistic than the measured test zone compressibility (4.3E-10 Pa^{-1} for PI and 4.2E-10 Pa^{-1} for PI2, see Appendix D). Several simulations showed that a variation of the c_{tz} parameter at values <1E-9 Pa^{-1} had a minor effect on the simulation result.

The SWS shut-in phase was chosen for the sequence log-log fit because it represents the longest individual test event of this test interval. The 12 hour long SWS is nonetheless mainly dominated by wellbore storage effect but shows a tendency toward infinite acting radial (IARF) flow at late time.

The SWS sequence is fitted in order to check if a prescribed parameter range with significantly higher values for the P_f parameter would produce similar results. The results of a combined fit log dP and log dP' are shown in Tab. 11.2 and in Fig. 11.3. The lower bound of the prescribed P_f parameter range (4500 kPa) was reached during the optimization process. The constrained P_f range results in a good quality fit to SWS pressure.

Tab. 11.2: Parameters estimates and 95% confidence intervals for the SWS diagnostic fit (combined fit log dP and log dP'), homogeneous model.

Parameter	Units	Fit Value SSE=2.76E+01	95% Confidence Intervals	
			Lower Value	Upper Value
K_fm	[m/s]	1.64E-14	1.20E-14	2.23E-14
P_fm	[kPa]	4500	4483	4517
ss_fm	[1/m]	3.39E-06	2.34E-06	4.90E-06

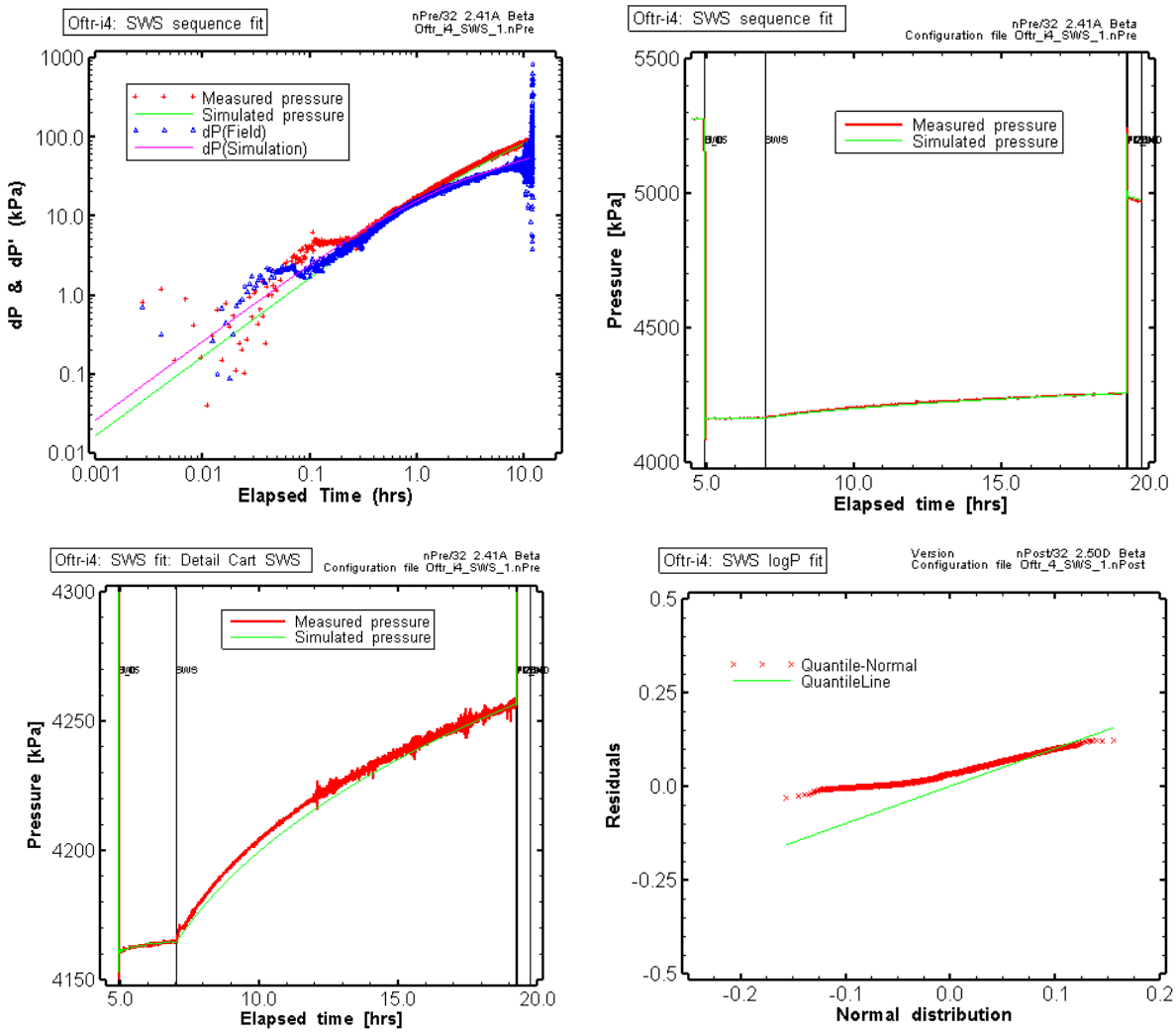

Fig. 11.3: Log-log fit for the SWS sequence (top left). Simulated Cartesian SWS pressure (top left and bottom left) and the distribution of the residuals (for the log dP fit) are shown using the formation parameter s obtained from the SWS fit.

11.4. Cartesian Fit to the SW-SWS Sequences

Based on the model configuration used for the SWS analysis a fit to the Cartesian pressure of the SW-SWS is performed. The pre-SWS test sequences INF-COM-PSR-PI are incorporated as pressure history, as well as the pre-test borehole history. Again, the static hydraulic pressure is allowed to very within the constrained range from 4500 to 5500 kPa.

Fig. 11.4 shows the results of the Cartesian fit to the SW-SWS sequence. The upper left and upper right plots show a good visual match to the SWS. The fitted formation parameters (Tab. 11.3) indicate a K-value of 1.73E-14 m/sec, an S_s -value of 3.36E-06 m^{-1}, and a P_f -value of 4500 kPa. The middle left plot in Fig. 11.4 shows the change in sensitivity coefficients of the three fitted parameters during the SW-SWS sequence. This indicates that the K is the most sensitive parameter and P_f is the least sensitive parameter and is still increasing at the end of the SWS sequence. The range between the upper and lower values for the 95th percentile confidence intervals are listed in Tab. 11.3 and shown in the bottom graphs of Fig. 11.4. The bottom plots in Fig. 11.4 provide the 95th percentile confidence regions for the estimation of the P_f and K parameter (left) and S_s and K parameters (right), with the shape of the ellipse indicating the degree of correlation between the parameters.

The confidence interval information indicates that the range in the fitted parameter values is relatively small for all three parameters. The middle right plot of Fig. 11.4 presents a comparison of the residuals (measured value minus simulated value) to that of a normal distribution. The residuals are essentially normally distributed which indicates that the residuals can be attributed to measurement error and not a systematic error indicating an erroneous conceptual model. Tab. 11.4 also includes the covariance correlation matrix which indicates that only K and S_S are highly correlated -0.989. This correlation is also observed in Fig. 11.4 by the almost linear nature (small minor axis) of the uncertainty ellipsoids.

Tab. 11.3: Parameters estimates and 95% confidence intervals for the SW-SWS Cartesian fit, homogeneous model.

Parameter	Units	Fit Value SSE=4.48E+04	95% Confidence Intervals	
			Lower Value	Upper Value
K_fm	[m/s]	1.73E-14	1.64E-14	1.83E-14
P_fm	[kPa]	4500	4478	4522
ss_fm	[1/m]	3.36E-06	3.11E-06	3.62E-06

Tab. 11.4: Covariance-Correlation matrix for homogeneous model (shaded cells denote correlation matrix elements).

Covariance/Correlation Matrix: Est. CART DAT_P			
	K_fm	P_fm	ss_fm
K_fm	8.85E-06	1.90E-05	-2.73E-05
P_fm	0.552	1.34E-04	-7.21E-05
ss_fm	-0.989	-0.669	8.63E-05

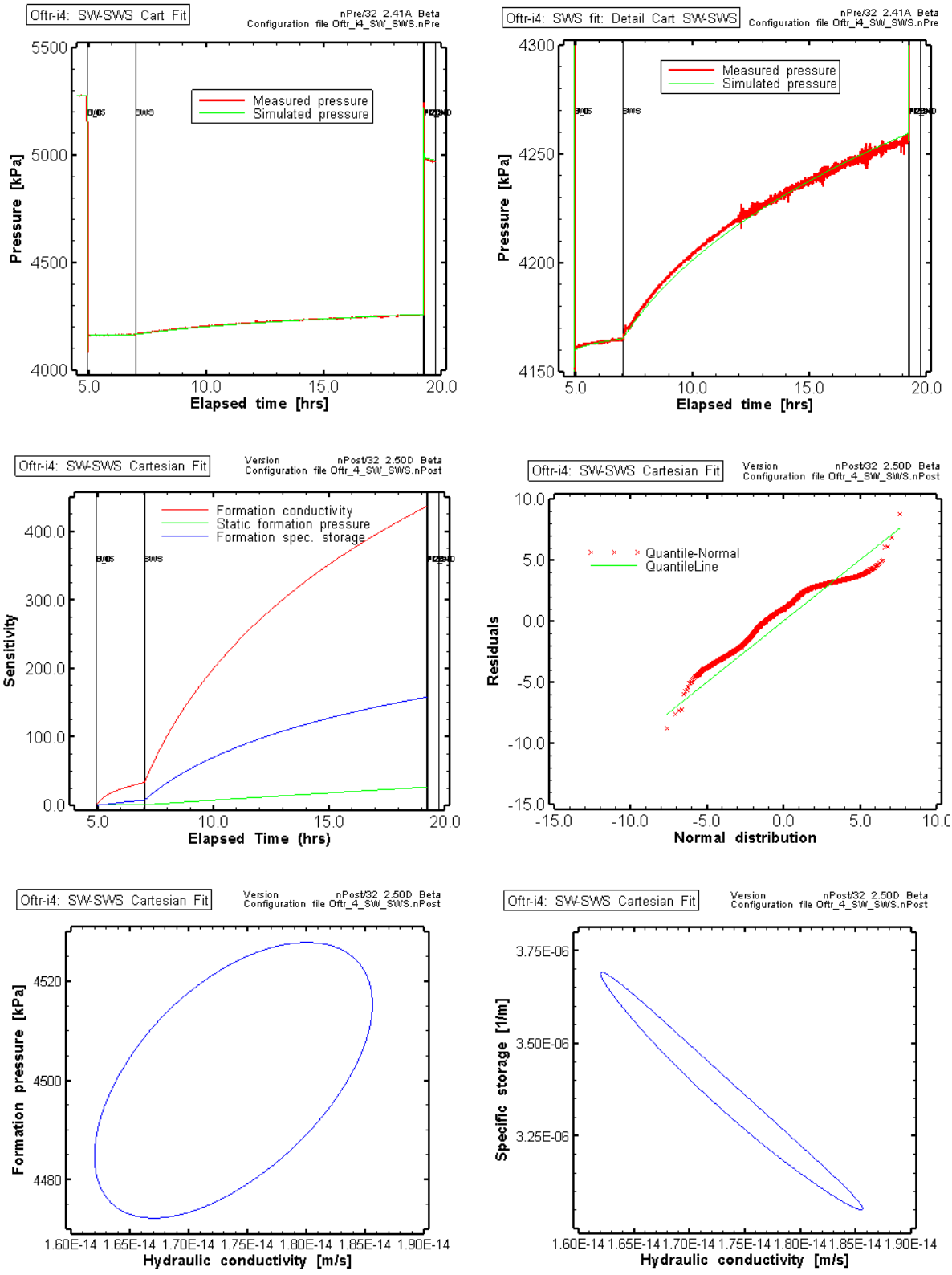

Fig. 11.4: Sequence SW-SWS optimization results fitted to the Cartesian pressure response (homogeneous model).

11.5. Perturbation Analysis for SW-SWS Using Extended Pf Range

Perturbation analyses were performed to test if the estimated parameters and differences were associated with a local minimum or represent a global minimum of the optimization. This was done by repeating the optimization with different starting values for the different parameters.

During a first perturbations analysis, the static head was allowed to vary within 4000 and 5500 kPa. 50 optimization runs were performed for which individual fits were computed using Simplex algorithm. The results are plotted as three dimensional plot of the SSE as a function of the best-fit values of formation conductivity and specific storage and as a function of the best-fit values of formation conductivity and formation pressure (Fig. 11.5, top graphs). In addition, the best-fit results (lowest SSE) are indicated as green filled circles for comparison with the distribution from the perturbation runs. Also indicated are the 95% confidence regions for the various realizations.

The 2D and 3D plots of Fig. 11.5 show several local minima. The lower left plot Fig. 11.5 indicates that higher K estimates are generally associated with lower S_S values. The upper left plot shows that lowest SSE (sum of square errors) corresponds to a parameter set with relatively high K and low S_S value. The 2D and 3D plots on the right of Fig. 11.5 suggest that the parameter space is less constrained for the P_f - K joint parameters. Most local minima and the global minimum are located near the lower end of the P_f axis (near Pf = 4000 kPa) but scatter along the K-axis between 1E-14 m/s and 3E-13 m/s. The parameters of the best fit estimate with lowest SSE (global minimum) are listed in the upper part of Tab. 11.5 (K = 2.05E-13 m/s, S_S = 2.40E-07 m^{-1} and P_f = 4020 kPa). Note that the P_f and S_S values represent the low extreme values of the configured parameter ranges ($4000 < P_f < 5500$ kPa).

A second perturbation analysis was carried out to see if an extension of the static formation pressure range would result in a better constrained parameter space. The static heads were allowed to vary within 3000 and 6000 kPa and 100 optimization runs were performed. Results are shown in Fig. 11.6 and the lower part of Tab. 11.5. Three regions can be identified in the parameters space. The one with the lowest SSE is now associated with a relatively high S_S value (left plots of Fig. 11.6) but low K value and low P_f value (left plots of Fig. 11.6): K = 1.90E-14 m/s, S_S = 5.02E-06 m^{-1} and P_f = 3724 kPa. The SSE value for best-fit realization of the 2nd perturbation analysis (SSE=7.077E+03) is not significantly lower compared to corresponding value of the 1st perturbation (8.834E+03).

The following can be concluded from the perturbation analyses:

- The space for the three optimized parameters K, S_S and P_f is not well constrained
- The K and S_S parameters are highly correlated
- The K and P_f parameter show a considerable degree of mutual independence
- The lowest SSE value (global minimum) is associated with an unrealistic low formation pressure
- The incorporation of the PSR-PI-SW sequences as pressure history provides generally lower head estimates

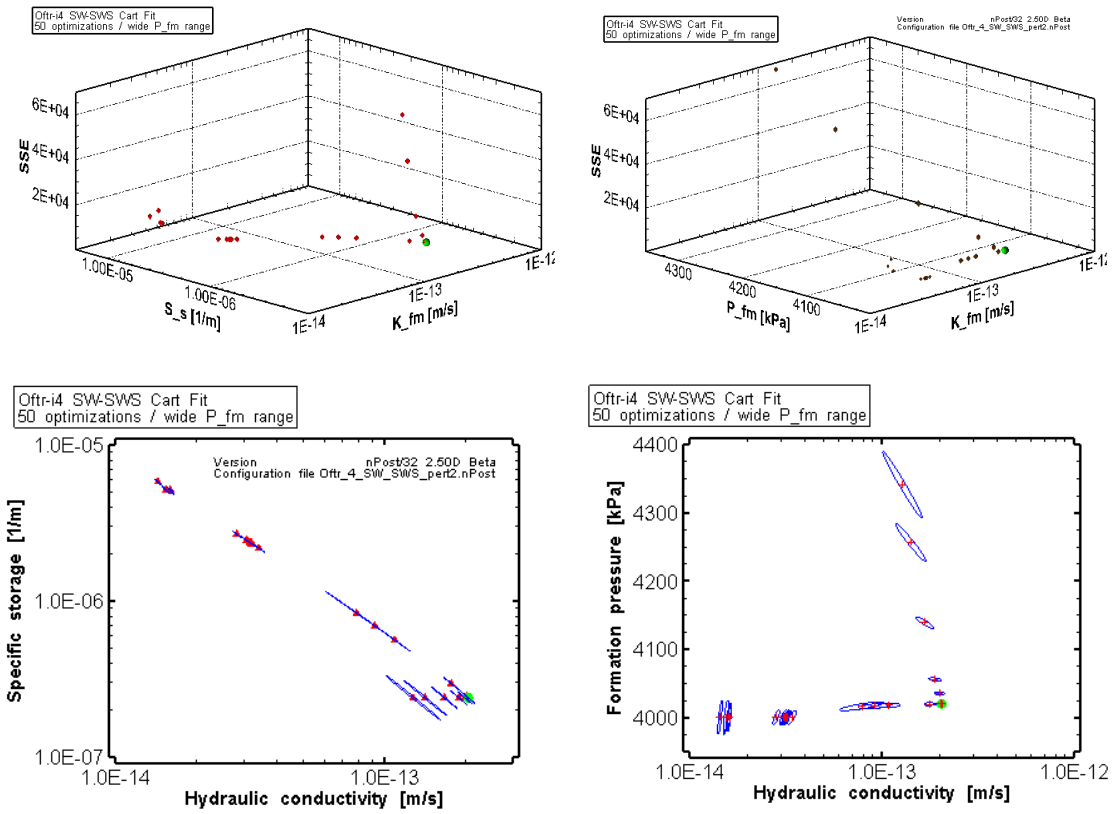

Fig. 11.5: Oftr-i4: Results from perturbation analysis of the nSights inverse simulation of the Cartesian pressure of the SW-SWS sequence using P_f range 4000 - 5500 kPa

Top left: multiple realizations with computed SSE (sum of square errors) versus S_S and K estimates, and top right, versus P_f and K estimates. Bottom: estimates of S_S and K (left) and P_f and K (right) and associated confidence regions for best-fit realizations (lowest SSE). For all optimizations the Simplex algorithm was used. The red symbol indicates the best-fit realization (lowest SSE).

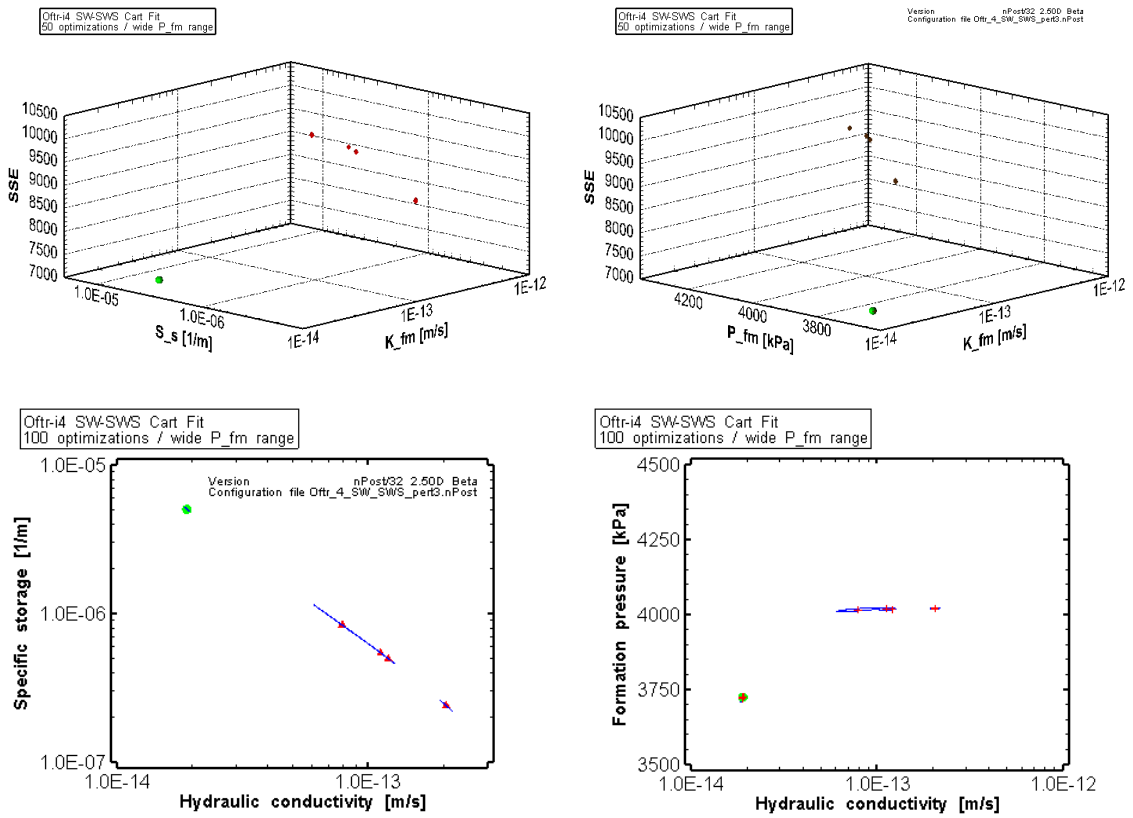

Fig. 11.6: Oftr-i4: Results from perturbation analysis of the nSights inverse simulation of the Cartesian pressure of the SW-SWS sequence using P_f range 3000 - 6000 kPa

Top left: multiple realizations with computed SSE (sum of square errors) versus S_S and K estimates, and top right, versus P_f and K estimates. Bottom: estimates of S_S and K (left) and P_f and K (right) and associated confidence regions for best-fit realizations (lowest SSE). For all optimizations the Simplex algorithm was used. The red symbol indicates the best-fit realization (lowest SSE).

Tab. 11.5: Best fit parameters estimates and 95% confidence intervals from perturbation analyses for the SW-SWS Cartesian fit, using different P_f-ranges

Parameter	Units	Values	95% Confidence Intervals	
			Lower Value	Upper Value
P_fm range: 4000 - 5500 (PERT2)				
SSE	8.834E+03			
K_fm	[m/s]	2.05E-13	1.96E-13	2.15E-13
P_fm	[kPa]	4020	4018	4021
ss_fm	[1/m]	2.40E-07	2.24E-07	2.57E-07
P_fm range: 3000 - 6000 (PERT3)				
SSE	7.077E+03			
K_fm	[m/s]	1.90E-14	1.87E-14	1.93E-14
P_fm	[kPa]	3724	3713	3734
ss_fm	[1/m]	5.02E-06	4.91E-06	5.14E-06

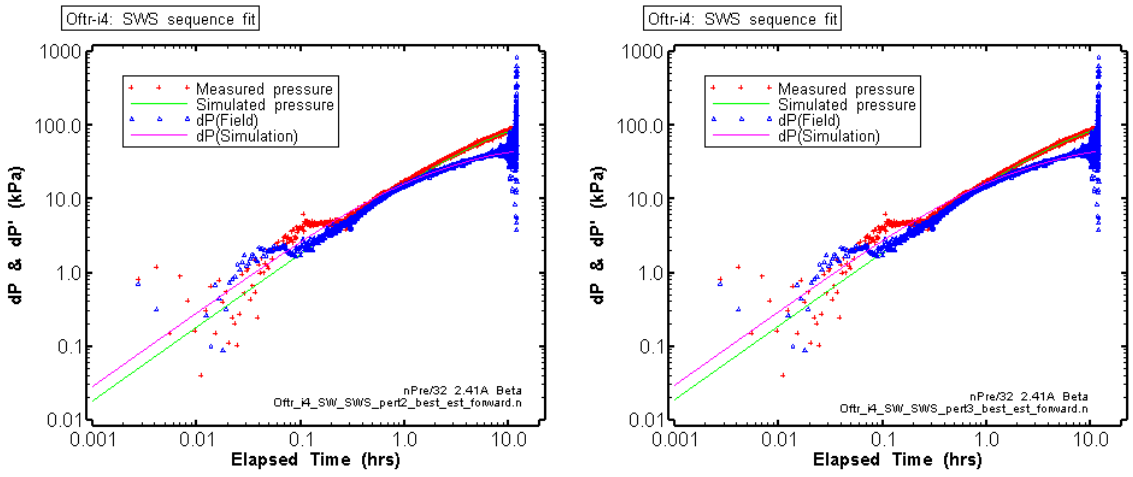

Fig. 11.7: Oftr-i4: SWS diagnostic plots showing the best estimate results (lowest SSE) of the perturbation analysis using P_f range 4000 - 5500 kPa (left) and the perturbation analysis using P_f range 3000 - 6000 kPa (right)

11.6. Role of Non-Fitting Parameters for SWS-SW Cartesian Fit

Given that the above tested conceptional models did not result in a well defined parameter space, even when widening the P_f range to unrealistic values, it was decided to investigate the role of non-fitting parameters. During the previous simulations, the non-fitting parameters such as borehole radius and test zone compressibility were assumed to be known with 100% certainty. This assumption is tested allowing a certain variation of these parameters. The aim of this exercise is to explore a potential improvement of the model due to revised fix-parameter assumptions.

In nSights, a user specified number of simulations can be run using the "Sampling" option. For each simulation, a set of non-fitting parameters are determined randomly from an uncertainty distribution (i.e. optimization-sampling mode) and the model re-optimizes the fitting parameters. Correlations between non-fitting and fitting parameters can be observed from the results.

11.6.1. Sampling of Test Zone Parameters

In a first step, the influence of the non-fitting parameters borehole radius, tubing radius and the shut-in test zone compressibility was investigated. In total, 200 simulations were run in nSights, each using a different set of the specified non-fitting parameters. For each simulation, the fitting parameters (K, S_S and P_f) were optimized and a SSE value was calculated. The sets of the non-fitting parameters were produced after defining lower and upper bound for each parameter (Tab. 11.6) using the Latin-Hyper Cube method. The P_f parameter was allowed to vary within 4000 and 5500 kPa. The result of parameter sampling and multiple realizations is shown in Tab. 11.7 and Fig. 11.8.

The bottom graph of Fig. 11.8 shows that the variation of the non-fitting parameters produced a majority of solutions with P_f close to 4000 kPa (= lower bound of parameter range), but a significant number of optimizations with P_f estimates greater than greater than 4500 kPa. An alignment of the best fit results with increased P_f estimates towards higher SSE values (sum of the square errors) can be recognized. This suggests that a variation of the non-fitting parameters c_{tz}, r_w , r_c is does not improve the model with regard to plausible P_f estimates.

Spearman correlation values for fitting and non fitting parameters are listed in Tab. 11.7. The non-fitting parameters r_w and r_c show no correlation to the fitting parameters and have little influence on the fit value. The c_{tz} parameter correlates significantly with P_f and K parameter and the fit value.

Tab. 11.6: Description of sampled parameters (200 samples)

Parameter		Sampling Type	Mean	Max	Min
c_{tz}	[1/Pa]	Log	1.9E-09	6.0E-09	6.0E-10
r_c	[m]	Lin	0.0047	0.0050	0.0044
r_w	[m]	Lin	0.075	0.080	0.070

11.6.2. Sampling of Pre-Test Open Borehole Pressure

For assumed borehole duration of 150 hrs, fixed pre-test borehole pressures between 4700 and 5100 kPa were sampled to investigate the effect of the borehole history to the Cartesian SW-SWS fit results. The fitting parameters were allowed to vary within extended ranges during the simulations: K from 1E-15 to 1E-11 m/s, S_S from 1E-7 to 1E-4 m^{-1} and P_f from 2000 to 6000 kPa. The results of 100 simulations are shown in 3D parameters space in the top left plot (SSE versus K and S_S) and top right plot (SSE versus K and P_f) of Fig. 11.9. Simulated Cartesian pressures of selected cases are shown in the bottom plots of Fig. 11.9. The bottom right plot presents a detailed view of the pressures during SW and start of SWS.

The 3D scatter plots of Fig. 11.9 suggest that the variation of the pre-test borehole history has a relatively small effect on the fitted parameters. The solutions with lowest SSE correspond to the cases with low pre-test borehole pressure and higher P_f estimates (e.g. case #10: pre-test pressure = 4713 kPa, P_f = 4311 kPa and SSE = 6890). However, the higher P_f estimates are still significantly below the expected range (4484 to 5465 kPa). The distribution of the solutions with SSE < 7300 is almost invariant to the K parameter (Fig. 11.9, plot SSE versus K and P_f). Most of the solutions whose SSE is greater 8000 are associated with pre-test borehole pressures higher than 5000 kPa.

From the sampling of the pre-test borehole pressure and the associated simulations it can be concluded that the generally low P_f estimates of the Cartesian fits to the SW-SWS sequence are not linked to the incertitude on the borehole pressure history.

Tab. 11.7: Correlation between fitting and non-fitting parameters

SpearmanR	K_fm	P_fm	ss_fm	c_{tz} (c_{tz})	r_c	r_w	Fit Value
K_fm	1.00	0.63	-0.85	0.67	0.16	0.00	0.64
P_fm		1.00	-0.38	0.88	-0.12	0.13	0.91
ss_fm			1.00	-0.40	0.02	-0.03	-0.41
c_{tz}				1.00	-0.02	0.05	0.97
r_c					1.00	-0.02	-0.11
r_w						1.00	0.16

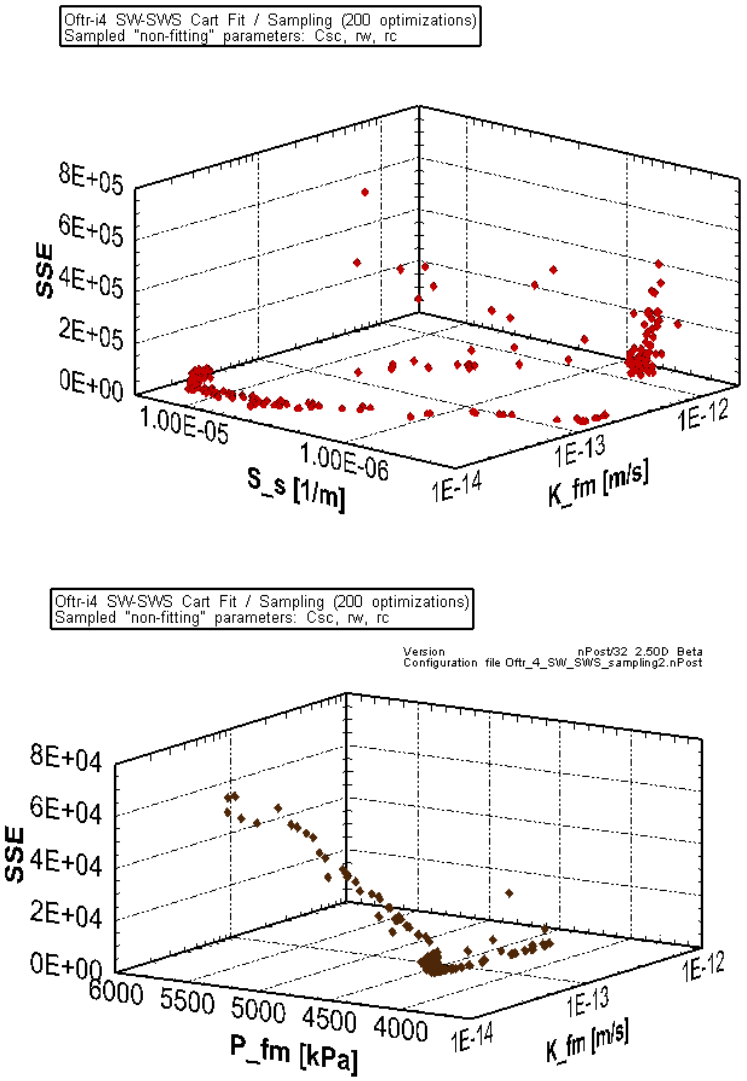

Fig. 11.8: Results from 200 inverse simulations based on sampling of the non-fitting parameters c_{tz} (c_{sc}), r_w and r_c.

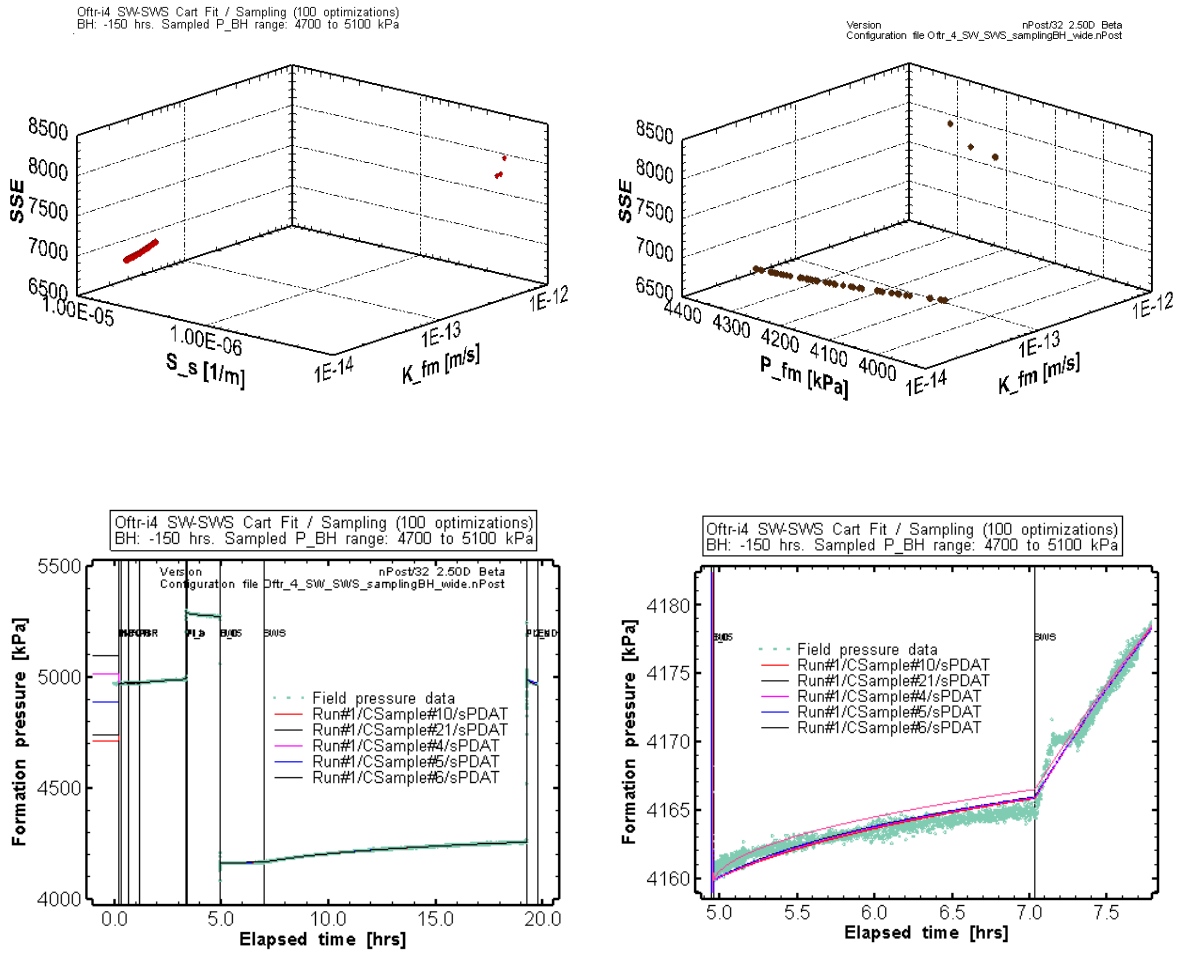

Fig. 11.9: Results from 100 inverse simulations based on sampling of fix pre-test borehole history pressures (BH duration = 150 hrs). Sampled P_{BH} range: 4700 to 5100 kPa

11.7. Perturbation Analysis for PI-SW-SWS Using Extended P_f Range

The analyses performed for the SW-SWS sequence were repeated after adding the PI sequence to Cartesian fit specification (PI-SW-SWS). Besides this, the same nSights configuration files were used as for the perturbations analyses described in Chapter 11.5. The aim of these additional simulations was to see how the additionally considered injection period (PI) would change the global and local minima in the parameter space and in particular if higher Pf estimates would be produced. The best-fit results for both perturbation runs are shown in Tab. 11.8 and in Fig. 11.10. The best-fit results from the perturbation analysis using a large P_f range (P_f was allowed to vary between 3000 - 6000 kPa, see lower half of Tab. 11.8), are very similar to those from the corresponding analysis for the SW-SWS Cartesian fit (Tab. 11.5). The P_f best estimate (3869 kPa) is only 145 kPa higher than the one from the SW-SWS analysis (3724 kPa). The top left and top right plot of Fig. 11.10 show that all perturbations scatter within in a single cluster. The 95% confidence regions of the best-fit estimate for the K - S_S and K - P_f joint parameters occupy very small areas in the parameter space, and no local minima are indicated.

The perturbation analysis using a limited range for the P_f parameter (upper part of Tab. 11.8) produced similar parameters estimates (with P_f at the lower bound of the input range), slightly increased and decreased S_S. The SSE value of the best-fit is very close to the one of the perturbation analysis with extended P_f range. The majority of the perturbations scatter close to the global minimum. A single perturbation case has a SSE value twice as high compared to the global minimum. It is associated with a relatively low K estimate and a relatively high S_S estimate (lower part of Fig. 11.10). The limited P_f input range did not force the optimization towards higher Pf values. The P_f estimates of all perturbations are around 4000 kPa, the lower bound of the input range (left plot in Fig. 11.10).

The residuals of the best-fit cases for both perturbation analyses are essentially normally distributed (Fig. 11.11).

Tab. 11.8: Best fit parameters estimates and 95% confidence intervals from perturbation analyses for the SW-SWS Cartesian fit, using different P_f-ranges

Parameter	Units	Values	95% Confidence Intervals	
			Lower Value	Upper Value
P_fm range: 4000 - 5500 (PERT2)				
SSE	2.360E+04			
K_fm	[m/s]	2.11E-14	2.07E-14	2.15E-14
P_fm	[kPa]	4000	3987	4013
ss_fm	[1/m]	3.71E-06	3.60E-06	3.82E-06
P_fm range: 3000 - 6000 (PERT3)				
SSE	2.308E+04			
K_fm	[m/s]	1.84E-14	1.81E-14	1.88E-14
P_fm	[kPa]	3869	3854	3884
ss_fm	[1/m]	4.71E-06	4.59E-06	4.85E-06

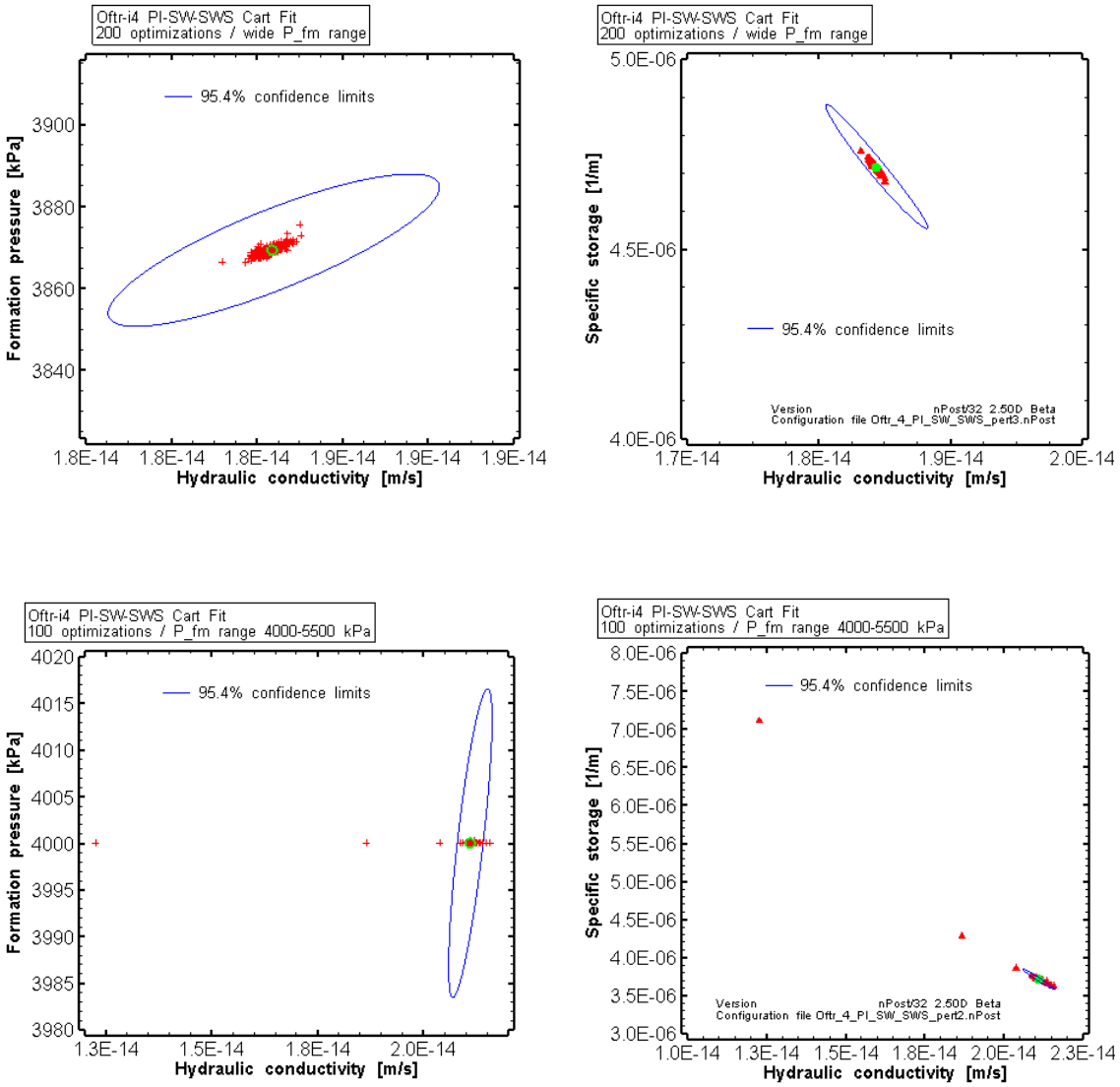

Fig. 11.10: Oftr-i4: Results from perturbation analyses of the nSights inverse simulation of the Cartesian pressure of the PI-SW-SWS sequence (2 cases).

Top plots: multiple realizations allowing P_f to vary from 3000 - 6000 kPa, with K versus P_f (left) and with K versus S_S estimates (right). 95% confidence limits are shown for the best-fit estimate. For all simulations the SSE varies in a very narrow range from 23080 to 23085. Bottom plots: multiple realizations allowing P_f to vary from 4000 - 5500 kPa, with K versus P_f (left) and with K versus S_S estimates (right). For the simulations results which plot in right half of each plot, the SSE varies in very narrow range 23600 to 23650. For the single value at the left half of each plot, SSE is at 45000.
For all optimizations the Simplex algorithm was used. The green symbol indicates the best-fit realization (lowest SSE).

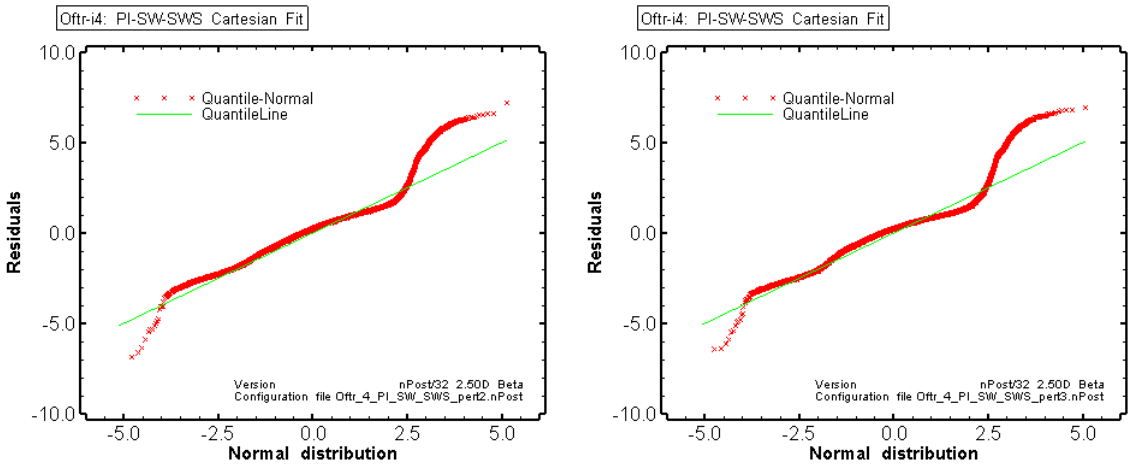

Fig. 11.11: Cartesian Fit PI-SW-SWS: Residuals compared to a normal distribution

Left: Residual plot of best-fit estimate of perturbation analysis using a wide P_f range (3000 to 6000 kPa). Right: Residual of perturbation analysis using a limited P_f range (4000 to 5500 kPa).

11.8. PI-SW-SWS-PI2 Composite Fits

The analyses presented in Sections 11.2 to 11.7 provide good quality fits to measured pressure data, however, the simulated formation pressure is below the expected range. Therefore, field data are re-evaluated (Section 11.8.1) and the process of inverse parameter estimated using adjusted fit constraints.

11.8.1. Smoothing and Filtering of Field Data

For test sequences where pressure varied only within limited range (e.g. SW, see top right plot of Fig. 11.12), the scatter of the pressure signal due to the NOK current transformation station is rather important. The amplitude of the scatter is not constant but day-time dependent. This can be seen for SWS (left bottom plot of Fig. 11.12; green symbols) where particularly the early and late time data are noisy. To remove data noise, pressure data of each fitted sequence PI, SW, SWS and PI2 were smoothed using the nSights smooth option. For SW and SWS, in maximum 20 data points left and right from the data point were used for the smooth operations. 5 data points (or less) left and right from the data point were used for smoothing of the pulse sequences (PI, PI2). The smoothed data curves are shown as blue lines in the individual plots of Fig. 11.12.

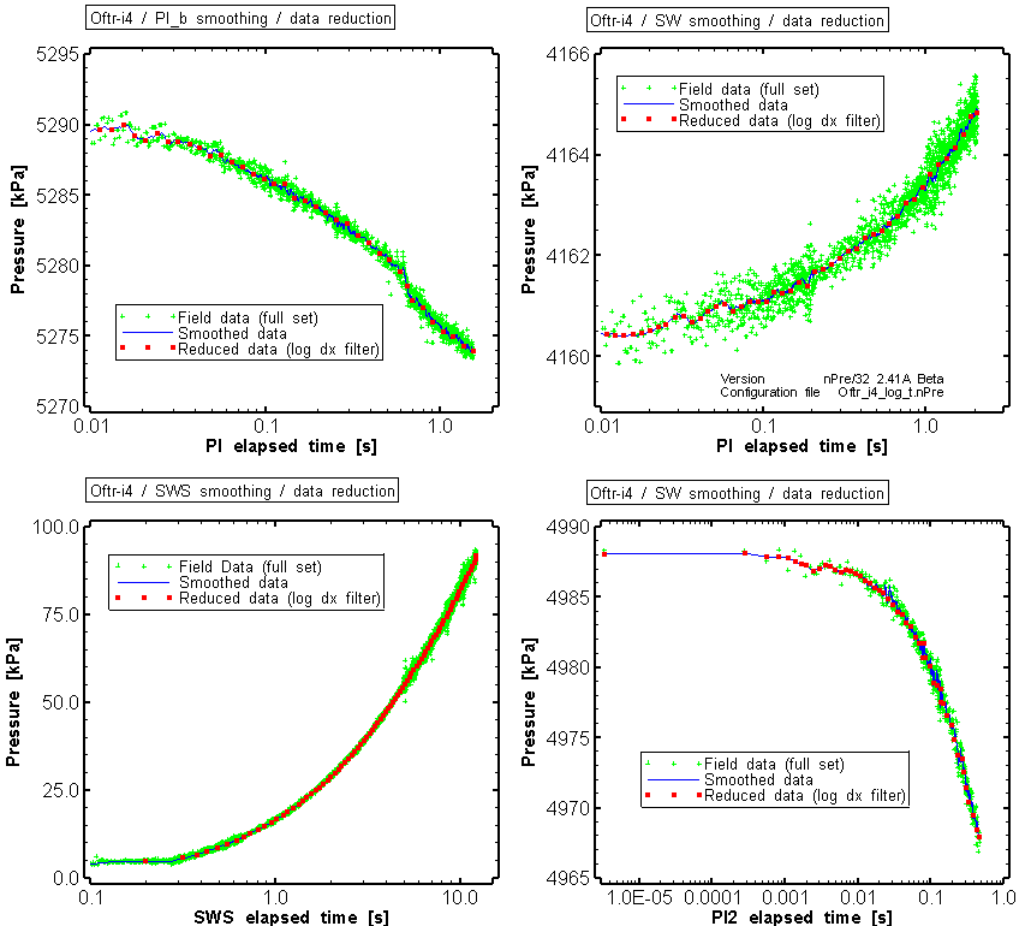

Fig. 11.12: Smoothing and filtering of field sequence data

11.8.2. Pressure versus log of time fit constraint

The PI, SW, SWS and PI2 sequence data were reduced using the nSights data reduction option "log x change". The data transformation results in consistent distribution of the reduced data points along the log time axis as shown in Fig. 11.12 (curves with red square symbols). The log distribution of data points on the time axis for each sequence emphasizes fitting of the early time data and therefore supports the verification of the hydraulic model. A composite fit was set up which includes P - log (t) fitting of the sequences PI, SW, SWS and PI2.

11.8.3. Result of the composite fit P vs. log(t) - homogeneous model

The result of the nSights inverse parameter optimization is presented in Tab. 11.9 and Fig. 11.15 and Fig. 11.13. The obtained fit is shown visually in the sequence plots P vs. log (t) of Fig. 11.13. The individual sequences are nicely fitted except of PI2, where the simulated pulse pressure decline is slightly slower than the measured pressure response. The early time data of SW are not fitted on purpose. The bump from 0.05 to 0.3 hours (see upper right plot in Fig. 11.13) is interpreted as a 'whole system' measuring effect of unknown mechanism not representing formation response. The lower fit range limit for the SWS sequence was set to 0.3 hrs. Parameter estimates and confidence limits for the K, Ss and P_f - parameters are shown in Tab. 11.9. The K-estimate for composite P - log(t) fit is slightly higher compared to the previous analyses of the SWS and the PI-SWS-SWS sequences. The estimated static formation pressure with P_f = 4503 kPa is now within the expected range.

Tab. 11.9: Parameters estimates and 95% confidence intervals for composite Fit, P vs. log(t) fit constraint, PI + SW + SWS + PI2 composite fit., homogeneous model.

Parameter	Units	Fit Value SSE= 6614	95% Confidence Intervals	
			Lower Value	Upper Value
K_fm	[m/s]	4.13E-14	3.52E-14	4.84E-14
P_fm	[kPa]	4552	4531	4572
ss_fm	[1/m]	1.10E-06	8.83E-07	1.37E-06

The residuals compared to a normal distribution are shown in Fig. 11.14 for each sub-fit. For comparison, the model has be re-run using the Cartesian fit specification (which does not include data smoothing and log t data reduction) and the residuals for this optimization are plotted on the same graph using grey symbols (Fig. 11.14). The residual plot illustrates the significant improvement due to data smoothing and log t data reduction.

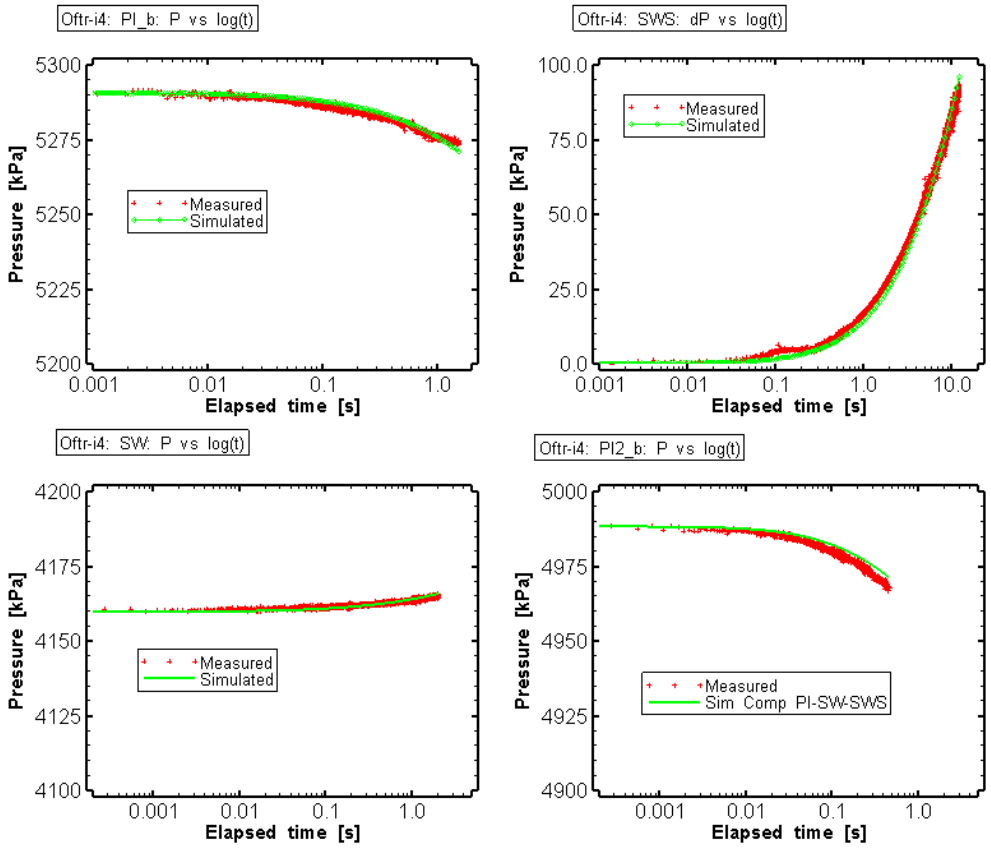

Fig. 11.13: Oftr-i4 - homogeneous model: Result of P vs. log(t) composite fit PI_b + SW + SWS + PI2_b shown for the individual test sequences.

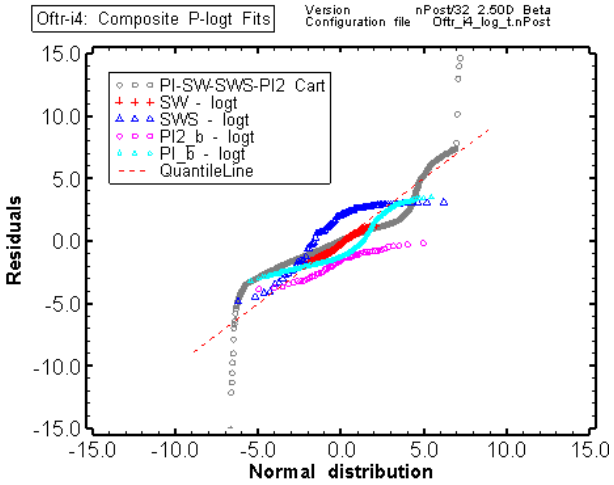

Fig. 11.14: Oftr-i4 - homogeneous model: computed residuals compared to a normal distribution for individual fits P - log(t) and for the Cartesian fit (PI_b to PI2_b)

11.8.4. Perturbation analysis of composite fit P vs. log(t) - homogeneous model

The initial estimates were perturbed during 50 optimizations in nSights to see if the object function results in a single minimum or if other local minima exist. The results with lowest SSE (best-estimate) are shown in Tab. 11.10 and Tab. 11.11. The parameter estimates are almost identical compared to the single optimization presented in the previous section. Joint confidence regions for the parameter pairs K- Ss and K- P_f are shown in Fig. 11.15, the parameter specific confidence limits in Tab. 11.10. The solutions scatter around a single global minim in the parameter space. The SSE values vary only within 6614 and 6716.

Tab. 11.10: Best-fit of perturbation analysis: parameters estimates and 95% confidence intervals for the composite P-log(t) PI+SW+SWS+PI2 fit, homogeneous model.

Parameter	Units	Fit Value SSE=6614.0	95% Confidence Intervals	
			Lower Value	Upper Value
K_fm	[m/s]	4.14E-14	3.53E-14	4.85E-14
P_fm	[kPa]	4551	4531	4571
ss_fm	[1/m]	1.09E-06	8.79E-07	1.36E-06

Tab. 11.11: Best-fit of perturbation analysis: Covariance-Correlation matrix for the composite P-log(t) PI+SW+SWS+PI2 fit, homogeneous model (shaded cells denote correlation matrix elements).

Covariance/Correlation Matrix: Est:Best:PI+SW+SWS+PI2			
	K_fm	P_fm	ss_fm
K_fm	7.41E-05	9.59E-06	-2.28E-04
P_fm	3.30E-01	1.14E-05	-2.95E-05
ss_fm	-9.99E-01	-3.30E-01	7.00E-04

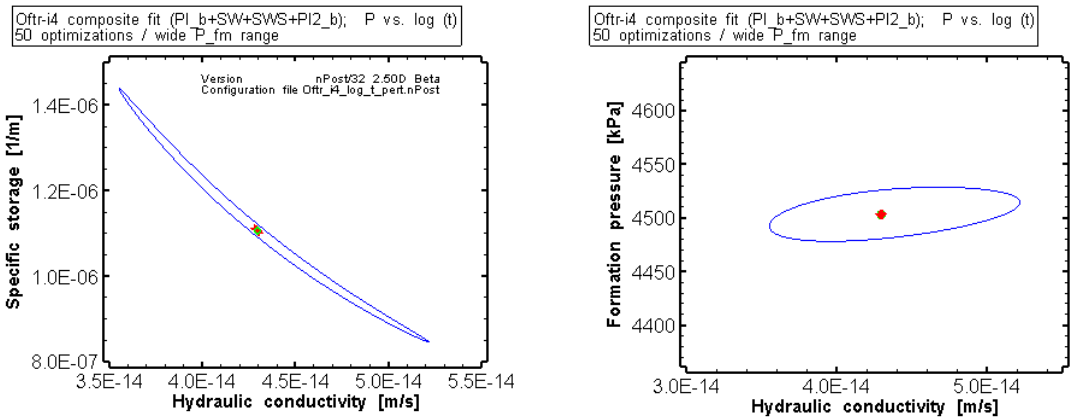

Fig. 11.15: Oftr-i4: Results from perturbation analysis of the nSights inverse simulation for the P vs. log(t) fit constraint, PI + SW + SWS + PI2 composite fit.

11.8.5. Result of the composite fit P vs. log(t) -- composite model (skin)

The homogenous model was extended to composite with a narrow cylindrical zone around the borehole of different properties (skin zone properties) compared to the formation properties. The results of the nSights inverse parameter optimization are shown in Tab. 11.12 and Tab. 11.13 and in Fig. 11.16. The introduction of a skin zone produces slightly improved visual fits, especially for the PI2 sequence (Fig. 11.16, upper right plot), and the SSE value is reduced from 6614 to 4552. The residuals were calculated for the sub-fits PI, SW, SWS and PI2. The distributions are in general agreement with a normal error distribution (Fig. 11.17) and suggest the absence of a systematic error or model mismatch.

During the simulations, the specific storage of the skin zone was held constant with S_{SS} = 5E-07 m^{-1}. The skin parameters values (K_S = 6.5E-14, t_S= 0.005 m in relation to the formation hydraulic conductivity (1.54E-14 m/s) correspond to a low skin factor of - 0.051. The low skin factor is mainly due to the relatively low contrast between formation conductivity and skin zone conductivity and the thin skin zone (0.005 m corresponds to the lower bound of the input range for this parameter). The skin zone conductivity is highly correlated with the radial thickness of the skin zone (Tab. 11.13). A comparison of the log-log diagnostic plots for the SWS sequence for homogeneous and composite model (Fig. 11.18) does not show visual differences.

Tab. 11.12: Parameters estimates and 95% confidence intervals for the PI+W+SWS+PI2 composite fit, composite skin model.

Parameter	Units	Fit Value SSE= 4555	95% Confidence Interval		
			Lower Value	Upper Value	Initial Value
K_fm	[m/sec]	1.54E-14	1.46E-14	1.63E-14	1.0E-13
K_s	[m/sec]	6.50E-14	5.23E-14	8.09E-14	1.0E-12
P_fm	[kPa]	4754	4723	4785	5000
Ss_fm	[1/m]	2.98E-06	2.67E-06	3.33E-06	2.20E-06
t_s	[m]	0.0050	0.0037	0.0063	0.05

Tab. 11.13: Covariance-Correlation matrix for skin model; composite Fit P-logt (shaded cells denote correlation matrix elements).

	K_fm	K_s	P_fm	ss_fm	t_s
K_fm	9.40E-06	2.45E-05	2.66E-06	-3.78E-05	3.17E-06
K_s	8.43E-01	9.01E-05	1.82E-05	-1.23E-04	1.23E-05
P_fm	1.68E-01	3.72E-01	2.66E-05	-1.80E-05	2.65E-06
ss_fm	-9.31E-01	-9.76E-01	-2.63E-01	1.75E-04	-1.65E-05
t_s	7.90E-01	9.93E-01	3.93E-01	-9.50E-01	1.71E-06

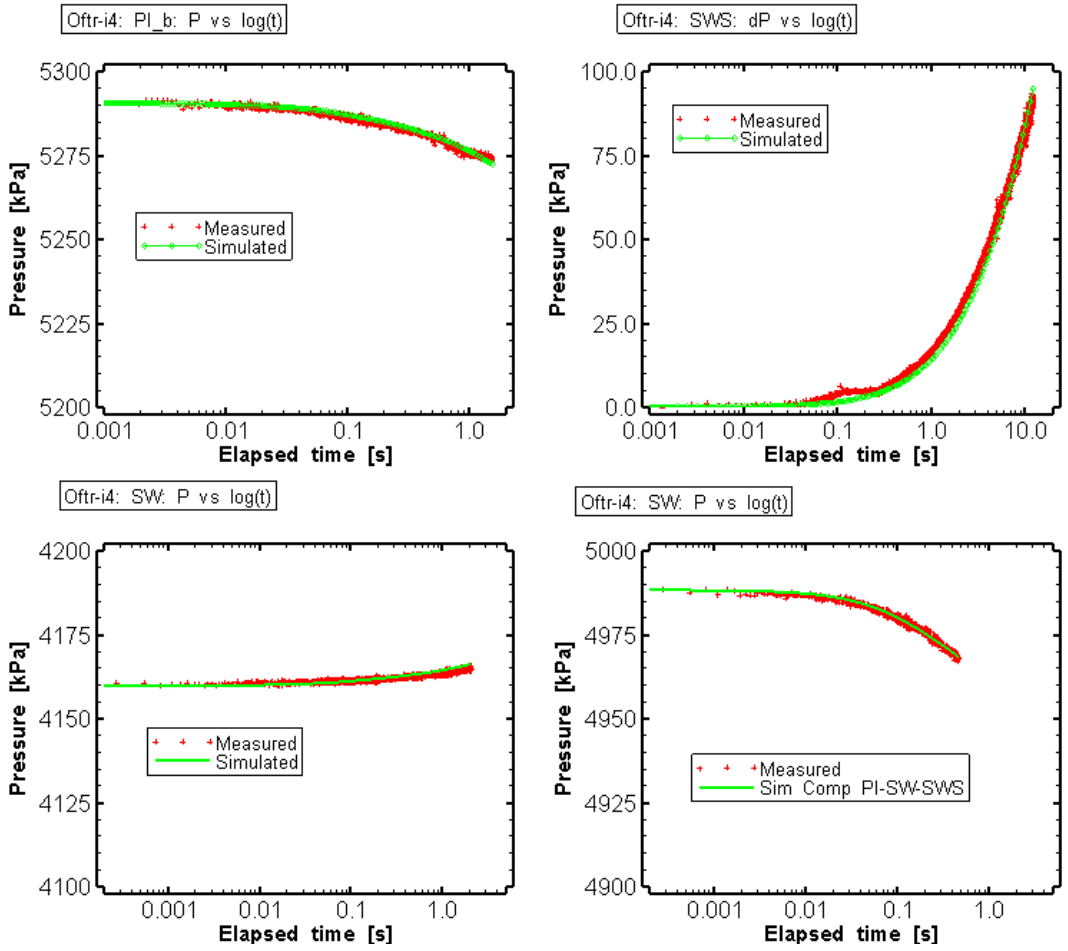

Fig. 11.16: Oftr-i4 - composite skin model: Result of P vs. log(t) composite fit PI_b + SW + SWS + PI2_b shown for the individual test sequences.

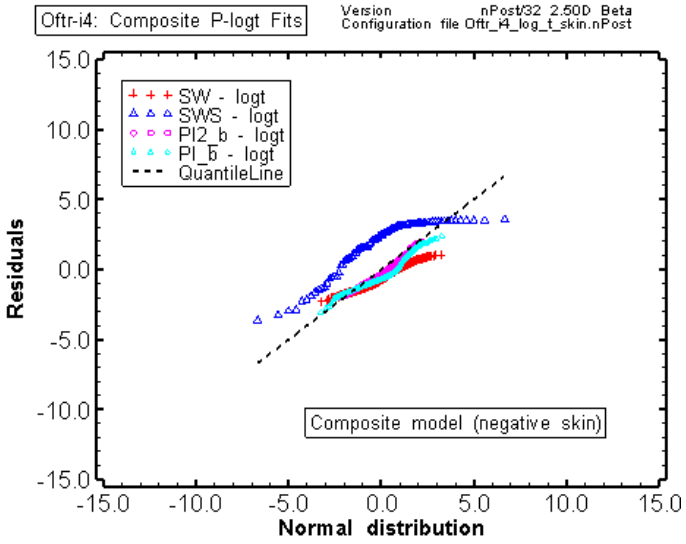

Fig. 11.17: Oftr-i4 - composite skin model: computed residuals compared to a normal distribution for individual fits P - log(t)

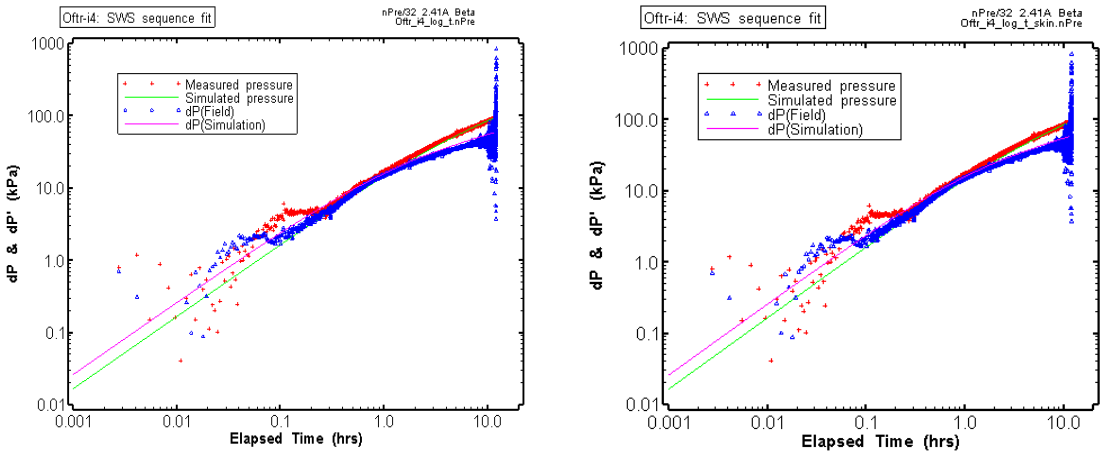

Fig. 11.18: Log-diagnostic plot for the SWS sequence, composite fit PI+SW+SWS+PI. Left: homogeneous model. Right: composite model (neg. skin)

11.8.6. Perturbation analysis of composite fit P vs. log(t) - composite model

The initial estimates were perturbed during 70 optimizations in nSights in order to see if the object function results in a single minimum or if other local minima exist. The parameter estimates associated with the lowest SSE value (best-estimate fit) are shown in Tab. 11.14 and Tab. 11.15. The parameter estimates are very similar to the fitted parameters of the single optimization presented in the previous section. Joint confidence regions for the parameter pairs K-Ss, K-P_f and K- Ks are shown in Fig. 11.19 and the parameter specific confidence limits in Tab. 11.14. The XY scatter plots of Fig. 11.19 and the 3D scatter plots of Fig. 11.20 show irregularly distributed multiple local minima and insular solutions in the 3D parameter space. Most of the cases scatter around the global minimum with SSE values slightly above 4500. The overall SSE values vary in a range from 4501 to 4.89E+06. The global minimum region comprises about 44 % of the cases with K-values ranging from 1.41E-14 to 1.88E-14 (see also histogram for the K-parameter at bottom right of Fig. 11.19.

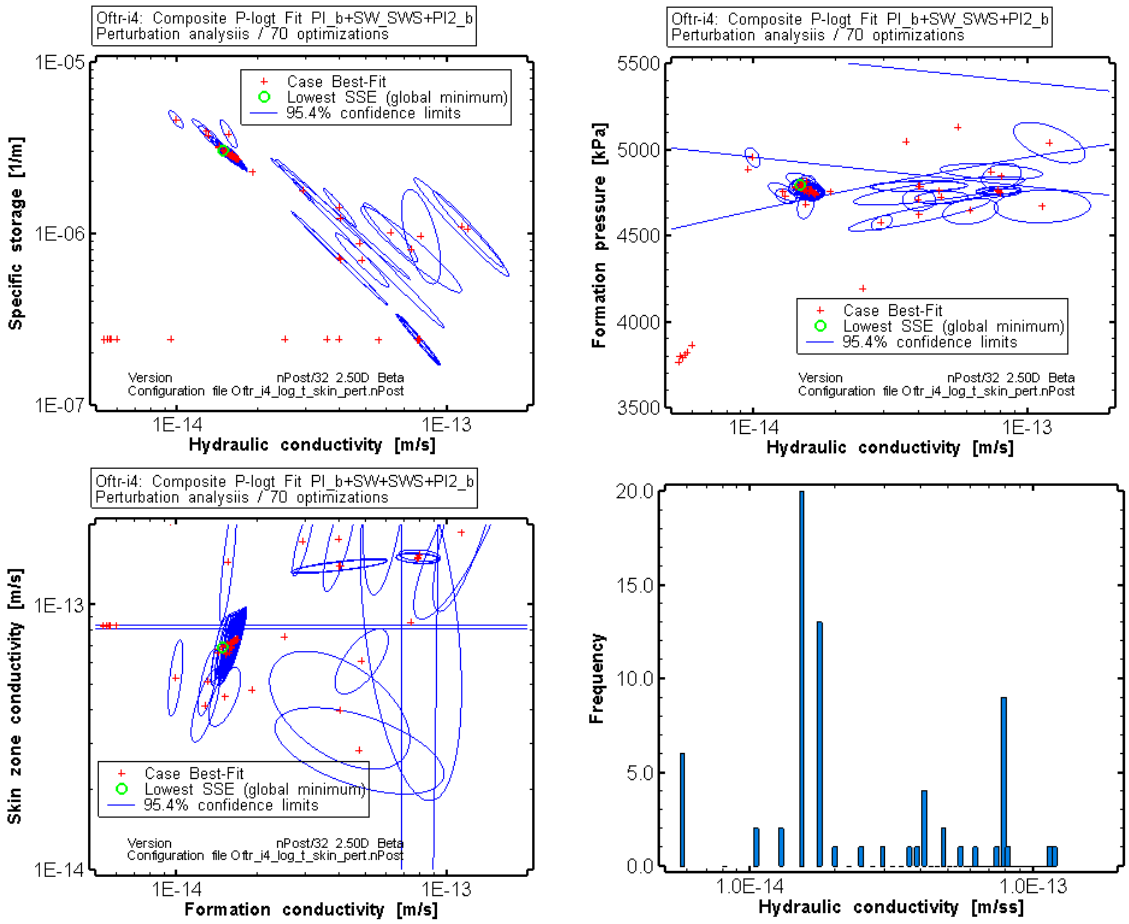

Fig. 11.19: Oftr-i4, composite model: results from perturbation analyses of the nSights inverse simulation for composite fit PI+SW+SWS+SWS (P - log (t)).

Confidence regions for the K - S_S joint parameters (top left), K - P_f joint parameters (top right) and K - K_S joint parameters (bottom left). The frequency distribution for the K-estimates is shown in the histogram at bottom right.

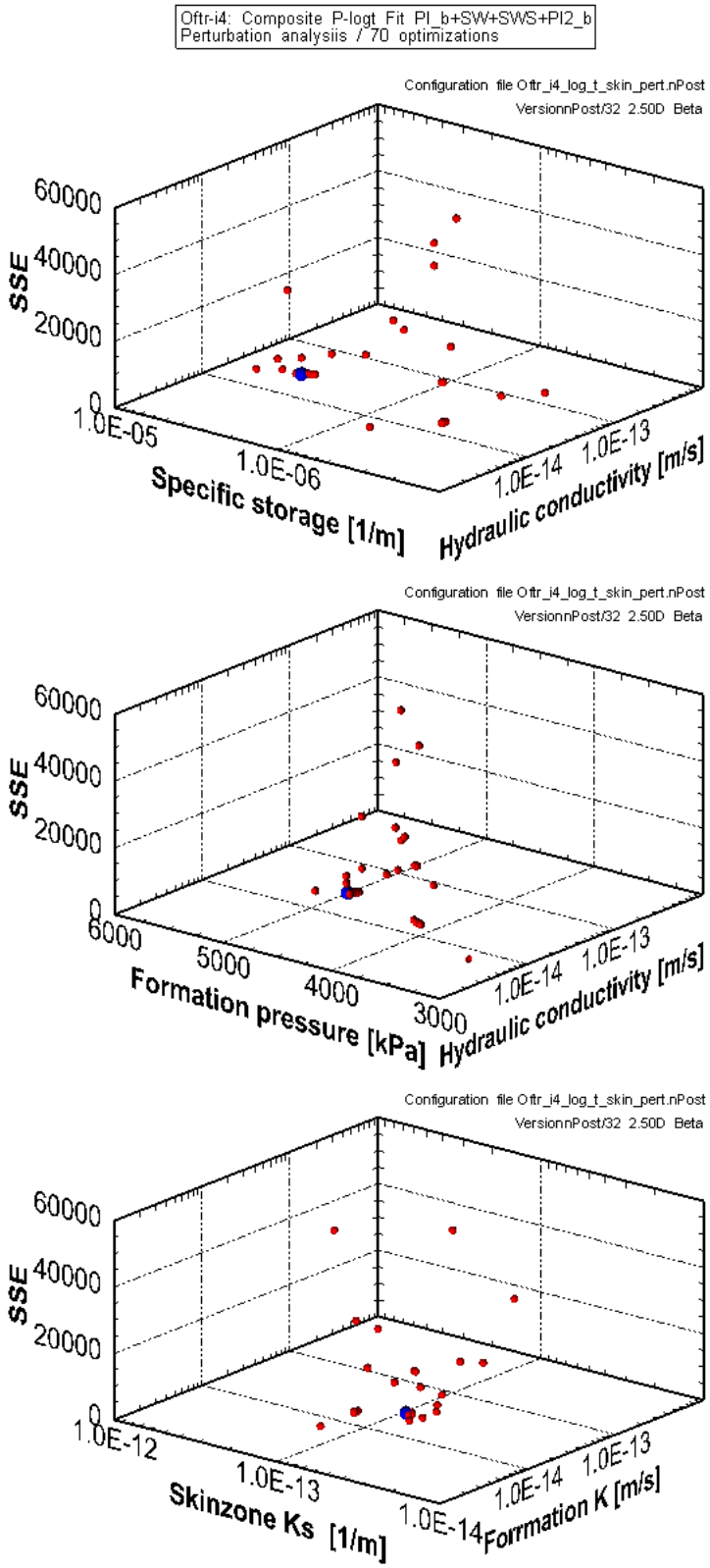

Fig. 11.20: Oftr-i4: composite model: results from perturbation analyses of the nSights inverse simulation for composite fit PI+SW+SWS+SWS (P - log (t)). Top: SSE versus S_S and K and S_S. Middle: SSE versus K and P_f. Bottom: SSE versus K and K_S.

Tab. 11.14: Perturbation analysis / Lowest SSE case: Parameters estimates and 95% confidence intervals for the PI+W+SWS+PI2 composite fit, composite skin model

Parameter	Units	Fit Value SSE= 4502	95% Confidence Interval	
			Lower Value	Upper Value
K_fm	[m/sec]	1.48E-14	1.40E-14	1.57E-14
K_s	[m/sec]	6.88E-14	5.47E-14	8.66E-14
P_fm	[kPa]	4794	4762	4826
Ss_fm	[1/m]	3.05E-06	2.72E-06	3.41E-06
t_s	[m]	0.0050	0.0037	0.0063

Tab. 11.15: Perturbation analysis/ Lowest SSE case: Covariance-Correlation matrix for skin model; composite Fit P-logt (shaded cells denote correlation matrix elements)

	K_fm	K_s	P_fm	ss_fm	t_s
K_fm	9.17E-06	2.65E-05	4.04E-06	-3.88E-05	3.43E-06
K_s	8.74E-01	9.98E-05	2.21E-05	-1.34E-04	1.35E-05
P_fm	2.49E-01	4.13E-01	2.86E-05	-2.35E-05	3.14E-06
ss_fm	-9.38E-01	-9.84E-01	-3.23E-01	1.87E-04	-1.79E-05
t_s	8.32E-01	9.94E-01	4.32E-01	-9.65E-01	1.85E-06

11.9. Summary for the standard "plus" analysis

Comprehensive analyses of test Oftr-i4 included:

- re-evaluation of the hydraulic model
- analysis of part-test sequences (SW, SW-SWS) including perturbation analyses
- testing of the role of non-fitting parameters
- adjustment of fitting constraints associated with smoothing and reduction of input data
- repetition of the statistical analyses

The incertitude to the static formation pressure indicated by the low sensitivity coefficient to P_f was recognized in the QLR. For the standard analysis, the effect of the P_f parameter was extensively investigated during perturbation analysis on the SW-SWS sequence and by setting different ranges within P_f was allowed to vary. Two cases were presented with P_f ranges 4000 - 5500 kPa and 3000 to 6000 kPa, respectively. The perturbation analyses for these two cases provided multiple minima in the parameter space within a K-range of roughly 1E-14 to 2E-13

m/s and S_S 2.4E-7 to 5E-06 m^{-1}. The solutions with lowest SSE values were associated with unrealistic values for the P_f parameter, i.e. at the lower bound of the pre-set P_f ranges.

After adjustment of fitting constraints (composite fit for PI+SW+SWS+PI2 with P as function of log t for each sub-fit) and smoothing/reduction of input data, a higher P_f estimate of 4552 kPa and a K-value of 4.1E-14 m/s was obtained. The initial estimates of the fitting parameters were varied during a perturbation analysis to see if the solution is associated with a global minimum in the parameter space and if other minima exist. The exercise showed that all solutions found are associated with single (global) minimum and the parameter estimates of all inverse simulations are located within the joint confidence regions of the best-fit estimate (lowest SSE). The residual distribution similar to the normal error distribution and the good fit quality give confidence to estimated parameters of this solution.

In a final step, a skin zone was added to see if the visual fits and the residuals would be further improved. The composite skin model resulted in a further reduced SSE-value and a better visual result for the PI2 fit. The obtained K-estimate of 1.5-14 m/s is lower than the one of the homogeneous model (4.1E-14 m/s) and the P_f estimate of 4754 kPa higher compared to the one of the homogeneous model (4502 kPa). The contrast between formation conductivity (K = 1.5E-14 m/s) and skin zone conductivity (K_S = 6.5E-14 m/s) is relatively small. The perturbation of the non-fitting parameters of the composite model confirms essentially the parameter estimates from the single realization (using unvaried initial estimates) but suggests a slightly higher P_f estimate of 4794 kPa. The perturbation analysis also shows that the parameter space for the composite model is less confined and multiple minima exist. Considering this, and in view of the relatively low K/K_S contrast and the very small radial skin thickness of the skin model (t_S = 0.005 m), the homogeneous model is preferred against the composite skin model.

Based on the results of the good quality simulation cases (tagged with the √ symbol in Tab. 11.16), the following parameter ranges were assessed:

- formation conductivity: 1.8E-14 to 2.2E-13 m/s
- specific storage: 2.2E-7 to 5.1E-06 1/m
- formation pressures: 3700 to 4580 kPa (with corresponding heads 303 - 393 m asl).

The above parameter ranges include the incertitude as indicated by the 95^{th} percentile confidence intervals for the individual minimum and maximum values.

The lowest P_f value was obtained when extending the permitted parameter range to unrealistic low values. The highest P_f value, associated with a K-estimate of 4.1E-14 m/s and a S_S value of 1.1E-06 m^{-1} was obtained using smoothed field data and adjusted fit constraints.

Level	Comments	
QLR best e.	Cart ESF	h
Standard plus	Sequence fit (diag) of SWS	h
Standard plus	Cart SW-SWS fit	h
Standard plus	Cart SW-SWS fit extended P_f range [1)]	h
Standard plus	Cart SW-SWS fit extended P_f range [2)]	h
Standard plus	Cart PI-SW-SWS fit extended P_f range [1)]	h
Standard plus	Cart PI-SW-SWS fit extended P_f range [2)]	h
Standard plus	CF PI+SW+SWS+ PI; ext. P_f range	h
Standard plus b. e.	CF PI+SW+SWS+ PI; ext. P_f range [2)]	h
Standard plus	CF PI+SW+SWS+ PI; ext. P_f range	c
Standard plus	CF PI+SW+SWS+ PI; ext. P_f range [2)]	c

best estimate case is shaded

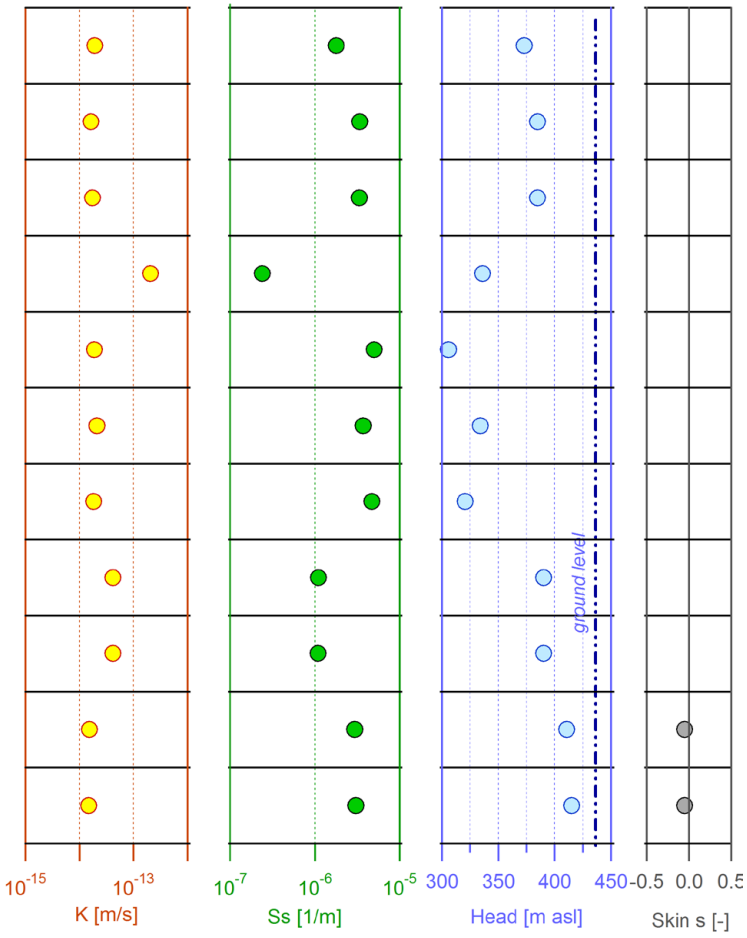

Fig. 11.21: Overview of results of inverse parameter estimations based on different models and fit configurations

QLR =	Quick Look Report
b.e.	best estimate
c =	composite skin model
CF	Composite fit
Cart ESF =	Cartesian entire sequence fit
diag.	diagnostic plot, composite fit of dP and dP'
h =	homogeneous model
[1)] =	perturbation analysis using extended P_f range 4000 - 5500
[2)] =	perturbation analysis using extended P_f range 3000 - 6000

Tab. 11.16: Oftr-i4: Overview of results of inverse parameter estimations

Case		K [m/s]	S_S [m^{-1}]	s [-]	h_s [m asl]	Fit quality	Remarks Plausibility	
Cart ESF	h	1.92E-14	1.79E-06		373.1	+		
Standard plus analysis:								
Sequence fit (diag) of SWS	h	1.64E-14	3.39E-06		384.9	+	P_f at lower limit	
Cart SW-SWS fit	h	1.73E-14	3.36E-06		384.9	+	P_f at lower limit	
Cart SW-SWS fit extended P_f range [1)]	h	2.05E-13	2.40E-07		336.0	+		√
Cart SW-SWS fit extended P_f range [2)]	h	1.90E-14	5.02E-06		305.8	+		√
Cart PI-SW-SWS fit extended P_f range [1)]	h	2.11E-14	3.71E-06		333.9	+		√
Cart PI-SW-SWS fit extended P_f range [2)]	h	1.84E-14	4.71E-06		320.6	+		√
CF PI+SW+SWS+ PI; ext. P_f range	h	4.13E-14	1.10E-06		390.2	+		√
CF PI+SW+SWS+ PI; ext. P_f range [2)]	h	4.14E-14	1.09E-06		390.1	+	**best estimate**	√
CF PI+SW+SWS+ PI; ext. P_f range	c	1.54E-14	2.98E-06	-0.05	410.8	+	t_S at lower limit	
CF PI+SW+SWS+ PI; ext. P_f range [2)]	c	1.48E-14	3.05E-06	-0.05	414.9	+	t_S at lower limit	

√ = good simulation results used to assess parameter ranges
QLR = Quick Look Report
c = composite skin model
CF Composite fit
Cart ESF = Cartesian entire sequence fit
diag. diagnostic plot, composite fit of dP and dP'
h = homogeneous model
[1)] = perturbation analysis using extended P_f range 4000 - 5500
[2)] = perturbation analysis using extended P_f range 3000 - 6000

12. Test Interval Oftr-i5: 449.9 - 499.9 m

Interpretation Level: Standard analysis

12.1. Introduction

Test Oftr-i5 consists of a COM and PSR phase followed by two pulse withdrawal tests (PW1 and PW2) and a short-term slug withdrawal test (SW). The initial analyses presented in the QLR (Appendix E) were expanded and additional numerical analyses were conducted to provide a greater level of confidence in the estimated formation properties. Borehole history effects were already included during the simulations for the QLR, as it was done for all intervals. The diagnostic plots presented in the QLR indicated that a homogeneous flow model is appropriate for this test interval. Three hours after begin of the PW1 test, the interval pressure showed a reversed trend (decreasing absolute pressure). The PW2 was initiated to record a greater percentage of pressure recovery and to confirm wellbore compressibility. A short duration slug withdrawal (SW) was performed to confirm the PW/PW2 results.

Downhole pressures of the entire test sequence of Test Oftr-i5 and packer pressures are shown in Fig. 12.3.

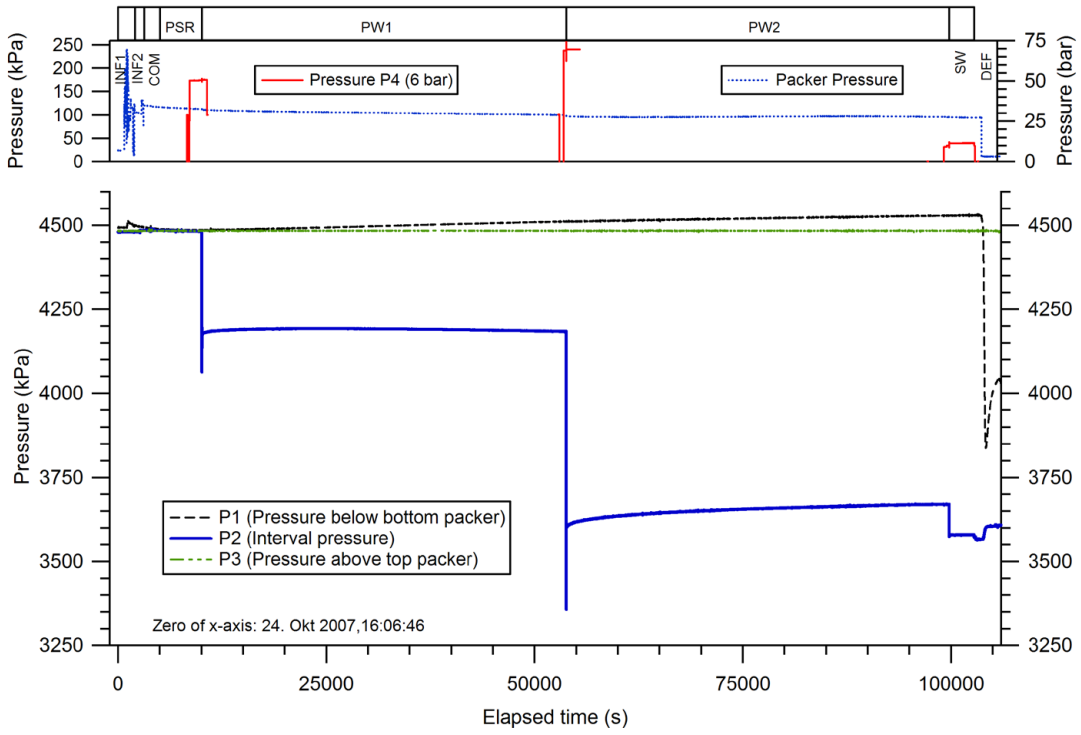

Fig. 12.1: Test Oftr-i5, 450.0 - 500.0 m: overview plot

12.1.1. Parameter Range and Best Estimate from the QLR

The range in fitted parameters of formation conductivities (K) was from 2.3E-14 to 8.7E-14 m/s and the estimates for specific storage (Ss) ranged from 4.9E-7 to 1.3E-6 m^{-1}. The estimated formation pressures indicated a relatively large range between 2880 and 3500 kPa, indicating hydraulic heads between about 270 m to 333 m asl which are significantly below the surface elevation of 433 m asl. The relatively high head values were based on the diagnostic fits of the PW1 sequence. Because of the low hydraulic conductivity of the formation and the relatively short duration of the test phases, only early time data were available for the extrapolation of formation pressures which is subject to large uncertainty. The uncertainty is also indicated by the low sensitivity of the analysis to the static formation pressure. The parameters obtained from the Cartesian fit to the entire testing sequence fit were considered the most representative parameter values: K = 2.3E-14 m/s, S_S = 1.3E-06 m^{-1} and P_f = 3109 kPa (see Tab. 12.2 and Appendix E). The Cartesian fit of the QLR best estimate is shown in Fig. 12.2.

The two pulse tests provided consistent measurements of the test zone compressibility, c_{tz} = 7.3E-10 Pa^{-1} for PW1 and 6.2E-10 Pa^{-1} for PW2.

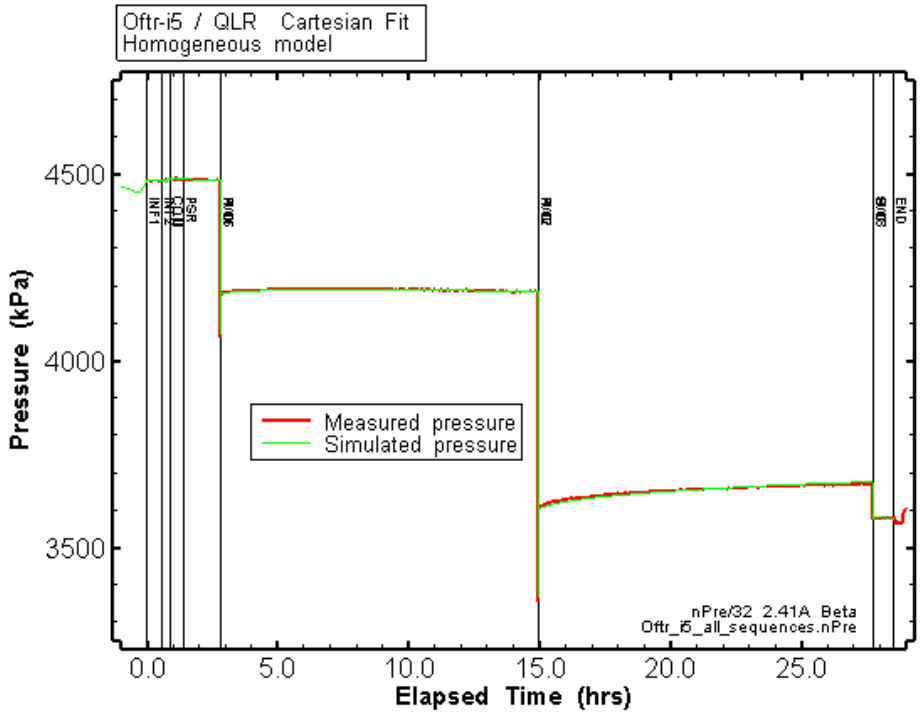

Fig. 12.2: Oftr-i5: Cartesian fit of the QLR best-estimate

Tab. 12.1: Oftr-i4: QLR best-fit parameters estimates and 95% confidence intervals for homogeneous model.

Parameter	Units	Fit Value SSE=1.30E+05	95% Confidence Intervals	
			Lower Value	Upper Value
K_fm	[m/s]	2.29E-14	2.09E-14	2.50E-14
P_fm	[kPa]	3109.4	3051.7	3167.2
ss_fm	[1/m]	1.30E-06	1.13E-06	1.50E-06

12.1.2. Data smoothing and filtering

For all sequences, the pressures varied only within a narrow range once the test was initiated (i.e. after the initial pulse or slug pressure change). The scatter of the pressure signal due to the NOK current transformation station is rather important. To remove data noise, pressure data of each fitted sequence PSR, PW1, PW2 and SW were smoothed using the nSights smooth option. For all sequences, 25 data points left and right from the data point were used for the smooth operations. The smoothed data curves are shown as blue lines in the individual plots of Fig. 12.7. The smoothing allows obtaining a more representative selection of field data when using the nSights data reduction option. The data reduction option was used for the P - log(t) fit constraint. The smoothing of field data had no noticeable effect on the inverse parameter optimizations associated with the Cartesian Fit constraint.

12.1.3. Incertitude with regard to the P_f parameter

Considering the very low hydraulic conductivity of test interval Oftr-i5 with a K-value smaller than 1E-12 m/s, the duration of the individual test sequences are too short to obtain a reliable estimate of static formation pressure (Fig. 12.3, middle left plot). The change of packer pressures during Test Oftr-i5 could have affected the interval pressure and consequently the P_f estimate (see Section 12.3)

12.2. Homogeneous model -- Cartesian fit PW1-PW2-SW

This Cartesian fit corresponds basically to the fit presented in the QLR but additionally includes the SW event. The field data were smoothed. Parameter ranges as defined in Section 7.3 were used with exception of the range for the P_f parameter which was extended to 2000 - 5000 kPa.

The optimization of the Cartesian pressure response of the PW1-PW2-SW sequence showed a fairly good fit. The simulation indicated a formation conductivity of 2.1E-14 m/s, a static formation pressure of 3052 kPa and a specific storage estimate of 1.5E-06 m^{-1}, Tab. 12.2. These results are very similar to the Cartesian Fit to the PW1-PW2 sequence of the QLR (Appendix E). The range between the upper and lower values for the 95th percentile confidence intervals are listed in Tab. 12.2 and shown in Fig. 12.3. The plots on the bottom of Fig. 12.3 provide the 95th percentile confidence regions for the estimation of the S_s and K parameters (bottom left) and P_f and K parameters (bottom right), with the shape of the ellipse indicating the degree of

correlation between the parameters. Tab. 12.3 includes the covariance correlation matrix (shaded cells) which indicates that the three fitting parameters are well correlated. This correlation is also observed in the confidence intervals plots of Fig. 12.3 by small minor axis of the uncertainty ellipsoids. The middle right plot in Fig. 12.3 shows a comparison of the residuals (measured value minus simulated value) to that of a normal distribution. The residuals are essentially normally distributed which indicates the absence of a systematic error and supports the conceptual model. Using the parameters estimates of the Cartesian fit (PW1-PW2-SW) for the diagnostic plots of the individual sequences resulted in good match of normalized pressure and derivative for the Ramey plots PW1 (not shown) and PW2 (top right plot of Fig. 12.3). The middle left plot in Fig. 12.3 shows the change in sensitivity coefficients of the three fitted parameters during the PW1-PW2-SW sequence. This indicates that the K is the most sensitive parameter and P_f is the least sensitive parameter and is still increasing at the end of the PW1 and PW2 sequence. The sensitivity coefficients for the SW sequence are zero. The SW phase is therefore not included during subsequent interpretation steps.

Tab. 12.2: Oftr-i5: Parameters estimates and 95% confidence intervals for the Cartesian all sequence fit, homogeneous model.

Parameter	Units	Fit Value SSE= 1.05+05	95% Confidence Intervals	
			Lower Value	Upper Value
K_fm	[m/s]	2.09E-14	1.92E-14	2.28E-14
P_fm	[kPa]	3050	2995	3106
ss_fm	[1/m]	1.46E-06	1.28E-06	1.66E-06

Tab. 12.3: Oftr-i5: Covariance-Correlation matrix for homogeneous model (shaded cells denote correlation matrix elements).

Covariance/Correlation Matrix: Est. All_Cart_smoothed			
	K_fm	P_fm	ss_fm
K_fm	9.86E-06	5.79E-05	-4.45E-05
P_fm	9.90E-01	3.47E-04	-2.63E-04
ss_fm	-9.98E-01	-9.95E-01	2.02E-04

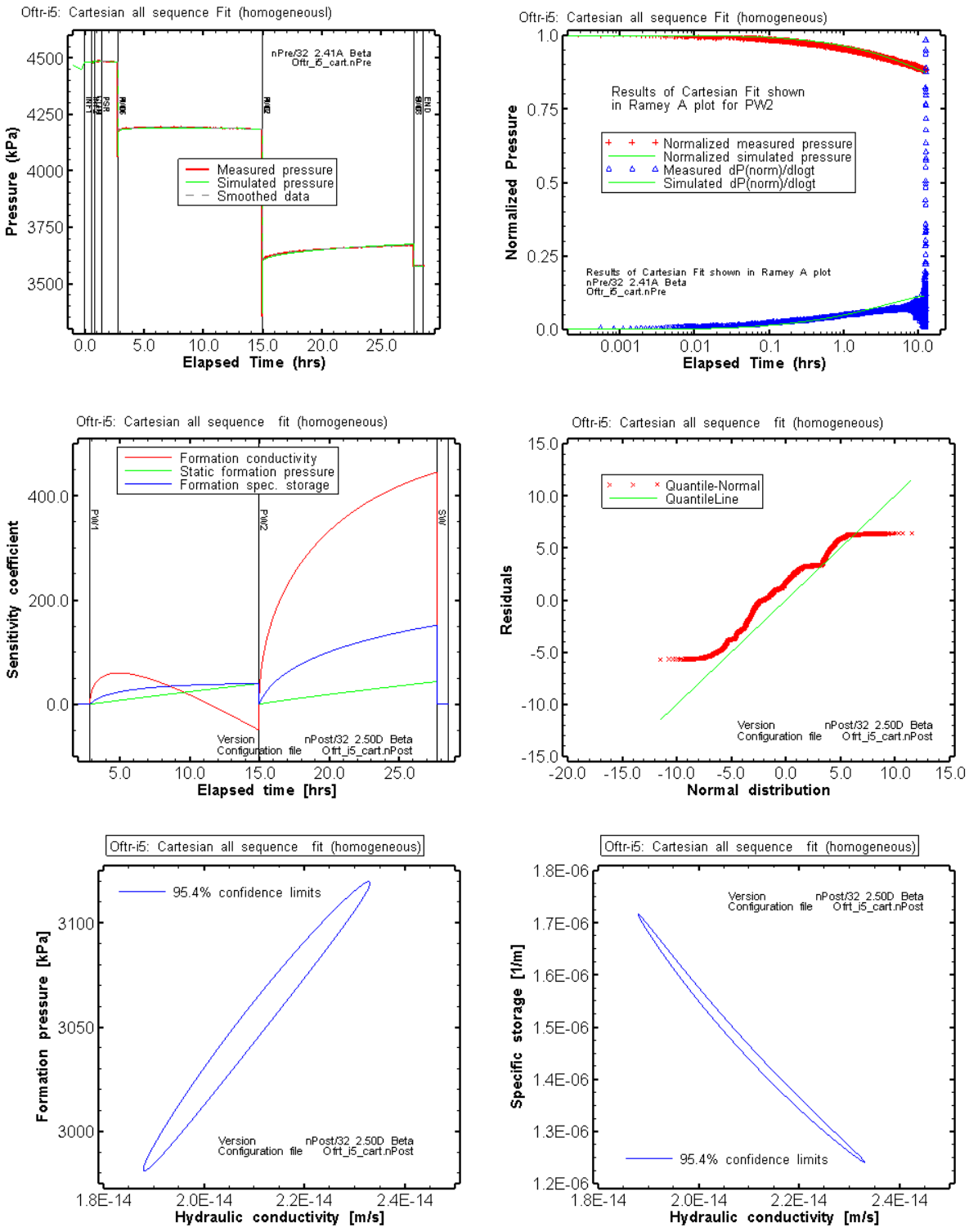

Fig. 12.3: Oftr-i5: Results from nSights inverse simulation of the Cartesian pressures of the entire test

Cartesian fit shown at top left; Ramey plot at top right; sensitivity plot at middle left; computed residual compared to a normal distribution at middle right; the confidence regions for the parameters K and P_f at bottom left and for K and S_S at bottom right.

12.3. Homogeneous Model -- Cartesian Fit with Limited P_f Range

This Cartesian fit corresponds to the fit presented in Section 12.2 but the variation of the P_f parameter was limited to the plausible range from 3993 kPa to 4974 kPa as defined in Section 7.3 (corresponding to static formation heads +/- 50 m above and below ground level: 383 to 483 m asl). The simulation indicated a formation conductivity of 3.00E-14 m/s, a specific storage estimate of 3.9E-07 m^{-1} and a static formation pressure at the lower bound of the pre-set range (3993 kPa, Tab. 12.4). Note that in comparison to the optimization with the extended P_f range (Section 12.2), the K-estimate for the limited P_f-range increased only by a factor of 1.4, whereas the S_S-estimate decreased by a factor of 3.8. Limiting of the P_f range resulted in inferior fit quality as it is shown in Fig. 12.4 for the Cartesian plot (upper left) and the Ramey A plots (result of Cartesian fit to normalized pressure and derivative) for the PW1 (upper right) and PW2 (middle left) sequences.

The sum of squared errors (SSE = 4.39E+05; Tab. 12.4) is significantly increased compared to the result of parameter optimization using an extended P_f range (SSE = 1.05+05, Tab. 12.2). The middle left plot in Fig. 12.4 shows a comparison of the residuals (measured value minus simulated value) to that of a normal distribution. The residuals are essentially normally distributed which indicates the absence of a systematic error and supports the conceptual model.

The range between the upper and lower values for the 95th percentile confidence intervals are listed in Tab. 12.4 and shown in Fig. 12.4. The two plots on the bottom left and bottom right side of Fig. 12.4 provide the 95th percentile confidence regions for the estimation of the P_f and K parameters (bottom left) and S_S and K parameters (bottom right), with the shape of the ellipse indicating the degree of correlation between the parameters. Tab. 12.5 includes the covariance correlation matrix (shaded cells) which indicates that the especially the Ss and K fitting parameters are well correlated. This correlation is also observed in the confidence intervals plots of Fig. 12.4 by small minor axis of the uncertainty ellipsoids.

Tab. 12.4: Oftr-i5: Parameters estimates and 95% confidence intervals for the Cartesian PW1-PW2 sequence fit, homogeneous model.

Parameter	Units	Fit Value SSE= 4.39E+05	95% Confidence Intervals	
			Lower Value	Upper Value
K_fm	[m/s]	3.00E-14	2.77E-14	3.26E-14
P_fm	[kPa]	3993	3966	4020
ss_fm	[1/m]	3.88E-07	3.38E-07	4.45E-07

Tab. 12.5: Oftr-i5: Covariance-Correlation matrix for the Cartesian PW1-PW2 sequence fit, homogeneous model (shaded cells denote correlation matrix elements).

Covariance/Correlation Matrix: Est. All_Cart_smoothed			
	K_fm	P_fm	ss_fm
K_fm	8.72E-06	3.10E-05	-4.35E-05
P_fm	7.49E-01	1.96E-04	-1.74E-04
ss_fm	-9.89E-01	-8.32E-01	2.22E-04

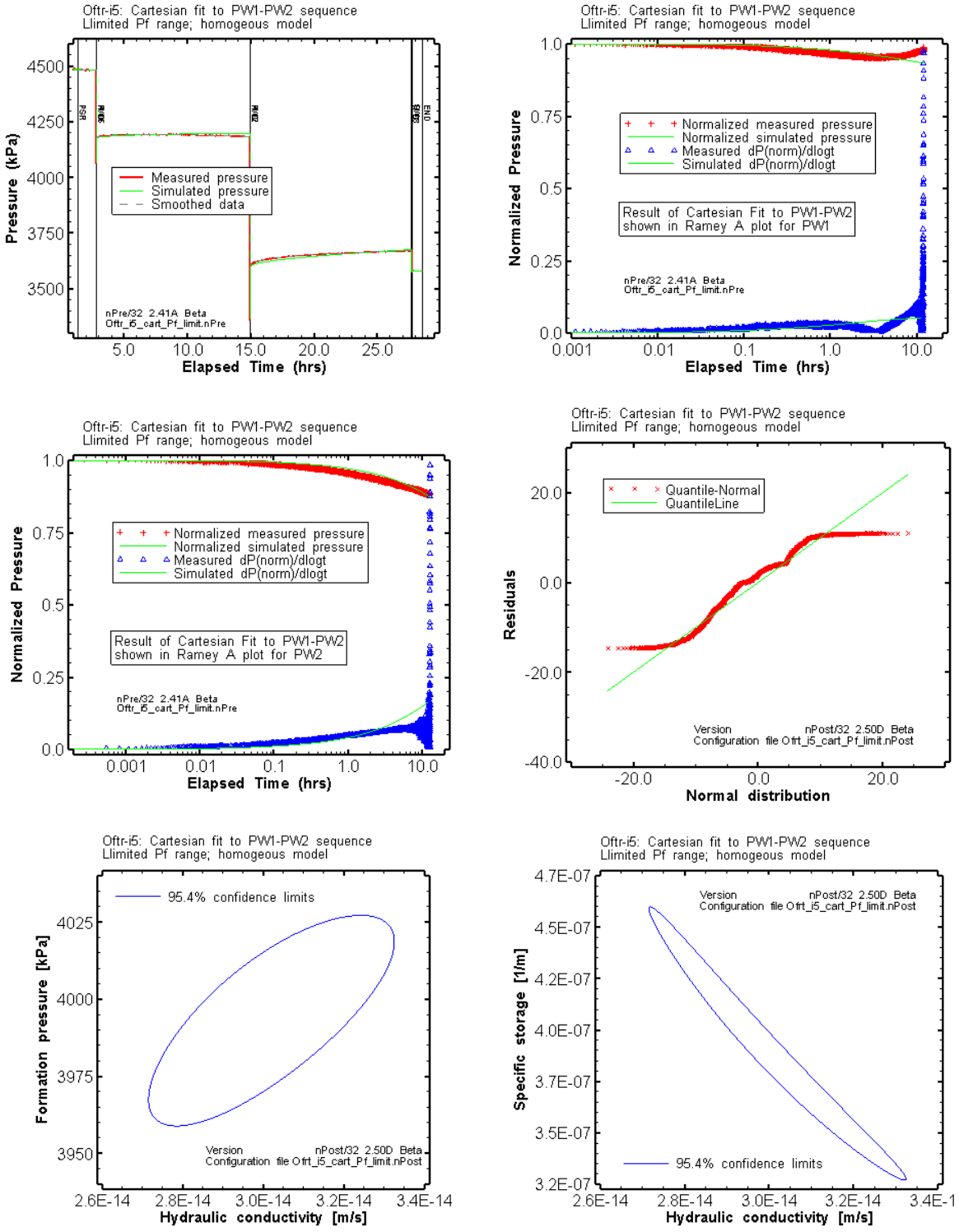

Fig. 12.4: Oftr-i5: Results from nSights inverse simulation of the Cartesian pressures of the PW1-PW2 sequence.

Results shown for the Cartesian pressure (top left) and for the PW1 (top right) and PW2 (middle left) Ramey A plots, the computed residual compared to a normal distribution (middle right) and the confidence regions for the parameters K and P_f (bottom left) and K and S_S (bottom right).

12.4. Potential Influence of Packer Pressure Change

The packer pressure continuously decreased during the hydraulic testing in Oftr-i5 (Fig. 12.5 and Tab. 12.6). Theoretically, the change in packer pressure could have resulted in slight movement of the packer sleeves at the packer ends facing towards the test zone. In case of packer pressure decrease, such an effect would cause an increase in test zone volume. In tight formation, an increase in test zone volume would be associated with a temporary decrease of interval pressure.

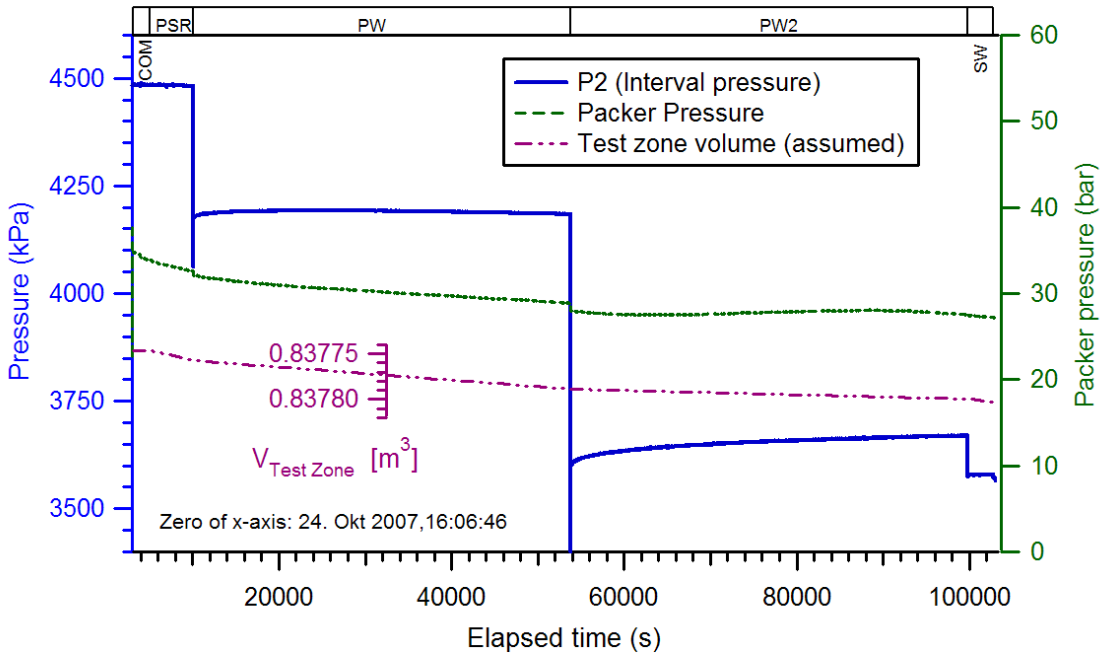

Fig. 12.5: Oftr-i5: Packer pressure data (shown with green line)

The potential influence of the packer pressure change associated with test zone volume change was estimated based on a assumed incremental movement of -0.5 mm per 1 bar change (decrease) in packer pressure (2 packers times -0.25 mm per packer). Assuming a movement perpendicular to the wellbore circular area, the test zone volume change becomes +8.37 ml/bar. The nominal test interval volume (≅ test zone volume V_{TZ}) is 0.8378 m^3. The measured changes in packer pressure per test event are transferred to volume changes and test zone volume values (Tab. 12.6). The varying test zone volumes as shown in Fig. 12.5 (magenta line) were incorporated in nSights as a wellbore boundary condition. The formation parameters were re-estimated during an inverse parameter optimization to quantify the effect of assumed test zone volume change on the P_f estimate. The results are shown in Fig. 12.6, Tab. 12.7 and Tab. 12.8 should be considered with care because the model is based on very rough assumptions. The sum of squared errors (Tab. 12.7) is by a factor of 2.4 higher in comparison to the case with constant test zone volume (Tab. 12.2). The K-estimate increased by factor of 1.6 and the P_f-estimate increased by 1100 kPa (P_f = 4150 kPa compared to 3050 kPa for the case with constant V_{TZ})

Tab. 12.6: Oftr-i5: Start and end packer pressures and relative pressure changes for individual test sequences.

OFTR-i5	Elapsed time		Packer pressures (at surface)			V_{TZ} [1)]
Event	Start [hrs]	End [hrs]	Start [bar]	End [bar]	Change [bar]	at end [m3]
COM	0.87889	1.40389	34.8	33.84	-0.96	0.8377470
PSR	1.40389	2.81861	33.84	32.58	-1.26	0.8377576
PW1	2.81861	14.9525	32.58	28.88	-3.70	0.8377885
PW2	14.9525	27.72417	28.88	27.61	-1.27	0.8377992
SW	27.72417	28.54694	27.61	27.2	-0.41	0.8378026

1) Test zone volume calculated based on an assumed volume change of 8.37 ml/bar (bar packer change) for end time of indicated event

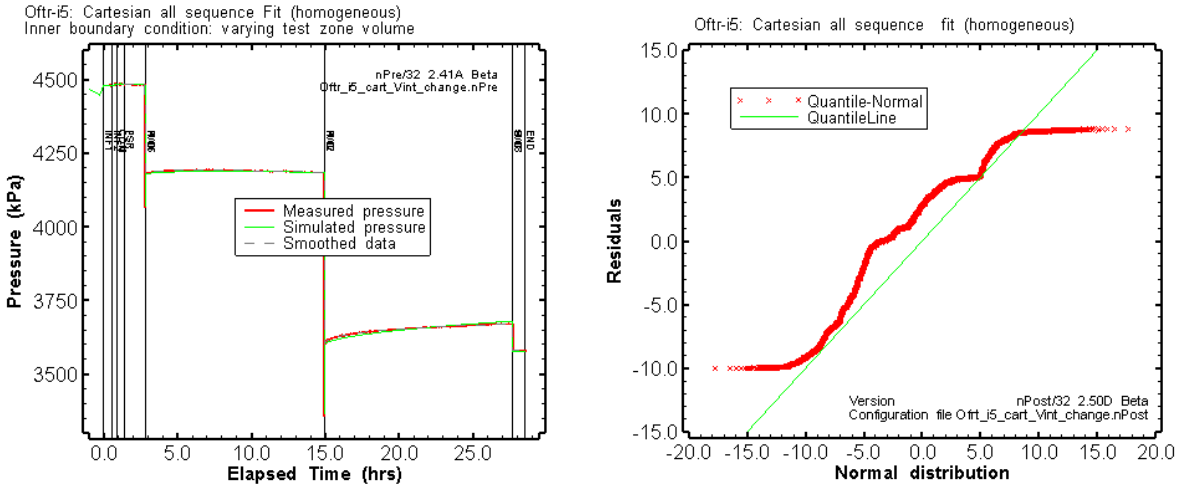

Fig. 12.6: Oftr-i5, varying test zone volume: Result of inverse parameter optimization to Cartesian pressure (left) and residual plot (right)

Tab. 12.7: Oftr-i5: Varying test zone volume. Parameters estimates and 95% confidence intervals for the Cartesian all sequence fit

Parameter	Units	Fit Value SSE= 2.49E+05	95% Confidence Intervals	
			Lower Value	Upper Value
K_fm	[m/s]	3.27E-14	2.78E-14	3.84E-14
P_fm	[kPa]	4150	4111	4188
ss_fm	[1/m]	2.46E-06	1.93E-06	3.14E-06

Tab. 12.8: Oftr-i5: Varying test zone volume. Covariance-Correlation matrix for homogeneous model (shaded cells denote correlation matrix elements).

Covariance/Correlation Matrix: Est. All_Cart_smoothed			
	K_fm	P_fm	ss_fm
K_fm	3.44E-05	3.27E-05	-1.55E-04
P_fm	8.75E-01	4.06E-05	-1.51E-04
ss_fm	-9.98E-01	-8.99E-01	6.97E-04

12.5. Homogeneous Model - Composite Fit PSR+PW1+PW2 for P vs. log(t)

The PSR, PW1 and PW2 sequence data were reduced using the nSights data reduction option "log x change". This reduction was applied on smoothed data (see Section 12.1.2).The data transformation results in consistent distribution of the reduced data points along the log time axis as shown in Fig. 12.7 (curves with red square symbols in the upper plots and the middle left plot). The log distribution of data points on the time axis for each sequence emphasizes fitting of the early time data and therefore supports the verification of the hydraulic model. A composite fit was set up which includes P - log (t) fitting of the sequences PSR, PW1 and PW2.

The result of the nSights inverse parameter optimization is presented in Tab. 12.9 and Fig. 12.7. The obtained fit is shown visually in the sequence plots P vs. log (t) of Fig. 12.7 (two upper plots and middle left plot). The individual sequences PSR and PW1 are rather poorly fitted whereas the fit to the PW2 sequence is of middle-rate quality. The K- and P_f-estimates from the composite P - log(t) fit are very similar to the K/P_f-estimates from Cartesian fit to the PSR-PW1-PW2 sequence (using extended P_f range, see Section 12.2). A visual comparison of the result of the two fit specifications is provided in Fig. 12.8.

Tab. 12.9: Parameters estimates and 95% confidence intervals for composite Fit, P vs. log(t) fit constraint, PSR + PW1 + PW2 composite fit., homogeneous model.

Parameter	Units	Fit Value = 1450	95% Confidence Intervals	
			Lower Value	Upper Value
K_fm	[m/s]	2.59E-14	1.02E-14	6.60E-14
P_fm	[kPa]	3079	2463	3694
ss_fm	[1/m]	1.29E-06	3.17E-07	5.24E-06

The residuals compared to a normal error distribution are shown in the middle right plot of Fig. 12.7 for each sub-fit. The residuals for the Cartesian fit specification (Section 12.2) are shown in the same plot for comparison. The residuals for the PSR and PW1 sub-fits do not follow a normal distribution whereas the residuals for the PW2 sub-fit are essentially normally distributed. This could be due the effect of decreasing packer pressure which was more pronounced for the PSR and PW1 sequences than for the PW2 sequence.

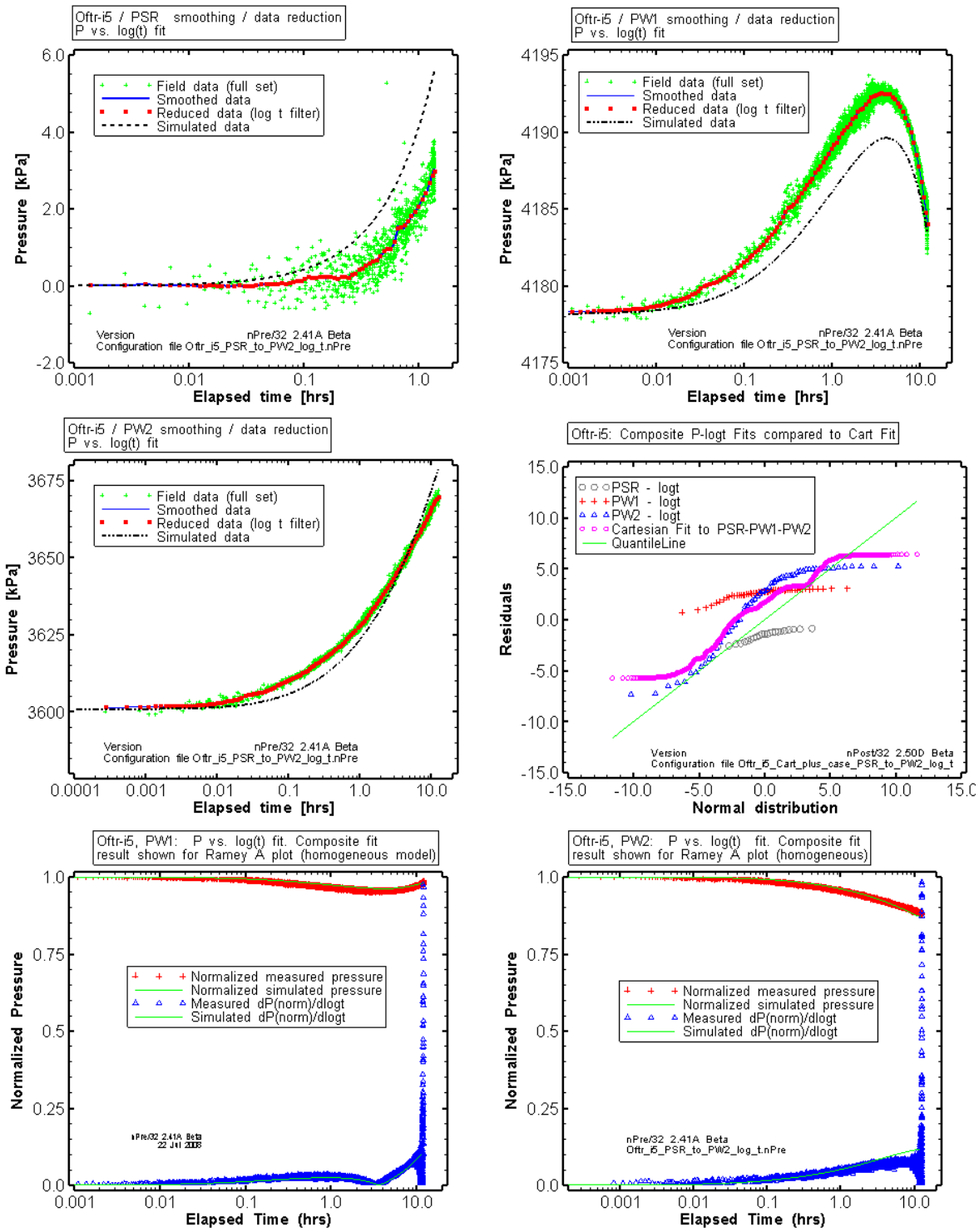

Fig. 12.7: Oftr-i5, homogeneous model: P vs. log(t) composite fit PSR+PW1+PW2.

Results shown for the individual test sequences. Bottom plots: Result of composite fit shown for Ramey A plots of PW1 and PW2. Middle right: computed residuals compared to normal distribution for P vs. log(t) sub-fits and for the Cartesian Fit PSR-PW1-PW2.

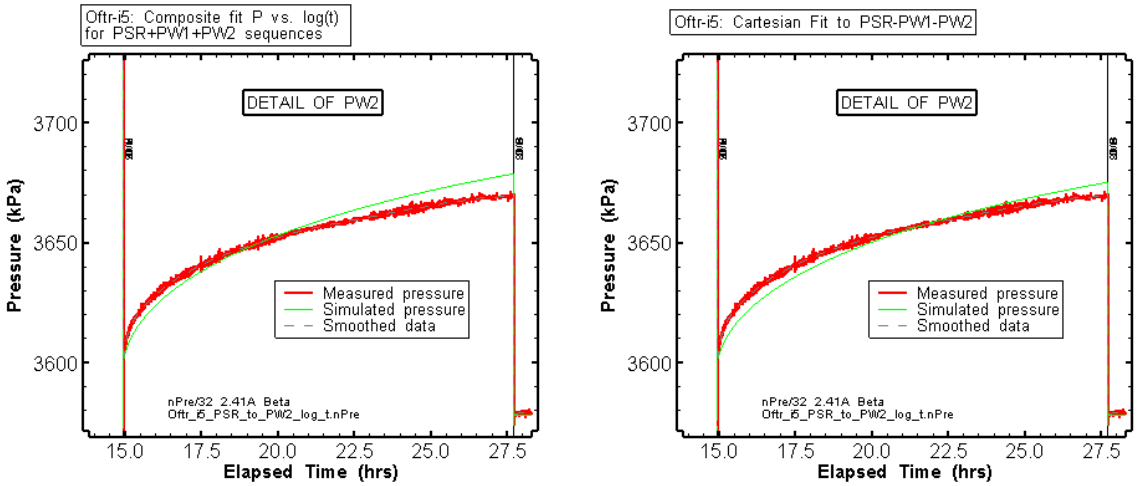

Fig. 12.8: Comparison of selected fits in a Cartesian detail view for PW2: Left: composite P vs. log(t) fit to PSR+PW1+PW2. Right: Cartesian fit to the PSR-PW1-PW2 sequence (Section 12.2).

12.6. Summary

During the "standard analysis" for test Oftr-i5, the homogeneous model was further tested using adjusted fit constraints. The significant incertitude with regard to the static formation pressure could not be fully cleared. The packer pressures decreased from 32.6 to 27.6 bar during the PSR-PW1-PW2 sequence. Test zone volume increase as a result of packer pressure decrease could have influenced the interval pressure. This effect was investigated by incorporating varying test volume as inner boundary condition in nSights. The relation used between packer pressure change and test zone volume change is based on an assumed packer displacement rates. The exercise showed that a half of millimetre displacement per bar (per bar of packer pressure change; the displacement is indicated in total for two packers) would result in a P_f-estimate which is increased by 1100 kPa (to 4150 kPa) compared to the case with constant inner boundary conditions (3050 kPa). The K- and S_S parameters proved to behave indifferently with regard to the change of the inner boundary conditions. For the case with constant test zone volume (assuming no effect due to packer pressure change) and based on a homogeneous model, a K-value of 2.1E-14 m/s and a S_S-estimate of 1.5E-6 m^{-1} was obtained. The model with varying test zone volume provided a slightly increased K-estimate of 3.3E-14 m/s and a S_S-estimate of 2.5E-6 m^{-1}.

An additional inverse parameter optimization was conducted with limited range for the P_f-parameter according to a plausible range for static heads +/- 50 meters above/below the surface level. This case provided a similar K-estimate (3.0E-14 m/s), a P_f-estimate at the lower limit of the input range (3993 kPa) and a relatively low S_S-estimate of 3.9E-7 m^{-1}.

The sum of squared errors (SSE) was lowest for the case with extended P_f range (SSE = 1.05E+05) and greatest for the case with confined P_f range (SSE = 4.4E+05). The optimization for the case with varying test zone volume produced an SSE-value of 2.5E+05.

Based on the results of the good quality simulation cases for the homogeneous model (tagged with the √ symbol in Tab. 12.10), the following parameter ranges were assessed:

- formation conductivity: 1.9E-14 to 3.8E-14 m/s
- specific storage: 3.4E-7 to 3.1E-06 1/m
- formation pressure: 2995 to 4188 kPa (with corresponding heads 282 - 403 m asl).

The above parameter ranges include the incertitude as indicated by the 95th percentile confidence intervals for the individual minimum and maximum values.

Note that the highest P_f value was obtained using assumed varying test zone volume based on a mechanism which is not supported by quantitative measurements. Therefore, the static formation pressure estimate has to be considered as highly uncertain for this test interval.

Level	**Comments**	
QLR best e.	Cart ESF	h
Standard	Cart PW1-PW2-SW fit, extended P_f range [1)]	h
Standard	Cart PW1-PW2-SW fit, **best estimate**	h
Standard	Cart PW1-PW2-SW fit, varying V_{TZ}	h
Standard	CF PSR+PW1+PW2; extended P_f range	h

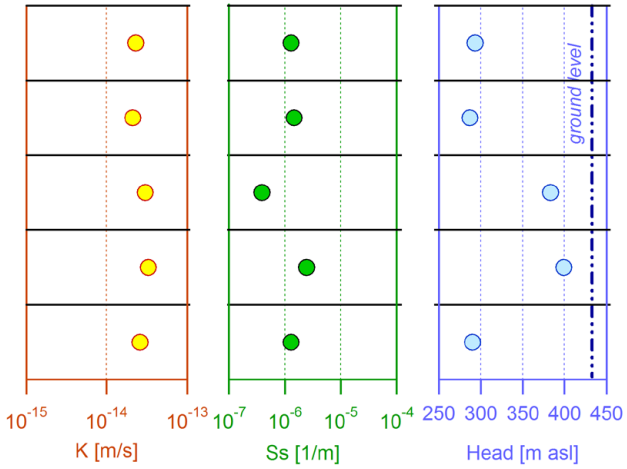

Fig. 12.9: Overview of results of inverse parameter estimations based on different models and fit configurations

QLR = Quick Look Report
c = composite skin model
CF Composite fit
Cart ESF = Cartesian entire sequence fit
h = homogeneous model
V_{TZ} test zone volume
[1)] = perturbation analysis using extended P_f range 2000 - 5000 kPa

Tab. 12.10: Oftr-i5: Overview of results of inverse parameter estimations

Case		**K [m/s]**	**S_S [m^{-1}]**	**s [-]**	**h_s [m asl]**	**Fit quality**	**Remarks Plausibility**	
Cart ESF	h	2.29E-14	1.30E-06		293.2		P_f, h_s are below expected range	
Standard analysis:								
Cart PW1-PW2-SW fit, extended P_f range	h	2.09E-14	1.46E-06		287.1	+	P_f, h_s are below expected range	√
Cart PW1-PW2-SW fit **best estimate**	h	3.00E-14	3.88E-07		383.2	+	P_f, h_s at lower limit of expected range	√
Cart PW1-PW2-SW fit, varying V_{TZ}	h	3.27E-14	2.46E-06		399.2	++	Varying test zone volume due to packer compliance considered	√
CF PSR+PW1+PW2; ext. P_f range	h	2.59E-14	1.29E-06		290.1	+	P_f, h_s are below expected range	√

√ = good simulation results used to assess parameter ranges
QLR = Quick Look Report
c = composite skin model
CF Composite fit
Cart ESF = Cartesian entire sequence fit
h = homogeneous model
V_{TZ} test zone volume
[1)] = perturbation analysis using extended P_f range 2000 - 5000 kPa

13. Test Interval Oftr-i6d: 408.5 - 417.6 m

Interpretation Level: Quick Look Report analysis

13.1. Summary of QLR Analysis

The analysis for the QLR provided the following parameters estimates:

$K = 4.0E\text{-}08$ m/s (2.4E-08 - 2.0E-06 m/s)
$S_S = 1.0E\text{-}06$ m^{-1} (1.0E-07 - 5.8E-06 m^{-1})
$P_f = 4065$ kPa (3919 - 4500 kPa)

The values in brackets indicate the lowest/highest estimates from several inverse parameter optimizations for different test periods and fit constraints using nSights. The large ranges for the individual fitting parameters reflect the uncertainty with regard to measured inconsistent formation responses. The drawdown tests (Fig. 13.1) initiated degassing of dissolved gases in the water of the test zone and possibly in the formation. The latter could possibly have resulted in two-phase flow conditions. The presence of gas was indicated by the high test zone compressibilities measured with c_{tz} -values ≥ 1.6E-06 Pa^{-1}. The best-estimate for the P_f parameter equals to the pressure at the end of the PSR sequence (4065 kPa) and corresponds to a formation head of 432.4 m, i.e. 0.6 meter below ground level.

No further analysis was performed beyond the QLR test interpretation (Annex F).

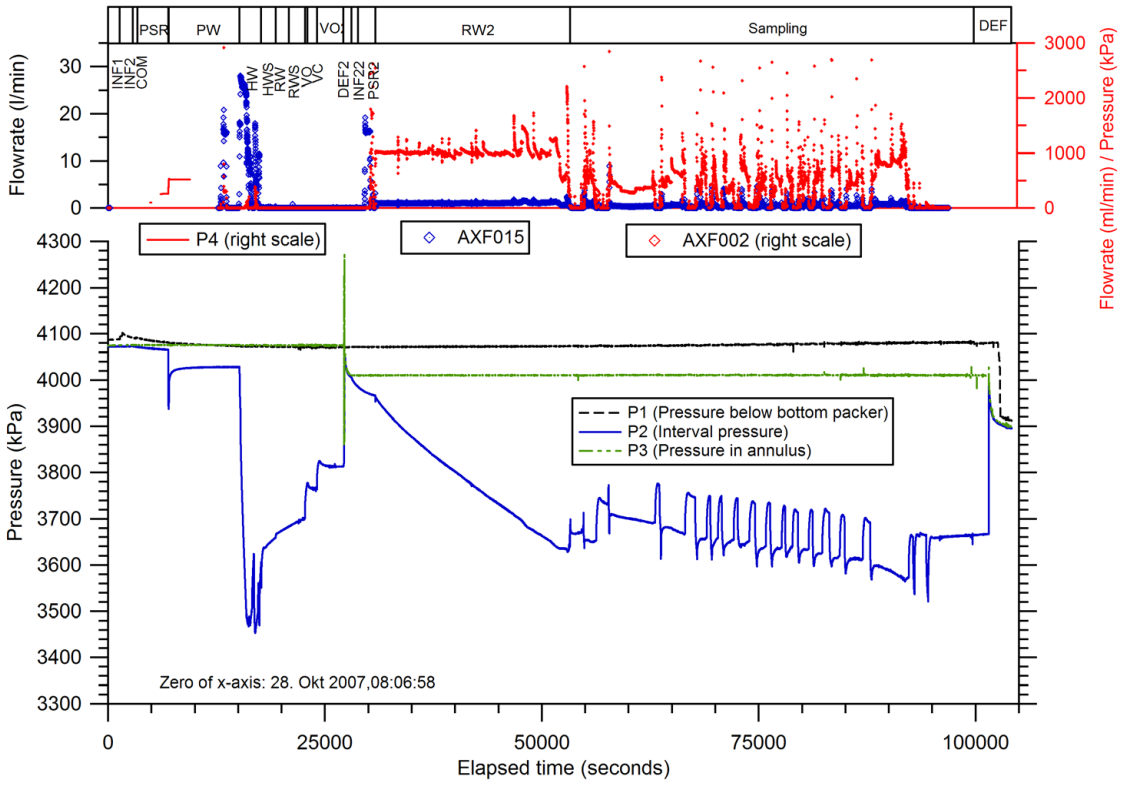

Fig. 13.1: Test Oftr-i6d, 408.5 - 417.6 m: overview plot

14. Test Interval Oftr-i7: 632.5 - 641.6 m

Interpretation Level: Standard analysis

14.1. Introduction

Test Oftr-i7 consists of a COM and PSR phase followed by a pulse withdrawal test (PW) and a pulse injection test (PI). For the standard analysis of test interval Oftr-i7, the earlier analyses presented in the QLR (Appendix G) were refined to better constrain the formation properties with focus on hydraulic conductivity and hydraulic head. Additional numerical analyses using nSights were conducted to provide a greater level of confidence in the estimated formation properties. Borehole history effects were already included during the simulations for the QLR, as it was done for all intervals. The diagnostic plots presented in the QLR indicated that a homogeneous flow model is appropriate for this test interval. The PI test was initiated to confirm wellbore compressibility estimate from PW.

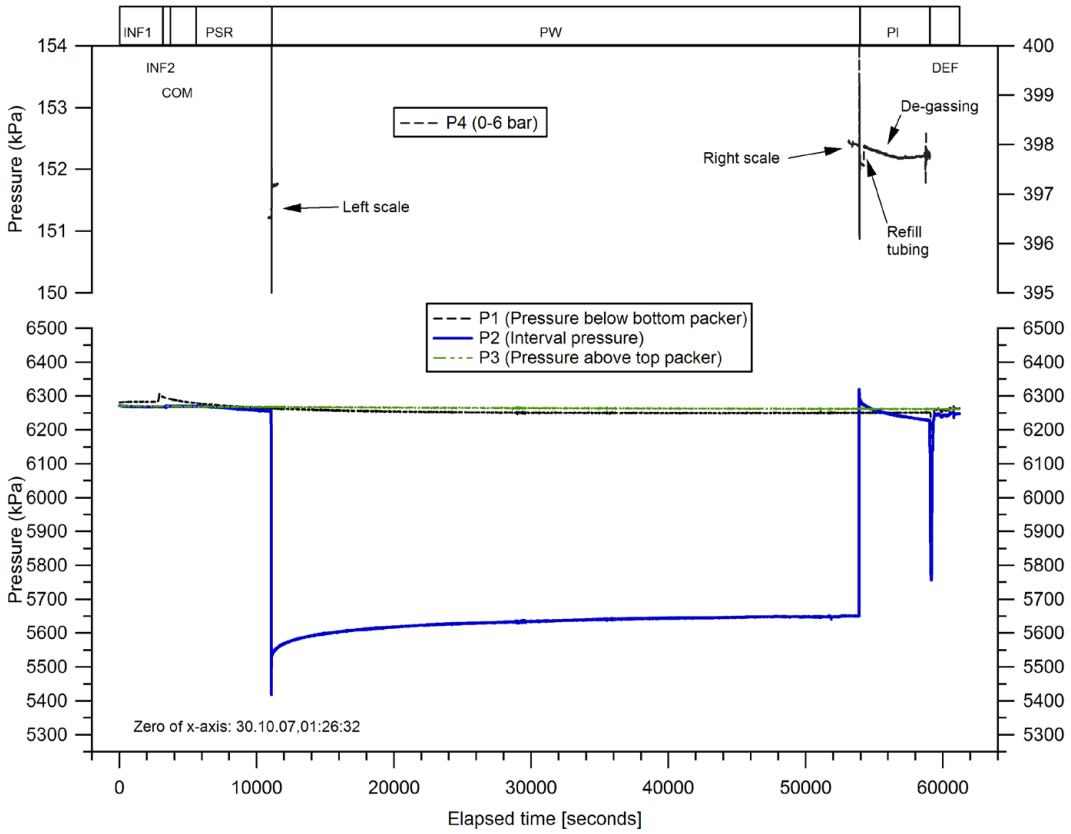

Fig. 14.1: Test Oftr-i7, 632.5 - 641.6 m: overview plot

14.2. Parameter Range and Best-Estimate from QLR

The numerical analyses for the QLR provided the following parameters estimates:

K = 7.6E-14 m/s (7.6E-14 - 1.5E-13 m/s)
S_S = 1.8E-06 m^{-1} (8.3E-07 - 1.8E-06 m^{-1})
P_f = 4795 kPa (4795 - 6326 kPa)

The values in brackets indicate the lowest/highest estimates from several inverse parameter optimizations for different test periods and fit constraints using nSights. In the preliminary analyses presented in the QLR, the estimates of the hydraulic pressures were below the lower limit of the expected values. The QLR best-estimate fit is based on a Cartesian fit specification and with use of wide P_f input range. The results are summarized in Tab. 14.1, Tab. 14.2 and Fig. 14.2. The computed residuals in comparison to a normal error distribution are shown of in the bottom right plot of Fig. 14.3.

Tab. 14.1: Oftr-i7 / QLR result: Parameters estimates and 95% confidence intervals for the Cartesian all sequence fit

Parameter	Units	Fit Value SSE= 2.61E+05	95% Confidence Intervals	
			Lower Value	Upper Value
K_fm	[m/s]	7.58E-14	7.21E-14	7.97E-14
P_fm	[kPa]	4795	4768	4822
ss_fm	[1/m]	1.76E-06	1.64E-06	1.88E-06

Tab. 14.2: Oftr-i7 /QLR result: Covariance-Correlation matrix for homogeneous model (shaded cells denote correlation matrix elements).

Covariance/Correlation Matrix: Est. Cart_Dat_P			
	K_fm	P_fm	ss_fm
K_fm	7.50E-06	1.45E-05	-1.36E-05
P_fm	9.84E-01	2.88E-05	-2.67E-05
ss_fm	-9.97E-01	-9.94E-01	2.50E-05

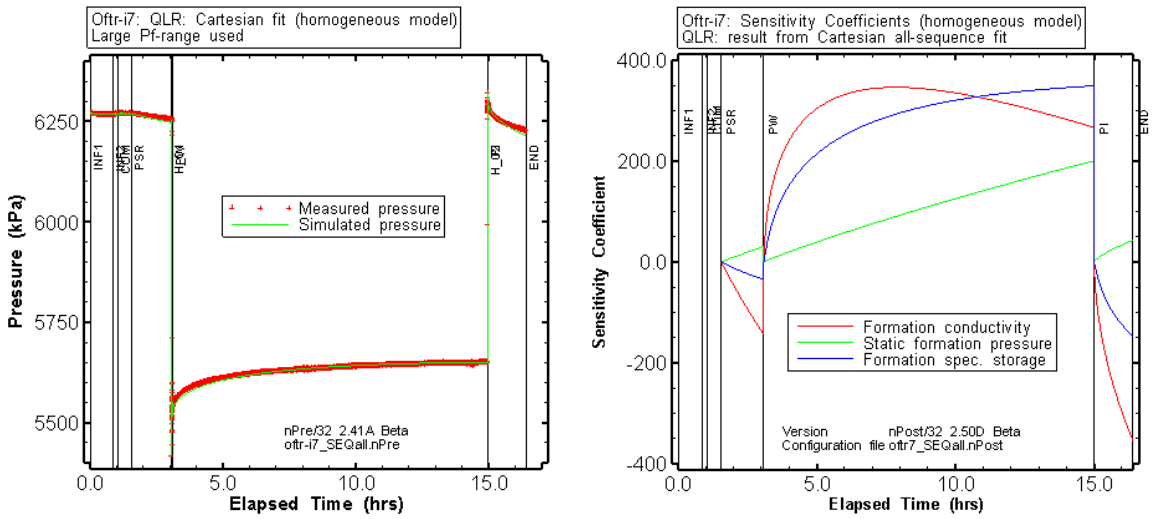

Fig. 14.2: Oftr-i7: Cartesian fit of QLR best-estimate. Left: result of inverse parameter estimation, Cartesian plot. Right: sensitivity coefficients for PSR, PW and PI.

14.3. Incertitude With regard to the P_f-Parameter

The QLR provided a best estimate of P_f = 4795 kPa corresponding to a hydraulic head of 282 m asl whereas the plausible range (Section 7.3.4) expects a static formation pressure value between 5784 and 6765 kPa (483 - 583 m asl). In general, the plausibility of P_f -estimates from interval Oftr-i7 also need to be checked against the head estimates from the adjacent intervals above (Oftr-i2) and below (Oftr-i1) of interval Oftr-i7. Test interval i7 (632.5 - 641.6 m) covers the lowest 7.5 meters of Interval i2 (590.0 - 640 m) and an extra 1.6 meters below interval i2 (total length 9.09 m). Interval i7 is located only a few meters above interval i1 (650 - 700 m). The detailed and standard analyses of interval i1 and i2 suggest formation heads of 456 and 436 m asl, respectively. Assuming that the hydraulic head of i7 is similar to the heads of intervals i1 and i2, a static formation pressure between 6300 to 6500 kPa is expected (corresponding to heads from 436 to 456 m asl). The QLR reported a relatively low sensitivity coefficient to the P_f parameter for all test sequences (right plot in Fig. 14.2) which makes the determination of a reliable P_f estimate difficult.

14.4. Homogeneous Model -- Cartesian Fit with Limited P_f Range

The Cartesian all-sequence homogeneous model from the QLR (Section 14.2) was adjusted by limiting the P_f input range according to the plausibility ranges as defined in Section 7.3.4. The result of the inverse parameter optimization is shown in Tab. 14.3, Tab. 14.4 and Fig. 14.3. The obtained P_f estimate of 5784 kPa is at the lower bound of the input range (5784 to 6765 kPa). The K- and S_S estimates are similar to the corresponding best-estimates of the QLR. However, the obtained fit is of inferior quality compared to the Cartesian fit using a wide P_f range (Section 14.2). This can also be noticed from the two bottom plots of Fig. 14.3 which show the residual distributions in comparison to a normal error distribution both for the case with limited P_f range (bottom left) and wide P_f range (bottom right). The residuals for the latter case are essentially normally distributed (bottom right) whereas the residuals for the case with limited P_f range (bottom left) deviate significantly from the quantile-normal line. This indicates the presence of a systematic error and a conceptual model mismatch. The sum of squared errors is an order of magnitude higher for the case with limited P_f range (SSE = 2.54E+06) compared to the case with wide P_f range (SSE = 2.61E+05). The range between the upper and lower values for the 95^{th} percentile confidence intervals are listed in Tab. 14.3 and shown in Fig. 14.3. The two plots of Fig. 14.3 provide the 95^{th} percentile confidence regions for the estimation of the P_f and K parameters (bottom left) and Ss and K parameters (bottom right), with the shape of the ellipse indicating the degree of correlation between the parameters. Tab. 14.4 includes the covariance correlation matrix (shaded cells) which indicates that the especially the Ss and K fitting parameters are well correlated. This correlation is also observed in the confidence intervals plots of Fig. 14.3 by small minor axis of the uncertainty ellipsoids.

The homogeneous model in combination with the pre-set fit constraints and the incorporated borehole pressure history does not satisfactorily reproduce the measured formation response. Therefore, new model features or other (non-hydraulic) effects need to be investigated.

Tab. 14.3: Oftr-i7: Parameters estimates and 95% confidence intervals for the Cartesian all sequence fit using limited P_f range

Parameter	Units	Fit Value SSE = 2.54E+06	95% Confidence Intervals	
			Lower Value	Upper Value
K_fm	[m/s]	4.49E-14	3.29E-14	6.13E-14
P_fm	[kPa]	5784	5754	5814
ss_fm	[1/m]	1.16E-06	7.77E-07	1.74E-06

Tab. 14.4: Covariance-Correlation matrix for homogeneous model fit using limited P_f range (shaded cells denote correlation matrix elements).

Covariance/Correlation Matrix: Est. Cart_Dat_P			
	K_fm	P_fm	ss_fm
K_fm	2.85E-04	-2.24E-05	-7.38E-04
P_fm	-8.69E-02	2.33E-04	1.69E-05
ss_fm	-9.98E-01	2.53E-02	1.92E-03

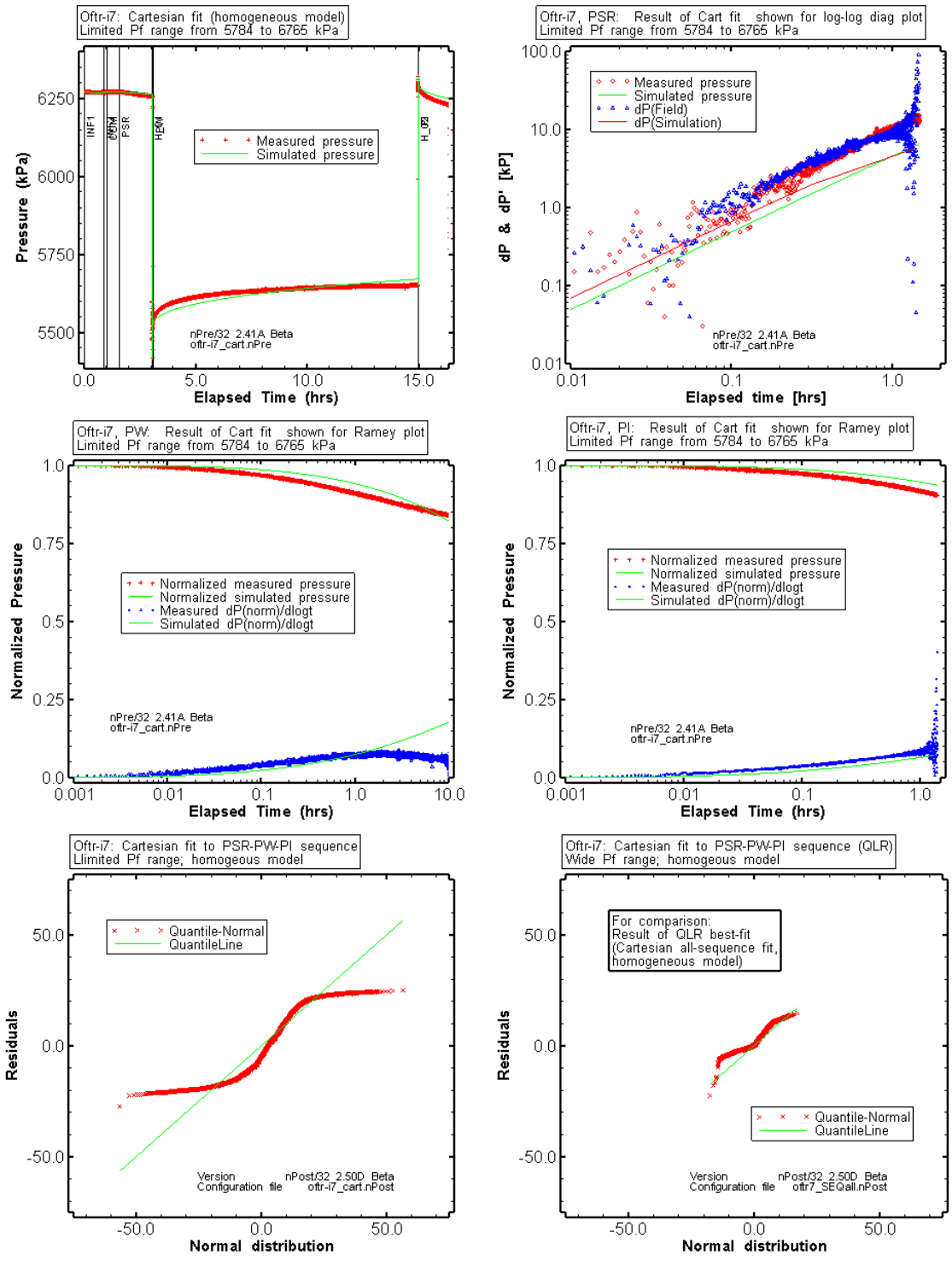

Fig. 14.3: Oftr-i7, homogeneous model / limited P_f range: fit plots and residual plots.

Results from nSights inverse parameter estimation fitting the Cartesian pressures of the entire test using a limited range for the P_f parameter. Cartesian plot of entire test (upper left) and results of Cartesian fit shown for log-log diagnostic plot of PSR (upper right), Ramey A plots of PW (middle left) and PI (middle right). The residual distributions are shown for two cases (both Cartesian fits), for the case with limited P_f input range (bottom left) and wide P_f input range (QLR fit, bottom right).

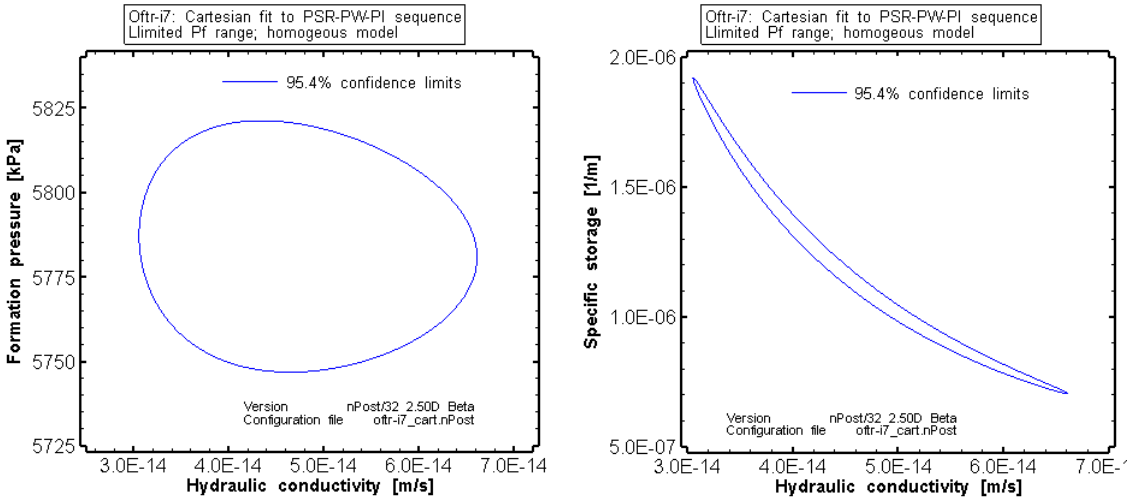

Fig. 14.4: Oftr-i7, Cartesian fit to the entire sequence (homogeneous model): confidence regions for the joint parameters K- P_f (left) and K - S_S (right)

14.5. Homogeneous Model -- Cartesian Fit to the PW-PI Sequence

Based on the model of the previous Section, an additional inverse parameter estimation with a slightly adjusted fit constraint was conducted. The case assumes that the PSR sequence was affected by ongoing compliance effects (decreasing packer pressure) and is not characteristic to the undisturbed formation response. The fit is therefore limited to the PW-PI sequence. The results (here not shown in detail) are very similar to the results of the entire sequence case (Section 14.4). The sum of square errors (SSE) is 2.62E+06 which almost equals to the SSE-value of the fit for the entire sequence (2.54E+06, Tab. 14.3).

14.6. Homogeneous Model -- Cartesian Fit with Limited P_f Range / No BH

The borehole pressure history is removed from the nSights configuration for this case in order to estimate its effect on the formation pressure parameter. The other nSights settings remained unchanged. The result of the inverse parameter optimization is shown in Tab. 14.5, Tab. 14.5 and Fig. 14.5. The P_f-estimate is at the lower limit of the input range. The fit quality is better compared to the previous case with limited P_f range and incorporated pre-test borehole history (Section 14.4). This can also be seen from the bottom left plot of Fig. 14.5 which shows the residual distributions in comparison to a normal error distribution (The residual distribution of the QLR best-estimate fit is provided in the bottom right plot of Fig. 14.5 for comparison). The residuals are essentially normally distributed (bottom right) indicating the absence of a systematic error. The sum of squared errors is half an order of magnitude lower for the case with no BH, limited P_f range (SSE = 6.03E+05) compared to the case with BH and same limited P_f range (SSE = 2.54E+06). The range between the upper and lower values for the 95th percentile confidence intervals are listed in Tab. 14.5 and shown in Fig. 14.6. The two plots of Fig. 14.6 provide the 95th percentile confidence regions for the estimation of the P_f and K parameters (bottom left) and Ss and K parameters (bottom right), with the shape of the ellipse indicating the degree of correlation between the parameters. Tab. 14.6 includes the covariance correlation matrix (shaded cells) which indicates that the especially the Ss and K fitting parameters are well correlated. This correlation is also observed in the confidence intervals plots of Fig. 14.6 by small minor axis of the uncertainty ellipsoids. The overall range of the confidence regions is relatively narrow.

The negation of borehole pressure history influence is not corroborated by particular observations. The role of pre-test borehole pressure history would be minor, for example if pre-test flow to or from the formation was hindered by positive skin, and if the skin then was removed prior to testing (see Enachescu et al., 2007).

Tab. 14.5: Oftr-i7: Parameters estimates and 95% confidence intervals for the Cartesian all sequence fit, no BH, using limited P_f range

Parameter	Units	Fit Value SSE = 6.03E+05	95% Confidence Intervals	
			Lower Value	Upper Value
K_fm	[m/s]	6.57E-14	5.96E-14	7.24E-14
P_fm	[kPa]	5784	5782	5786
ss_fm	[1/m]	2.00E-06	1.75E-06	2.29E-06

Tab. 14.6: Covariance-Correlation matrix for homogeneous model fit, no BH, using limited P_f range (shaded cells denote correlation matrix elements).

Covariance/Correlation Matrix: Est. Cart_Dat_P			
	K_fm	P_fm	ss_fm
K_fm	2.82E-05	1.32E-06	-7.74E-05
P_fm	2.14E-01	1.36E-06	-4.87E-06
ss_fm	-9.97E-01	-2.86E-01	2.14E-04

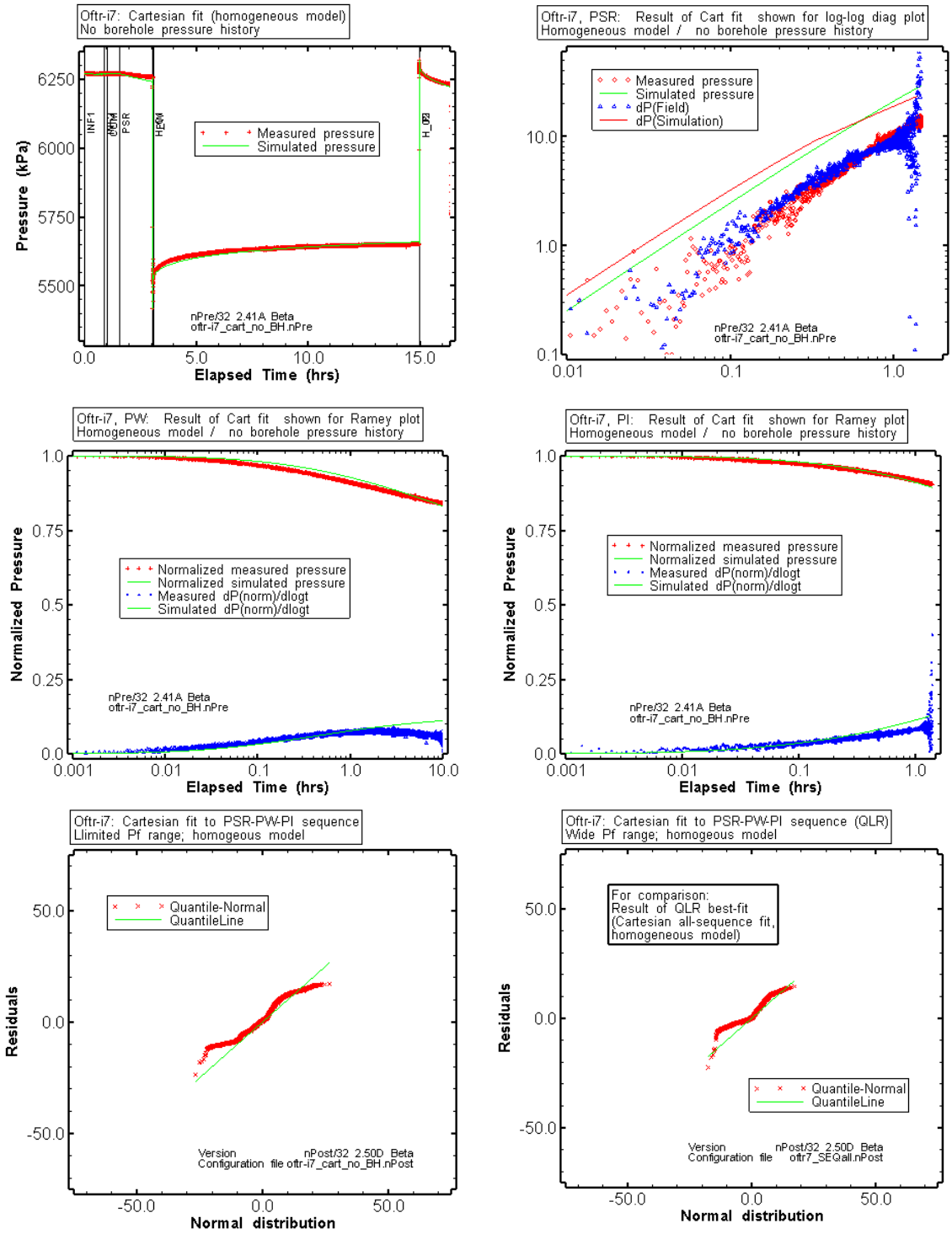

Fig. 14.5: Oftr-i7: homogeneous model / no BH history: fit plots and residual plots.

Results from nSights inverse parameter estimation fitting the Cartesian pressures of the entire test using a limited range for the P_f parameter and assuming no borehole pressure history. Cartesian plot of entire test (upper left) and results of Cartesian fit shown for log-log diagnostic plot of PSR (upper right), Ramey A plots of PW (middle left) and PI (middle right). The residual distributions are shown for this case (without BH effects, bottom left) and for the best-estimate case from QLR which includes BH effects(bottom right).

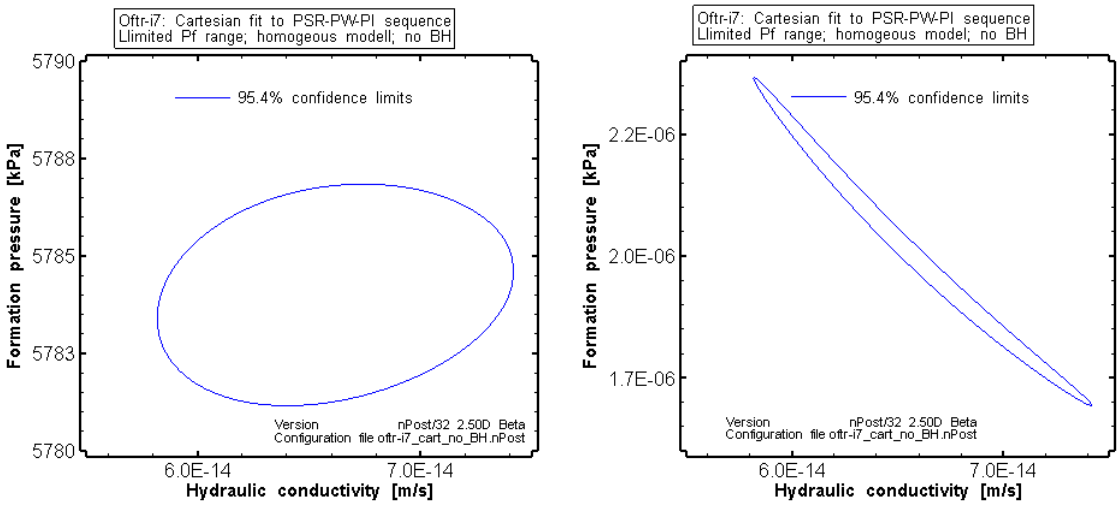

Fig. 14.6: Oftr-i7, Cartesian fit to the entire sequence; no BH (homogeneous model): confidence regions for the joint parameters K- P_f (left) and K - S_S (right)

14.7. Composite Skin Model -- Cartesian Fit with Limited P_f Range

The homogenous model was extended to composite to see if a narrow cylindrical zone around the borehole of different properties (skin zone properties) compared to the formation properties would result in comparable fit quality and significantly increased formation pressure.

The results of the nSights inverse parameter optimization are shown in Tab. 14.7 and Tab. 14.8 and in Fig. 14.8. A relatively low formation conductivity of K=1.0E-14 m/s and a P_f-estimate of 6422 kPa was obtained. The introduction of a skin zone produces improved visual fits, especially for the late time data of the Ramey plot for PW and PI (middle left and middle right plot of Fig. 14.8), and the SSE value is reduced to 4.70E+04. The residual distribution is in general agreement with a normal error distribution (bottom left blot of Fig. 14.8) and suggests the absence of a systematic error or model mismatch. During the simulations, the storage constant of the skin zone was held constant with S_{SS} = 1E-06 m^{-1}. The skin parameters values (K_S = 2.8E-13, t_S= 0.0374 m in relation to the formation hydraulic conductivity (1.0E-14 m/s) correspond to a skin factor of -0.4. The ratio between formation conductivity and skin zone conductivity equals to 26. The formation conductivity is highly correlated with the radial thickness of the skin zone and the formation storage constant (Tab. 14.8).

Fig. 14.7 provide the 95th percentile confidence regions for the estimation of the P_f and K parameters (left) and S_s and K parameters (right), with the shape of the ellipse indicating the degree of correlation between the parameters. The confidence interval information indicates that the range in the fitted parameter values is large for all three parameters. The large confidence intervals for the S_S and in particular to the P_f parameter is also reflected by the low sensitivity to theses parameters (Fig. 14.9).

Tab. 14.7: Oftr-i7: Parameters estimates and 95% confidence intervals for the Cartesian PW-PI fit using limited P_f range, composite skin model

Parameter	Units	Fit Value SSE= 4.70E+04	95% Confidence Interval	
			Lower Value	Upper Value
K_fm	[m/sec]	1.08E-14	4.94E-15	2.36E-14
K_s	[m/sec]	2.83E-13	2.81E-13	2.85E-13
P_fm	[kPa]	6422	6285	6558
Ss_fm	[1/m]	7.30E-07	2.69E-07	1.98E-06
t_s	[m]	0.0374	0.0364	0.0385

Tab. 14.8: Covariance-Correlation matrix for the Cartesian PW-PI fit using limited P_f range, composite skin model (shaded cells denote correlation matrix elements).

	K_fm	K_s	P_fm	ss_fm	t_s
K_fm	1.80E-03	1.67E-05	-4.64E-03	-4.58E-03	1.11E-04
K_s	8.20E-01	2.31E-07	-4.56E-05	-4.20E-05	9.74E-07
P_fm	-7.87E-01	-6.82E-01	1.93E-02	1.12E-02	-2.59E-04
ss_fm	-9.97E-01	-8.09E-01	7.41E-01	1.17E-02	-2.84E-04
t_s	9.88E-01	7.68E-01	-7.05E-01	-9.95E-01	6.96E-06

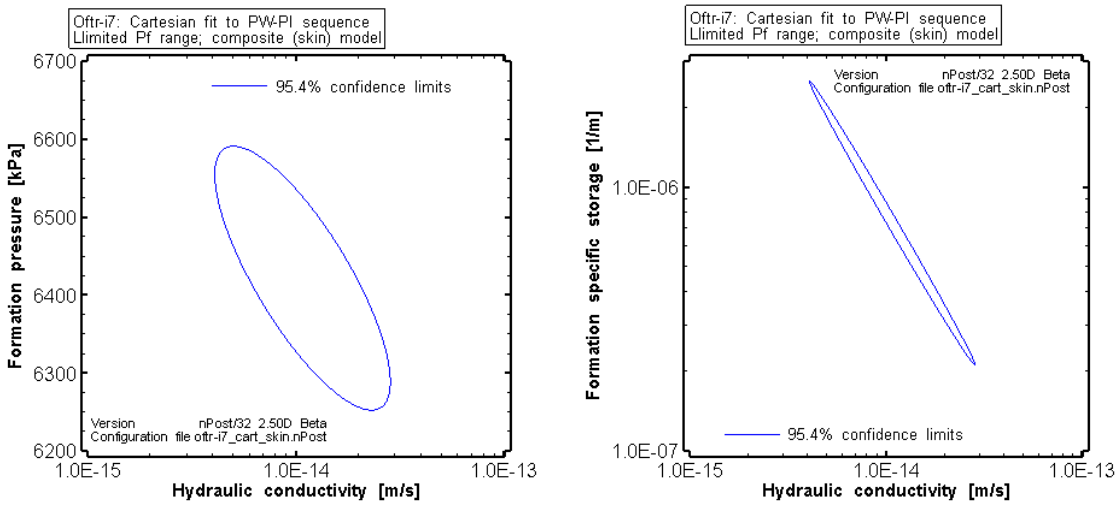

Fig. 14.7: Oftr-i7, composite skin model / Cartesian fit to PW-PI: confidence regions for the joint parameters K-P_f (left) and K - S_S (right).

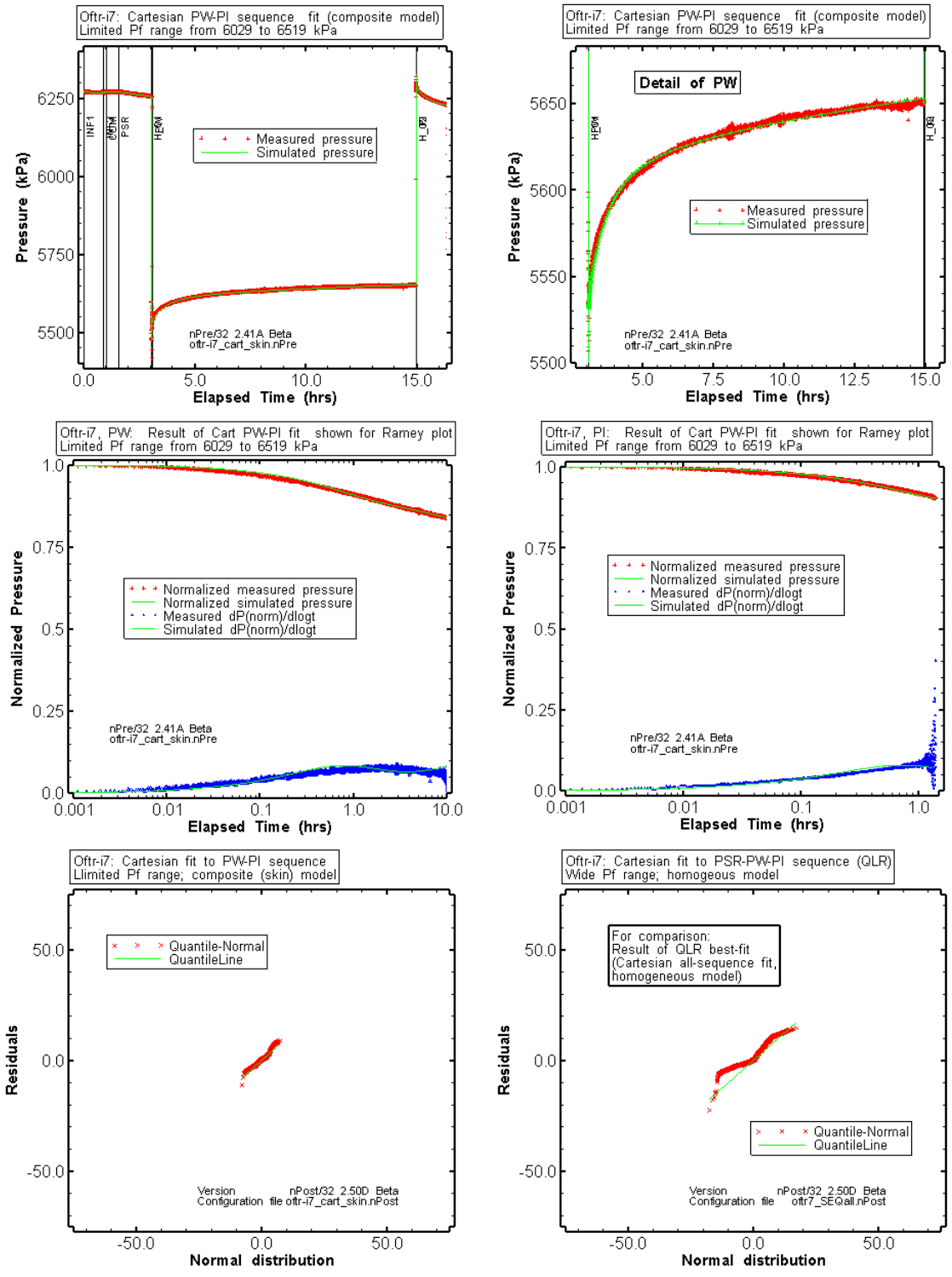

Fig. 14.8: Oftr-i7: composite skin model / limited P_f range: fit plots and residual plots.

Results from nSights inverse parameter estimation fitting the Cartesian pressures of the PW-PI sequence using a limited range for the P_f parameter (6029 - 6519 kPa). Cartesian plot (upper left) with detail for PW (upper right) and results of Cartesian fit shown for the Ramey A plots of PW (middle left) and PI (middle right). The residual distributions are

shown for this case (with skin & BH, bottom left) and for the best-estimate case from QLR (bottom right).

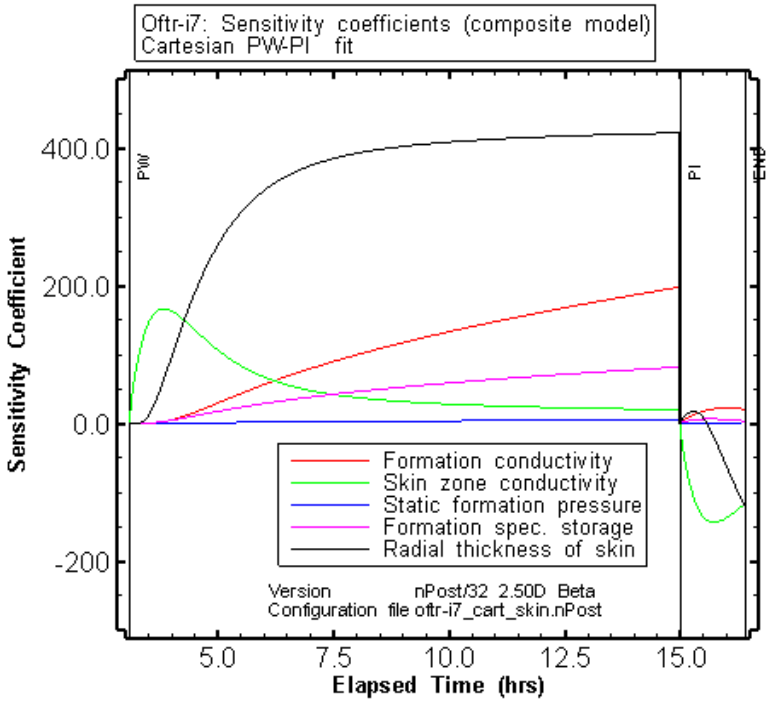

Fig. 14.9: Sensitivity coefficients for the Cartesian PW-PI sequence, composite skin model. The sensitivity to the formation pressure parameter is close to zero.

14.7.1. Perturbation analysis

A perturbation analysis was performed to test if the estimated parameters and differences were associated with a local minimum or represent a global minimum of the optimization. This was done by repeating the optimization with different starting values for the different parameters. For this case 100 optimization runs were performed for which individual fits were computed. The simplex optimization algorithm was used.

Fig. 14.10 shows the best fit values and the 95% confidence regions from all perturbation runs for the K-S_S (top left) and K-P_f (top right) joint parameters. Frequency histograms for the K- and P_f -parameters are given provided on the bottom left and bottom right of Fig. 14.10. The P_f parameter shows a bi-modal frequency distribution. The largest frequency in the P_f histogram shows the class with the highest P_f -values adjacent to the upper limit of the pre-set P_f range (bottom right plot of Fig. 14.10). The perturbation results are plotted Fig. 14.11 as three dimensional plot of the SSE as a function of the best-fit values of formation conductivity and formation pressure (top) and as a function of the best-fit values of formation conductivity and specific storage (bottom). The best-fit results are indicated as green squares for comparison with the distribution from the perturbation runs.

Tab. 14.9: Oftr-i7: Composite skin model, perturbation analysis statistics

Run	K_fm [m/sec]	K_s [m/sec]	P_fm [kPa]	ss_fm [1/m]	t_s [m]
Best	**1.42E-14**	**2.84E-13**	**6029**	**7.23E-07**	**0.0372**
Max	1.66E-14	2.86E-13	6519	3.86E-06	0.0377
Min	4.14E-15	2.77E-13	6029	5.21E-07	0.0316
Mean	1.10E-14	2.83E-13	6349	8.41E-07	0.0372
StdDev	2.07E-15	1.08E-15	152.3	4.86E-07	8.74E-04

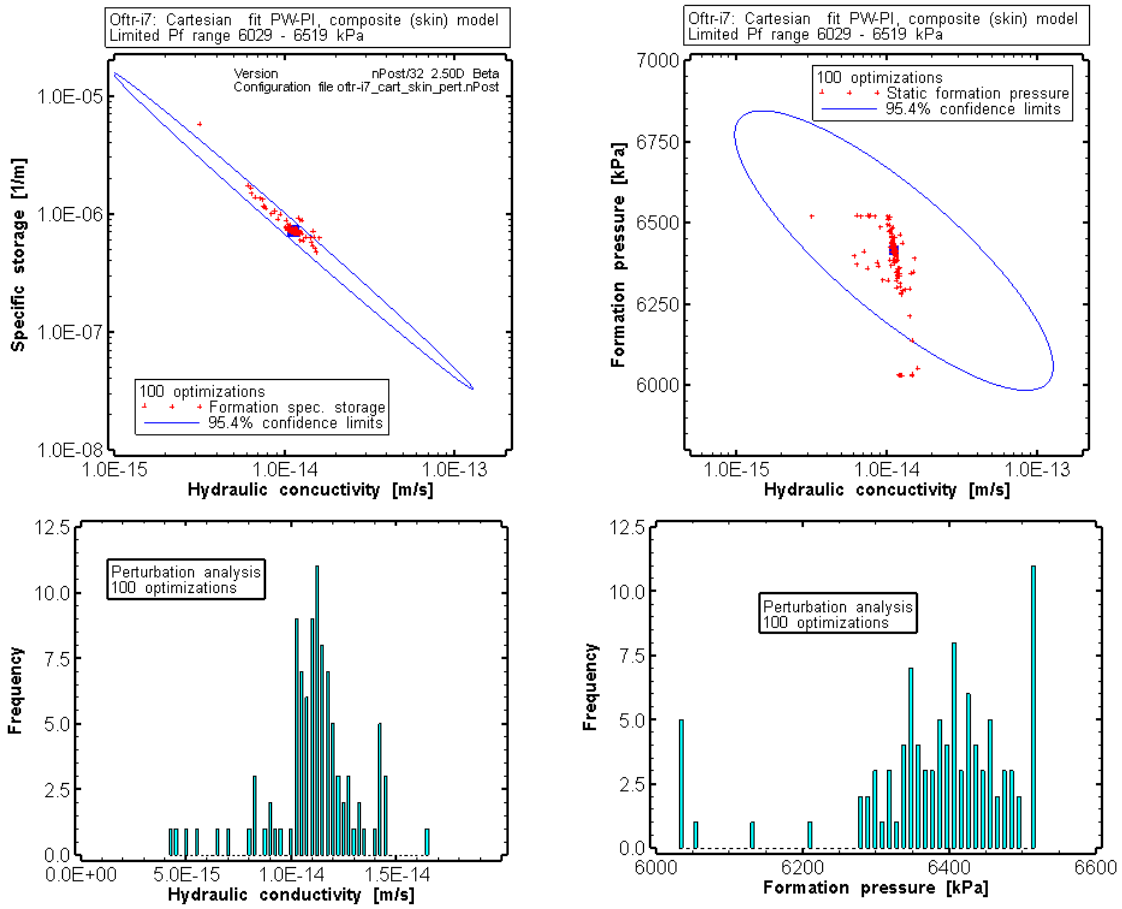

Fig. 14.10: Oftr-i7, composite skin model: results from perturbation analysis of nSights inverse simulation Cartesian fit to PW-PI sequence.

Confidence regions for the K- S_S joint parameters (left top), K-P_f joint parameters (top right) and the frequency distributions for the K- (bottom left) and the P_f estimates (bottom right).

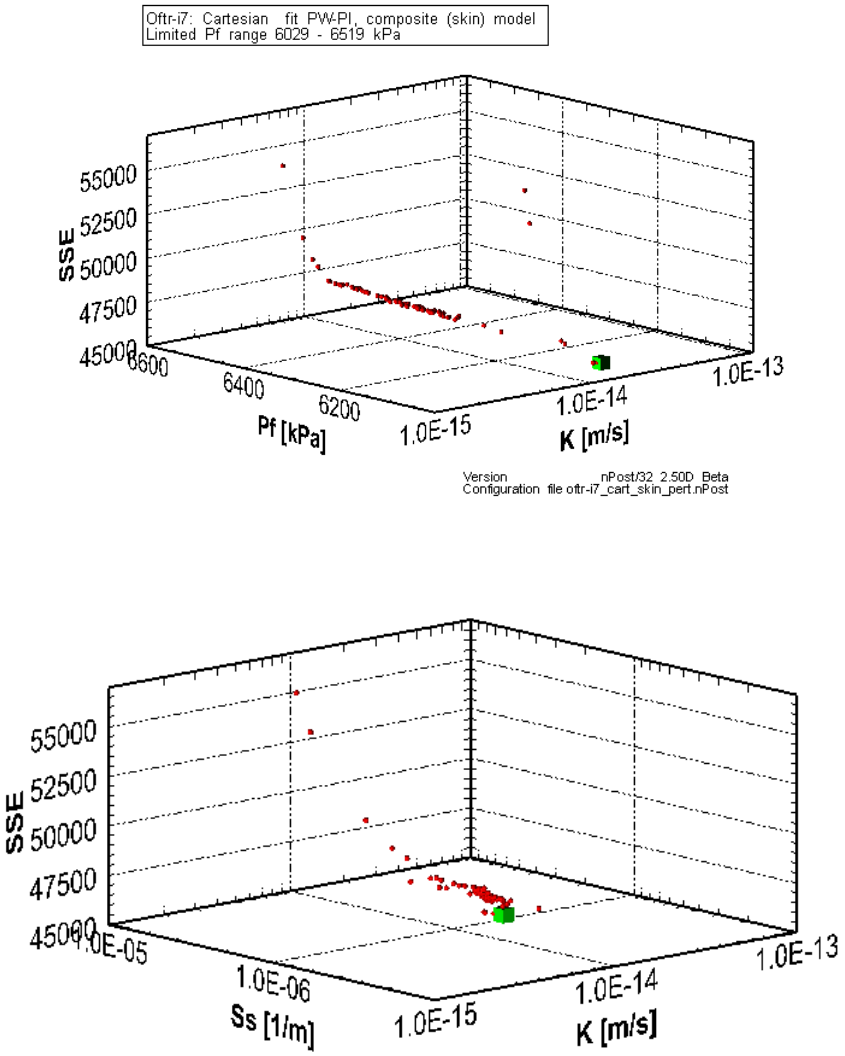

Fig. 14.11: Oftr-i7, composite skin model / Cartesian fit to the PW-PI sequence: Perturbation analysis

Top: SSE versus K and P_f . Bottom: SSE versus K and S_S. The best-estimate solution with lowest SSE value is shown in the green cube symbol.

14.8. Composite Skin Model -- Composite Fit to PW+PI P vs. log(t)

The fit constraint is adjusted towards stronger weighting of the early time data of the individual test sequences to test the quality of the composite model. For this purpose, a composite fit is specified in nSights consisting of sub-fits for the PW and PI test sequences. The data for each sequence were smoothed (15 data points left and right of the point) and reduced on log-scale basis (upper plots of Fig. 14.13). The smoothed data curves are shown as blue lines, the reduced data with red and the original field data with green data points.

The results of the nSights inverse parameter optimization are shown in Tab. 14.10 and Tab. 14.11 and in Fig. 14.13. The K-estimate (K = 2.4E-14 m/s) from the composite fit is about a factor 2.2 higher compared to the Cartesian fit (1.0E-14 m/s, see Section 14.7). The formation pressure estimate (P_f = 6029 kPa) is 393 kPa lower than the corresponding value from the Cartesian fit (6422 kPa). The comparable lower P_f value for the composite fit disagrees with the observed higher simulated pressure at late time of PW (Fig. 14.14). Overall, the composite P vs. log(t) produces a similar visual fit quality as the Cartesian fit. A detailed view shows that as expected the early/middle-time data are better matched using the P vs. log(t) fit specification, whereas the measured late time data are more precisely re-produced when using the Cartesian fit constraint (Fig. 14.14). The S_S estimates are almost identical for both fit constraints (Tab. 14.7 and Tab. 14.10). The SSE values for the two cases are not comparable because of the different fit specifications used. The residual distribution both for the sub-fit PW and sub-fit PI is in general agreement with a normal error distribution (bottom left blot of Fig. 14.8) and suggests the absence of a systematic error or model mismatch. During the simulations, the storage constant of the skin zone was held constant with S_{SS} = 1E-06 m^{-1}. The skin parameters values (K_S = 3.8E-13, t_S= 0.031 m in relation to the formation hydraulic conductivity (2.4E-14 m/s) correspond to a skin factor of -0.33. The ratio between formation conductivity and skin zone conductivity equals to 16. The formation conductivity is highly correlated with the radial thickness of the skin zone and the formation storage constant (Tab. 14.11). Fig. 14.12 provides the 95th percentile confidence regions for the estimation of the P_f and K parameters (left) and S_s and K parameters (right), with the shape of the ellipse indicating the degree of correlation between the parameters. The confidence interval information indicates that the range in the fitted parameter values is extremely large for the K and S_S parameters, and considerably large for the formation pressure (P_f). The confidence limit values are listed for each fitted parameter in Tab. 14.10.

Tab. 14.10: Oftr-i7: Parameters estimates and 95% confidence intervals for the composite PW+PI fit P vs. log(t) using limited P_f range, composite skin model

Parameter	Units	Fit Value	95% Confidence Interval	
		SSE= 1.42E+03	Lower Value	Upper Value
K_fm	[m/sec]	2.39E-14	2.40E-16	2.38E-12
K_s	[m/sec]	3.76E-13	3.54E-13	3.99E-13
P_fm	[kPa]	6029	5614	6444
Ss_fm	[1/m]	8.83E-07	2.59E-09	3.01E-04
t_s	[m]	0.0306	0.0231	0.0381

Tab. 14.11: Covariance-Correlation matrix for the composite PW+PI fit P vs. log(t) using limited P_f range, composite skin model (shaded cells denote correlation matrix elements).

	K_fm	K_s	P_fm	ss_fm	t_s
K_fm	6.24E-02	7.36E-04	-4.92E-02	-1.58E-01	4.66E-03
K_s	6.89E-01	1.83E-05	-8.80E-04	-1.80E-03	4.70E-05
P_fm	-4.65E-01	-4.86E-01	1.79E-01	1.07E-01	-2.25E-03
ss_fm	-9.97E-01	-6.66E-01	4.01E-01	4.01E-01	-1.20E-02
t_s	9.71E-01	5.73E-01	-2.77E-01	-9.85E-01	3.68E-04

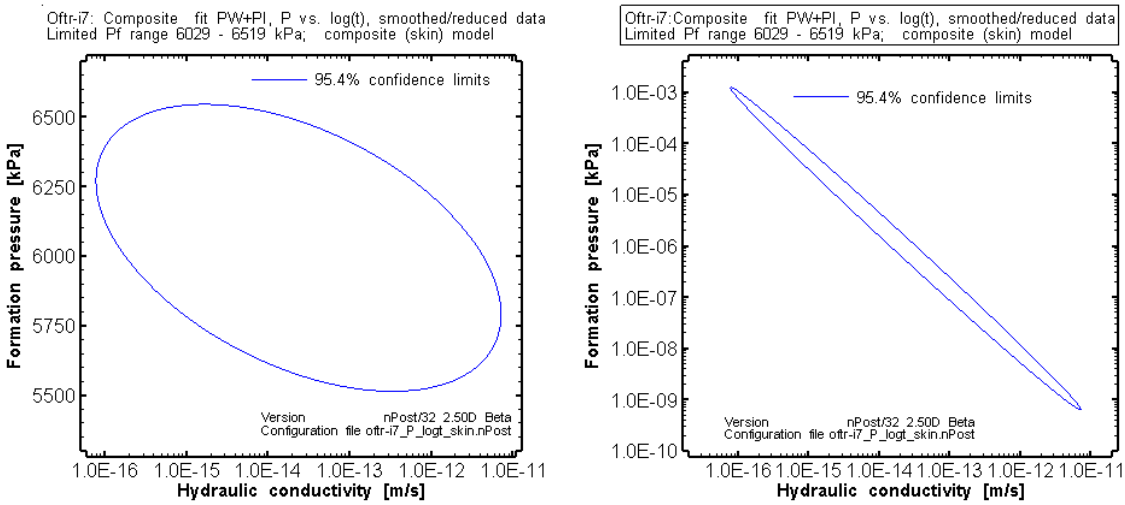

Fig. 14.12: Oftr-i7: Composite skin model / composite P vs. log(t) fit to PW+PI: confidence regions for the joint parameters K-P_f (left) and K - S_S (right).

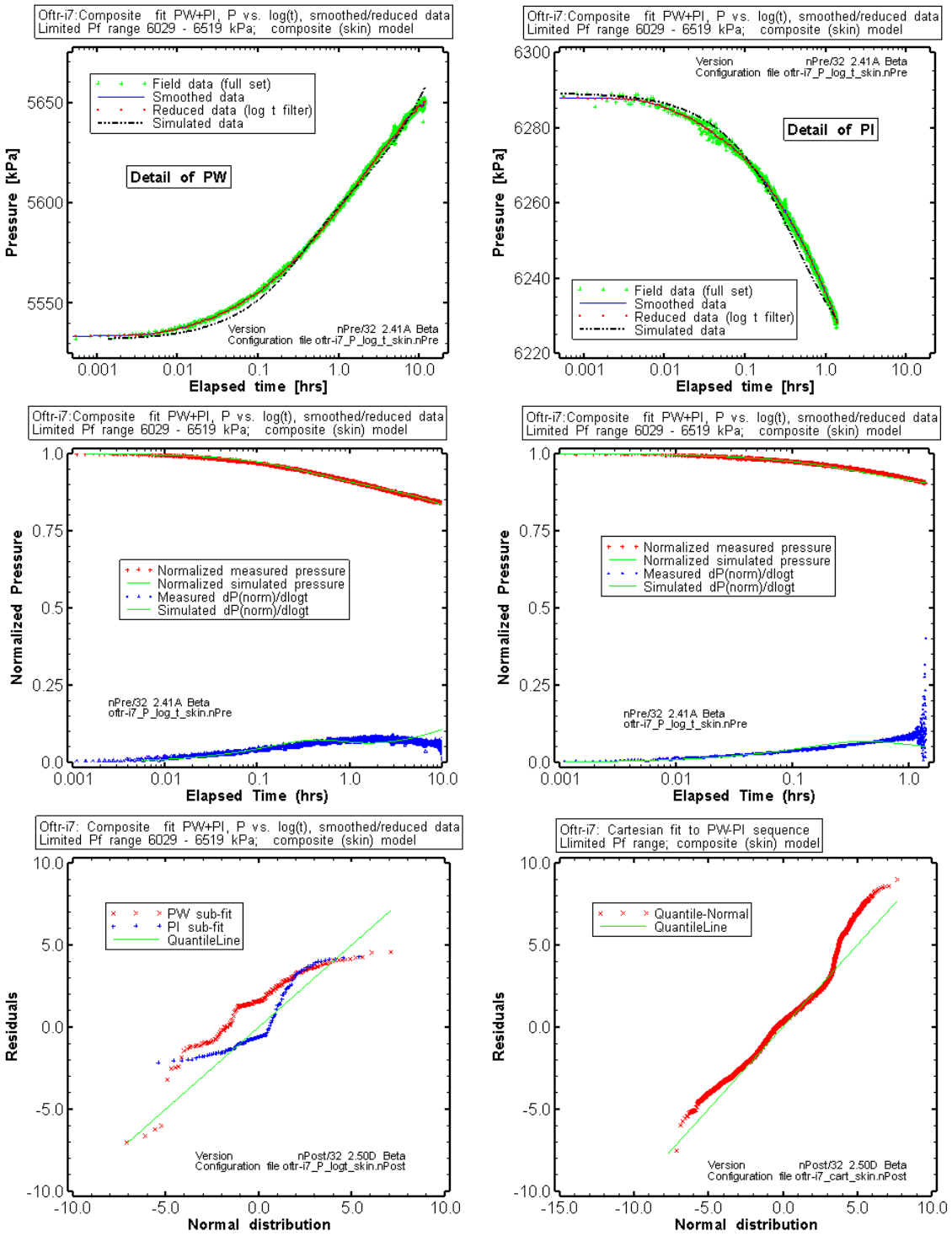

Fig. 14.13: Oftr-i7, composite skin model: Results of P vs. log(t) composite fit PW+PI shown for the individual test sequences.

Top plots: Field data, smoothed/ reduced data and simulated data shown for PW (left) and PI (right). Middle plots: Result of composite fit P vs. log(t) shown for Ramey A plots of PW (left) and PI (right). Bottom left: computed residuals compared to normal distribution for the P vs. log(t) sub-fits. Bottom right: For comparison, the residual plot of the Cartesian PW-PI of the same model is shown.

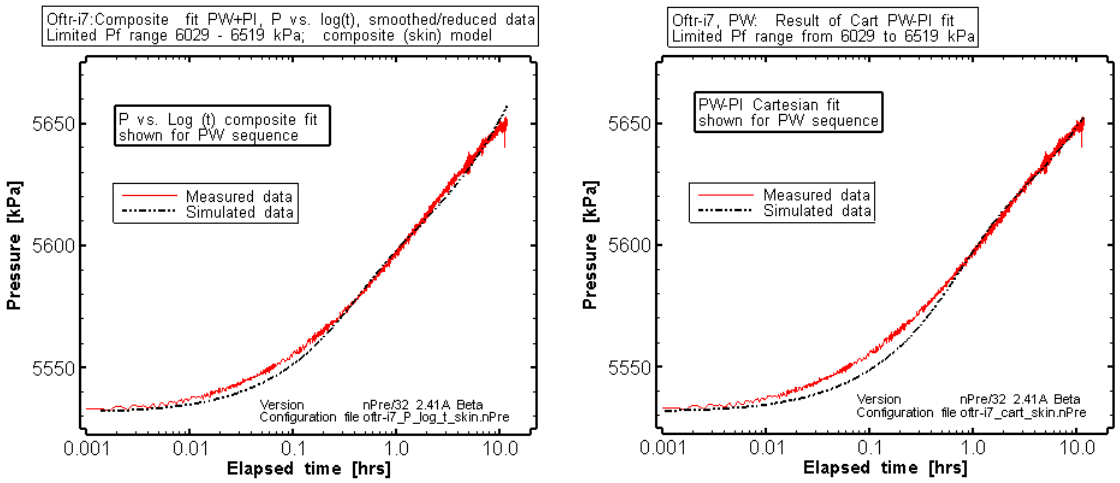

Fig. 14.14: Effect of fit-specification. Left: composite fit (PW+PI) with P vs. log(t). Right: Cartesian fit for the PW-PI sequence.

14.8.1. Perturbation analysis

A perturbation analysis was performed to test if the estimated parameters and differences were associated with a local minimum or represent a global minimum of the optimization. This was done by repeating the optimization with different starting values for the different parameters. For this case 100 optimization runs were performed for which individual fits were computed. The simplex optimization algorithm was used.

Fig. 14.15 shows the best fit values and the 95% confidence regions from all perturbation runs for the K-S_S (top left) and K-P_f (top right) joint parameters. Frequency histograms for the K- and P_f -parameters are given provided on the bottom left and bottom right of Fig. 14.15. Both the K- and P_f parameters show bi-modal frequency distributions. The largest frequency in the P_f histogram shows the class with the lowest P_f -values adjacent to the lower limit of the pre-set P_f range (bottom right plot of Fig. 14.15). The perturbation results are plotted in Fig. 14.16 as three dimensional plot of the SSE as a function of the best-fit values of formation conductivity and formation pressure (top) and as a function of the best-fit values of formation conductivity and specific storage (bottom). The best-fit results are indicated as green squares for comparison with the distribution from the perturbation runs.

Tab. 14.12: Oftr-i7, composite skin model / composite fit P vs. log(t): perturbation analysis statistics

Run	K_fm [m/sec]	K_s [m/sec]	P_fm [kPa]	ss_fm [1/m]	t_s [m]
Best	**2.39E-14**	**3.81E-13**	**6029**	**8.84E-07**	**0.0307**
Max	2.62E-14	3.86E-13	6514	1.19E-06	0.0320
Min	1.58E-14	3.69E-13	6029	7.29E-07	0.0301
Mean	2.04E-14	3.75E-13	6272	8.44E-07	0.0314
StdDev	2.34E-15	3.92E-15	156	6.19E-08	0.0005

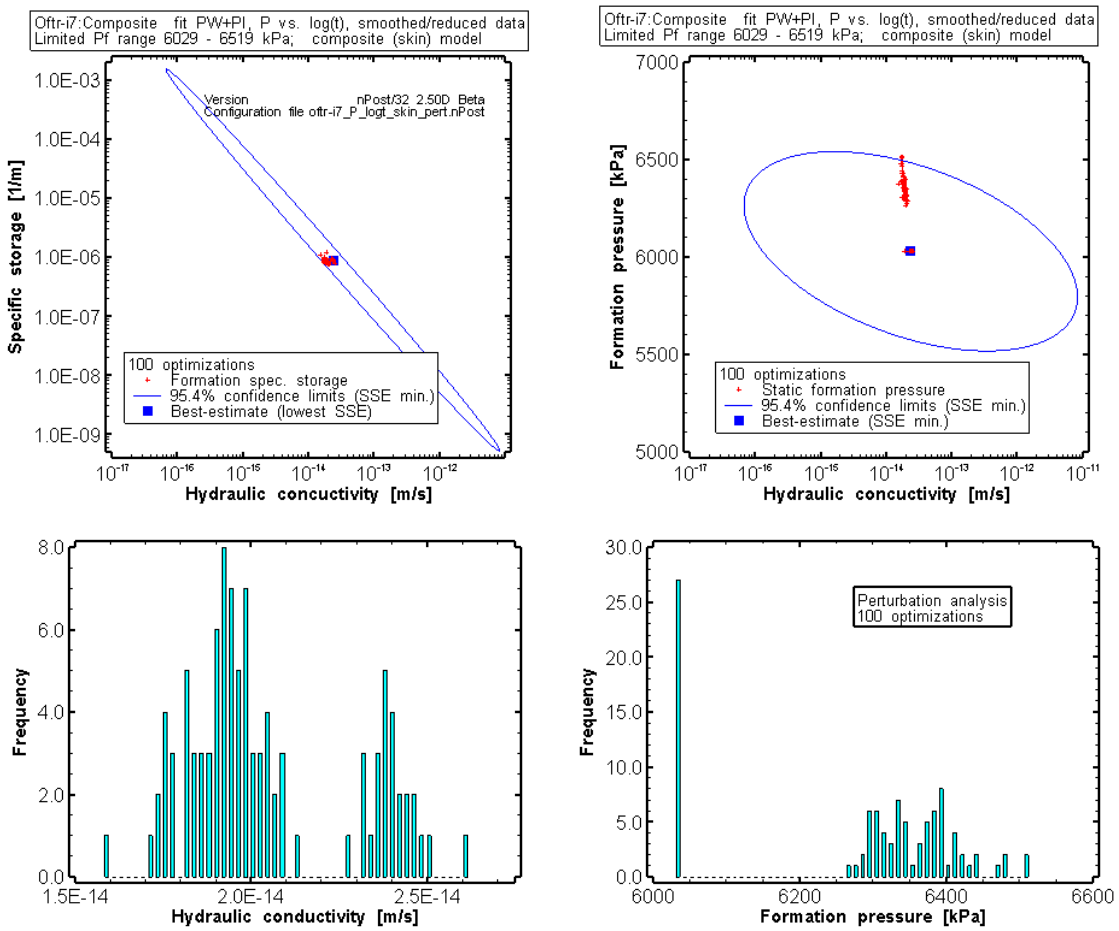

Fig. 14.15: Oftr-i7, composite model: results from perturbation analysis of nSights inverse simulation for composite fit PW+PI, P vs. log(t).

Confidence regions for the K- S_S joint parameters (left top), K-P_f joint parameters (top right) and the frequency distributions for the K- (bottom left) and the P_f estimates (bottom right).

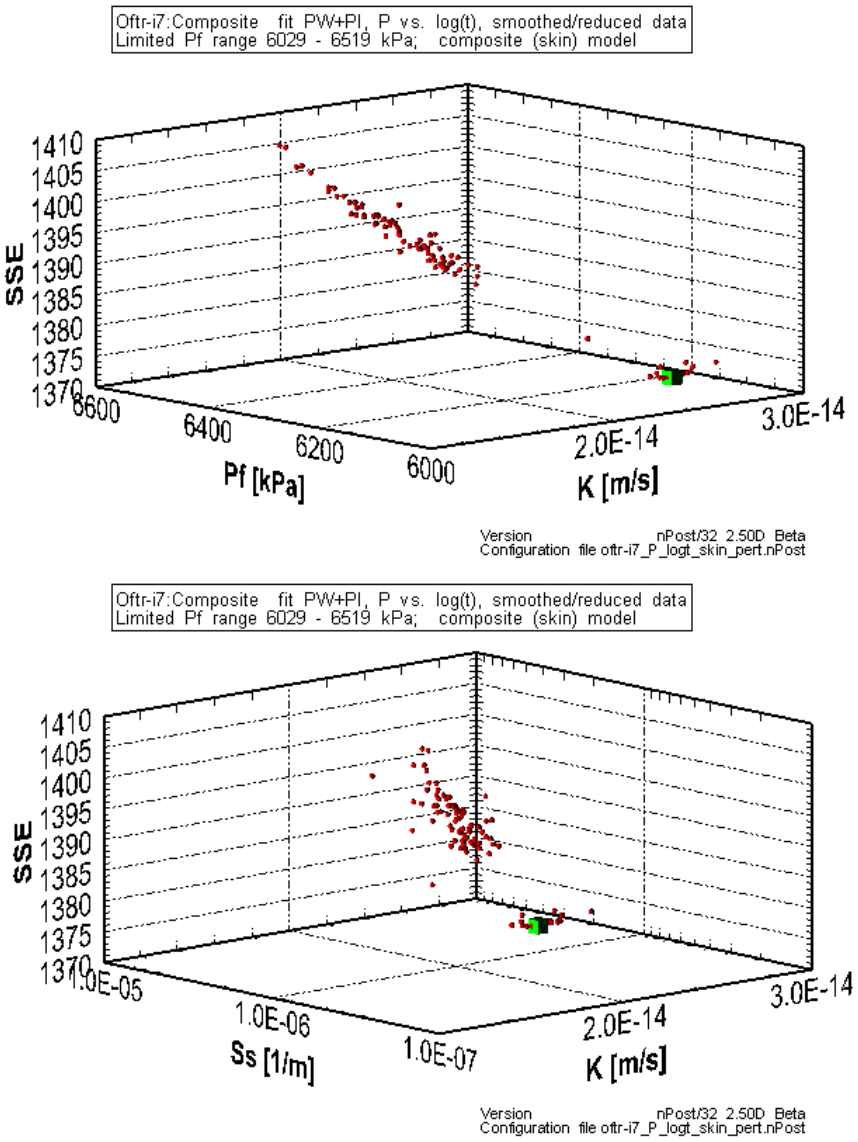

Fig. 14.16: Oftr-i7, composite skin model / composite fit P vs. log(t) fit to PW+PI: Perturbation analysis

Top: SSE versus K and P_f . Bottom: SSE versus K and S_S. The best-estimate solutions with lowest SSE value are shown the green cube symbol.

14.9. Potential Influence of Packer Pressure Change

The packer pressure continuously decreased during the hydraulic testing in Oftr-i7 (Fig. 14.17 and Tab. 14.13). Theoretically, the change in packer pressure could have resulted in slight movement of the packer sleeves at the packer ends facing towards the test zone. In case of packer pressure decrease, such an effect would cause an increase in test zone volume. In tight formation, an increase in test zone volume would be associated with a temporary decrease of interval pressure.

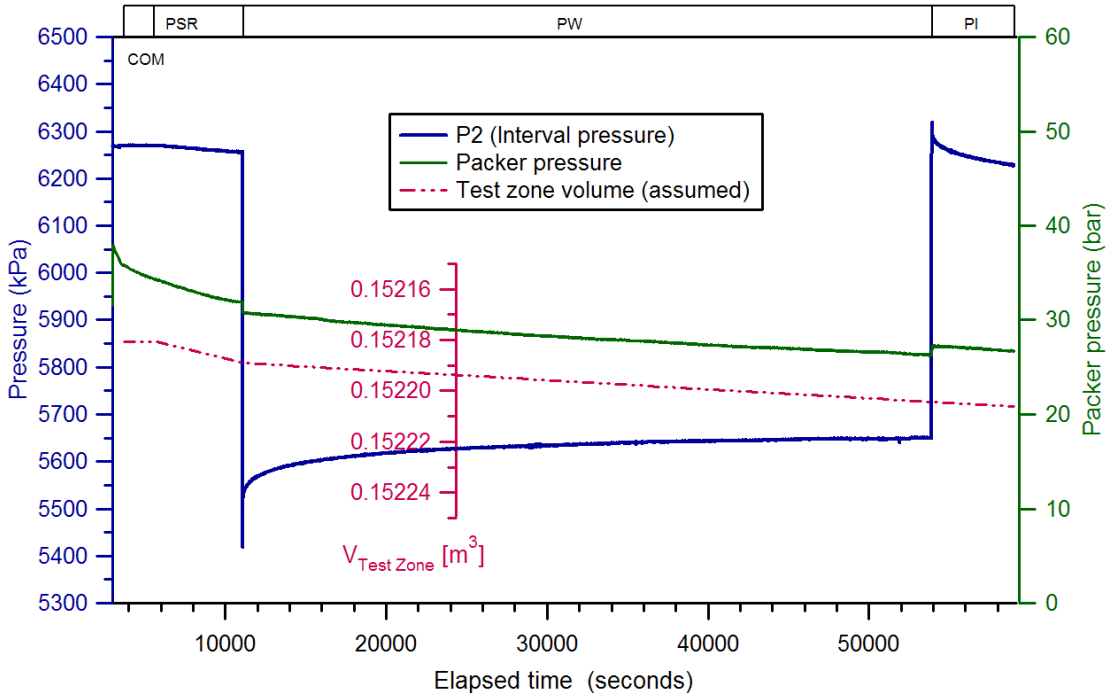

Fig. 14.17: Packer pressure (green line) and assumed varying test zone volume (magenta line)

The potential influence of the packer pressure change associated with test zone volume change was estimated based on a assumed incremental movement of -0.2 mm per 1 bar change (decrease) in packer pressure (2 packers times -0.1 mm per packer). Assuming a movement perpendicular to the wellbore circular area, the test zone volume change becomes +3.35 ml/bar. The nominal test interval volume (≅ test zone volume V_{TZ}) is 0.15218 m^3. The measured changes in packer pressure per test event are transferred to volume changes and test zone volume values (Tab. 14.13). The varying test zone volumes as shown in Fig. 14.17 (magenta line) were incorporated in nSights as a wellbore boundary condition. The formation parameters were re-estimated during an inverse parameter optimization to quantify the effect of assumed test zone volume change on the P_f estimate. The results shown in Fig. 14.18, Tab. 14.14 and Tab. 14.15 should be considered with care because the model is based on very rough assumptions. The visual fit quality is fairly good for the PW and PI sequences, whereas the fit to the PSR pressure is poor. The packer pressure change effect could be overestimated for the PSR

period because displacement due to packer pressure change could be less significant at high inflation pressures. The sum of squared errors (Tab. 14.14) is similar to the corresponding value from the QLR case with constant test zone volume and wide P_f-range (Tab. 14.1). The K- and S_S- estimates of the two cases are almost identical. The exercise shows that a minor compensation for packer pressure change allows to obtain a 1580 kPa higher formation pressure (P_f = 6375 kPa compared to 4795 kPa) with otherwise very similar model parameters.

Tab. 14.13: Oft-i7: Start and end packer pressures and calculated test zone volume based on a assumed ratio of volume change to packer pressure change.

OFTR-i7	Elapsed time		Packer pressures (at surface)			V_{TZ} [1)]
Event	Start [hrs]	End [hrs]	Start [bar]	End [bar]	Change [bar]	at end [m3]
COM	1.03139	1.6	35.81	34.34	-1.47	0.1521807
PSR	1.6	3.08917	34.34	31.85	-2.49	0.1521890
PW	3.08917	14.99	30.79	26.26	-4.53	0.1522042
PI	14.99	16.40361	27.25	26.69	-0.56	0.1522060

1) Test zone volume calculated based on a assumed volume change of 3.35 ml/bar (bar packer change) for end time of indicated event

Tab. 14.14: Oftr-i7: Varying test zone volume. Parameters estimates and 95% confidence intervals for the Cartesian all sequence fit

Parameter	Units	Fit Value SSE= 2.62E+05	95% Confidence Intervals	
			Lower Value	Upper Value
K_fm	[m/s]	6.97E-14	6.58E-14	7.39E-14
P_fm	[kPa]	6375	6359	6391
ss_fm	[1/m]	2.03E-06	1.88E-06	2.19E-06

Tab. 14.15: Oftr-i7: Varying test zone volume. Covariance-Correlation matrix for homogeneous model (shaded cells denote correlation matrix elements)

Covariance/Correlation Matrix: Est. All_Cart_smoothed			
	K_fm	P_fm	ss_fm
K_fm	9.86E-06	-2.35E-05	-2.61E-05
P_fm	-8.97E-01	6.98E-05	6.01E-05
ss_fm	-9.97E-01	8.62E-01	6.97E-05

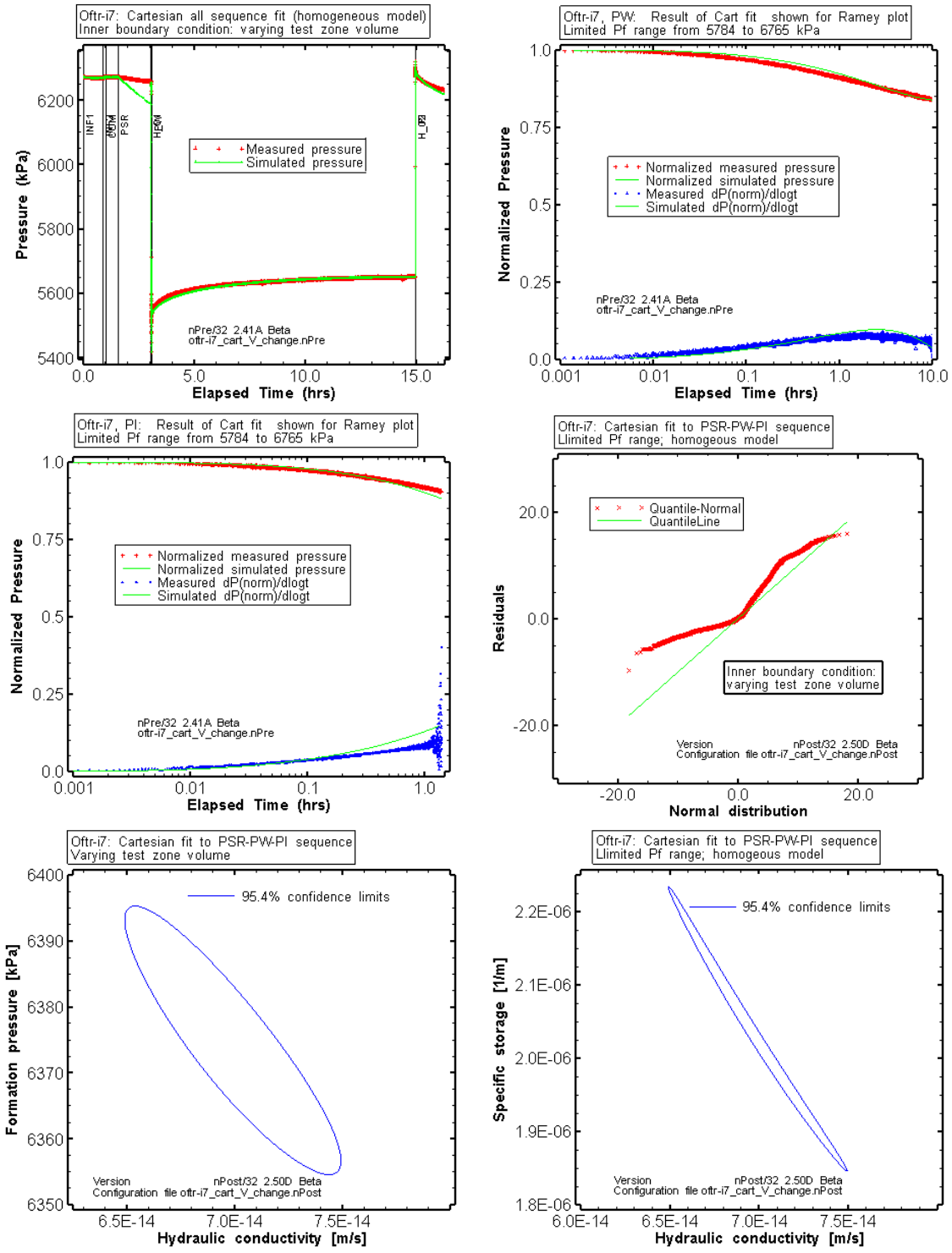

Fig. 14.18: Oftr-i7, homogeneous model / varying test zone volume

Results from nSights inverse parameter estimation using varying test zone volume as inner boundary condition. Top left: Cartesian plot. Top right/ middle left: Result of all-sequence Cartesian fit shown to the Ramey A plots for PW / PI. Middle right: residual distribution in comparison to normal error distribution. Bottom: confidence regions shown for the K-P_f (left) and K-S_S joint parameters.

14.10. Summary

During the "standard analysis" for test Oftr-i7, the homogeneous model was further tested using adjusted model parameters such as the span of the pre-set P_f range (outside and within the plausibility range), incorporation or exclusion of borehole pressure history and adjustment of fit constraints. The limited P_f-range with plausible values equivalent to fresh water heads +/- 50 m bgl resulted in a general decrease of fit quality. A slightly improved fit was obtained when no pre-test borehole pressure was considered.

The homogeneous type models provided K-estimates ranging between 4.5E-14 and 7.6E-14 m/s and S_S-estimates between 1.2E-6 m^{-1} and 2.0E-6 m^{-1}. The narrow ranges reflect the low sensitivity to the P_f-parameter.

During a more detailed analysis, two additional models were tested to "force" the formation pressure towards more reasonable values: a composite skin model and a model with varying test zone volume. The latter case accounts for possible volume changes due the observed gradual decrease of packer pressure during the testing. Given that near near-surface heads were indicated by the results from the adjacent test intervals Oftr-i1 and Oftr-i2, the P_f-ranges were further narrowed to pressures equivalent to heads +/-25 m surface.

The skin model produced fits of fairly good quality. Note that the sensitivity to the formation pressure is further decreased for the composite skin model. Perturbation analyses using two different fit specifications (Cartesian and composite P vs. log(t)) resulted in P_f -estimates scattering between the lower and upper limit of the pre-set P_f -range. For both fit-specifications, the values with the lowest sum of square errors (SSE) were located at the lower limit of the P_f range (6029 kPa). Significant frequencies with higher P_f-estimates were recognized as well. The solutions with higher P_f-estimates are associated with SSE-values that are only marginally increased compared to the best estimate SSE. The perturbation of the initial parameters proved to be nearly indifferent with respect to hydraulic conductivity. The Cartesian fit specification produced K-values mainly between 1E-14 and 1.5E-14 m/s, whereas the P vs. log(t) composite fit resulted in K-estimates mainly between 1.7E-14 and 2.5E-14 m/s. Despite the reasonable fit quality for the composite skin model, presence of (negative) skin remains uncertain because of the imperfect residual distribution and because the relatively large confidence regions.

In a further interpretation step, the effect of volume displacement due to packer pressure change was investigated. The packer pressures decreased from 34.3 to 26.7 bar during the PSR-PW-PI sequence. Test zone volume increase as a result of packer pressure decrease could have influenced the interval pressure. This effect was investigated by incorporating varying test volume as inner boundary condition in nSights. The relation used between packer pressure change and test zone volume change is based on assumed packer displacement rates. The exercise showed that 0.2 millimetre displacement per bar (per bar of packer pressure change; the displacement is indicated in total for two packers) would result in a P_f-estimate which is increased by 1580 kPa compared to the case with constant inner boundary conditions. The K- and S_S parameters proved to behave indifferently with regard to the change of the inner boundary conditions. For the case with constant test zone volume (assuming no effect due to packer pressure change), use of wide P_f range in combination with a homogeneous model, a K-value of 7.6E-14 m/s and a S_S-estimate of 1.8E-6 m^{-1} was obtained. The model with varying test zone volume provided a slightly increased K-estimate of 7.0E-14 m/s and a S_S-estimate of 2.0E-6 m^{-1}.

To summarize, the multiple cases of inverse parameter estimations performed for the homogeneous and composite skin model provided the following results:

- formation conductivities ranged from 1.0E-14 to 8.0E-14 m/s
- specific storage values ranged from 7E-07 to 2.0E-06 m^{-1}
- formation pressures ranged from 4795 to 6420 kPa

Note that highest P_f values were obtained either by using a composite model or by an assumed varying test zone volume. The mechanism for the latter case is not supported by quantitative measurements. Therefore, the static formation pressure estimate has to be considered as highly uncertain for this test interval.

Based on the results of the preferred homogeneous model (good quality simulation cases; tagged with the √ symbol in Tab), the following parameter ranges were assessed:

- formation conductivity: 3.3E-14 - 8.0E-14 m/s
- specific storage: 7.8E-07 - 2.2E-06 m^{-1}
- formation pressures: 4768 - 6391 kPa (corresponding heads 279 - 445)

The above parameter ranges include the incertitude as indicated by the 95^{th} percentile confidence intervals for the individual minimum and maximum values.

The suggested best estimate K-value is 6.2E-14 m/s and represents the geometric mean of the K-results of the indicated good quality simulations. The suggested value is about a factor 8 smaller than the best estimate K-value from test interval Oftr-i2 (Oftr-i7 represents a subsection of Oftr-i2). The best estimate for the formation pressure equals to the lower limit of the plausibility range for this parameter (5784 kPa, corresponding head h_s = 383 m asl) and should be considered with care. The hydraulic head estimated for test interval Oftr-i2 is about 50 meter higher.

Level	Comments	
QLR **best e.**	Cart ESF, wide P_f range	h
Standard	Cart ESF, plausible P_f range (Section 7.3.4)	h
Standard	Cart ESF, no BH	h
Standard	Cart PW-PI fit, limited P_f range [2)]	c
Standard	Cart PW-PI fit, limited P_f range [3)]	c
Standard	CF PW+PI, limited P_f range [2)]	c
Standard	CF PW+PI, limited P_f range [3)]	c
Standard	Cart PW-PI fit, varying V_{TZ}. [2)]	h

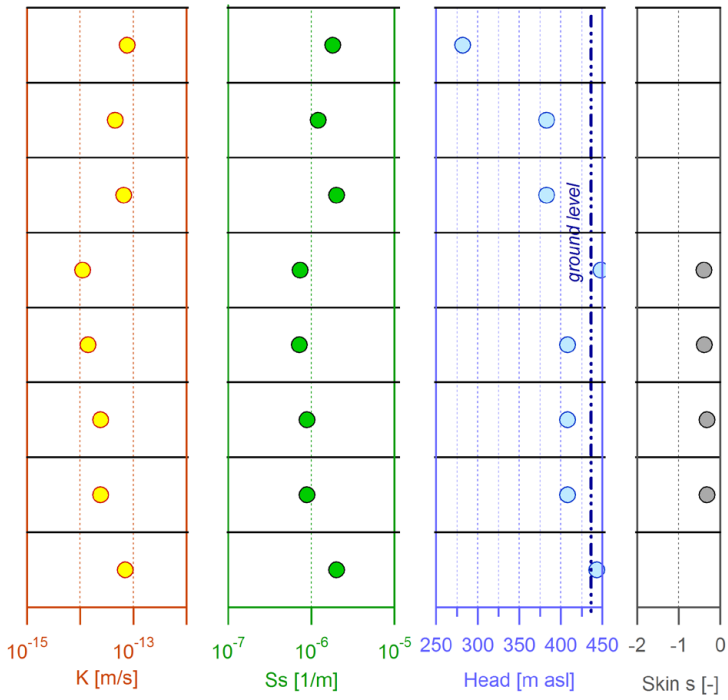

Fig. 14.19: Overview of results of inverse parameter estimations based on different models and fit configurations

Shaded cells denote "good estimates"
QLR = Quick Look Report
best e. best estimate
c = composite skin model
CF Composite fit
Cart ESF = Cartesian entire sequence fit
h = homogeneous model
V_{TZ} test zone volume
[1)] = limited P_f range 5784 - 6765 kPa
[2)] = limited P_f range 6029 - 6519 kPa
[3)] = perturbation analysis, limited P_f range 6029 - 6519 kPa

Tab. 14.16: Oftr-i7: Overview of results of inverse parameter estimations

Case		K [m/s]	S_S [m^{-1}]	s [-]	h_s [m asl]	Fit quality	Remarks Plausibility	
Cart ESF, wide P_f range	h	7.6E-14	1.8E-06		282.2	+	Unrealistic low P_f	√
Standard analysis:								
Cart ESF, plausible P_f range (Section 7.3.4)	h	4.5E-14	1.2E-06		383.0	**(+)**	P_f at lower limit	√
Cart ESF, no BH	h	6.6E-14	2.0E-06		383.0	+	P_f at lower limit	
Cart PW-PI fit, limited P_f range [2)]	c	1.1E-14	7.3E-07		448.1	+	wide range of K confidence limits	
Cart PW-PI fit, limited P_f range [3)]	c	1.4E-14	7.2E-07	-0.40	408.0	+	local SSE minima exist	
CF PW+PI, limited P_f range [2)]	c	2.4E-14	8.8E-07	-0.39	408.0	+	wide range of K confidence limits	
CF PW+PI, limited P_f range [3)]	c	2.4E-14	8.8E-07	-0.33	408.0	+	Frequency plot shows bimodal K_f distribution; wide range of K confidence limits	
Cart PW-PI fit, varying V_{TZ}. [2)]	h	7.0E-14	2.0E-06	-0.33	443.3	+	poor match for PSR	√

√ = good simulation results used to to assess parameter ranges and to calculate mean K-value as best estimate
QLR = Quick Look Report
c = composite skin model
CF Composite fit
Cart ESF = Cartesian entire sequence fit
h = homogeneous model
[1)] = limited P_f range 5784 - 6765 kPa
[2)] = limited P_f range 6029 - 6519 kPa
[3)] = perturbation analysis, limited P_f range 6029 - 6519 kPa

15. Test Interval Oftr-i8c: 621.5 - 630.6 m

Interpretation Level: Standard analysis

15.1. Introduction

The testing procedure of Test Oftr-i8c is identical to the one from Test Oftr-i7: COM and PSR phase are followed by a pulse withdrawal test (PW) and a pulse injection test (PI). The PI test was conducted to confirm the wellbore compressibility estimate from PW. For the standard analysis of test interval Oftr-i8c, the earlier analyses presented in the QLR (Appendix H) were refined to better constrain the formation properties with focus on hydraulic conductivity and hydraulic head. Additional numerical analyses using nSights were conducted to provide a greater level of confidence in the estimated formation properties. Borehole history effects were already included during the simulations for the QLR, as it was done for all intervals. The diagnostic plots presented in the QLR indicated that a homogeneous flow model is appropriate for this test interval. The 9.09 m long test interval Oftr-i8c (621.5 -630.6 m) represents a subsection of the 50.04 m long test interval Oftr-i2 (590.0 - 640.04 m). An overview plot of the Oftr-i8c test sequence is provided in Fig. 15.1. The total test duration of interval Oftr-i8c is 11-½ hrs. This is short compared to other tests in the NOK-EWS borehole which lasted at least 19-½ hours.

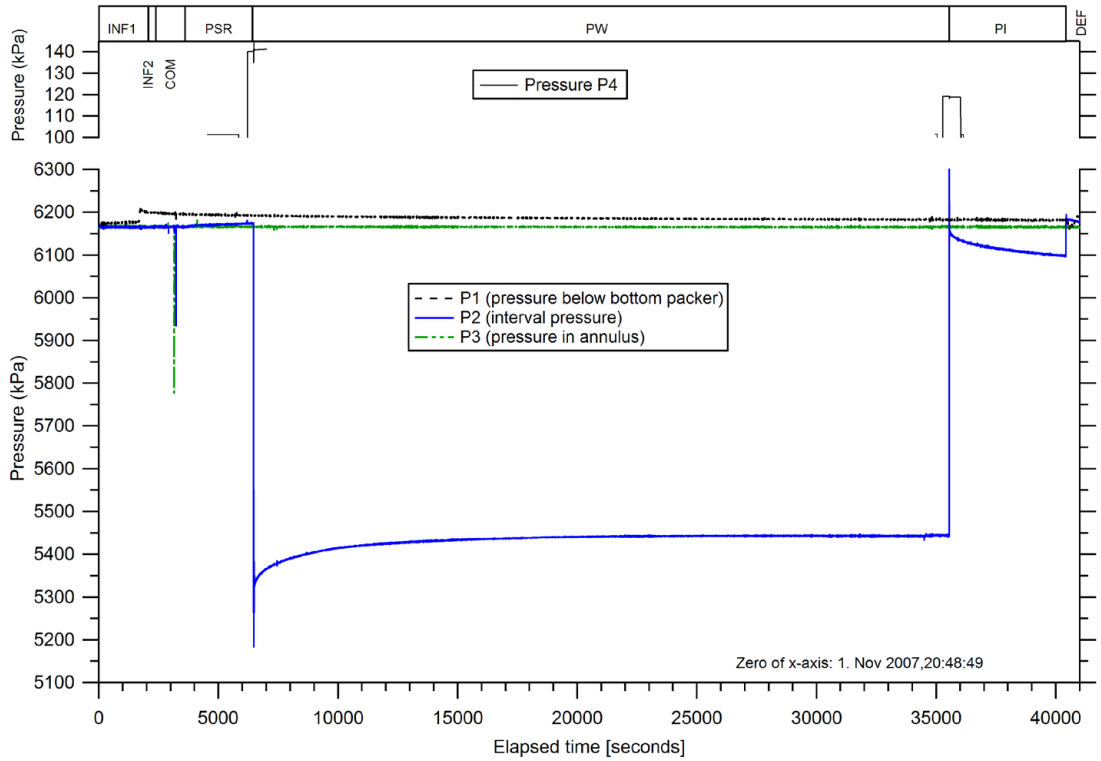

Fig. 15.1: Test Oftr-i8c, 621.5 - 630.6 m: overview plot

15.2. Parameter Range and Best-Estimate from QLR

The numerical analysis for the QLR provided the following parameters estimates:

K = 1.2E-13 m/s (1.2E-13 - 5.3E-13 m/s)
S_S = 2.7E-06 m^{-1} (6.4E-07 - 2.7E-06 m^{-1})
P_f = 3857 kPa (3857 - 6692 kPa)

The values in brackets indicate the lowest/highest estimates from several inverse parameter optimizations for different test periods and fit constraints using nSights. In the preliminary analyses presented in the QLR, the estimates of the hydraulic pressures were below the lower limit of the expected values. The QLR best-estimate fit is based on a Cartesian fit specification and with use of wide P_f input range. The results are summarized Tab. 15.1, Tab. 15.2 and Fig. 15.2. The computed residuals in comparison to a normal error distribution are shown of in the bottom right plot of Fig. 15.3.

Tab. 15.1: Oftr-i8c / QLR result: Parameters estimates and 95% confidence intervals for the Cartesian all sequence fit

Parameter	Units	Fit Value SSE= 1.38E+06	95% Confidence Intervals	
			Lower Value	Upper Value
K_fm	[m/s]	1.16E-13	1.00E-13	1.35E-13
P_fm	[kPa]	3857	3703	4012
ss_fm	[1/m]	2.73E-06	2.21E-06	3.37E-06

Tab. 15.2: Oftr-i8c / QLR result: Covariance-Correlation matrix for homogeneous model (shaded cells denote correlation matrix elements).

Covariance/Correlation Matrix: Est. Cart_Dat_P			
	K_fm	P_fm	ss_fm
K_fm	4.19E-05	1.49E-04	-5.90E-05
P_fm	9.87E-01	5.48E-04	-2.14E-04
ss_fm	-9.96E-01	-9.96E-01	8.38E-05

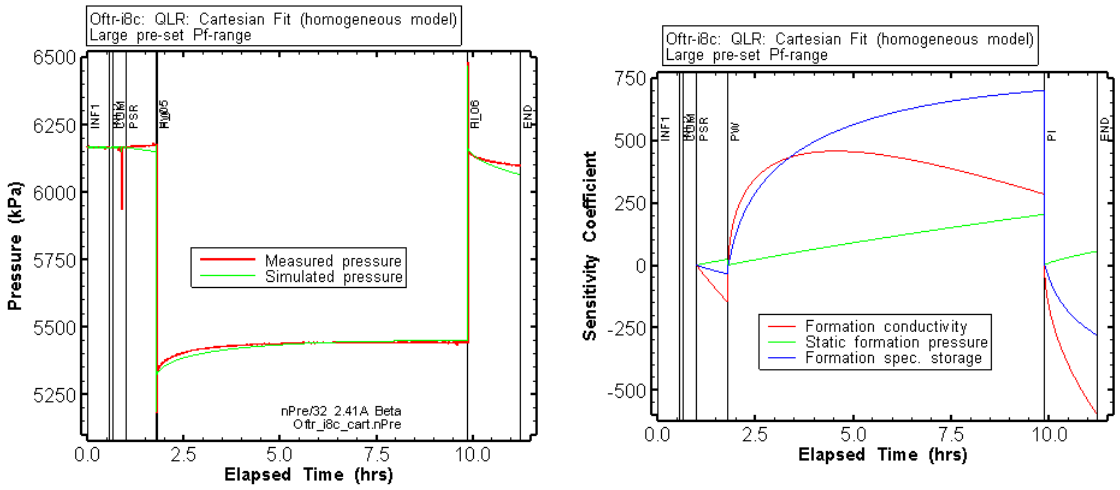

Fig. 15.2: Oftr-i8c: Cartesian fit of QLR best-estimate. Left: result of inverse parameter estimation, Cartesian plot. Right: sensitivity coefficients for PSR, PW and PI.

15.3. Incertitude With Regard to the P_f-Parameter

The QLR provided a best estimate of P_f = 3857 kPa corresponding to a hydraulic head of 197.1 m asl whereas the plausible range (Section 7.3.4) expects a static formation pressure value between 5676 and 6657 kPa (483 - 583 m asl). In general, the plausibility of P_f -estimates from interval Oftr-i8c also need to be checked against the head estimate of test interval Oftr-i2 which includes interval i8c (Section 15.1), and against interval Oftr-i1. Test interval i8c is separated from the more transmissive interval Oftr-i1 only by 19.4 m. The detailed and standard analyses of interval i1 and i2 suggest formation heads of 456 and 436 m asl, respectively. Assuming that the hydraulic head of test interval Oftr-i8c is similar to the heads of intervals i1 and i2, a static formation pressure between 6193 to 6302 kPa would be expected (corresponding to heads from 436 to 456 m asl). The QLR reported a relatively low sensitivity coefficient to the P_f parameter for all test sequences (right plot in Fig. 15.2) which makes the determination of a reliable P_f estimate difficult.

15.4. Homogeneous Model -- Cartesian Fit with Limited Pre-set P_f-Range

The Cartesian all-sequence fit model from the QLR (Section 15.2) was adjusted by limiting the P_f input range according to the plausibility ranges as defined in Section 7.3.4. The result of the inverse parameter optimization is shown in Tab. 15.3, Tab. 15.4 and Fig. 15.3. The obtained P_f estimate of 5784 kPa is at the lower bound of the input range (5676 to 6657 kPa). The K- and S_S estimates are similar to the corresponding best-estimates of the QLR. However, the obtained fit is of inferior quality compared to the Cartesian fit using a wide P_f range (Section 15.2). This can also be noticed from the two bottom plots of Fig. 15.3 which show the residual distributions in comparison to a normal error distribution both for the case with limited P_f range (bottom left) and wide P_f range (bottom right). The residuals for the latter case are essentially normally distributed (bottom right) whereas the residuals for the case with limited P_f range (bottom left) deviate significantly from the quantile-normal line. This indicates the presence of a systematic error and a conceptual model mismatch. The sum of squared errors is an order of magnitude higher for the case with limited P_f range (SSE = 3.58E+06) compared to the case with wide P_f range (SSE = 1.38E+06). The range between the upper and lower values for the 95th percentile confidence intervals are listed in Tab. 15.3 and shown in Fig. 15.3. The two plots of Fig. 15.3 provide the 95th percentile confidence regions for the estimation of the P_f and K parameters (bottom left) and Ss and K parameters (bottom right), with the shape of the ellipse indicating the degree of correlation between the parameters. Tab. 15.3 includes the covariance correlation matrix (shaded cells) which indicates that the especially the Ss and K fitting parameters are well correlated. This correlation is also observed in the confidence intervals plots of Fig. 15.3 by small minor axis of the uncertainty ellipsoids.

The homogeneous model in combination with the pre-set fit constraints and the incorporated borehole pressure history does not satisfactorily reproduce the measured formation response. Therefore, new model features or other (non-hydraulic) effects need to be investigated.

Tab. 15.3: Oftr-i8c: Parameters estimates and 95% confidence intervals for the Cartesian all sequence fit using limited P_f range

Parameter	Units	Fit Value SSE = 3.58E+06	95% Confidence Intervals	
			Lower Value	Upper Value
K_fm	[m/s]	6.25E-14	3.75E-14	1.04E-13
P_fm	[kPa]	5676	5592	5760
ss_fm	[1/m]	1.59E-06	8.15E-07	3.12E-06

Tab. 15.4: Covariance-Correlation matrix for homogeneous model fit using limited P_f range (shaded cells denote correlation matrix elements).

Covariance/Correlation Matrix: Est. Cart_Dat_P			
	K_fm	P_fm	ss_fm
K_fm	3.44E-04	9.09E-05	-1.35E-03
P_fm	1.14E-01	1.84E-03	-5.61E-04
ss_fm	-9.98E-01	-1.80E-01	5.31E-03

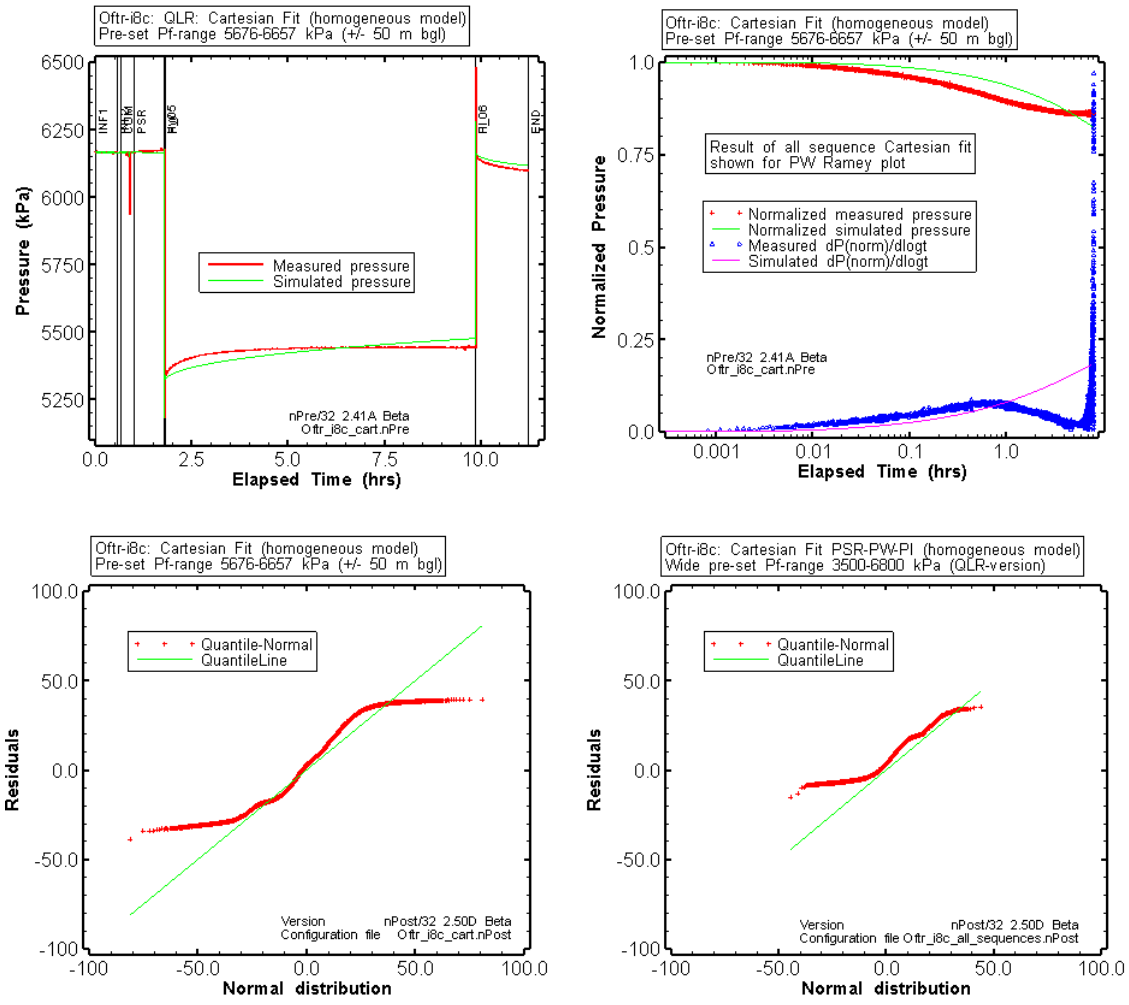

Fig. 15.3: Oftr-i8c, homogeneous model / limited P_f range: fit plots and residual plots.

Results from nSights inverse parameter estimation fitting the Cartesian pressures of the entire test using a limited range for the P_f parameter (5676 - 6657 kPa). Cartesian plot of entire test (upper left) and results of Cartesian fit shown for the PW Ramey A plot (upper right). The residual distributions are shown for two cases (both Cartesian fits): for the case with limited pre-set P_f range (bottom left) and wide pre-set P_f range (QLR fit, bottom right).

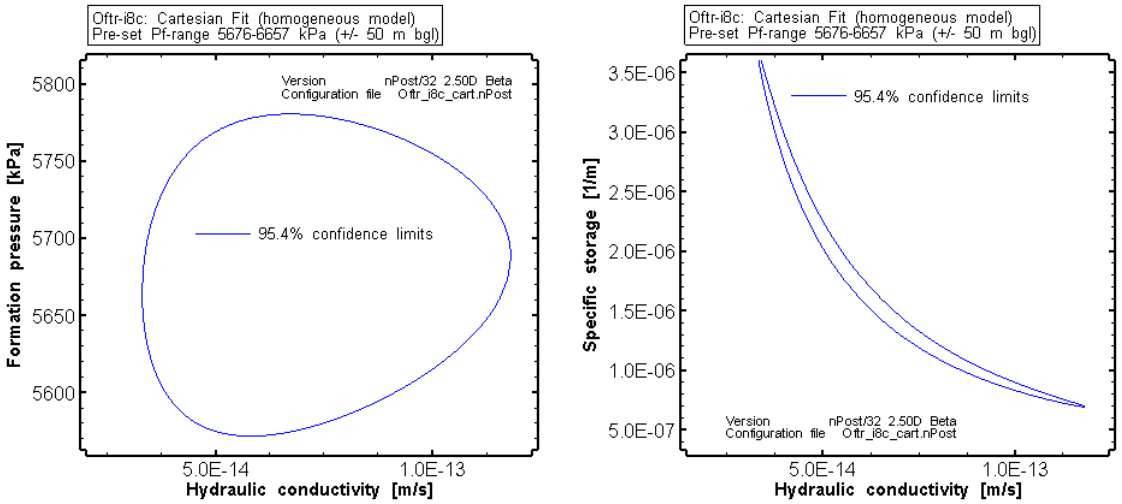

Fig. 15.4: Oftr-i8c, Cartesian fit to the entire sequence (homogeneous model): confidence regions for the joint parameters K- P_f (left) and K - S_S (right)

15.5. Homogeneous Model -- Cartesian Fit to the PW-PI Sequence

Based on the model of the previous Section, additional inverse parameter estimation with a slightly adjusted fit constraint was conducted. The case assumes that the PSR sequence was affected by ongoing compliance effects and is not characteristic to the undisturbed formation response. The fit is therefore limited to the PW-PI sequence. The results (here not shown in detail) are very similar to the results of the entire sequence case (Section 15.4. The sum of square errors (SSE) is 3.56E+06 which almost equals to the SSE-value of the fit for the entire sequence (3.58E+06, Tab. 15.3).

15.6. Composite (Skin) Model -- Cartesian Fit with Limited P_f Range

The homogenous model was extended to composite to see if a narrow cylindrical zone around the borehole of different properties (skin zone properties) compared to the formation properties would result in comparable fit quality and significantly increased formation pressure.

The results of the nSights inverse parameter optimization are shown in Tab. 15.5 and Tab. 15.6, Fig. 15.6 and Fig. 15.7. An unrealistic low formation conductivity of K=1.3E-15 m/s and a P_f-estimate of 6657 kPa was obtained. The introduction of a skin zone produces improved visual fits, especially for the middle/late time data of the Ramey plot for PW (middle left plot of Fig. 15.7), and the SSE value is reduced to 2.67E+05. The residual distribution is essentially in agreement with a normal error distribution (bottom left blot of Fig. 15.7) and suggests the absence of a systematic error or model mismatch. The skin parameters values (K_S = 2.1E-13, t_S= 0.024 m in relation to the formation hydraulic conductivity (1.3E-15 m/s) correspond to a skin factor of -0.28. The ratio between formation conductivity and skin zone conductivity equals to 158. The thickness of the skin zone is highly correlated (R > 0.9) with the skin conductivity and highly negatively correlated with the specific storage of the skin zone (Tab. 15.6). K_S and S_{SS} are fully negatively correlated (R = -1.00).

The parameter variance (diagonal elements) is large for the P_f parameter (Tab. 15.6). Given that the parameters are estimated by nSights using a normalized scale of 0 to 1, the maximum theoretical variance would correspond to the case where all values in this range are equally likely represented by a uniform distribution with a theoretical variance of 1/12 or 8.33E-2. The parameter variance for the P_f parameter is above this value which indicates that the estimated parameter distributions are widely scattered around the mean value.

Fig. 15.5 provides the 95th percentile confidence regions for the estimation of the P_f and K parameters (left) and S_s and K parameters (right), with the shape of the ellipse indicating the degree of correlation between the parameters. The confidence interval information indicates that the range in the fitted parameter values is large for the P_f and S_S parameters. The large confidence intervals for the S_S and the P_f parameters are also reflected by the low sensitivity to these parameters (Fig. 15.7).

Tab. 15.5: Oftr-i8c: Parameters estimates and 95% confidence intervals for the Cartesian entire using limited pre-set P_f range, composite skin model

Parameter	Units	Fit Value SSE= 2.67E+05	95% Confidence Interval	
			Lower Value	Upper Value
K_fm	[m/sec]	1.31E-15	8.99E-16	1.90E-15
K_s	[m/sec]	2.07E-13	1.10E-13	3.90E-13
P_fm	[kPa]	6657	4741	8573
Ss_fm	[1/m]	2.27E-06	1.79E-07	2.88E-05
Ss_s	[1/m]	1.79E-06	8.52E-07	3.77E-06
t_s	[m]	0.0242	0.0037	0.0447

Tab. 15.6: Covariance-Correlation matrix for the Cartesian PSR-PW-PI fit using limited P_f range, composite skin model (shaded cells denote correlation matrix elements).

	K_fm	K_s	P_fm	ss_fm	Ss_s	t_s
K_fm	4.13E-04	3.61E-04	-3.63E-03	-2.81E-03	-9.47E-04	2.44E-03
K_s	3.87E-01	2.11E-03	1.40E-02	-7.75E-03	-5.70E-03	1.12E-02
P_fm	-1.83E-01	3.12E-01	**9.54E-01**	-1.99E-01	-3.73E-02	1.26E-01
Ss_fm	-5.02E-01	-6.12E-01	-7.40E-01	7.62E-02	2.06E-02	-5.81E-02
Ss_s	-3.75E-01	-1.00E+00	-3.07E-01	6.02E-01	1.54E-02	-3.03E-02
t_s	4.68E-01	9.54E-01	5.04E-01	-8.20E-01	-9.50E-01	6.59E-02

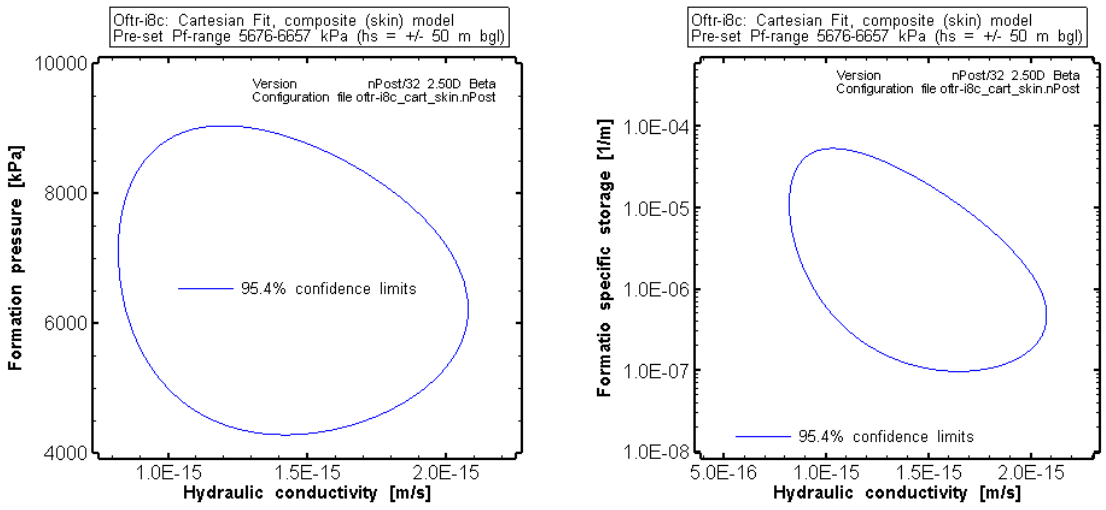

Fig. 15.5: Oftr-i8c, composite skin model / Cartesian fit to PW-PI: confidence regions for the joint parameters K-P_f (left) and K - S_S (right).

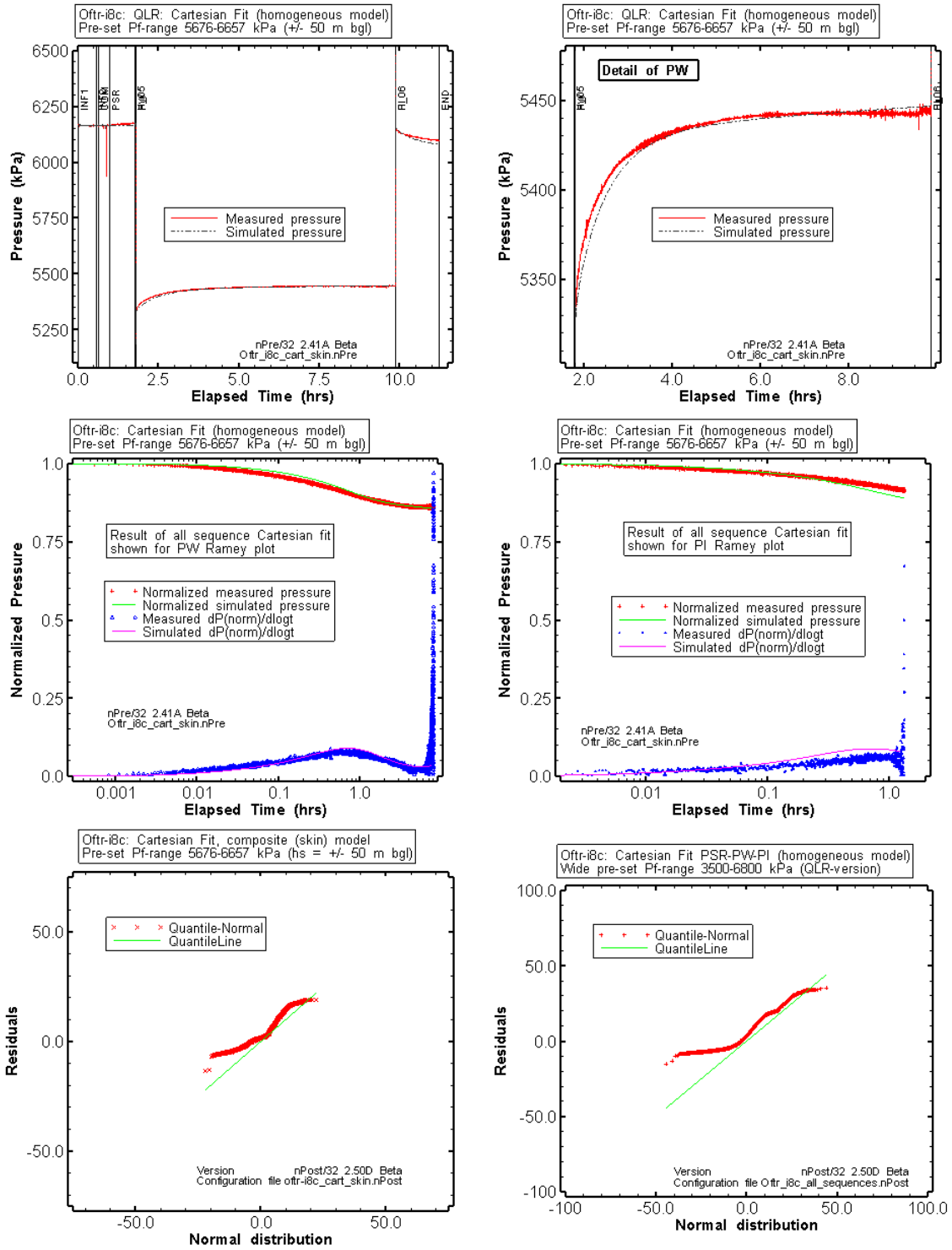

Fig. 15.6: Oftr-i8c: composite skin model / limited P_f range: fit plots and residual plots.

Results are shown from nSights inverse parameter estimation fitting the Cartesian pressures of the PSR-PW-PI sequence and using a limited range for the P_f parameter (5676 - 6657 kPa). The Cartesian plot (upper left) is shown with detailed view for PW sequence (upper right). The parameters of Cartesian fit were applied for the Ramey A plots of PW (middle left) and PI (middle right). The residual distributions are shown for this case (with skin, bottom left) and for the best-estimate case from QLR (bottom right).

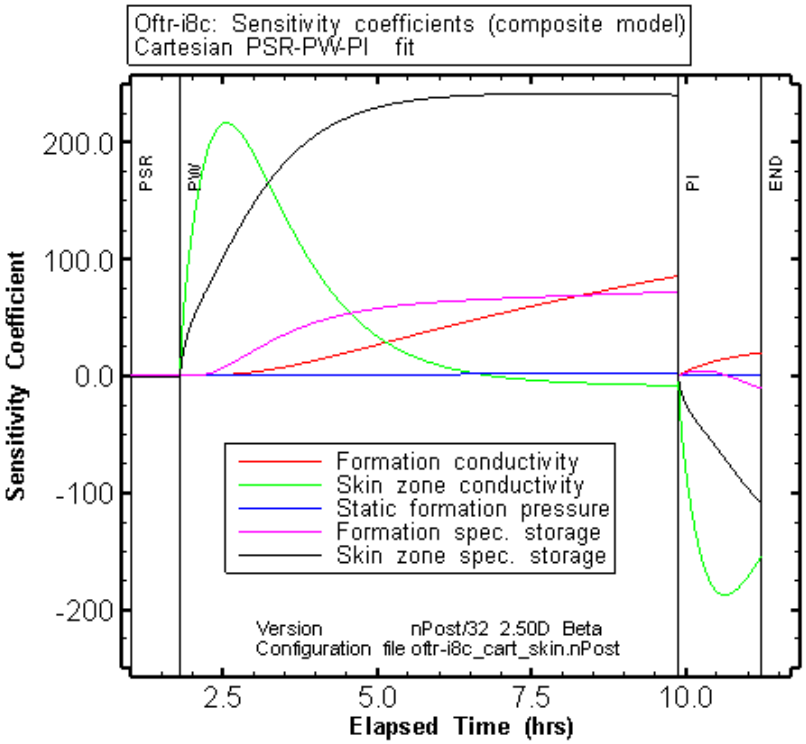

Fig. 15.7: Oftr-i8c: composite skin model / limited P_f range: Sensitivity coefficients.

The sensitivity coefficients are shown for the Cartesian PSR-PW-PI (entire) sequence fit, composite skin model. The sensitivity to the formation pressure parameter is close to zero.

15.7. Composite Skin Model -- Use of Other Fit Specifications

Based on the composite model described in the previous section, multiple trials with different fit specifications were undertaken. The following fit constraints were used: composite PW-PI sequence fit to pulse normalized pressure, sequence fit to pulse derivative function and sequence fit to both normalized pressure and derivative (combined fit). The simulations (not shown) produced the following parameters: K= 1.3E-15 to 6.7E-15 m/s, K_S = 1.1E-13 to 2.7E-13 m/s, P_f = 6621 to 6657 kPa, S_S = 1.9E-07 to 4.1E-6 m^{-1}, S_S = 1.3E-06 to 3.6E-06 m^{-1}, t_S = 0.012 to 0.028 m.

15.7.1. Perturbation analysis

A perturbation analysis was performed to see if other local or global minima would exist and in particular if such a local/global minima would be associated with a more realistic estimate for the K-parameter. This was done after increasing the lower limit of K-range from 1E-15 to 1E-14 m/s and by repeating the optimization with different starting values for the different parameters. For this case 100 optimization runs were performed for which individual fits were computed. The skin storage constant was not varied but entered as constant (S_{SS} = 1E-6 m^{-1}) and a test zone compressibility value of 1.0E-9 Pa^{-1} was used. The perturbation was run using the simplex optimization algorithm. The result of the best estimate (case with lowest SSE) is shown graphically in the plots of Fig. 15.10. The perturbation statistics of Tab. 15.7 indicates for each fitted parameter the maximum and minimum values and the values of the best estimate case. The latter is associated to the optimization with the lowest SSE-value.

Fig. 15.8 shows the results from all perturbation runs for the K-S_S and K-P_f joint parameters (top left and top right). The 95% confidence regions are shown for the best estimate. Frequency histograms for the K- and P_f -parameters are given provided on the bottom left and bottom right of Fig. 15.8. 84% of the K-values belong to the class at the lower limit of the pre-set K-range (84 values between 1.00E-14 and 1.01E-14 m/s). The P_f parameter shows similar frequencies for most of the 50 classes. The highest frequency is located at the upper limit and the 2nd highest frequency at the lower limit of the pre-set range. The perturbation results are plotted in Fig. 15.9 as three dimensional plots of the SSE as a function of the best-fit values of formation conductivity and formation pressure (top), as a function of the best-fit values of formation conductivity and specific storage (middle) and as function of skin and formation conductivity. The best-fit results are indicated as green squares for comparison with the distribution from the perturbation runs.

The perturbation analysis was successful by demonstrating that the skin model represents a plausible scenario that is not restricted to unrealistic low formation values. The best estimate optimization (lowest SSE) is associated with a K-value of 1.0E-14 m/s (at the lower bound of the pre-set range of 1E-14 to 1E-11 m/s) and the obtained SSE-value of 2.78E+05 is only slightly above the SSE-value of the single realization (SSE= 2.67E+05, see Tab. 15.5).

The perturbation analysis was not successful in terms that the optimizations based on perturbed initial parameters did not lead to a well confined parameter space.

Tab. 15.7: Oftr-i8c, composite skin model: perturbation analysis statistics (100 optimizations)

Run	K_fm [m/sec]	K_s [m/sec]	P_fm [kPa]	ss_fm [1/m]	t_s [m]	SSE
Best	**1.00E-14**	**3.58E-13**	**6637**	**1.90E-07**	**0.0409**	2.78E+05
Max	1.52E-14	6.24E-13	6657	1.50E-06	0.0420	4.93E+05
Min	1.00E-14	3.44E-13	5676	1.90E-07	0.0317	2.78E+05
Mean	1.03E-14	3.67E-13	6283	2.73E-07	0.0406	2.91E+05
StdDev	9.20E-16	4.05E-14	308.1	2.53E-07	0.0021	3.50E+04

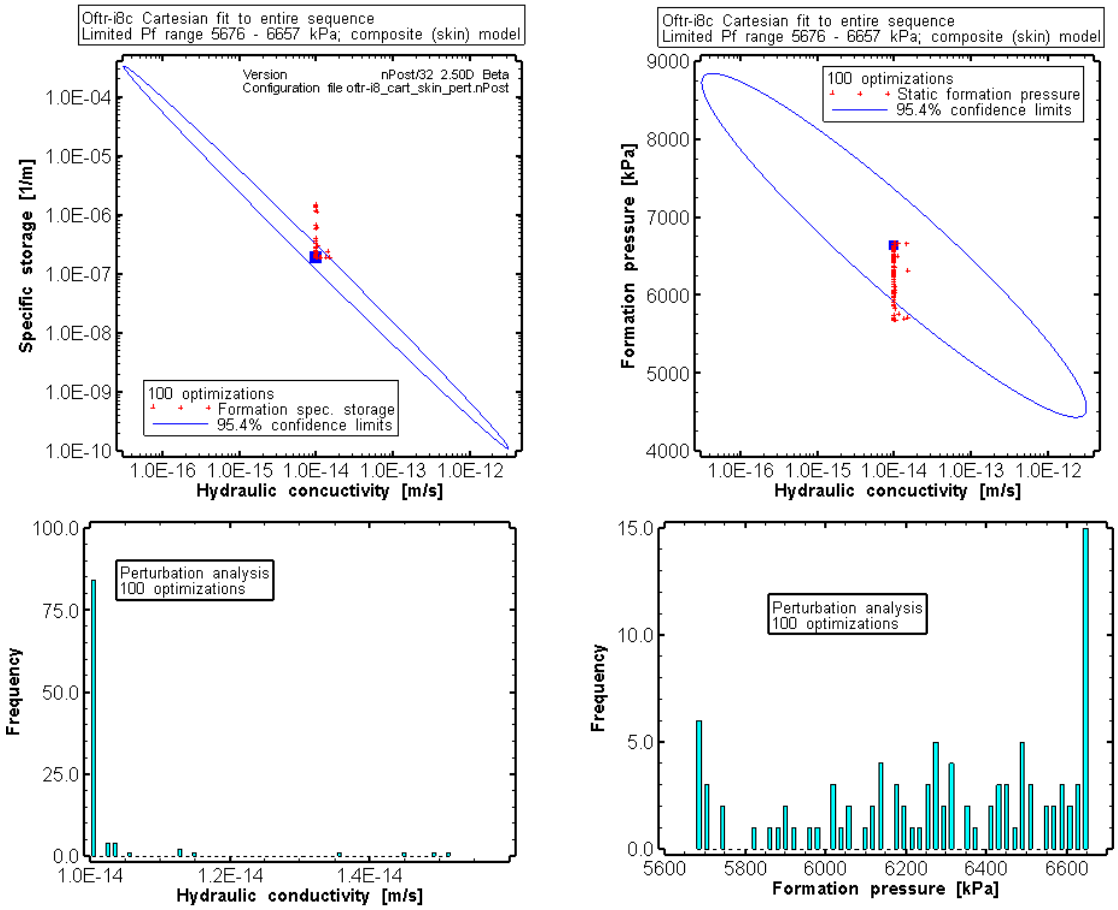

Fig. 15.8: Oftr-i8c, composite skin model: results from perturbation analysis of nSights inverse simulation Cartesian fit to PW-PI sequence.

Confidence regions for the K- S_S joint parameters (left top), K-P_f joint parameters (top right) and the frequency distributions for the K- (bottom left) and the P_f estimates (bottom right).

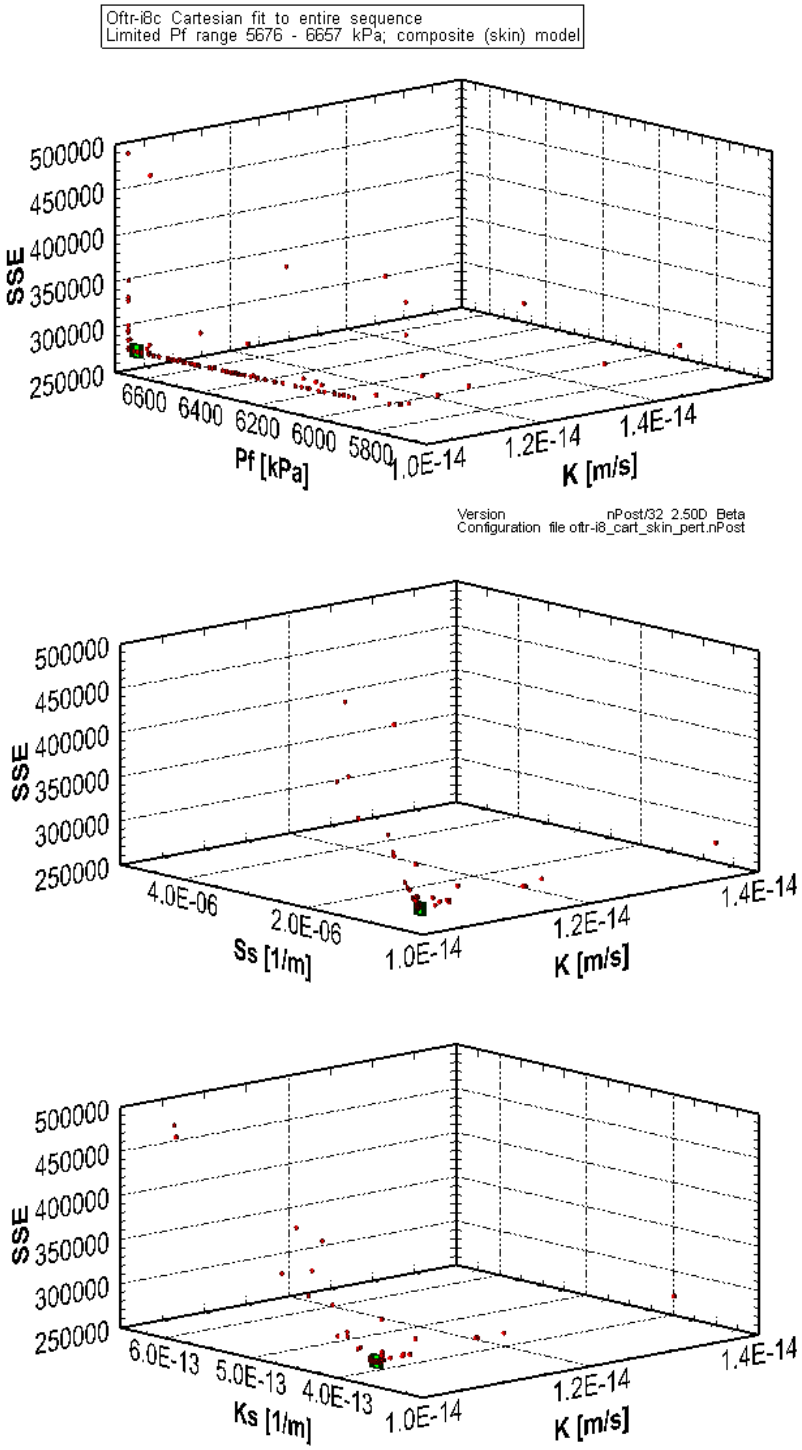

Fig. 15.9: Oftr-i8c, composite skin model / Cartesian fit to the PW-PI sequence: Perturbation analysis

Top: SSE versus K and P_f . Middle: SSE versus K and S_S. Bottom: SSE versus K and K_S. The best-estimate solutions with lowest SSE value are shown the green cube symbol.

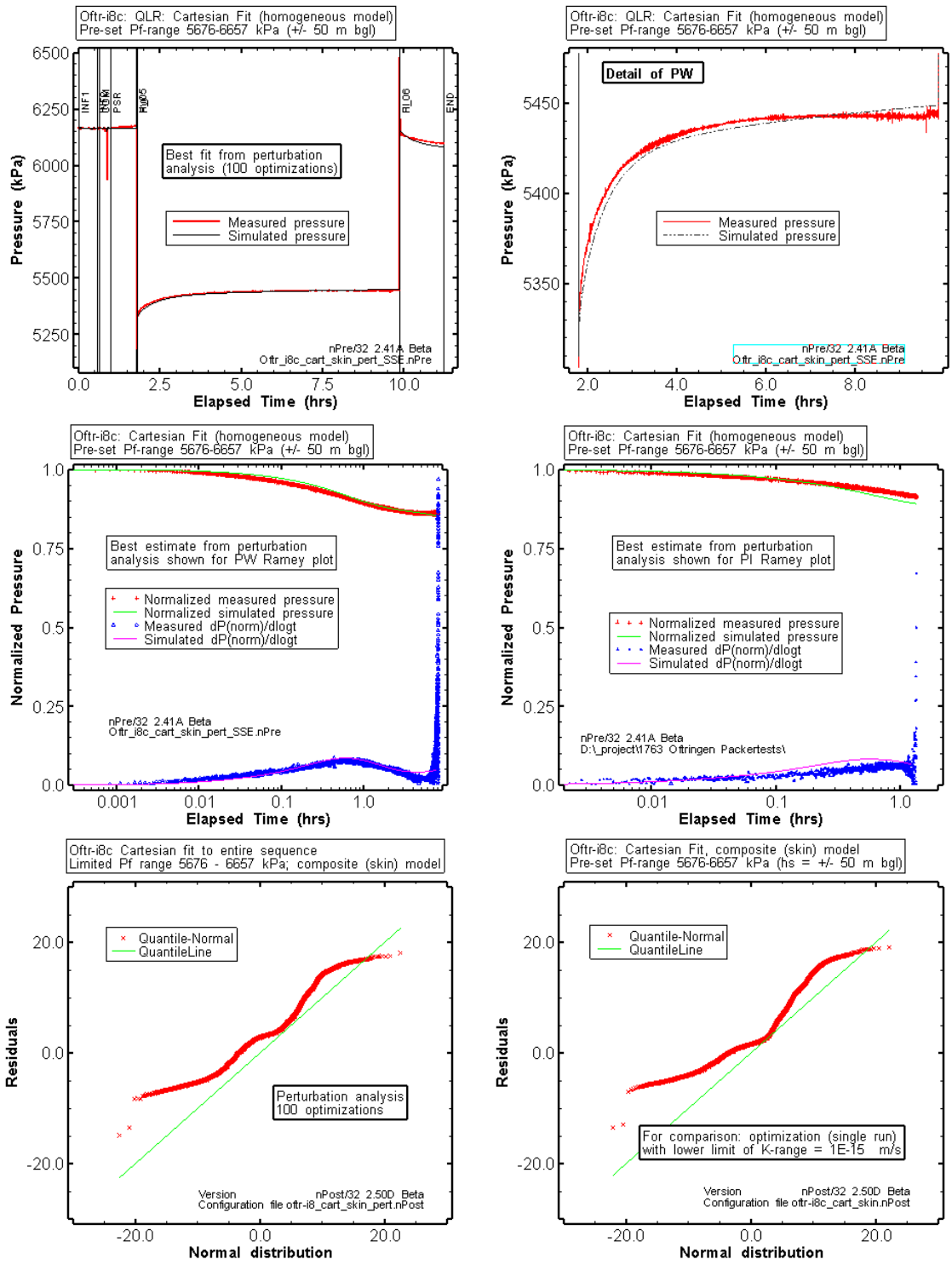

Fig. 15.10: Oftr-i8c - composite skin model / perturbation analysis: Fits and residuals.

Results from nSights inverse parameter estimation fitting the Cartesian pressures of the PSR-PW-PI sequence using a limited range for the P_f parameter (5676 - 6657 kPa) and the K-parameter (1E-14 to 1E-11 m/s). Best estimate (lowest SSE value) for 100 realizations is based on perturbed initial estimates of fitted parameters. Cartesian plot (upper left) with detail for PW (upper right) and results of Cartesian fit shown for the Ramey A plots of PW (middle left) and PI (middle right). The residual distributions are shown for this case (with

skin, pre-set K-range 1.0E-14 - 1.0E-11 m/s, bottom left) and for the best-estimate case from the single run optimization, using a pre-set K-range from 1.0E-15 to 1.0E-11 m/s (bottom right).

15.8. Potential Influence of Packer Pressure Change

The packer pressure continuously decreased during the hydraulic testing in Oftr-i8c (Fig. 15.11), from 37.9 bar (at start of the PSR) to 32.6 bar (at end of PI). Theoretically, the change in packer pressure could have resulted in slight movement of the packer sleeves at the packer ends facing towards the test zone. In case of packer pressure decrease, such an effect would cause an increase in test zone volume. In tight formation, an increase in test zone volume would be associated with a temporary decrease of interval pressure. The effect of varying test zone volume was not investigated for this interval.

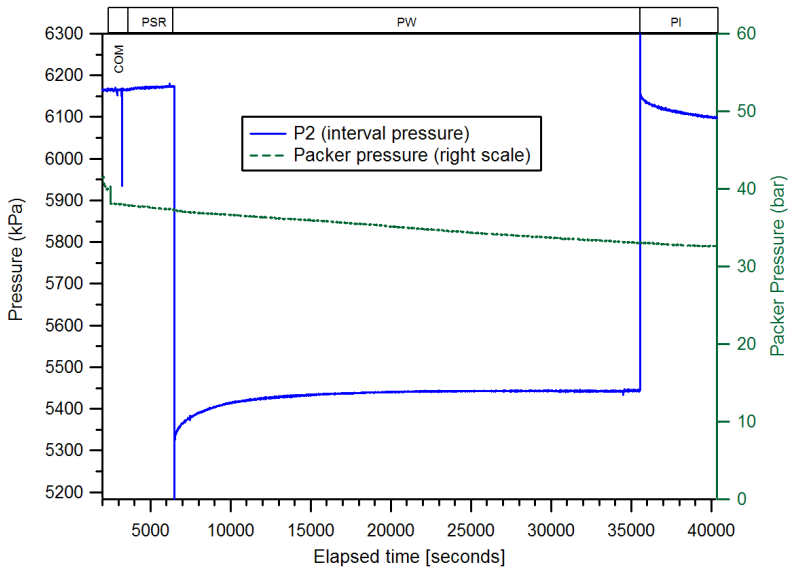

Fig. 15.11: Packer pressure decrease during testing in Oftr-i8c (green line)

15.9. Summary

During the "standard analysis" for test Oftr-i8c, the homogeneous model was additionally used with adjusted model parameters (e.g. pre-set P_f range according the plausibility range) and with a composite skin model. For the homogeneous model, the use of a limited P_f-range (plausible values equivalent to fresh water heads +/- 50 m bgl) decreased the overall fit quality. The homogeneous type models provided K-estimates ranging between 6.3E-14 and 1.2E-13 m/s and S_S-estimates between 1.6E-6 m^{-1} and 1.8E-6 m^{-1}. The higher K-estimate (result of QLR) is associated with a hydraulic head of 3857 kPa which is outside of the plausibility range. The formation pressure estimate for the case with narrowed P_f range equals to 5576 kPa. This value corresponds to the lower limit of the pre-set range, i.e. to a freshwater head of 50 m bgl.

A composite skin model was tested to see if the formation pressure would approach more reasonable values. The skin model produced fits of fairly good quality. However, the sensitivity to the formation pressure is almost zero for this model. A perturbation analysis was performed to see if other local or global minima would exist and in particular if such a minima would provide a more realistic estimate for the K-parameter. This was done after increasing the lower limit of K-range from 1E-15 to 1E-14 m/s and by repeating the optimization with different starting values for the different parameters. The obtained P_f -estimates scattered between the lower and upper limit of the P_f -range used, whereas the K-values of all optimizations were located at the lower limit of the pre-set K-range (1.0E-14 m/s, or slightly higher). A large number of solutions have very similar K- and SSE-values but differ with regard to the P_f-parameter. Despite the reasonable fit quality for the composite skin model, presence of (negative) skin remains uncertain because of the imperfect residual distribution and because the relatively large confidence limits for the P_f and S_S parameters.

The possibility that the measured pressure response was affected by the measured decrease in packer pressure during testing of Oftr-i8c can not be excluded. Simulations of non-hydraulic effects for in similar impermeable rock (Oftr-i5 and Oftr-i7) demonstrate that only small incremental volume changes are required to obtain significantly increased estimates for the formation pressure parameter (Sections 12.4 and 14.9). Such a scenario would possibly imply slightly increased K-estimates.

The multiple cases of inverse parameter estimations performed for the homogeneous and composite skin model provided the following parameter ranges:

- formation conductivities ranged from 1.3E-15 to 1.2E-13 m/s.
- specific storage values ranged from 2E-07 to 4E-06 m^{-1}
- formation pressures ranged within the pre-set range from 5676 to 6657 kPa

The K-values <1E-14 m/s are considered unrealistic. For comparison, the QLR suggested a K-value of 1.1E-13 m/s based on an extended P_f-range and a P_f best-estimate of 3857 kPa. The QLR also reported relatively "high" K-estimates for the individual sequence fits for PW (K= 4.0E-13 m/s) and PI (K=5.5E-13 m/s). The values from the individual sequence fits were considered as less representative of the formation properties. During the Standard analysis, the highest P_f values were obtained in combination with a composite skin model. Non-hydraulic effects could have affected the estimated parameters and in particular the formation pressure estimates. Therefore, the static formation pressure estimates have to be considered rough estimates.

Based on the results of the preferred homogeneous model (good quality simulation cases; tagged with the √ symbol in Tab. 15.8), the following parameter ranges were assessed:

- formation conductivity: 3.7E-14 - 1.4E-13 m/s
- specific storage: 8.2E-07 - 3.4E-06 m^{-1}
- formation pressures: 3703 - 5760 kPa (corresponding heads 182 - 392 m asl)

The above parameter ranges include the incertitude as indicated by the 95th percentile confidence intervals for the individual minimum and maximum values.

The suggested best estimate K-value of 6.25E-14 m/s (Tab. 15.8) is by a factor 7.5 smaller than the best estimate K-value from test interval Oftr-i2 (Oftr-i8 represents a subsection of Oftr-i2). The best estimate for the formation pressure equals to the lower limit of the plausibility range for this parameter corresponding to a head of 383 m asl and should be considered with care. The hydraulic head estimated for test interval Oftr-i2 is about 50 meter higher.

Level	**Comments**	
QLR	Cart ESF, wide P_f range	h
Standard best estimate	Cart ESF, plausible P_f range [1] (Section 7.3.4)	h
Standard	Cart ESF, plausible P_f range [1]	c
Standard	Cart ESF, plausible P_f range [2]	c
Standard (not shown)	CF PW+PI P(norm) [1]	c
Standard (not shown)	CF PW+PI dP(norm) [1]	c
Standard (not shown)	CF PW+PI P(norm) & dP(norm) [1]	c

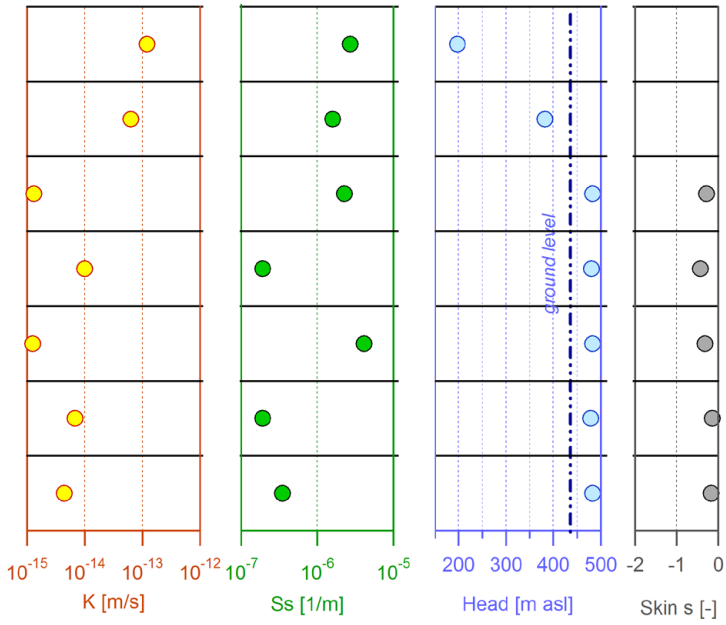

Fig. 15.12: Overview of results of inverse parameter estimations based on different models and fit configurations

QLR =	Quick Look Report
c =	composite skin model
Cart ESF =	Cartesian entire sequence fit
CF	composite fit
h =	homogeneous model
[1] =	Plausible P_f range 5676 - 6657 kPa, see Section 7.3.4
[2] =	perturbation analysis, P_f range 5676 - 6657 kPa

Tab. 15.8: Oftr-i8c: Overview of results of inverse parameter estimations

Case		K [m/s]	S_S [m^{-1}]	s [-]	h_s [m asl]	Fit quality	Remarks Plausibility	
QLR best estimate Cart ESF, wide P_f range	h	1.2E-13	2.7E-06		197.1	+	unrealistic low P_f	√
Standard analysis								
Cart ESF, plausible P_f range [1], **best estimate**	h	6.25E-14	1.59E-06		382.5	**(+)**	P_f at lower limit	√
Cart ESF, plausible P_f range [1]	c	1.31E-15	2.27E-06	-0.28	482.5	+	large confidence limits for P_f-S_S, near zero sensitivity to P_f	
Cart ESF, plausible P_f range [2]	c	1.00E-14	1.90E-07	-0.43	480.5	+		
CF PW+PI P(norm) [1]	c	1.25E-15	4.12E-06	-0.32	482.5	+	not shown	
CF PW+PI dP(norm) [1]	c	6.74E-15	1.90E-07	-0.14	478.8	+	not shown	
CF PW+PI P(norm) & dP(norm) [1]	c	4.40E-15	3.50E-07	-0.17	482.5	-	not shown, rather poor fit for PW	

√ = good simulation results used to to assess parameter ranges
QLR = Quick Look Report
c = composite skin model
Cart ESF = Cartesian entire sequence fit
CF composite fit
h = homogeneous model
[1] = Plausible P_f range 5676 - 6657 kPa, see Section 7.3.4
[2] = perturbation analysis, P_f range 5676 - 6657 kPa

16. Test Interval Oftr-i9: 583 - 592.1 m

Interpretation Level: Standard analysis

16.1. Introduction

The 9.09 m long test interval Oftr-i9 covers a subsector of interval Oftr-i3, 550 - 600.04 m bgl. During the temperature and salinity logging undertaken by BLM, a possible minor inflow zone at 588.7 m was identified. An overview plot of the Oftr-i9 test sequence is provided in Fig. 16.1. The test Oftr-i9 was recorded during 19 hrs and consisted of an initial pressure recovery PSR phase followed by a pulse withdrawal test (PW) and a slug withdrawal test and a pulse injection test (PI). The PI test was conducted to confirm the wellbore compressibility estimate from PW. The PSR phase might be influenced by compliance effects which may not have fully dissipated prior to start of PSR. The temperature shows an increasing trend especially at the beginning of the sequence with a flattening at late time and an overall temperature increase of 4.0° C. For the standard analysis of test interval Oftr-i9, the earlier analyses presented in the QLR (Appendix I) were refined to better constrain the formation properties with focus on hydraulic conductivity and hydraulic head. Additional numerical analyses using nSights were conducted to provide a greater level of confidence in the estimated formation properties. Borehole history effects were already included during the simulations for the QLR. The diagnostic plots presented in the QLR indicated that a composite skin flow model is appropriate for this test interval.

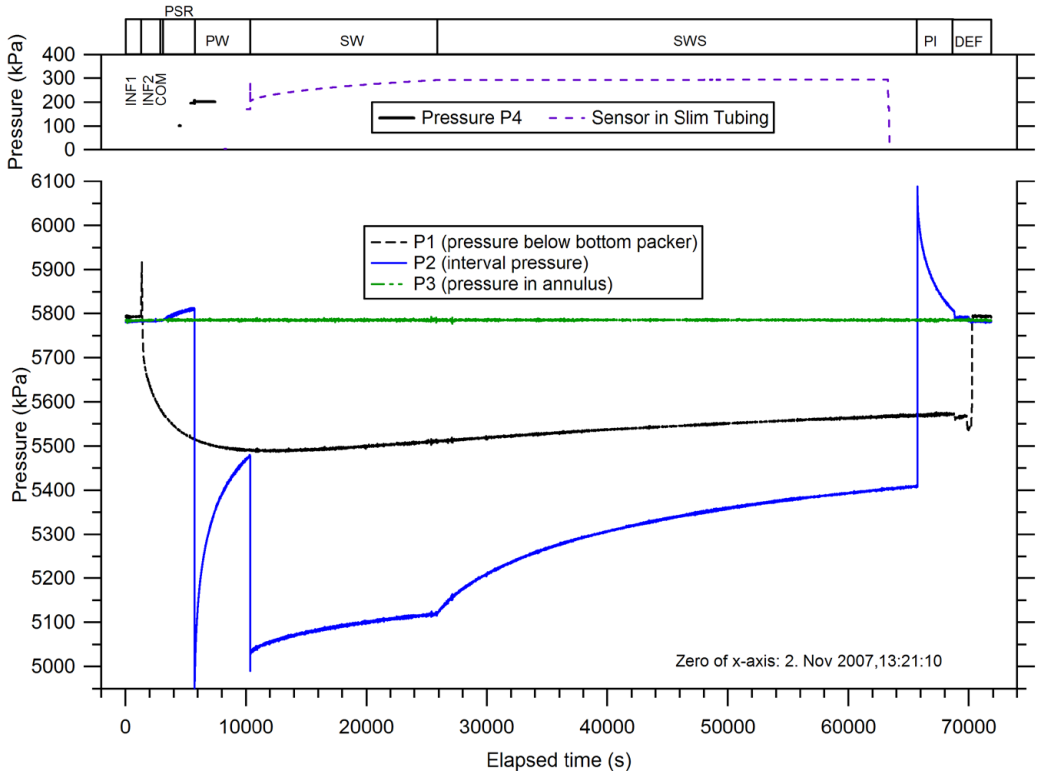

Fig. 16.1: Test Oftr-i9, 583.0 - 592.1 m: overview plot

16.2. Parameter Range and Best-Estimate from QLR

The numerical analysis for the QLR provided the following parameters estimates:

K = 1.7E-12 m/s (1.7E-12 - 8.0E-11 m/s)
S_S = 1.0E-05 m^{-1} (9.9E-06 - 9.1E-05 m^{-1})
P_f = 5523 kPa (4828 - 6000 kPa)

The values in brackets indicate the lowest/highest estimates from several inverse parameter optimizations for different test periods and fit constraints using nSights. The lowest K-estimate was obtained using a composite skin model. The homogeneous model provided K-values ranging between 2E-11 m/s and 8.0E-11 m/s. The estimates of the hydraulic pressures from composite skin model (QLR analysis) were below the lower limit of the expected values. The QLR best-estimate fit was based on a Cartesian fit specification and with use of wide P_f input range. The results for the skin case are summarized Tab. 16.1, Tab. 16.2 and Fig. 16.2. The computed residuals in comparison to a normal error distribution are shown of in the bottom right plot of Fig. 16.2. Note that the results shown in Tab. 16.1 differ slightly from the values presented in the QLR. The time steps of the history sequences (transition between SWS and PI) were synchronized with the time intervals of measured to eliminate irrelevant residuals. This correction leaded to slightly different parameter estimates.

Tab. 16.1: Oftr-i9 / QLR result: Parameters estimates and 95% confidence intervals for the Cartesian all sequence fit

Parameter	Units	Fit Value SSE= 1.67E+06	95% Confidence Interval	
			Lower Value	Upper Value
K_fm	[m/sec]	1.48E-12	8.95E-13	2.44E-12
K_s	[m/sec]	9.27E-11	8.38E-11	1.03E-10
P_fm	[kPa]	5531	5499	5563
Ss_fm	[1/m]	1.00E-05	5.03E-06	1.99E-05
Ss_s	[1/m]	1.07E-06	8.18E-07	1.41E-06
t_s	[m]	0.28669	0.24208	0.33130

Tab. 16.2: Oftr-i9 / QLR result: Covariance-Correlation matrix for homogeneous model (shaded cells denote correlation matrix elements).

	K_fm	K_s	P_fm	ss_fm	Ss_s	t_s
K_fm	4.72E-04	2.13E-05	-1.80E-04	-2.35E-03	-9.94E-05	9.08E-05
K_s	1.79E-01	2.99E-05	-1.70E-05	-3.09E-04	-1.60E-04	5.96E-05
P_fm	-9.33E-01	-3.50E-01	7.90E-05	9.48E-04	8.44E-05	-5.01E-05
Ss_fm	-9.43E-01	-4.92E-01	9.30E-01	1.31E-02	1.60E-03	-8.48E-04
Ss_s	-1.55E-01	-9.98E-01	3.23E-01	4.74E-01	8.65E-04	-3.21E-04
t_s	3.73E-01	9.73E-01	-5.03E-01	-6.60E-01	-9.73E-01	1.26E-04

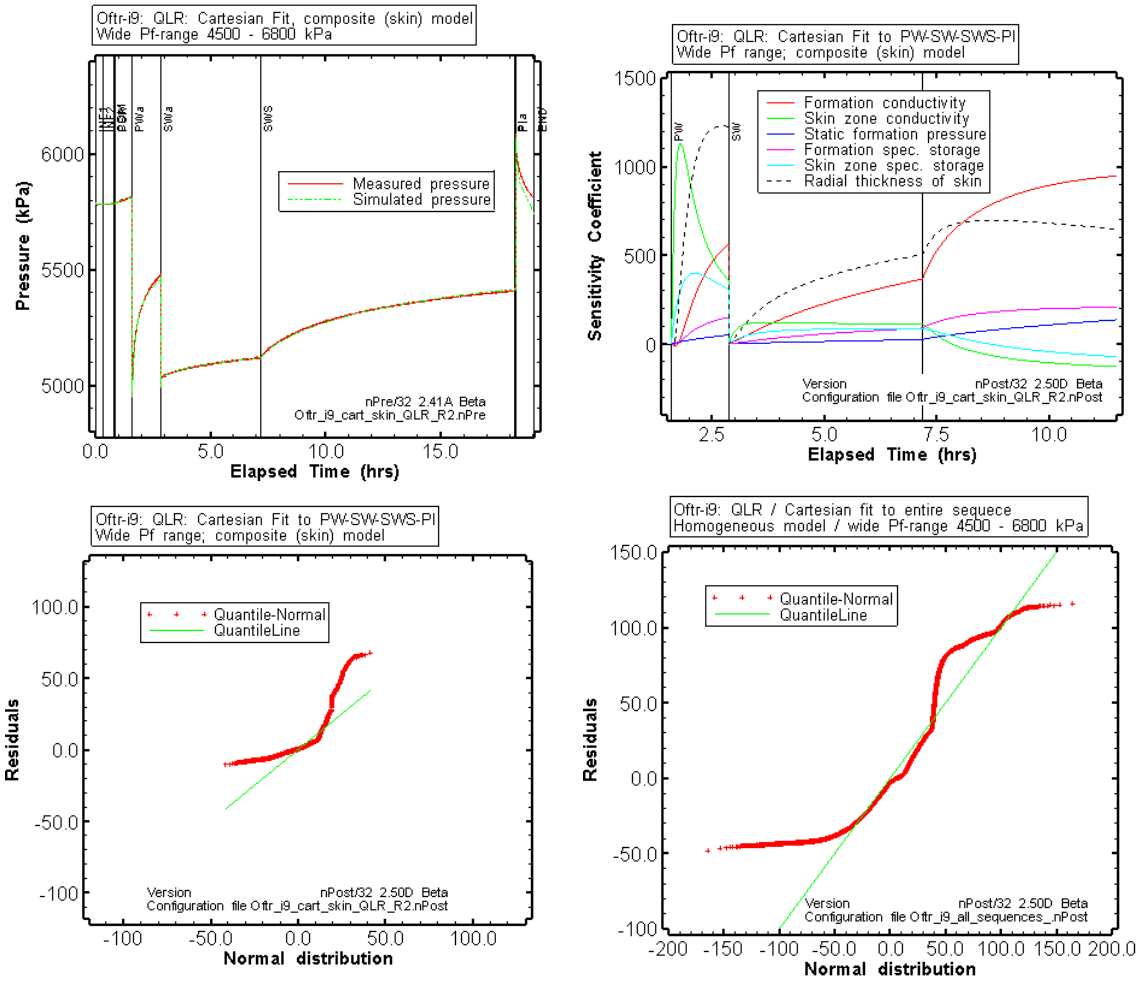

Fig. 16.2: Oftr-i9: Cartesian fit of QLR best-estimate (model setup slightly adjusted).

Top left: result of inverse parameter estimation, Cartesian plot. Top right: sensitivity coefficients for PW, SW, SWS and PI sequences. Bottom left: residuals compared to normal error distribution for the composite skin model. Bottom right: residual distribution of the homogeneous case (QLR analysis) shown for comparison.

16.2.1. Parameters for the homogeneous model from QLR

The QLR-result for the homogeneous model without skin is shown for comparison in Tab. 16.3, Tab. 16.4 and in Fig. 16.3. The inverse parameter estimation using a homogeneous model in combination with the entire sequence fit constraint resulted in a poor fit. The residual distribution for this case in comparison to a normal error distribution is shown in the bottom right plot of Fig. 16.2. The visual fit quality and the residual distribution suggest that the homogeneous model is not appropriate to describe the formation properties.

Tab. 16.3: Oftr-i9: QLR / homogeneous model: Parameters estimates and 95% confidence intervals for the Cartesian all sequence fit using a wide P_f range

Parameter	Units	Fit Value SSE = 2.63E+07	95% Confidence Intervals	
			Lower Value	Upper Value
K_fm	[m/s]	4.05E-11	4.00E-11	4.10E-11
P_fm	[kPa]	5176	5174	5179
ss_fm	[1/m]	1E-5 (pre-set constant)		

Tab. 16.4: Covariance-Correlation matrix for homogeneous model fit using limited P_f range (shaded cells denote correlation matrix elements).

Covariance/Correlation Matrix: Est. Cart_Dat_P		
	K_fm	P_fm
K_fm	2.78E-07	-1.58E-07
P_fm	-5.06E-01	3.53E-07

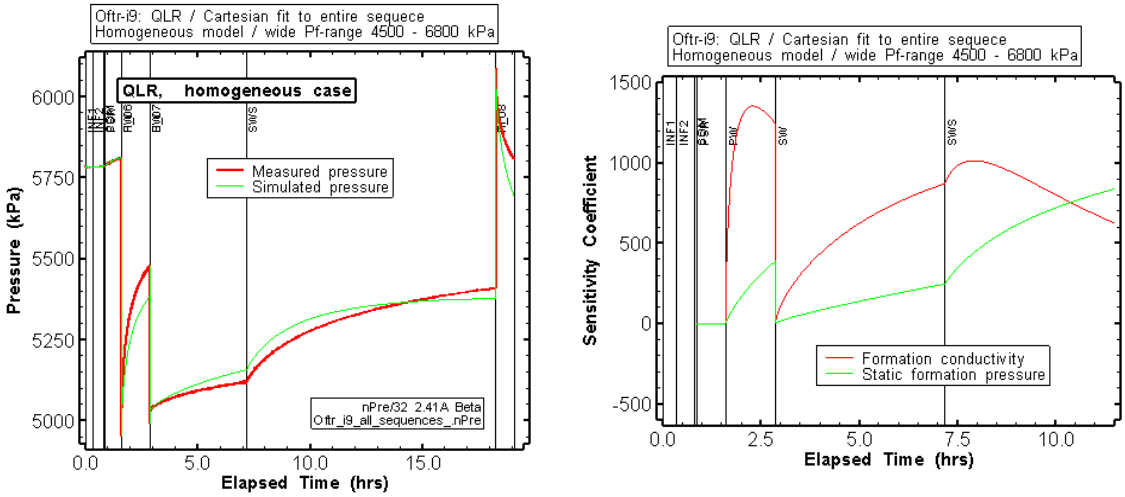

Fig. 16.3: Oftr-i9: QLR / Cartesian fit to the entire test sequence, homogeneous model.

Left: result of inverse parameter estimation, Cartesian plot. Right: sensitivity coefficients to the entire sequence.

16.3. Incertitude With Regard to the P_f-Parameter

The QLR provided a best estimate of P_f = 5523 kPa corresponding to a hydraulic head of 404.5 m asl using a composite skin model. These values are in the plausible range (Section 7.3.4) which expects static formation pressure values between 5300 and 6280 kPa (483 - 583 m asl). The plausibility of corresponding heads should be compared with the head estimates of the adjacent lower test intervals Oftr-i2 and Oftr-i1. Test interval i9 is separated from interval Oftr-i2 by 7 m. The detailed and standard analyses of interval i1 and i2 suggest formation heads of 456 and 436 m asl, respectively. Assuming that the hydraulic head of test interval Oftr-i9 is similar to the heads of intervals i1 and i2, a static formation pressures between 5815 to 6014 kPa would be expected (corresponding to a range in heads between 436 and 456 m asl).

16.4. Homogeneous Model -- Cartesian SW-SWS-PI Fit with Limited P_f-Range

The Cartesian all-sequence fit model from the QLR (Fig. 16.3, see also Annex I) adjusted by limiting the P_f input range according to the plausibility ranges as defined in Section 7.3.4 and by changing by limiting the fit constraint to the SW-SWS-PI sequence. The PW period (only poorly matched using the entire fit specification; see Fig. 16.3) is incorporated as pressure history period. The case assumes that the PSR-PW sequence was affected by ongoing compliance and other transient effects and is not characteristic to the undisturbed formation response. The result of the inverse parameter optimization is shown in Tab. 16.5, Tab. 16.6 and Fig. 16.4. The visual fit quality is good for all three fitted sequences SW, SWS and PI (Fig. 16.4, top plots). The parameters of the Cartesian fit were used to produce Ramey A plot for the PW (Fig. 16.4, middle left plot) and PI (not shown) sequences which all showed a good agreement between measured and simulated data. The SWS dP and dP' (derivative) data are also nicely fitted, as shown in the log-log diagnostic plot of Fig. 16.3 (middle right plot).

The obtained P_f estimate of 5300 kPa is at the lower bound of the plausible range (i.e. pre-set P_f range 5300 - 6280 kPa corresponding to heads +/ 50 m bgl). The formation conductivity estimate of K= 1.3E-11 m/s is about a factor three smaller than the corresponding value from the entire sequence fit (QLR, Tab. 16.3) but an order of magnitude higher than the K-estimate from the composite skin model (Tab. 16.1). The S_S estimate corresponds to the lower limit of the revised plausibility range for this parameter (1.9E-9 m^{-1}). The residuals for the latter case are essentially normally distributed (bottom right plot in Fig. 16.5) which supports the conceptional model with reservation that the PSR-PW was not included in the fit constraint.

The range between the upper and lower values for the 95th percentile confidence intervals are listed in Tab. 16.5 and shown in Fig. 16.4. The two plots of Fig. 16.4 provide the 95th percentile confidence regions for the estimation of the P_f and K parameters (left) and Ss and K parameters (right), with the shape of the ellipse indicating the degree of correlation between the parameters. Tab. 16.6 includes the covariance correlation matrix (shaded cells) which indicates that the especially the Ss and K fitting parameters are well correlated. This correlation is also observed in the confidence intervals plots of Fig. 16.4 by small minor axis of the uncertainty ellipsoids. The parameter variances (diagonal elements) are low resulting in a narrow range of the confidence intervals.

Tab. 16.5: Oftr-i9, homogeneous model, Cartesian fit to SW-SWS-PI: parameters estimates and 95% confidence intervals using limited P_f range

Parameter	Units	Fit Value SSE = 2.58E+05	95% Confidence Intervals	
			Lower Value	Upper Value
K_fm	[m/s]	1.25E-11	1.23E-11	1.26E-11
P_fm	[kPa]	5300	5299	5301
ss_fm	[1/m]	1.90E-05	1.86E-05	1.94E-05

Tab. 16.6: Covariance-Correlation matrix for homogeneous model fit using limited P_f range (shaded cells denote correlation matrix elements).

Covariance/Correlation Matrix: Est. Cart_Dat_P			
	K_fm	P_fm	ss_fm
K_fm	2.99E-07	-2.63E-07	-1.29E-06
P_fm	-8.37E-01	3.31E-07	1.03E-06
ss_fm	-9.83E-01	7.47E-01	5.76E-06

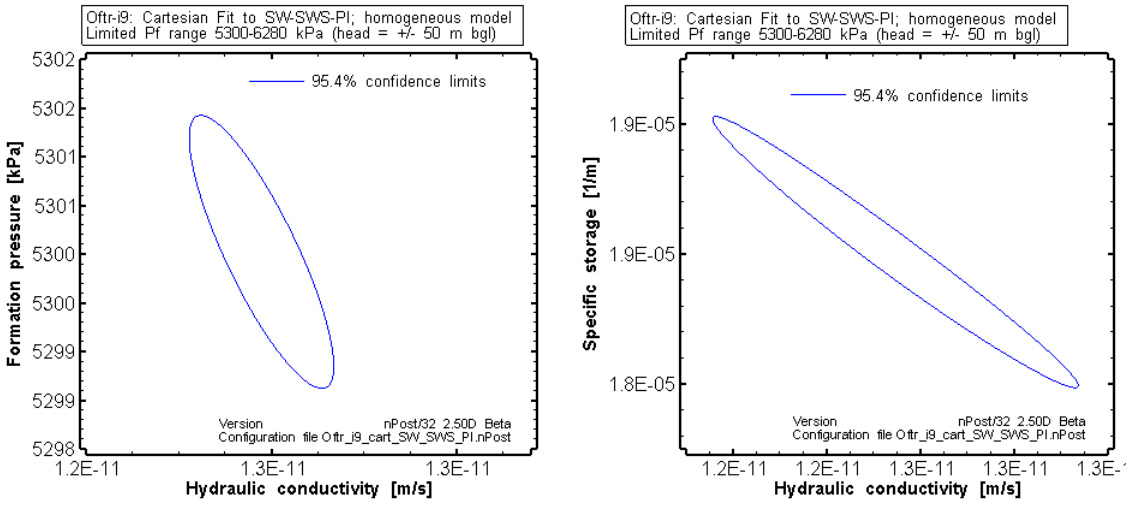

Fig. 16.4: Oftr-i9, Cartesian fit to the SW-SWS-PI sequence (homogeneous model): confidence regions for the joint parameters K- P_f (left) and K - S_S (right)

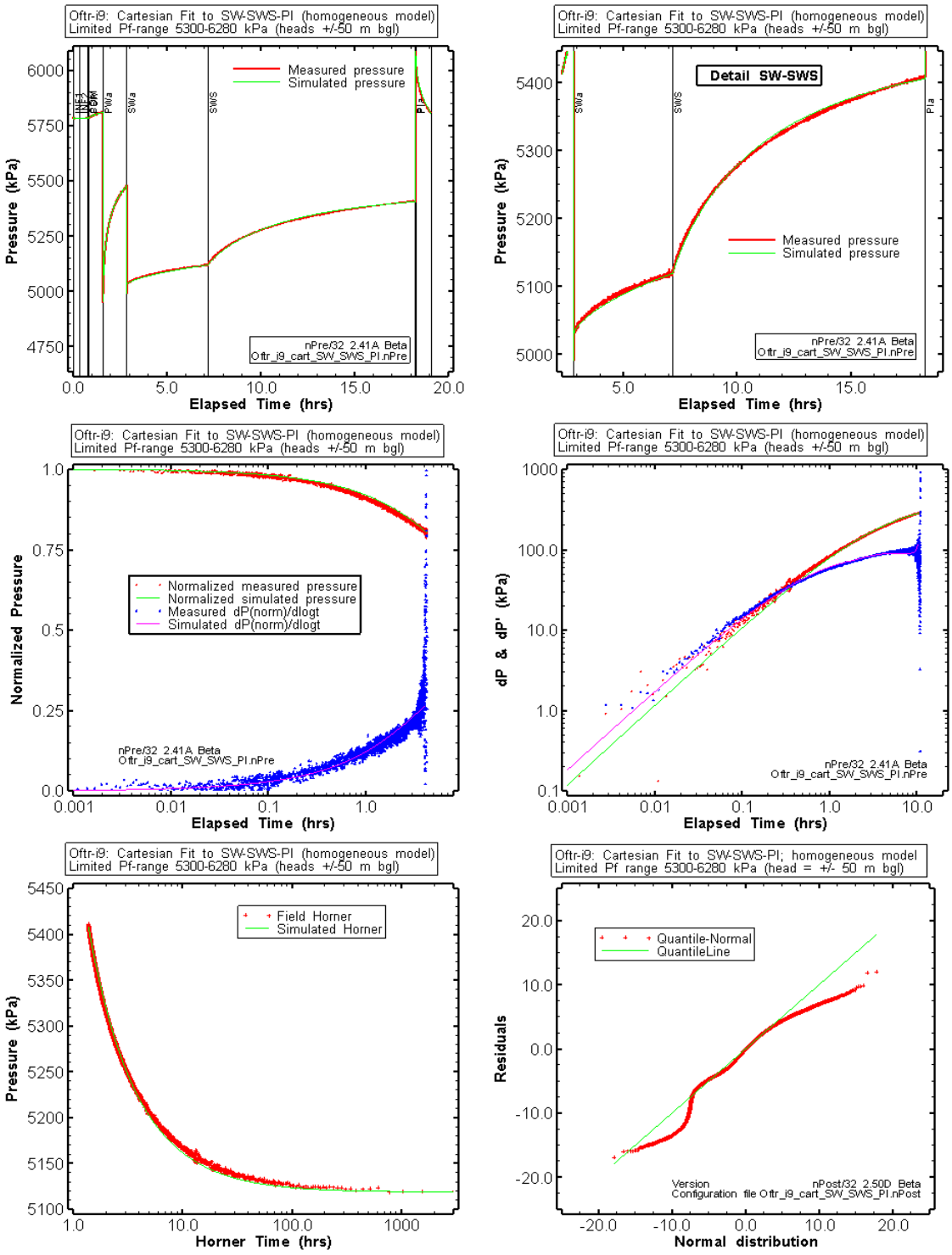

Fig. 16.5: Oftr-i9: homogeneous model, SW-SWS-PI sequence Cartesian fit / limited P_f range: fit plots and residual plots.

Results from nSights inverse parameter estimation fitting the Cartesian pressures of the entire test using a limited range for the P_f parameter (5300 - 6280 kPa). Cartesian plot of entire test (upper left) and results of Cartesian fit shown for the PW Ramey A plot (upper right). The residual distributions are shown for two cases (both Cartesian fits): for the case with limited pre-set P_f range (bottom left) and wide pre-set P_f range (QLR fit, bottom right).

16.5. Perturbation Analysis / Homogeneous Model / Wide P_f-Range

Two perturbation analyses were performed to see (1) if the result of the inverse parameters optimization represents belongs to a local/global minimum region in the parameter space and (2) if a perturbation analysis with wider pre-set ranges for P_f and S_S would provide similar parameter estimates. The results are presented in Subsection 16.5.1 for the perturbation analysis using a wide pre-set P_f-range (4000-7000 kPa) and in Subsection 16.5.2 for the perturbation with additionally extended S_S-range (1.0E-07-1.0E-4 m^{-1}).

16.5.1. Wide P_f-range

During this perturbations analysis, the static head was allowed to vary within 4000 and 7000 kPa. 100 optimization runs were performed for which individual fits were computed using Simplex algorithm. The results of the perturbation analysis are shown graphically in Fig. 16.6 and Fig. 16.7. The results of the best-estimate solution with lowest sum of squared errors (SSE) are presented in Tab. 16.7 and Tab. 16.8.

The parameters from 100 perturbations are plotted as three dimensional plot of the SSE as a function of the best-fit values of formation conductivity and formation pressure (Fig. 16.6, top graph), as a function of the best-fit values of formation conductivity and specific storage (Fig. 16.6, middle graph) and as a function of the best-fit values of specific storage and formation pressure (Fig. 16.6, bottom graph). In addition, the best-fit results (lowest SSE) are indicated as green filled cubes for comparison with the distribution from the perturbation runs. The 3D plots of Fig. 16.6 suggest that no other local minima exist besides the global minimum. All solutions are associated with S_S values at the upper limit of the pre-set range for this parameter (S_S = 1.9E-06 m^{-1}). The estimated P_f values vary with a very narrow range between 5276 and 5286 kPa. The obtained P_f best-estimate is only 20 kPa below the lower limit of the plausible range for this parameter. The top right plot Fig. 16.7 and the two plots in the middle of Fig. 16.7 show 2D scatter plots for the various realizations. The confidence regions of the best-estimate solution (lowest SSE case) for all presented joint parameters (K-P_f, K-S_S, S_S-P_f) include most of the other realizations. The residuals of the best-estimate solution are essentially normally distributed (top left plot of Fig. 16.7). The frequency plots at the bottom of Fig. 16.7 confirm the well confined ranges for the K- (bottom left) and P_f-parameters (bottom right).

Tab. 16.7: Oftr-i9, homogeneous model, Cartesian fit to SW-SWS-PI: parameters estimates and 95% confidence intervals using wide P_f range (4000-7000 kPa)

Parameter	Units	Fit Value SSE = 1.95E+05	95% Confidence Intervals	
			Lower Value	Upper Value
K_fm	[m/s]	1.32E-11	1.30E-11	1.33E-11
P_fm	[kPa]	5280	5279	5281
ss_fm	[1/m]	1.90E-05	1.86E-05	1.94E-05

Tab. 16.8: Covariance-Correlation matrix for homogeneous model fit using limited P_f range (shaded cells denote correlation matrix elements).

Covariance/Correlation Matrix: Est. Cart_Dat_P			
	K_fm	P_fm	ss_fm
K_fm	2.15E-07	-5.15E-08	-9.33E-07
P_fm	-7.88E-01	1.98E-08	1.99E-07
ss_fm	-9.82E-01	6.89E-01	4.19E-06

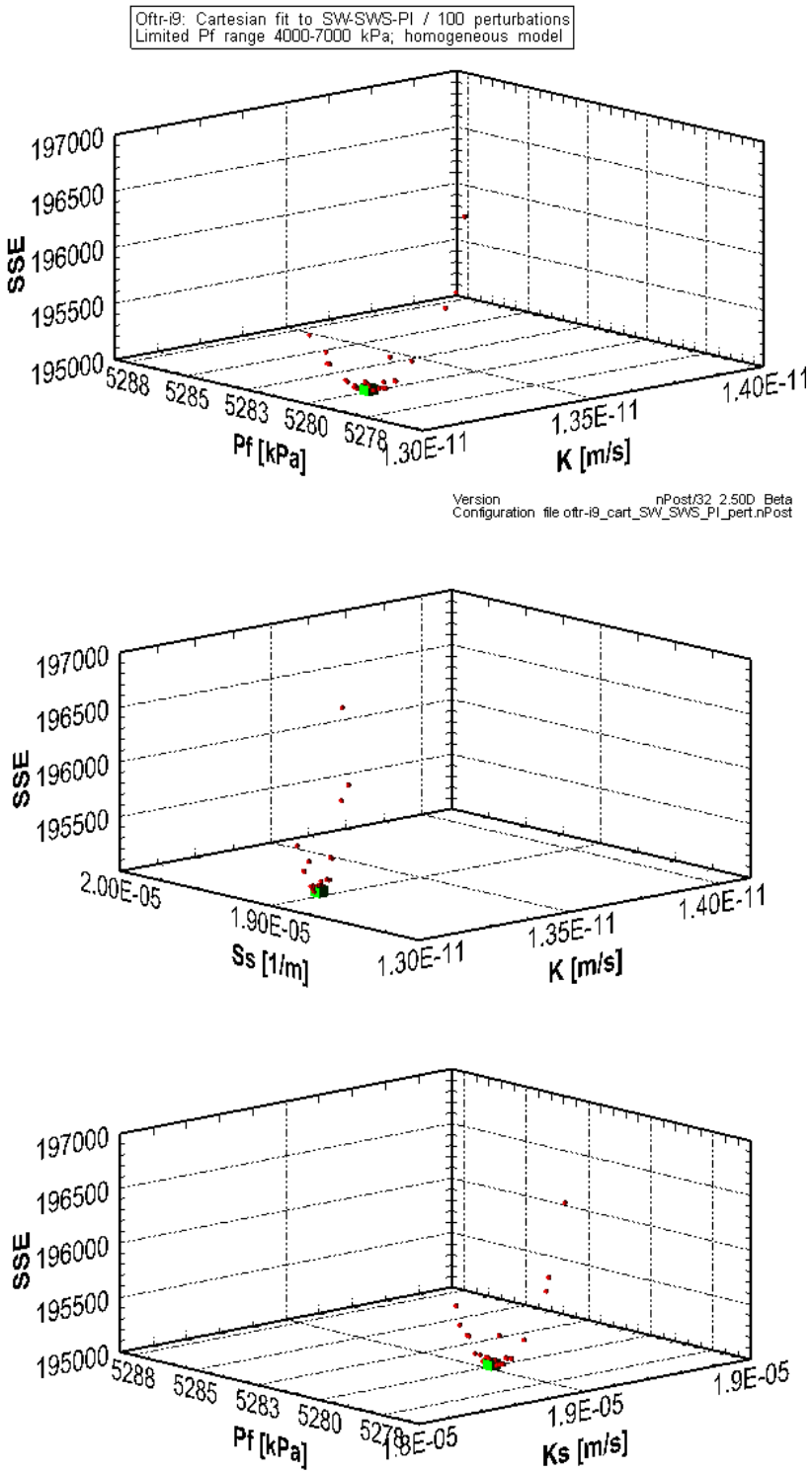

Fig. 16.6: Oftr-i9, homogeneous model / perturbation analysis: Cartesian fit to the SW-SWS-PI sequence.

Perturbation analysis with 100 realizations using wide P_f-range. The best estimate solutions associated with lowest SSE value are shown in green cube symbol

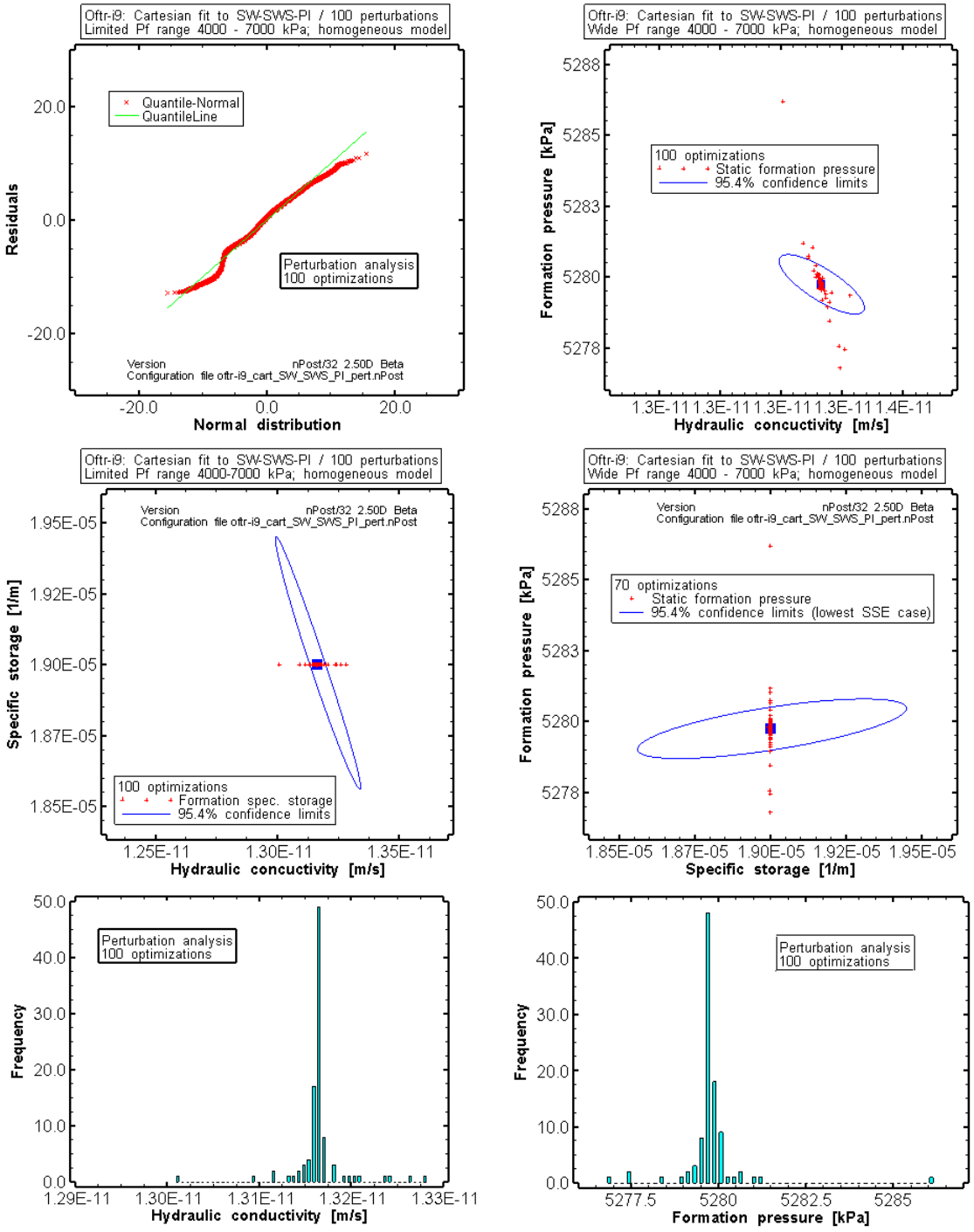

Fig. 16.7: Results from 100 perturbations using the Cartesian SW-SWS-PI sequence fit constraint in combination with large pre-set range for the P_f parameter.

Top left: residual distribution of best-estimate optimization (lowest SSE case) in comparison to normal error distribution. Top right to middle right: results (red crosses) and confidence regions for the K-Pf, K-S_S and SS-P_f joint parameters. The lowest SSE cases are shown as blue squares but may be hidden behind the red crosses. Bottom: frequency distributions for the K- (bottom left) and Pf -estimates (bottom right).

16.5.2. Wide P_f-range / wide S_S range

During this perturbations analysis, the static head was allowed to vary within 4000 and 7000 kPa and the S_S range was extended to 1.0E-7 to 1E-4 m^{-1}. 70 optimization runs were performed for which individual fits were computed using Simplex algorithm. The results of the perturbation analysis are shown graphically in Fig. 16.8 and Fig. 16.9. The results of the best-estimate solution associated with lowest SSE value are presented in Tab. 16.9 and Tab. 16.10.

The parameters estimates of 67 of 70 perturbation runs vary within very narrow ranges. This can be observed from the 2D scatter plots shown in Fig. 16.9. For the presented joint parameters K-P_f (top right), K-S_S (middle left) and S_S-P_f (middle right), a number of 67 solutions are within the confidence regions of the best-estimate solution (lowest SSE case). The insular solutions of the parameters space (not shown) are associated with significantly higher SSE values. The residuals of the best-estimate solution are essentially normally distributed (top left plot of Fig. 16.7). The frequency plots at the bottom of Fig. 16.9 show that 65 of 70 values belong to one single class (of total 50 classes) and confirm the well confined ranges for the K- (bottom left) and P_f-parameters (bottom right).

Tab. 16.9: Oftr-i9, homogeneous model, Cartesian fit to SW-SWS-PI: Best estimate parameters of 70 perturbations and 95% confidence intervals (wide P_f / S_s ranges)

Parameter	Units	Fit Value SSE = 9.11E+04	95% Confidence Intervals	
			Lower Value	Upper Value
C_tz	[1/Pa]	5.08E-09	5.07E-09	5.09E-09
K_fm	[m/s]	7.98E-12	7.87E-12	8.10E-12
P_fm	[kPa]	5313	5312	5314
ss_fm	[1/m]	4.44E-05	4.35E-05	4.54E-05

Tab. 16.10: Covariance-Correlation matrix for homogeneous model fit / perturbation analysis / wide P_f / S_s ranges (shaded cells denote correlation matrix elements).

Covariance/Correlation Matrix: Est. Cart_Dat_P				
	C_tz	K_fm	P_fm	ss_fm
C_tz	1.51E-07	8.66E-08	-1.22E-08	-1.37E-07
K_fm	3.58E-01	3.89E-07	-9.91E-08	-9.38E-07
P_fm	-1.74E-01	-8.76E-01	3.29E-08	2.34E-07
ss_fm	-2.32E-01	-9.86E-01	8.46E-01	2.33E-06

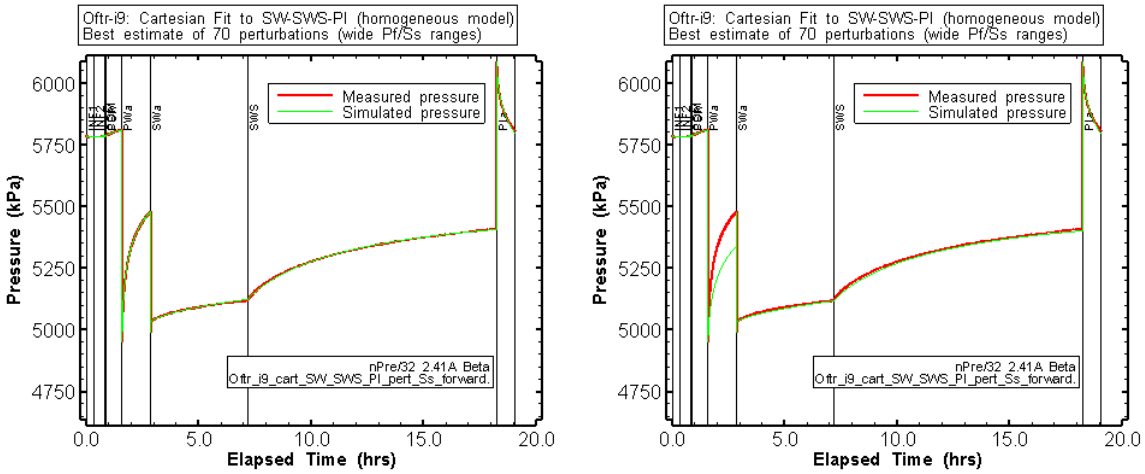

Fig. 16.8: Measured and simulated Cartesian pressures using best-estimate parameters from 70 perturbations (wide P_f/S_S range); homogeneous model.

Left: best fit of perturbation analysis using PSR-PW sequence as incorporated pressure history. Right: forward simulation using best fit parameters but with PW included in simulation.

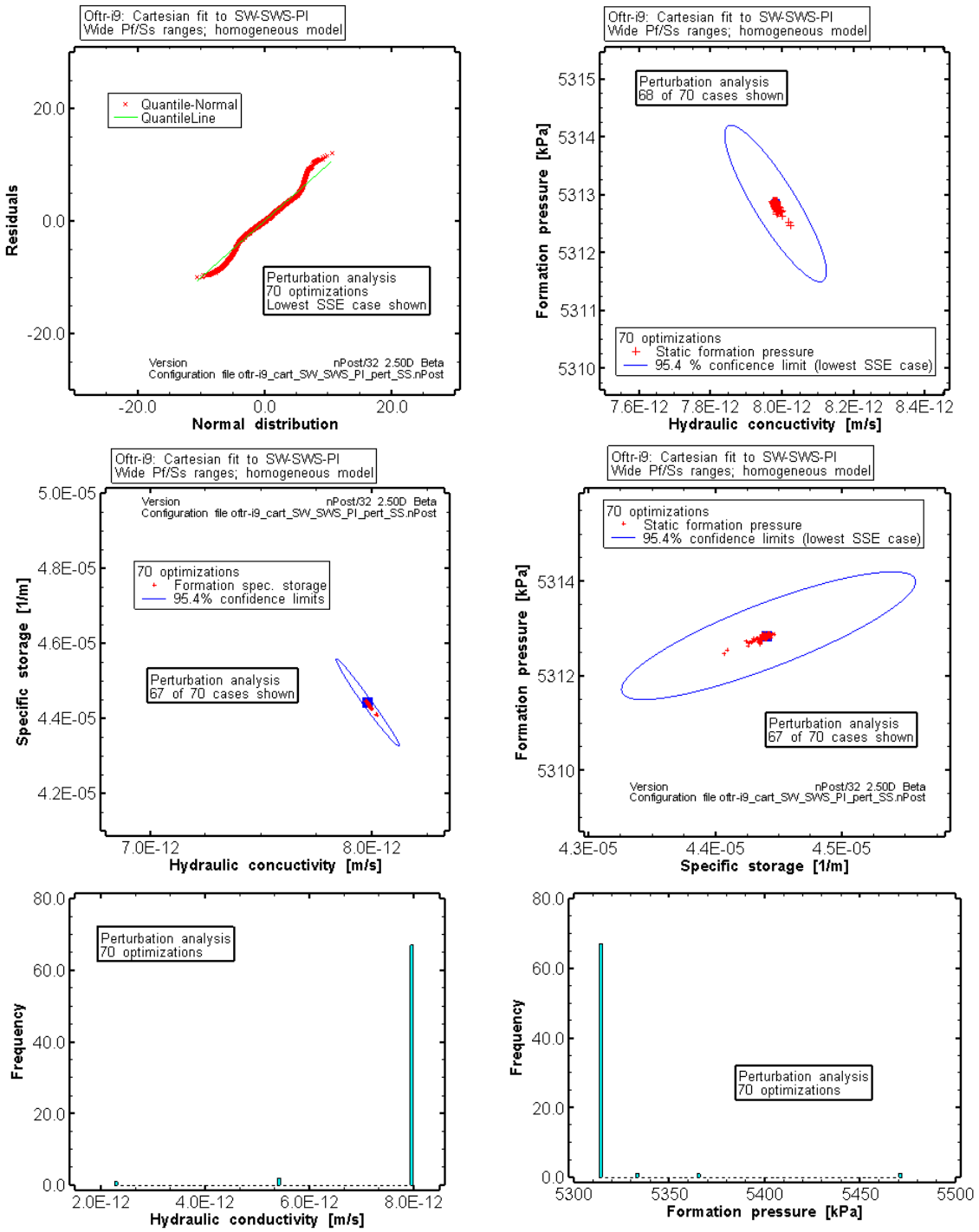

Fig. 16.9: Results from 70 perturbations using the Cartesian SW-SWS-PI sequence fit constraint in combination with large pre-set ranges for the P_f and S_S parameters.

Top left: residual distribution of best-estimate optimization (lowest SSE case) in comparison to normal error distribution. Top right to middle right: results (red crosses) and confidence regions for the K-Pf, K-S_S and SS-P_f joint parameters. The lowest SSE cases are shown as blue squares but may be hidden behind the red crosses. Bottom: frequency distributions for the K- (bottom left) and Pf -estimates (bottom right).

16.6. Summary for Homogeneous Model

The results of the simulated cases for the homogeneous model are summarized in Tab. 16.11. The best fit quality indicated by low SSE value was obtained from the last case with unrealistic high S_S-value. The shaded cells show the case with plausible best-estimate parameters. The SSE value for this case is by a factor 2.8 higher compared to the lowest SSE case.

Tab. 16.11: Oftr-i9: Summary for homogeneous model.

Case	K [m/s]	S_S [m^{-1}]	P_f [kPa]	SSE	Pre-set parameter ranges	Fit quality	Remarks Plausibility
QLR-Entire	4.07E-11	(1E-06)	5176	2.63E+07	wide Pf [1)]	--	P_f below plausibility range
SW-SWS-PI	1.25E-11	1.90E-05	5300	2.58E+05	limited Pf [2)]	+	P_f at lower limit S_S at upper limit
SW-SWS-PI Perturbation	1.32E-11	1.90E-05	5280	1.95E+05	wide Pf [3)]	+	Good fit
SW-SWS-PI Perturbation	7.98E-12	4.44E-05	5313	9.11+04	wide Pf wide S_S [4)]	++	P_f in pl. range S_S about pl. range

[1)] 4500-6800 kPa [2)] 5300-6280 kPa [3)] 4000-7000 kPa [4)] 1E-07 - 1E-04 m^{-1}

16.7. Improvement of Composite Skin Model Based on QLR Result

Despite of the good visual fit of the composite model (Fig. 16.2, top left plot) and the low SSE value (Tab. 16.1), the residual distribution as shown in bottom left plot of Fig. 16.2 show some discrepancy to a normal error distribution (bottom left of Fig. 16.2). Therefore, additional simulations were undertaken to see if further improvement of the composite model can be achieved. The results are presented graphically in Fig. 16.10 and Fig. 16.11. A perturbation analyses was carried out using slightly adjusted fit constraints (Cartesian fit with 250 log-stepped points for each subsequence PW, SW, SWS, PI) and updated parameter ranges. The S_S -parameter was allowed to vary between 1.9E-7 and 1.9E-5 m^{-1}, and the Pf -parameter was limited to the plausible range from 5300 to 6280 kPa.

The best-estimate Cartesian fit and the associated residual distribution are shown in Fig. 16.10. The residuals show similar discrepancies to the normal distribution as the single optimization case presented in Section 16.2, bottom left plot of Fig. 16.2. Similarly low SSE were found for the majority of the 50 optimization runs (see SSE histogram, bottom right plot in Fig. 16.11) with formation- and skin-parameter estimates widely scattered in the parameter space (Fig. 16.11).

The best estimate parameters and corresponding confidence intervals are listed in Tab. 16.12 and Tab. 16.13, respectively. The values are similar as the single optimization presented in Section 16.2 but with a P_f-estimate at the upper bound of the pre-set range.

Tab. 16.12: Oftr-i9, composite skin model: Perturbation analysis / lowest SSE case.

Parameters estimates and 95% confidence intervals for the Cartesian all sequence fit

Parameter	Units	Fit Value SSE= 5.65E+06	95% Confidence Interval	
			Lower Value	Upper Value
K_fm	[m/sec]	9.95E-13	8.21E-13	1.21E-12
K_s	[m/sec]	1.56E-10	1.27E-10	1.92E-10
P_fm	[kPa]	6280	6233	6327
Ss_fm	[1/m]	1.62E-05	7.74E-06	3.39E-05
Ss_s	[1/m]	1.56E-06	8.84E-07	2.74E-06
t_s	[m]	0.30000	0.19614	0.40385

Tab. 16.13: Covariance-Correlation matrix for composite skin model (shaded cells denote correlation matrix elements).

	K_fm	K_s	P_fm	ss_fm	Ss_s	t_s
K_fm	6.94E-05	6.82E-05	-9.43E-05	-5.45E-04	-2.92E-04	9.63E-04
K_s	6.09E-01	1.81E-04	-1.68E-04	-1.02E-03	-8.24E-04	2.40E-03
P_fm	-4.72E-01	-5.21E-01	5.74E-04	9.47E-04	7.41E-04	-2.12E-03
Ss_fm	-8.17E-01	-9.50E-01	4.94E-01	6.42E-03	4.60E-03	-1.39E-02
Ss_s	-5.71E-01	-9.98E-01	5.04E-01	9.36E-01	3.77E-03	-1.09E-02
t_s	6.46E-01	9.96E-01	-4.95E-01	-9.67E-01	-9.95E-01	3.21E-02

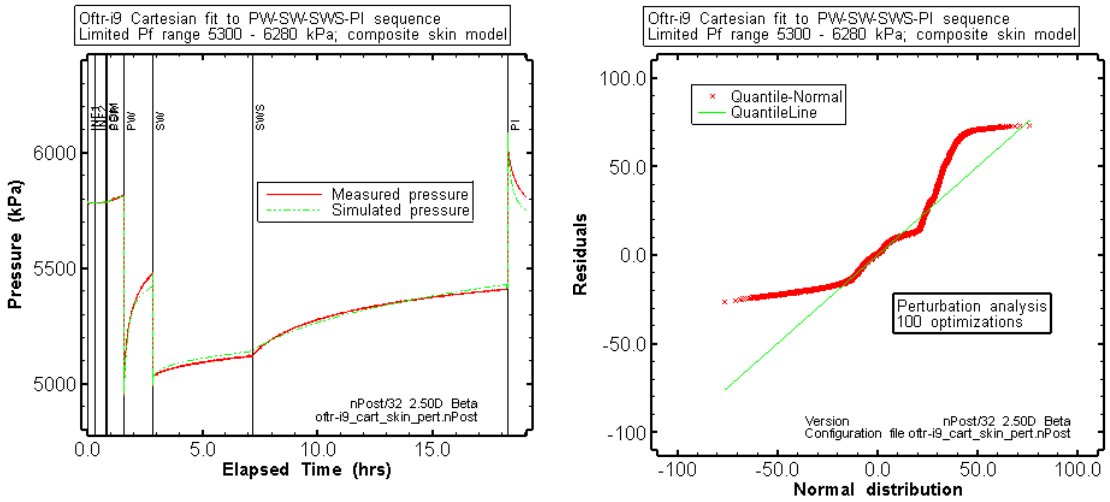

Fig. 16.10: Oftr-i9, composite skin model / perturbation analysis: Cartesian fit of best-estimate realization (lowest SSE; left) and residual distribution (right).

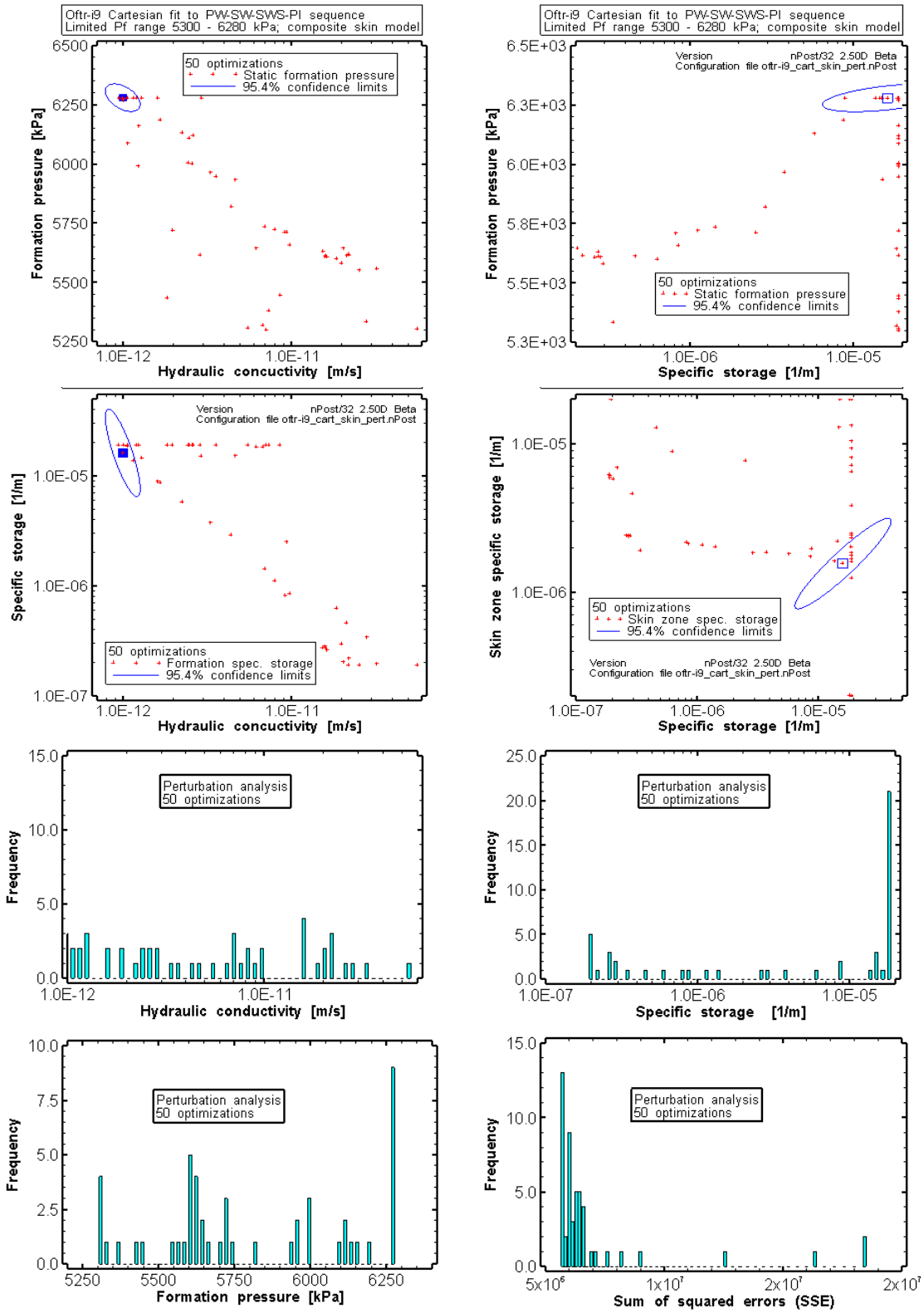

Fig. 16.11: Oftr-i9, composite skin model / 50 perturbations: joint parameter scatter plots and frequencies for individual parameters.

16.8. Possible Influences of Temperature and Packer Pressure Change

The packer pressure dropped by 2.5 bar between start of PW and end of PI (30.1 - 27.6 bar, Fig. 16.12). The change in packer pressure over 17.6 hours is considered low and should not have affected the interval pressure. Relatively cool fresh water was injected into the borehole during packer deflation of the previous test interval Oftr-i8c to accelerate loosening of packers. At beginning of test Oftr-i9, the interval temperature showed 37.1 °C and increased to 39.3 °C by end of PW. Subsequent PW, the temperature increased at lower rates and stabilized at 41 °C by end of PI (Fig. 16.12).

The differential temperature changes are highest for the PSR and PW sequences. Given that the PSR sequence was poorly fitted both when using the homogeneous and composite skin model, the influence of a possible temperature effect was investigated. The measured temperature curve was incorporated as a varying test zone condition in nSights. The model parameters from the Cartesian fit to the SW-SWS-PI sequence were used but with inclusion of PW as fitted sequence (see Section 16.4 for the homogenous model and 16.7 for the skin model). A thermal expansion coefficient of 2.07E-04 $°C^{-1}$ was assumed. The results of inverse parameter optimization are shown graphically for both the homogeneous model (Fig. 16.13, left) and for the composite skin model (right). For both models, no improvement of the fit quality can be observed. It appears that the measured temperature change did not significantly impact the interval pressure.

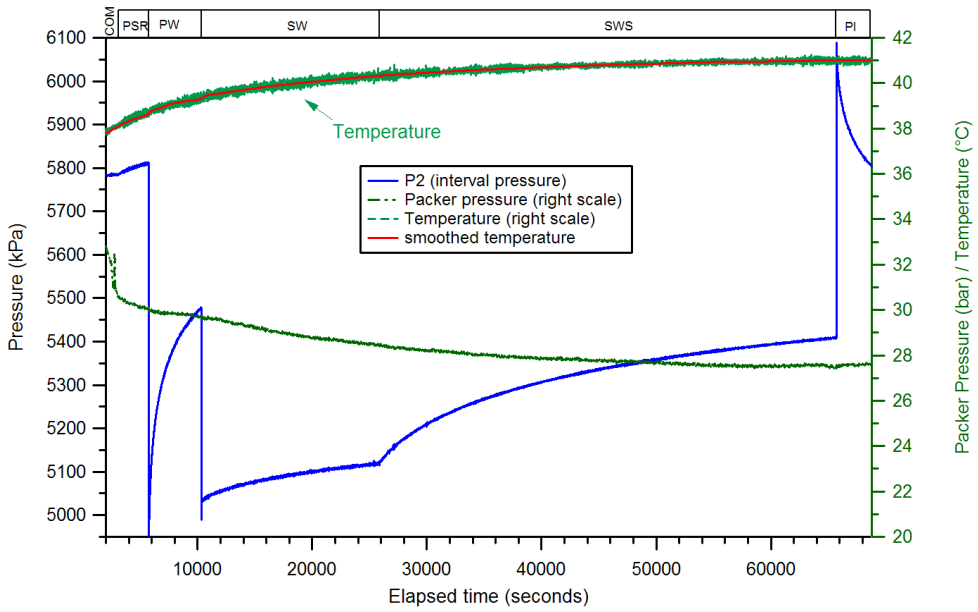

Fig. 16.12: Oftr-i9: Change of interval temperature and packer pressure during testing

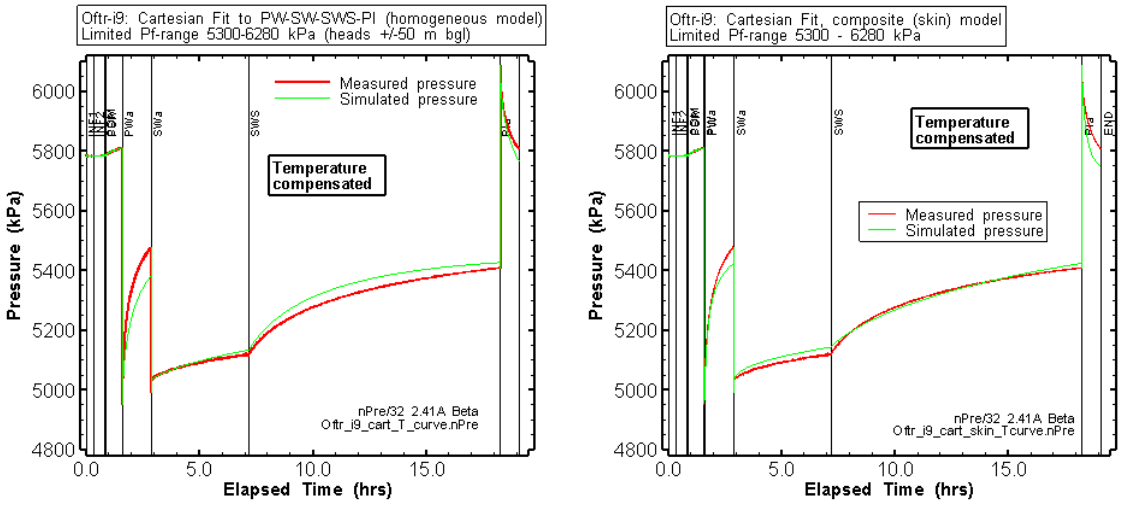

Fig. 16.13: Temperature compensation applied to the homogenous (left) and composite skin model (right).

16.9. Summary

During the "standard analysis" for test Oftr-i9, both the homogeneous model and the composite skin model were refined using adjusted model parameters such as pre-set ranges for the P_f and S_S parameters (according the plausibility ranges described in Section 7.3). The entire sequence optimization (all events but PSR) showed a poor fit when using the homogeneous model. Additional simulations were performed on the part sequence SW-SWS-PI assuming that the PW sequence was affected by ongoing compliance effects or other transient effect not characteristic to the formation. The nSights simulations using a Cartesian fit to the SW-SWS-PI sequence, homogenous model, provided a good quality fit. Extending this model using larger pre-set P_f- and S_S-ranges to values outside of the plausibility ranges resulted in slightly improved fits associated with similar K- and P_f -estimates.

The composite skin model was tested to see if the parameters of the QLR belong to a global or local minimum in the parameter space and if other plausible parameter sets could be obtained. The skin model produced fits of fairly good quality. However, the sensitivity to the formation pressure is relatively low for this model. The initial parameter estimates were disturbed during a perturbation analysis. The P_f- and S_S-parameters were allowed to vary within the pre-set plausibility ranges. The obtained P_f -estimates scattered between the lower and upper limit of the P_f -range used, whereas the K-values scattered within a large range between 9.4E-13 and 5.7E-11 m/s. The P_f- and S_S- parameter also showed +/- similar frequencies over the entire prescribed ranges with partially significantly increased frequencies at the range limits. Despite the reasonable fit for the composite skin model, the presence of (negative) skin is considered uncertain because of the lack a clearly located global minimum in the parameter space and because of the imperfect residual distribution for the best-estimate (lowest SSE) optimization. The composite skin model is therefore rejected. Possible temperature effects considered during additional detailed analyses for the homogeneous and composite skin model proved irrelevant.

Based on multiple cases of inverse parameter estimations performed for the homogeneous model (good quality simulation cases; tagged with the √ symbol in Tab. 16.14), the following parameter ranges were assessed:

- formation conductivity: 7.8E-12 - 1.3E-11 m/s
- specific storage: 1.9E-05 to (4.5E-5 m^{-1}) $m^{-1:}$
- formation pressure: (5279) - 5314 kPa, with corresponding heads 381 - 384 m asl.

The above parameter ranges include the incertitude as indicated by the 95th percentile confidence intervals for the individual minimum and maximum values. Nonetheless, the above indicated formation pressure range seems too small given the known incertitude inherent in test performance. Therefore, the above given uncertainty range for the formation pressure parameter (derived from P_f values of good quality simulation cases) is discarded. Based on expert judgement, also taking into account the results from the QLR, the following range is given:

- formation pressure: 5000 - 5600 kPa, with corresponding heads 352 - 414 m asl.

The 9.09 m long test interval Oftr-i9 covers a subsector of interval Oftr-i3. The best estimate K-value of 1.3E-11 m/s (Tab. 16.14) corresponds to a transmissivity value of 1.1E-10 m^2/s. This value is very similar to the best estimate transmissivity for the 50.04 m long interval Oftr-i3 (T = 1.0E-10 m^2/s). Assuming a homogenous distribution of K-values within interval Oftr-i3 and according the ratio of interval lengths, the transmissivity of Oftr-i9 would be expected to be about 5 times smaller than the T-value of Oftr-i3. Instead, the actual T/K-best estimates for intervals Oftr-i3 and Oftr-i9 suggest non-homogeneous distribution with potential conductive features mainly restricted to the depth sector of interval Oftr-i9 (Oftr-i9 contributes principally to the transmissivity measured in Oftr-i3). A non-homogeneous distribution of K-values is supported by the temperature /salinity log of BLM which indicates a possible minor inflow zone within interval Oftr-i9, at 588.7 m.

The head estimate for Oftr-i3 seems underestimated in comparison with adjacent interval Oftr-i2 where the head estimates are ≥ 50 meters higher. The discrepancy in head may be due to imprecision of the measurements because of limited testing time.

Level	Comments	
QLR	Cart ESF, wide P_f range [1]	h
QLR best e.	Cart ESF, wide P_f range [1]	c
Standard	Cart SW-SWS-PI, plausible P_f range [2]	h
Standard	Cart SW-SWS-PI, pert, extended P_f range [3]	h
Standard	Cart SW-SWS-PI, pert, extended P_f / S_S ranges [4]	h
Standard	Cart PW-SW-SWS-PI wide P_f range [5]	c
Standard	Cart PW-SW-SWS-PI [2], perturbation analysis	c

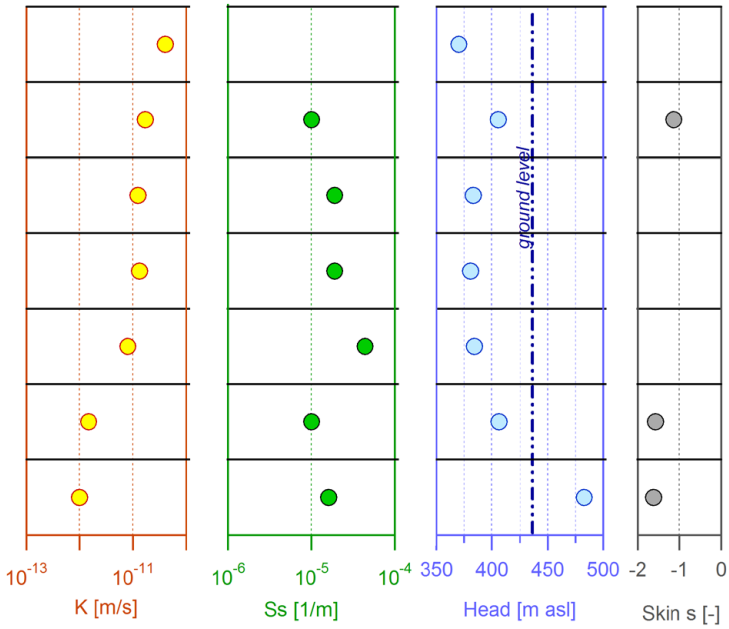

Fig. 16.14: Overview of results of inverse parameter estimations based on different models and fit configurations

QLR =	Quick Look Report
c =	composite skin model
CF	composite fit
Cart ESF =	Cartesian entire sequence fit
h =	homogeneous model
pert	perturbation analysis
[1] =	wide P_f range 4500 - 6800 kPa
[2] =	P_f range 5300 - 6280 kPa according to heads +/- 50 m asl Section 7.3.4
[3] =	extended P_f range 4000 - 7000 kPa
[4] =	extended P_f range 4000 - 7000 kPa, extended S_S range 1E-07 - 1E-04 m^{-1}
[5] =	case similiar to that of QLR best estimate but with improved fit constraints

Tab. 16.14: Oftr-i9: Overview of results of inverse parameter estimations

Case		K [m/s]	S_S [m^{-1}]	s [-]	h_s [m asl]	Fit quality	Remarks Plausibility	
Cart ESF, wide P_f range [1]	h	4.05E-11	(1.0E-06)		370.3	- -	P_f below plausibility range	
Cart ESF, wide P_f range [1] QLR best estimate	c	1.70E-11	1.00E-05	-1.14	405.7	+	thick skin zone (0.26 m), P_f within pl. range.	
Standard analysis:								
Cart SW-SWS-PI, plausible P_f range [2]	h	1.25E-11	1.90E-05		383.0	+	P_f at lower limit, S_S at upper limit	√
Cart SW-SWS-PI, pert, extended P_f range [3]	h	1.32E-11	1.90E-05		380.9	+	low P_f, S_S at upper limit	√
Cart SW-SWS-PI, pert, extended P_f / S_S ranges [4]	h	8.00E-12	4.40E-05		384.3	++	P_f in plausibility range S_S above pl. range	√
Cart PW-SW-SWS-PI wide P_f range [5]	c	1.48E-12	1.00E-05	-1.57	406.5	++	thick skin zone (0.29 m)	
Cart PW-SW-SWS-PI [2], pert, adjusted fit constraints	c	9.95E-13	1.62E-05	-1.62	482.9	(+)	P_f at upper limit; thick thin zone, lack of clearly located SSE-minimum	

√ = good simulation results used to to assess parameter ranges and to calculate mean K-value as best estimate
QLR = Quick Look Report
c = composite skin model
CF composite fit
Cart ESF = Cartesian entire sequence fit
h = homogeneous model
pert perturbation analysis
[1] = wide P_f range 4500 - 6800 kPa
[2] = P_f range 5300 - 6280 kPa according to heads +/- 50 m asl Section 7.3.4
[3] = extended P_f range 4000 - 7000 kPa
[4] = extended P_f range 4000 - 7000 kPa, extended S_S range 1E-07 - 1E-04 m^{-1}
[5] = case similiar to that of QLR best estimate but with improved fit constraints

17. Test Interval Oftr-i10: 408.5 - 417.6 m

Interpretation Level: Quick Look Report analysis

Test interval Oftr-i10 has identical packer positions as the previously test interval Oftr-i6. The test objectives of the second test in this borehole section, Test Oftr-i10, were to retry extraction of a representative formation sample and to obtain improved estimates of interval transmissivity and fresh-water hydraulic head. The analysis for the QLR (Appendix J) provided the following parameters estimates:

$K = 2.5E\text{-}06$ m/s (7.4E-07 - 4.9E-06 m/s)
$S_S = 1.0E\text{-}07$ m^{-1} (1.0E-07 - 1E-05 m^{-1})
$P_f = 4016$ kPa (3576 - 4283 kPa)

The values in brackets indicate the lowest/highest estimates from several inverse parameter optimizations for different test periods and fit constraints using nSights. The large ranges for the individual fitting parameters reflect the uncertainty with regard to measured inconsistent formation responses. Same as during test Oftr-i6, the drawdown tests Fig. 17.1 initiated degassing of dissolved gases in the water of the test zone and possibly in the formation. The latter could possibly have resulted in two-phase flow conditions. The presence of gas was indicated by the high test zone compressibilities measured with c_{tz} -values > 1E-07 Pa^{-1}. The best estimate of the QLR is based on the numerical analysis of the SW2 sequence which suggests a P_f value of 4016 kPa corresponding to a head of 426.8 kPa. Considering possible de-gassing effects during SW2, the measured pressure at end of the PSR sequence of 4055 kPa is deemed more representative to the formation. The P_f value of 4055 corresponds to a formation head of 430.7 m asl, i.e. 2.3 m below ground level. No further analysis was performed beyond the QLR test interpretation (Annex J).

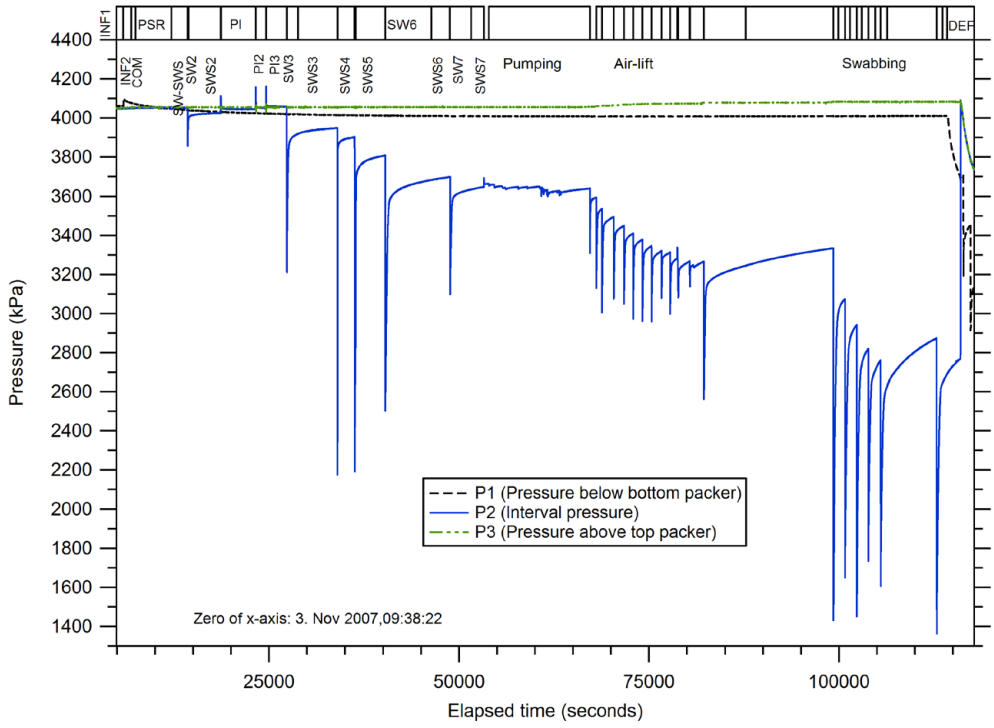

Fig. 17.1: Test Oftr-i10, 408.5 -417.6 m: overview plot

18. Quality Assurance

Solexperts is certificated by the International Organization for Standardization (ISO-9000:2000) and operates according to the Solexperts' Quality Assurance System. The quality securing measures are defined in the Solexperts Quality Management Handbook. It contains the overall concept and it regulates the responsibilities and the internal and external processes. The operative instrument for our production orders and services is the Quality Management Plan (QM-plan). It comprise all project relevant information, regulates the responsibilities, manage the dates and refers to quality-relevant documents like test logs, certificates and specification sheets for the equipment etc. The project manager establishes a QM-plan and keeps it updated during the project.

In addition, the requirements from the Nagra quality policy have been obeyed. It includes the quality guidelines no. 10 "Hydrotesting Mobilization", no. 11 "Durchführung von Hydro- und Gastests" and no. 90 "Sicherheit auf Bohrstellen" for the field work and no. 15 "Interpretation Hydrotests (Einzeltests)" including cited guidelines therein for the data interpretation.

18.1. Project Related Quality Assurance Measures

Prior to mobilization, the equipment was tested on functionality and measuring accuracy with respect to the project requirements. System specifications, test logs, data sheets and calibration protocols were provided to NAGRA in the mobilization report, which is part of the Nagra project documentation.

The pressure sensors from the Triple Sub Surface Probe were recalibrated in September 2006 at the Federal office of Metrology METAS in Wabern, Bern. Prior to running the system into the borehole and after finishing the tests the sensors were checked on surface against atmospheric pressure (pre- and post-test bench test). There was no evidence of a significant change over the whole test time. The transducers were also checked during installation and on the particular test depths prior to packer inflation. A density range of 0.997 to 0.999 g/cm3 was calculated from the pressure readings assuming verticality of the borehole. Volumetric measurements with measuring cylinder and a stopwatch were made in the field to gauge the different flow-meters used. The pre- and post-test bench tests for the sensors and the verification of the flow-meters are included in the QLRs (Appendix A to J).

For traceability of the field work, the activities were documented for each test interval in a logbook. Tally lists and installation protocols were created and provided to the project manager for approval. On line analysis of the test sequences were used to optimize test process.

The measurements were written to a data file (or a number of data files) on the PC hard drive in real-time to minimize a potential loss of information in case of a power outage. In addition, the data were transferred to another network PC every 10 seconds for "online" analysis and data back-up. Moreover the data were stored every 12 hours to an external hard drive disk. An uninterruptible power supply was utilized to protect the system from short power interruptions.

For each test zone, a Quick Look Reports (QLR) was written and reviewed by AF-Colenco and Nagra. AF-Colenco provided for each QLR a written review report with comments on test data and analysis to the project management (see memoranda in Appendix L). A reply of Solexperts and Intera to these comments is given in Appendix L.

18.2. Quality Control Documentation

The field operations, data interpretation and reporting conform to the requirements of the master testing plan of Nagra. The evidence of conformity is provided in the master testing data forms (MTDF) which were developed by Nagra during previous projects together with various contractors. The MTDF are compulsory for project documentation and are filled and updated on completion of important project events during field work, during preliminary reporting (QLRs) and during revision of the final report.

The master testing data forms (MTDF) are included in Appendix M.

19. Summary and Conclusions

Ten hydraulic tests using double-packer testing equipment were carried out in the NOK-EWS borehole at Oftringen in October/November 2007. The deepest test interval from 650 - 700 m bgl covers a limestone section (Hauptrogenstein) in the Dogger formation. All other test intervals are situated in limestone (Geissberg Member), marls or limestone-marl interbedded strata (Effingen Member) of the Malm formation. The hydraulic tests Oftr-i1 to Oftr-i5 were performed using a uniform packer straddle length of 50.04 m. The packer straddle length for tests Oftr-i6 to Oftr-i10 was 9.09 m.

Two tests (Oftr-i6d and Oftr-i10) were conducted in limestone of the Geissberg member at identical depth position. The aim of the second test (Oftr-i10) was to retrieve a representative formation water sample which could not be completed during test Oftr-i6d. Three additional tests were conducted to investigate subsections of previously tested larger test zones. Tests Oftr-i7 and Oftr-i8 cover subsections of test interval Oftr-i2 and test Oftr-i9 covers a subsection of test interval Oftr-i3.

Pressure and flow data recorded during the tests and used in the analyses (flow data only for Oftr-i1) are shown graphically in Chapters 8 to 17 and in the Appendices A to J. Eight of ten tests were subject to standard or detailed analysis according to Nagra's terms of reference. For the test intervals Oftr-i6d and Oftr-i10, no additional analysis was done in addition to the QLR-interpretation.

The results of all tested intervals are summarized in Tab. 19.1 and Tab. 19.2. The hydraulic parameters transmissivity (T), hydraulic conductivity (K) and hydraulic head (h) are plotted versus borehole depth in Fig. 19.1 to Fig. 19.3. Intrinsic permeability values (k, in m^2; Tab. 19.1) were calculated based on water density and viscosity values given in Chapter 7. For each test interval, the uncertainty ranges are indicated. The ranges represent the span of minimum/maximum "good estimate" parameters for an individual interval and for the indicated hydraulic model. In two cases, the uncertainty ranges are based on expert judgement.

In the formation of the Effingen Member below 450 m depth, the best-estimate hydraulic conductivity values vary between 3.0E-14 m/s and 1.3E-11 m/s. Note that the given K-values represent average hydraulic conductivities. In heterogeneous medium, the average K-value may be lower than the hydraulic conductivity of an individual higher transmissive feature (e.g. fracture or micro-fracture) or higher than the actual K-value of the matrix or the undisturbed low porosity rock section.

The uppermost tests Oftr-i6d and Oftr-i10 (408.5 - 417.6 m bgl) cover a fractured zone in the limestone of the Geissberg Member. The hydraulic tests in this zone were disturbed by degassing effects. As a consequence, a relatively wide range of results were obtained especially with respect to the hydraulic conductivity parameter. The best-estimate K-value of test Oftr-i10 (K = 2.5E-6 m/s) is significantly higher than the best-estimate K-value from Oftr-i6d (K=4.0E-08 m/s). Assuming that the interference of gas-phase was less for the analyzed test sequence of Oftr-i10, the value of 2.5E-6 m/s is considered more representative of the formation.

In contrast to the Hauptrogenstein in Western Switzerland where this geological unit is used as a groundwater resource, the Hauptrogenstein at Oftringen proved to be very low permeable. A K-value of 7.0E-12 m/s was obtained from Oftr-i1, the only test interval in the Dogger formation (mainly Hauptrogenstein). The hydraulic conductivity of interval Oftr-i1 is slightly higher compared to the K-values measured in the overlaying very low permeable Effingen strata.

The vertical distribution of the estimated hydraulic heads is shown graphically in Fig. 19.3. Reliable head estimates were obtained from the relatively permeable test intervals Oftr-i1, Oftr-i6d and Oftr-i10. It was expected that the relatively tight test intervals located between the more permeable intervals Oftr-i1 and Oftr-i6d/-i10 would show basically similar hydraulic heads ranging from roughly -23 m bgl (artesian head estimate of Oftr-i1) and 6 m bgl (head estimate of Oftr-i10).

However, a number of head estimates (Oftr-i4, -i5, -i7, -i8c, -i9) indicate distinct lower heads, 30 meters or more below surface level. A decrease in packer pressure by 3 to 4.5 bar was observed during testing of intervals Oftr-i5, i7 and i8c. The packer decrease could cause an increase in test zone volume which in turn could affect the measured interval pressure. In impermeable rock, even small gradual changes in test zone volume over a period of several hours may affect the measured interval pressure, leading to erroneous parameter estimates. The possible impact of changing test zone volume due to packer pressure change was investigated for the test intervals Oftr-i5 and Oftr-i7. The detailed analyses showed that a minor compensation for gradual volume change (associated with packer pressure change) provides 100 to 160 m higher heads using very similar model parameters. The use of varying test zone volumes associated with the above mentioned head changes in head estimate had only minor influence on the formation conductivity values calculated during numerical analyses (inverse parameters optimization).

The modelling of varying test zone volume was not based on a quantitatively recorded mechanism and is therefore expected to provide only rough results. The corresponding head estimates are not shown in the plot head versus depth (Fig. 19.3). Nonetheless, the varying test zone simulation demonstrated that the low head-estimates for the above mentioned test intervals could reflect non-ideal test conditions and that the formation heads are possibly underestimated.

Tab. 19.2 and Fig. 19.3 show that the head uncertainty ranges of the intervals Oftr-i2 to i5 and Oftr-i7 to i9 overlap more or less with the uncertainty ranges of the higher transmissive intervals Oftr-i1 and i6/i10 which are located below and above, respectively.

Tab. 19.1: Oftringen borehole: summary of hydraulic testing: transmissivity, hydraulic conductivity and permeability

Test interval details and hydraulic model							Transmissivity, hydraulic conductivity and permeability								
Test Name	Interval depth				Interval length: [m]	Model	**Best estimates**			Lowest estimates			Highest estimates		
	from: [m bgl]	to: [m bgl]	from: [m asl]	to: [m asl]			T [m^2/s]	K [m/s]	k [m^2]	T_{min} [m^2/s]	K_{min} [m/s]	k_{min} [m^2]	T_{max} [m^2/s]	K_{max} [m/s]	k_{max} [m^2]
Oftr-i1	650.00	700.04	-217.00	-267.04	50.04	Composite skin	3.5E-10	7.0E-12	4.8E-19	1.7E-10	3.3E-12	2.3E-19	7.0E-10	1.4E-11	9.6E-19
Oftr-i2	590.00	640.04	-157.00	-207.04	50.04	Homogeneous	2.4E-11	4.7E-13	3.4E-20	1.8E-11	3.6E-13	2.6E-20	2.8E-10	5.6E-12	4.1E-19
Oftr-i3	550.00	600.04	-117.00	-167.04	50.04	Homogeneous	1.0E-10	2.0E-12	1.6E-19	4.0E-11	8.0E-13	6.2E-20	2.0E-10	4.0E-12	3.1E-19
Oft-i4	500.00	550.04	-67.00	-117.04	50.04	Homogeneous	2.1E-12	4.1E-14	3.4E-21	9.0E-13	1.8E-14	1.5E-21	1.1E-11	2.2E-13	1.8E-20
Oftr-i5	449.85	499.89	-16.85	-66.89	50.04	Homogeneous	1.5E-12	3.0E-14	2.6E-21	9.5E-13	1.9E-14	1.7E-21	1.9E-12	3.8E-14	3.3E-21
Oftr-i6d	408.50	417.59	24.50	15.41	9.09	Homogeneous	3.6E-07	4.0E-08	3.6E-15	2.2E-07	2.4E-08	2.2E-15	1.8E-05	2.0E-06	1.8E-13
Oftr-i7	632.50	641.59	-199.50	-208.59	9.09	Homogeneous	5.6E-13	6.2E-14	4.3E-21	3.0E-13	3.3E-14	2.3E-21	7.3E-13	8.0E-14	5.5E-21
Oftr-i8c	621.50	630.59	-188.50	-197.59	9.09	Homogeneous	5.7E-13	6.3E-14	4.4E-21	3.4E-13	3.7E-14	2.6E-21	1.3E-12	1.4E-13	9.8E-21
Oftr-i9	583.00	592.09	-150.00	-159.09	9.09	Homogeneous	1.1E-10	1.3E-11	9.3E-19	7.1E-11	7.8E-12	5.8E-19	1.2E-10	1.3E-11	9.6E-19
Oftr-i10	408.50	417.59	24.50	15.41	9.09	Homogeneous	2.3E-05	2.5E-06	2.3E-13	6.7E-06	7.4E-07	6.7E-14	4.5E-05	4.9E-06	4.4E-13

The lowest and highest estimates for a given parameter are based on "good simulation results" as presented in the chapters for each test interval.

Tab. 19.2: Oftringen borehole: summary of hydraulic testing: hydraulic head estimates

Test interval details and hydraulic model							Hydraulic heads m bgl			Hydraulic heads m asl			Formation pressures		
Test Name	Interval depth				Interval length:	Model	**Best** h	Lowest h_{min}	Highest h_{max}	**Best** h	Lowest h_{min}	Highest h_{max}	**Best** P_f	Lowest P_{min}	Highest P_{max}
	from: [m bgl]	to: [m bgl]	from: [m asl]	to: [m asl]	[m]		[m bgl]	[m bgl]	[m bgl]	[m asl]	[m asl]	[m asl]	[kPa]	[kPa]	[kPa]
Oftr-i1	650.00	700.04	-217.00	-267.04	50.04	Composite skin	-23	-9	-24	456	442	457	6671	6530	6678
Oftr-i2	590.00	640.04	-157.00	-207.04	50.04	Homogeneous	-1	5	-24	434	428	457	5863	5808	6091
Oftr-i3	550.00	600.04	-117.00	-167.04	50.04	Homogeneous	23	37 [1)]	-14 [1)]	411	396 [1)]	447 [1)]	5242	5100 [1)]	5600 [1)]
Oft-i4	500.00	550.04	-67.00	-117.04	50.04	Homogeneous	43	130	40	390	303	393	4551	3700	4580
Oftr-i5	449.85	499.89	-16.85	-66.89	50.04	Homogeneous	50	152	30	383	282	403	3993	2995	4188
Oftr-i6d	408.50	417.59	24.50	15.41	9.09	Homogeneous	1	16	-43	432	417	476	4065	3919	4500
Oftr-i7	632.50	641.59	-199.50	-208.59	9.09	Homogeneous	50	154	-12	383	279	445	5784	4768	6391
Oftr-i8c	621.50	630.59	-188.50	-197.59	9.09	Homogeneous	50	251	41	383	182	392	5676	3703	5760
Oftr-i9	583.00	592.09	-150.00	-159.09	9.09	Homogeneous	49	81 [1)]	19 [1)]	383	352 [1)]	414 [1)]	5313	5000 [1)]	5600 [1)]
Oftr-i10	408.50	417.59	24.50	15.41	9.09	Homogeneous	6	51	-21	427	382	454	4016	3576	4282

The lowest and highest estimates for a given parameter are based on "good simulation results" as presented in the chapters for each test interval.

[1)] Based on expert judgement. Besides the results of the Standard Analysis, the results of the QLR are taken into account.

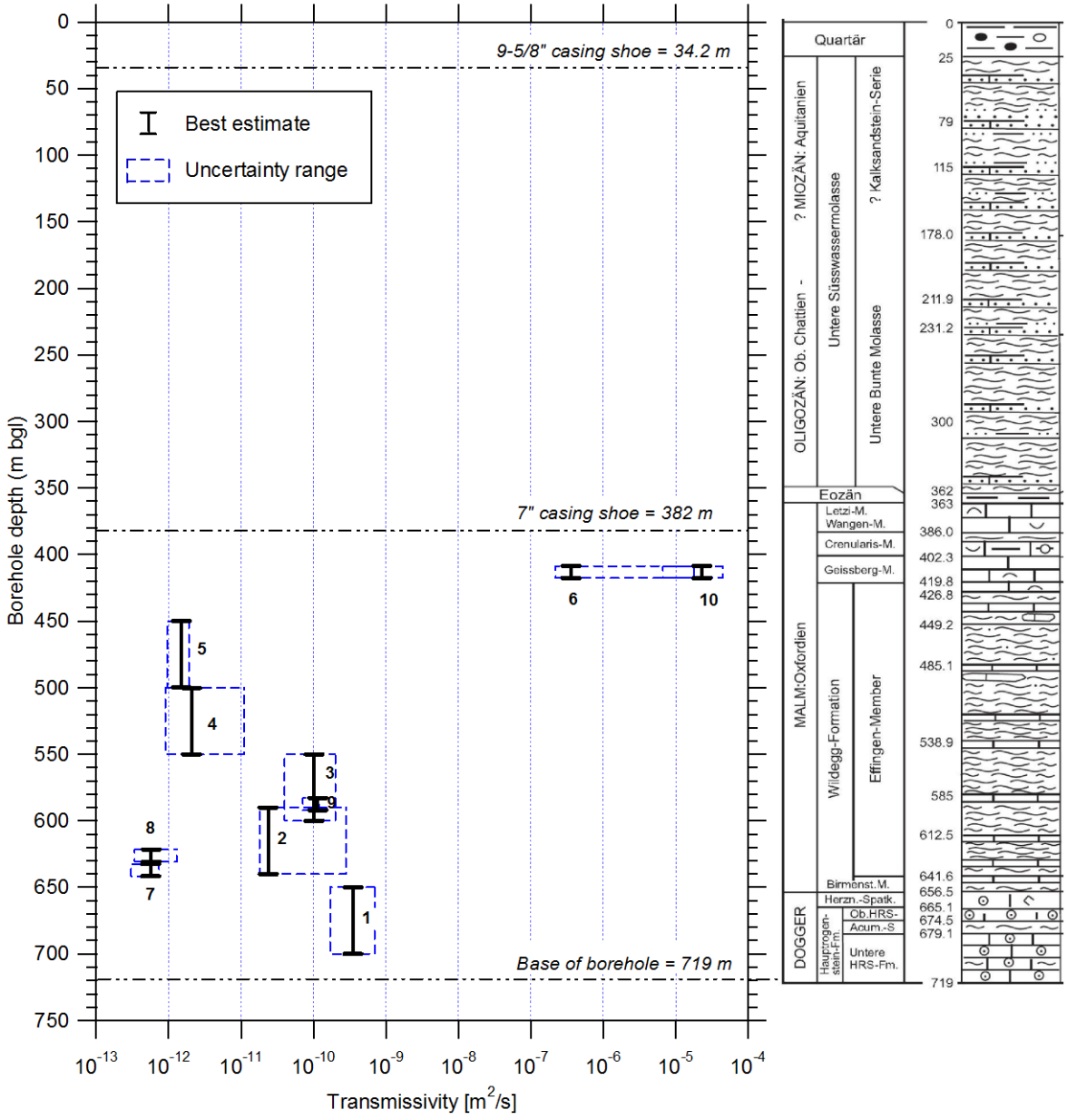

Fig. 19.1: Oftringen borehole summary: transmissivity profile

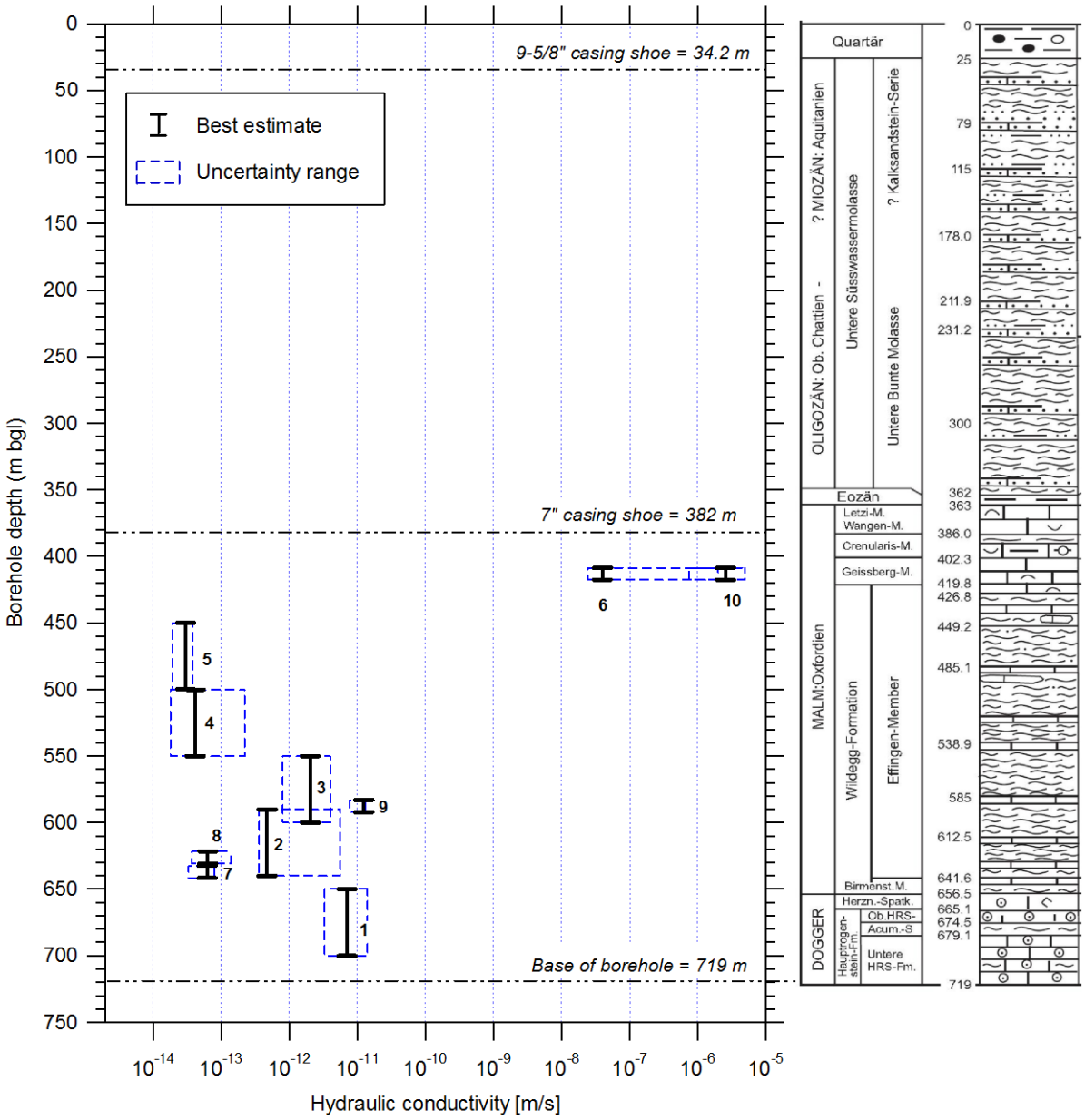

Fig. 19.2: Oftringen borehole summary: formation hydraulic conductivity profile

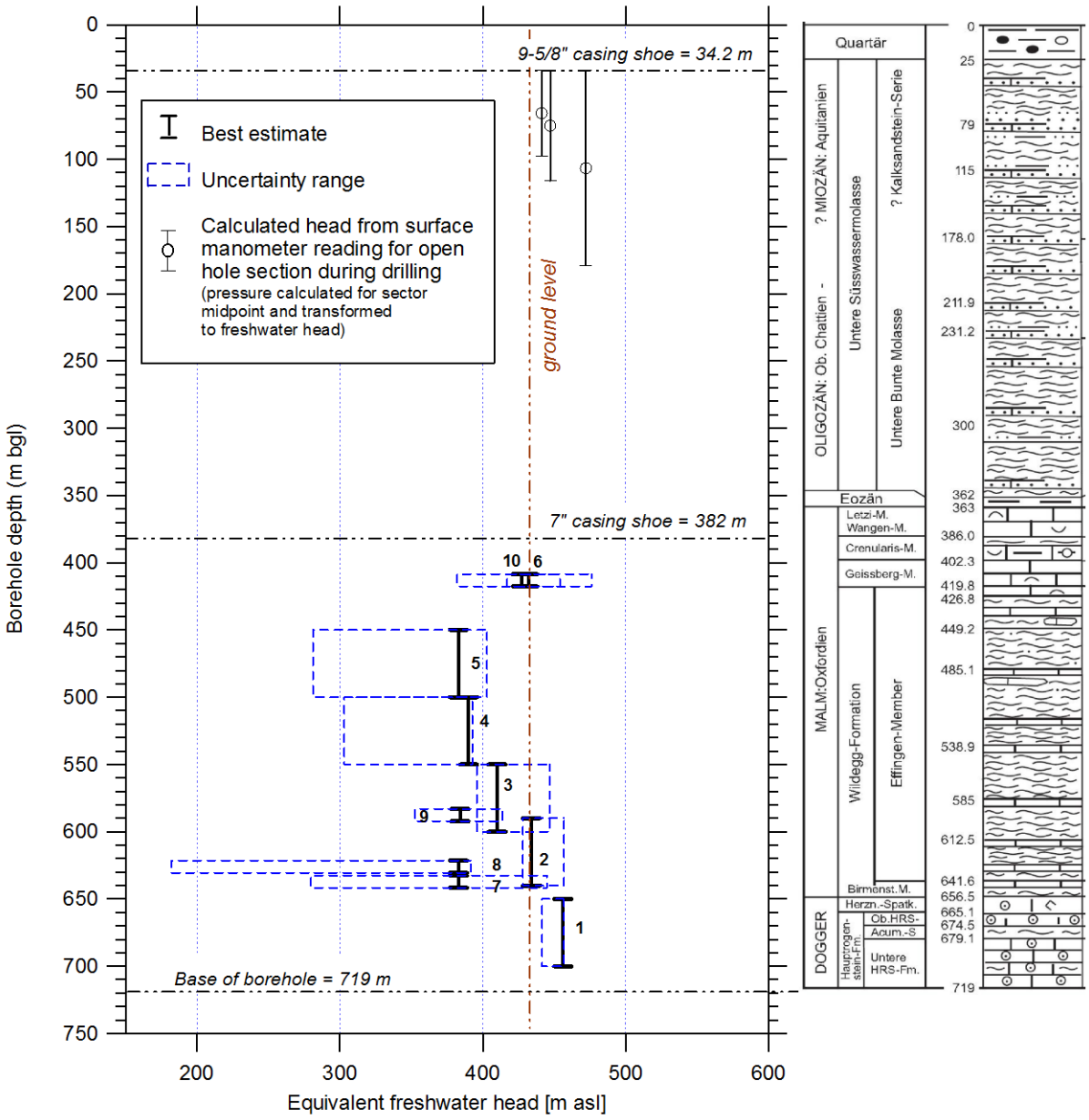

Fig. 19.3: Oftringen borehole summary: formation hydraulic head profile

20. References

American Society of Mechanical Engineers (ASME). 1990. Quality assurance requirements of computer software for nuclear facility applications. ASME NQA-2a-1990 addenda, Part 2.7, ASME, New York.

Adams, J. & Wyss, E. (1994): Hydraulic Packer Testing in the Wellenberg Boreholes SB1 and SB2. Methods and Field Results. Nagra Tech. Rep. NTB 93-38; Wettingen (Nagra)

Albert, W. & Bläsi, H.R. (2008): NOK EWS-Bohrung Oftringen: Geologische, mineralogische und bohrochgeophysikalische Untersuchungen (Rohdatenbericht). - Nagra Arbeitsbericht, NAB 08-02; Wettingen (Nagra)

Almen, K.E., Andersson, J.-E., Carlsson, L., Hansson, K. & Larsson, N-A. (1986): Hydraulic Testing in Cristalline Rock. A Comparative Study of Single-Hole Test Methods. SKB Technical Report 86-27.

Agarwal, R.G., Al-Hussainy, R. & Ramey, H.J., Jr. (1970): An Investigation of Wellbore Storage and Skin Effect in Unsteady Liquid Flow: I. Analytical Treatment. Soc. Pet. Eng. J., pp.279-290, Trans. AIME, 249.

Agarwal, R.G. (1980): A New Method to Account for Producing Time Effects When Drawdown Type Curves Are Used to Analyze Pressure Buildup and Other Test Data, Soc. of Petroleum Engineers, SPE Paper 9289, presented at SPE-AIME Meeting, Dallas, Texas, September 21-24

Barker, J.A. & Black, J.H. (1983): Slug Tests in Fissured Aquifers, Water Resour. Res. 19 (6), 1558 - 1564.

Black, J.H. (1985): The Interpretation of Slug Tests in Fissured Rocks, Q. Jour. Eng. Geology, Vol. 18, pp. 161-171.

Bourdet, D., Ayoub, J.A. & Pirard, Y.M. (1989): Use of Pressure Derivative in Well-Test Interpretation. - Soc. of Petroleum Engineers, SPE Formation Evaluation, pp. 293-302.

Bredehoeft J.D. , Papadopulos, S.S. (1980): A Method for Determining the Hydraulic Properties of Tight Formations. Water Resour. Res. Vol. 16 (1). 233-238.

Chakrabarty, C., & Enachescu C. (1997): Using deconvolution approach for slug test analysis: theory and application. – Groundwater Vol. 35 No. 5, September-October.

Cooper, H.H. JR., Bredehoeft, J.D. & Papadopulos, S.S.(1967): Response of a Finite-Diameter Well to an Instantaneous Charge of Water, Water Resour. Res., First Quarter 1967, 263-269.

Cooper, H.H. & Jacob, C.E. (1946): A Generalized Graphical Method for Evaluating Formation Constants and Summarizing Well-Field History, Transactions of the American Geophysical Union, Vol. 27, No. IV, pp 526-532.

Doe, T.W. & Geier, J.E. (1990): Interpretation of Fracture System Geometry Using Well Test Data, Technical Report 91-03, Swedish Nuclear Fuel and Waste Management Co. (STRIPA), Stockholm, Sweden.

Earlougher, R.C. JR. (1977): Advances in Well Test Analysis, Soc. of Petroleum Engineers, Monograph Volume 5 of the Henry L. Doherty Series, 264 p.

Ehlig-Economides, C.A. & Ramey, H.J.JR. (1981): Pressure Buildup for Wells Produced at a Constant Pressure, Society of Petroleum Engineers, SPE Journal, Feb. 1981, pp.105-114.

Enachescu, C., Lavanchy, J.M., Ostrowski, L., Senger, R. & Wosniewicz, J. (1997): Hydrogeolocical Investigations at Wellenberg: Hydraulic Packer Testing in Boreholes SB4a/v and SB4a/s - Methods and Field Results. - Nagra Technical Report, NTB 95-02; Nagra, Wettingen.

Enachescu, C., Frieg, B. Rohs, S. & Paris, B. (2007): Poster presented at the Meeting "Lille 2007" - 3rd International Meeting on "Clay in Natural and Engineered Barriers for Radioactive Waste Confinement", 17 to 20 September 2007, International Convention Centre in Lille (France).

Freeze, R.A., & Cherry, J.A. (1979): Groundwater, Prentice-Hall Inc., Englewood Cliffs, N.J.

Gringarten, A.C., Bourdet, D.P., Landel, P.A. & Kniazeff, V.J. (1979): A Comparison Between Different Skin and Wellbore Storage Type-Curves for Early Time Transient Analysis. SPE Paper 8205, presented at SPE-AIME 54th Annual Technical Conference, Las Vegas, Nevada, Sept. 23-35.

Horne, R. N. (1995): Modern Well Test Analysis - A Computer-Aided Approach. - 2. Edit., Petroway Inc., 251 p.

Horner, D.R. (1951): Pressure Build-Up in Wells, Third World Pet. Congress, E.J. Brill, Leiden II, pp. 503-521

Hvorslev, M. J. (1951): Time lag and soil permeability in ground-water observations. U.S. Army Corps of Engineers, Waterways Experiment Station, Bulletin No. 36McElwee, C.D. (2001): Application of a Nonlinear Slug Test Model. Ground Water Vol. 39, No. 5, pp. 737-744.

Intera Engineering Ltd., nSIGHTS Version 2.3 User Manual, ERMS# 530161, Sandia National Laboratories, 2005

Jacob, C.E. & Lohman, S.W. (1952): Nonsteady Flow to a Well of Constant Drawdown in an Extensive Aquifer, Transactions, American Geophysical Union, Vol. 33, No. 4, pp. 559-569

Karasaki, K., Long, C.S. & Whiterspoon, P.A. (1988): Analytical Models of Slug Tests. Water Res. Res. 24 (1), 115 - 126.

Nagra (2001): Sondierbohrung Benken. Textband. Nagra Tech. Bericht NTB 00-01.

Nagra (2002a): Projekt Opalinuston - Konzept für die Anlagen und den Betrieb eines geologischen Tiefenlagers. - Entsorgungsnachweis für abgebrannte Brennelemente, verglaste hochaktive sowie langlebige mittelaktive Abfälle. - Nagra Technical Report, NTB 02-02; Wettingen (Nagra).

Nagra (2002b): Projekt Opalinuston - Synthese der geowissenschaftlichen Untersuchnungs-ergebnisse - Entsorgungsnachweis für abgebrannte Brennelemente, verglaste hochaktive

sowie langlebige mittelaktive Abfälle. - Nagra Technical Report, NTB 02-03; Wettingen (Nagra).

Ostrowski L.P. & Kloska, Mr. B. (1989): Use of derivatives presses in analysis of Slug-test and DST flow period dated, SPE Production Operation Symposium, Oklahoma City, Oklahoma, March 13-14, 1989.

Papadopulos, S.S., Bredehoeft J.D. & Cooper H.H. (1973): On the Analysis of 'Slug Test' Data. Water Resour. Res. Vol. 9 (4). 1087-1089.

Ramey, J. J., Henry, J., Agarwal, R. G. & Martin, J. (1975): Analysis of slug test at DST flow period data. - Journal Canadian Petroleum Technology, 14, S. 37 - 42; Montreal

Peres, A.M., Onur, M. & Reynolds, A.C. (1989). A new analysis procedure for determining aquifer properties from slug test data. Water Resources Research, vol. 25, no. 7, pp. 1591-1602.

Pickens, J. F., Grisak, G. E., Avis, J. D., Belanger, D. W. & Thury, M. (1987): Analysis and Interpretation of Borehole Hydraulic Tests in Deep boreholes: Principles, Model Development, and Applications. - Water Resources Research, Vol. 23, No. 7, pp. 1341-1375.

Zeigler, T.W. (1976): Determination of Rock Mass Permeability, U.S. Army Engineering Waterways Experiment Station, Technical Report S-76-2, Vicksburg, Mississippi

21. Abbreviations, Nomenclature and Definitions

21.1. Abbreviations

	Test phases
INF	Packer inflation
INF1	Inflation of lower packer (INF2 = Inflation of upper packer)
DEF	Packer deflation
DEF1	Deflation of lower packer (DEF2 = Deflation of upper packer)
PSR	Static pressure recovery (shut-in valve closed)
SI	Slug injection test
SIS	Pressure recovery after slug injection test (shut-in)
SW	Slug withdrawal test
SWS	Pressure recovery after slug withdrawal test (shut-in)
PI	Pulse injection test
PW	Pulse withdrawal test
HI	Constant head injection test (constant pressure difference)
HIS	Pressure recovery after constant head injection test (shut-in)
HW	Withdrawal test applying constant differential head
HWS	Pressure recovery after constant head withdrawal test (shut-in)
MR	Multi-rate test: Test with variable flow rate
MRS	Pressure recovery after test with variable flow rate
RW	Pump test with constant flow rate
RWS	Pressure recovery after pump test with constant flow rate (shut-in)
RI	Constant flow injection test
RIS	Pressure recovery after constant flow injection test (shut-in)
VC	Shut-in valve is closed
VO	Shut-in valve is open
	General
CBP	Cooper, Bredehoeft, Papadopulos (type-curve matching method)
DAS	Data acquisition system
FS	Full scale
IARF	Infinite Acting Radial Flow
LC	Log cycle
m agl	Meters above ground level
m bgl	Meters below ground level
m asl	Meters above sea level
OD	Outer diameter

PVT	Pressure volume temperature correlation
SLA	Straight-line analysis
SSE	Sum of squared errors
TOC	Top of casing
WC	Water content
WL	Water level (or WT = Water table)

21.2. Nomenclature

	Description	SI-Unit		Description	SI-Unit
b	Y-intercept of linear regression		r_c	Tubing radius	m
C	Wellbore storage constant	$m^3\ Pa^{-1}$	r_w	Wellbore radius	m
C_S	Wellbore storage constant, shut-in	$m^3\ Pa^{-1}$	R_1	Radius, composite model	m
C_D	Dimensionless wellbore constant	-	R_D	Dimensionless radius	-
c_f	Formation compressibility (Pore volume based)	Pa^{-1}	S	Storage	-
c_r	Rock compressibility	Pa^{-1}	S’	Storativity	$m\ Pa^{-1}$
c_{sc}	System compressibility (= test zone compressibility c_{tz})	Pa^{-1}	S_S	Specific storage	m^{-1}
c_w	Water compressibility	Pa^{-1}	S'_S	Specific Storativity	Pa^{-1}
E	Young’s modulus	Pa	S_C	Sensitivity coefficient	
g	Acceleration of gravity (9.81)	$m\ s^{-2}$	S_{SC}	Scaled sensitivity coefficient	
Δh	Differential head	m	s	Skin factor	-
h_S	Static head		S_{SS}	Specific storage of skin zone	m^{-1}
k	Intrinsic permeability	m	t, Δt	Time, elapsed time	s
K, K_f	Hydraulic conductivity of formation () special case	m^2	t_c	Critical time	s
K_s	Hydraulic conductivity of skin zone () special case	m/s	t_D	Dimensionless time	-
L	Interval length	m	Δt_e	Equivalent time (after Agarwal)	s
m	slope (regression)	m	Δt_H	Horner time	-
P	Pressure		t_p	Production time	s
P_0	Minimal or maximal pressure	Pa, kPa	t_p*	Corrected production time	s
P_{atm}	Probe signal at atmospheric pressure	Pa, kPa	t_m	Match time	s
ΔP	Differential pressure, pressure change	Pa, kPa	t_0	X-intercept of linear regression	s
P_D	Dimensionless pressure	Pa, kPa	t_s	Thickness of skin zone	m
P_f	Static formation pressure	-	T	Transmissivity	m^2/s
Pi	Initial pressure	Pa, kPa	T_W	Water temperature	°C
$P_{min/max}$	Minimal/maximal pressure	Pa, kPa	V	Volume	m^3
P_{S1}	Static pressure in P1-Interval (below bottom packer)	Pa, kPa	z_1	P1 sensor depth	m
P_{S2}, P_f	Static pressure in test interval	Pa, kPa	z_2	P2 sensor depth	m
P_{S3}	Static pressure in annulus (above upper packer)	Pa, kPa	z_3	P3 sensor depth	m
q	Flow rate	Pa, kPa	α ,β	Type-curve match parameter	-
q_{end}, q_e	Last flow rate	$m^3\ s^{-1}$	μ	Dynamic viscosity	Pa·s
Q, Q_{tot}	Cumulative flow	$m^3\ s^{-1}$	ν	Poisson’s ratio	-
r_e	Effective radius (Slug, Pulse test)	m^3	θ	Porosity	-
R_i	Radius of influence	m	ρ_w	Density of fresh water	kg/m^3
R^2	Correlation coefficient	-			

21.3. Definitions

$C_D = \frac{\rho\ g C}{2\pi\ S r_{w^2}}$	Wellbore constant, dimensionless
$c_t = c_f + c_w$	Total compressibility
$H_D = \frac{P - P_i}{P_0 - P_i}$	Dimensionless pressure (slug und pulse tests)
$K = \frac{k\ \rho\ g}{\mu}$	Hydraulic conductivity
$P_D = \frac{2\pi\ T \Delta h}{q}$	Dimensionless pressure
$\Delta P = \rho\ g \Delta h$	Differential pressure
$q_D = \frac{q}{2\pi\ T \Delta h}$	Dimensionless flow
$t_D = \frac{t\ T}{r_w^2 S}$	Dimensionless time
$S = \phi c_t\ h \rho_w g$	Storage or storage coefficient
$S = S_S\ h$	Storage or storage coefficient
$S_S = \rho g\ (c_r + \theta\ c_w)$	Specific storage
$S' = \phi c_t\ h$	Storativity
$S' = S'_S\ h$	Storativity
$s = \left(\frac{K_f}{K_s} - 1\right) \ln\left(\frac{r_w + t_s}{r_w}\right)$	Skin factor

Definitions (continued)

$S_C = \frac{\partial P}{\partial r}$	Sensitivity coefficient
where ∂P is the partial derivative of the calculated system response (i.e., pressure) with respect to a parameter varied by the derivative span ∂r . For comparison of sensitivity coefficients for different parameters, the sensitivity coefficients are typically scaled by inverses of the respective standard deviations as follows: $S_{sc} = S_C \frac{\sigma_r}{\sigma_P} = \frac{\partial P}{\partial r} \cdot \frac{\sigma_r}{\sigma_P}$ where S_{sc} is the scaled sensitivity coefficient, σ_r is the a priori standard deviation of the measurement error, and σ_P is the estimated standard deviation of the parameter. If not otherwise stated, default values σ_r = 1 and σ_P = 1 were used.	
$T = K\ L$	Transmissivity
$\frac{t_D}{C_D} = \frac{2\pi T t}{\rho\ g C}$	Dimensionless time axis
$t_e = \frac{t_p \cdot \Delta t}{t_p + \Delta t}$	Dimensionless Agarwal time (Agarwal, 1980)
$t_e^* = \frac{t_p^* \cdot \Delta t}{t_p^* + \Delta t}$	Modified Agarwal time (using corrected production time)
$t_p^* = \frac{Q}{q_{end}}$	Modified production time (Ehlid-Economides and Ramey, 1980)